

RETURNING MATERIALS:
Place in book drop to remove this checkout from your record. FINES will be charged if book is returned after the date stamped below.

TOURS AND THE STATE OF THE STAT

SEISMIC ANALYSES OF TWO STEEL DECK ARCH BRIDGES

Ву

Ralph Alan Dusseau

A THESIS

Submitted to
Michigan State University
in partial fulfillment of the requirements
for the degree of

MASTER OF SCIENCE

Department of Civil and Sanitary Engineering
1982

ABSTRACT

SEISMIC ANALYSES OF TWO STEEL DECK ARCH BRIDGES

by

Ralph Alan Dusseau

Seismic analyses of two steel deck arch bridges were conducted. The bridges chosen were the 193 foot South Street Bridge (SSB) in Connecticut and the 700 foot Cold Springs Canyon Bridge (CSCB) in California. The analyses consisted of computer modeling utilizing the response spectrum method.

The response spectra used in the analyses were the Normalized Rock Spectra. Maximum ground accelerations of 0.09g for SSB and 0.50g for CSCB were set based on AASHTO site seismicity specifications. No attenuation of member responses was allowed for ductility.

The calculated fundamental periods were 0.64 seconds for SSB and 0.37 seconds for CSCB. For the arch ribs and the deck, the analyses indicated acceptable responses for SSB, but stresses approaching the yield stress for CSCB. The results also indicated that the cables in CSCB and certain deck abutment, arch rib abutment and column connections in both bridges might experience distress.

To my wife Ann
for her love and encouragement
on this and every project.

ACKNOWLEDGEMENTS

It is with deep gratitude and thanks that I wish to acknowledge the substantial contributions to this study which were made by Dr. Robert K. L. Wen, Professor of Civil Engineering, Michigan State University. In addition to his official roles as study coordinator and thesis advisor, Dr. Wen was also indispensable as a counselor, a seismic and structures expert, a devil's advocate, and a good friend. Without the aid of Dr. Wen this study would not have been possible.

I would also like to thank both the Division of Engineering
Research and the Department of Civil and Sanitary Engineering at
Michigan State University for their generous support. Finally, I would
like to thank my good friend Jalil for his good natured and always
helpful assistance.

TABLE OF CONTENTS

Chapter				Page
	LIST	OF TAB	LES	viii
	LIST	OF FIG	ur es	x
I	INTRO	DUCTIO	N	1
	1.1	Study	Motivation and Goals	1
	1.2	Bridge	s Analyzed	2
	1.3	Finite	Element Program	2
II	BRID	E MODE	LING AND PRECURSORY ANALYSES	4
	2.1	Genera	l Modeling Notes	4
	2.2	Modeli	ng of South Street Bridge	6
		2.2.1	Description of the Bridge	6
		2.2.2	Modeling Goal and Final Bridge Model	7
		2.2.3	Arch Ribs	7
		2.2.4	Arch Struts	8
		2.2.5	Arch Diagonals	8
		2.2.6	Columns	8
		2.2.7	Deck	.12
		2.2.8	Lumped Masses	.17
	2.3	Modeli	ng of Cold Springs Canyon Bridge	.18
		2.3.1	Description of the Bridge	.18
		2.3.2	Modeling Goal and Final Bridge Models	.19
		2.3.3	Arch Ribs	. 20

TABLE OF CONTENTS (Continued)

Chapter				Page
		2.3.4	Arch Crossframes	21
		2.3.5	Arch Laterals	22
		2.3.6	"Arch Elements"	22
		2.3.7	Cables	25
•		2.3.8	Columns	27
		2.3.9	Towers	29
•		2.3.10	Deck	30
		2.3.11	Lumped Masses	34
	2.4	Gravity	and Wind Load Responses	••35
		2.4.1	Dead Load Responses	••35
		2.4.2	Live Load Stresses	••35
		2.4.3	Wind Load Responses	••37
	2.5	Natural	Frequencies and Mode Shapes	••37
		2.5.1	General Comments	••37
		2.5.2	South Street Bridge Mode Shapes	38
		2.5.3	Cold Springs Canyon Bridge Mode Shapes With	
			Cables	••39
		2.5.4	Cold Springs Canyon Bridge Mode Shapes Without	
			Cables	40
III	RESP	ONSE SPE	CTRUM ANALYSES	41
	3.1	General	Notes	42
		3.1.1	Method of Analysis	42
		3.1.2	Response Spectra	43
		3.1.3	Definitions	47

TABLE OF CONTENTS (Continued)

Chapter			Page
	3.2	Arch Rib Stresses	48
		3.2.1 Axial Stresses	.49
		3.2.2 Major Axis Bending Stresses	50
		3.2.3 Minor Axis Bending Stresses	52
		3.2.4 Combined Stresses	52
	3.3	Arch Rib Displacements	••53
		3.3.1 X Axis Displacements	• • 54
		3.3.2 Y Axis Displacements	••55
		3.3.3 Z Axis Displacements	••55
	3.4	Deck Stresses	56
		3.4.1 Axial Stresses	 5 8
		3.4.2 Vertical Bending Stresses	••59
		3.4.3 Lateral Bending Stresses	60
		3.4.4 Combined Stresses	61
	3.5	Deck Displacements	62
		3.5.1 X Axis Displacements	63
		3.5.2 Y Axis Displacements	64
		3.5.3 Z Axis Displacements	65
	3.6	Other Member or Connection Responses	65
		3.6.1 Deck Expansion Joint Responses	68
		3.6.2 Arch Rib Hinge Responses	6 8
		3.6.3 Column to Floorbeam Connection Responses	70
		3.6.4 Column Base Connections	71
		3.6.5 CSCB Responses With and Without Cables	72

TABLE OF CONTENTS (Continued)

Chapter			Page
	3.7	Deck Lumped Masses	73
	3.8	Deck Torsion Constants	. 74
	3.9	Deck Concrete Effectiveness	75
IV	SUMM	ARY AND CONCLUSION	78
	4.1	Summary	78
	4.2	Concluding Remarks	81
	TABL	ES	83
	FIGU	RES	104
	LIST	OF REFERENCES	.262
	APPR	NDTX - CLOSSARY OF SYMBOLS	264

LIST OF TABLES

Tabl	e	Page
1	SSB Mode Shapes Characterized by Z Axis Displacements	
	and/or X Axis Rotations	83
2	SSB Mode Shapes Characterized by X Axis Displacements	
	and/or Y Axis Displacements	84
3	CSCB Mode Shapes Characterized by Z Axis Displacements	
	and/or X Axis Rotations for the Model with Cables	85
4	CSCB Mode Shapes Characterized by X Axis Displacements	
	and/or Y Axis Displacements for the Model with Cables	86
5	CSCB Mode Shapes Characterized by Z Axis Displacements	
	and/or X Axis Rotations for the Model without Cables	87
6	CSCB Mode Shapes Characterized by X Axis Displacements	
	and/or Y Axis Displacements for the Model without Cables	88
7	SSB Responses as a Function of Deck Mass Distribution	
	Under X Axis Accelerations of 0.09g	89
8	SSB Responses as a Function of Deck Mass Distribution	
	Under Y Axis Accelerations of 0.09g	90
9	SSB Responses as a Function of Deck Mass Distribution	
	Under Z Axis Accelerations of 0.09g	91
10	SSB Responses as a Function of Deck Torsion Constant	
	Under Z Axis Accelerations of 0.09g	92

LIST OF TABLES (Continued)

[abl	e Page
11	CSCB Responses as a Function of Deck Torsion Constant
	Under Z Axis Accelerations of 0.50g (Model Without Cables)93
12	SSB Responses as a Function of Concrete Effectiveness
	Under X Axis Accelerations of 0.09g
13	SSB Responses as a Function of Concrete Effectiveness
	Under Y Axis Accelerations of 0.09g95
14	SSB Responses as a Function of Concrete Effectiveness
	Under Z Axis Accelerations of 0.09g%
15	CSCB Responses as a Function of Concrete Effectiveness
	Under X Axis Accelerations of 0.50g (Model With Cables)97
16	CSCB Responses as a Function of Concrete Effectiveness
	Under Y Axis Accelerations of 0.50g (Model With Cables)98
17	CSCB Responses as a Function of Concrete Effectiveness
	Under Z Axis Accelerations of 0.50g (Model With Cables)99
18	SSB and CSCB Geometric and Design Characteristics100
19	Largest SSB and CSCB Arch Rib Responses101
20	Largest SSB and CSCB Deck Responses102
21	Other Key SSB and CSCB Responses103

LIST OF FIGURES

Figu	re Page
1	South Street Bridge Profile104
2	South Street Bridge Cross-section105
3	Final South Street Bridge Model106
4	Arch Abutment Hinge Connection107
5	Column to Floorbeam Expansion Joints108
6	Column Base Connections109
7	Deck Abutment Connections110
8	Deck Expansion Joints at F and F'111
9	Cold Springs Canyon Bridge Profile112
10	Cold Springs Canyon Bridge Cross-section113
11	Cold Springs Canyon Bridge Models114
12	Arch Rib Abutment Connection115
13	Arch Rib to Column to Crossframe Connection116
14	Arch Laterals Plan View117
15	Arch Element Configuration118
16	Arch Cross-section as Modeled119
17	Lateral Cables120
18	Longitudinal Cables121
19	Column Cross-section and Pedestal Connection
20	Tower Elevation View123
21	Tower Model

F	igu	re
	22	Deck Laterals125
	23	Deck Expansion Connections at Panel Point 1126
	24	Deck Bearing Connections at Panel Point 20127
	25	SSB Mode 1128
	26	SSB Mode 2129
	27	SSB Mode 3130
	28	SSB Mode 4131
	29	SSB Mode 5132
	30	SSB Mode 6
	31	SSB Mode 7134
	32	SSB Mode 8135
	33	SSB Mode 9
	34	SSB Mode 10
	35	SSB Mode 11
	36	SSB Mode 12139
	37	SSB Mode 13140
	38	SSB Mode 14141
	39	SSB Mode 15142
	40	SSB Mode 16143
	41	SSB Mode 17144
	42	SSB Mode 18145
	43	SSB Mode 19146
	44	SSB Mode 20147
	45	SSB Mode 21148

Figu	re	Page
46	SSB Mode 22	149
47	SSB Mode 23	150
48	SSB Mode 24	151
49	SSB Mode 25	152
50	SSB Mode 26	153
51	SSB Mode 27	154
52	SSB Mode 28	155
53	SSB Mode 29	156
54	SSB Mode 30	157
55	SSB Mode 31	158
56	SSB Mode 32	159
57	SSB Mode 33	160
5 8	SSB Mode 34	161
59	SSB Mode 35	162
60	SSB Mode 36	163
61	CSCB Mode 1 With Cables	164
62	CSCB Mode 2 With Cables	165
63	CSCB Mode 3 With Cables	166
64	CSCB Mode 4 With Cables	167
65	CSCB Mode 5 With Cables	168
66	CSCB Mode 6 With Cables	169
67	CSCB Mode 7 With Cables	170
68	CSCB Mode 8 With Cables	171
69	CSCB Mode 9 With Cables	

Figu	re		Page
70	CSCB Mode	10 With Cables	.173
71	CSCB Mode	11 With Cables	.174
72	CSCB Mode	12 With Cables	.175
73	CSCB Mode	13 With Cables	.176
74	CSCB Mode	14 With Cables	.177
75	CSCB Mode	15 With Cables	.178
76	CSCB Mode	16 With Cables	.179
77	CSCB Mode	17 With Cables	.180
78	CSCB Mode	18 With Cables	.181
79	CSCB Mode	19 With Cables	.182
80		20 With Cables	_
81		21 With Cables	
		22 With Cables	_
_		23 With Cables	
		24 With Cables	
_		25 With Cables	
86		26 With Cables	
87		1 Without Cables	-
88		2 Without Cables	-
89		3 Without Cables	
90 91		4 Without Cables	
•		6 Without Cables	
		7 Without Cables	106

Figu	re	Page
94	CSCB Mode 8 Without Cables	.197
95	CSCB Mode 9 Without Cables	.198
96	CSCB Mode 10 Without Cables	.199
97	CSCB Mode 11 Without Cables	. 200
98	CSCB Mode 12 Without Cables	. 201
99	CSCB Mode 13 Without Cables	. 202
100	CSCB Mode 14 Without Cables	. 203
101	CSCB Mode 15 Without Cables	. 204
102	CSCB Mode 16 Without Cables	. 205
103	CSCB Mode 17 Without Cables	. 206
104	CSCB Mode 18 Without Cables	. 207
105	CSCB Mode 19 Without Cables	. 208
106	CSCB Mode 20 Without Cables	. 209
107	CSCB Mode 21 Without Cables	.210
108	CSCB Mode 22 Without Cables	. 211
109	CSCB Mode 23 Without Cables	. 212
110	CSCB Mode 24 Without Cables	.213
111	CSCB Mode 25 Without Cables	. 214
112	CSCB Mode 26 Without Cables	. 215
113	Normalized Rock Spectra	. 216
114	NRC Spectra	. 217
115	SSB Arch Rib Stresses in Elements DE Versus X Axis	
	Acceleration	.218

Figu	re Page
116	SSB Arch Rib Stresses in Elements D'C' Versus Y Axis
	Acceleration219
117	SSB Arch Rib Stresses in Elements CD Versus Z Axis
	Acceleration220
118	CSCB Arch Rib Stresses in Elements 15c-16 Versus X Axis
	Acceleration221
119	CSCB Arch Rib Stresses in Elements 13c-14 Versus Y Axis
	Acceleration222
120	CSCB Arch Rib Stresses in Elements 6c-7 Versus Z Axis
	Acceleration223
121	SSB Arch Rib Responses to X Axis Application of Self Weight224
122	SSB Arch Rib Displacements at X Axis Accelerations of 0.09g225
123	SSB Arch Rib Displacements at Y Axis Accelerations of 0.09g226
124	SSB Arch Rib Displacements at Z Axis Accelerations of 0.09g227
125	CSCB Arch Rib Displacements at X Axis Accelerations of 0.50g228
126	CSCB Arch Rib Displacements at Y Axis Accelerations of 0.50g229
127	CSCB Arch Rib Displacements at Z Axis Accelerations of 0.50g230
128	SSB Arch Rib Displacements Versus X Axis Acceleration231
129	SSB Arch Rib Displacements Versus Y Axis Acceleration232
130	SSB Arch Rib Displacements Versus Z Axis Acceleration233
131	CSCB Arch Rib Displacements Versus X Axis Acceleration234
132	CSCB Arch Rib Displacements Versus Y Axis Acceleration235
133	CSCB Arch Rib Displacements Versus Z Axis Acceleration236
134	SSB Deck Stresses in Element DE Versus X Axis Acceleration237

Figure	
135	SSB Deck Stresses in Element D'C' Versus Y Axis Acceleration238
136	SSB Deck Concrete Stress in Element CD Versus Z Axis
	Acceleration
137	CSCB Deck Stresses in Element 15-16 Versus X Axis
	Acceleration240
138	CSCB Deck Stresses in Element 15-16 Versus Y Axis
	Acceleration241
139	CSCB Deck Concrete Stresses in Element 10-11 Versus Z Axis
	Acceleration242
140	SSB Deck Displacements at X Axis Accelerations of 0.09g243
141	SSB Deck Displacements at Y Axis Accelerations of 0.09g244
142	SSB Deck Displacements at Z Axis Accelerations of 0.09g245
143	CSCB Deck Displacements at X Axis Accelerations of 0.50g246
144	CSCB Deck Displacements at Y Axis Accelerations of 0.50g247
145	CSCB Deck Displacements at Z Axis Accelerations of 0.50g248
146	SSB Deck Displacements Versus X Axis Acceleration249
147	SSB Deck Displacements Versus Y Axis Acceleration250
148	SSB Deck Displacements Versus Z Axis Acceleration251
149	CSCB Deck Displacements Versus X Axis Acceleration252
150	CSCB Deck Displacements Versus Y Axis Acceleration253
151	CSCB Deck Displacements Versus Z Axis Acceleration254
152	Limits of Assumption Validity for SSB Under X Axis
	Acceleration

Figu	re	Page
153	Limits of Assumption Validity for SSB Under Z Axis	
	Acceleration	. 256
154	Limits of Assumption Validity for CSCB With Cables Under	
	X Axis Acceleration	. 257
155	Limits of Assumption Validity for CSCB With Cables Under	
	Y Axis Acceleration	. 258
156	Limits of Assumption Validity for CSCB With Cables Under	
	Z Axis Acceleration	. 259
157	Limits of Assumption Validity for CSCB Without Cables Under	
	Z Axis Acceleration	. 260
158	Typical SSB Column to Pedestal Joint and Linear Joint Stress	
	Distribution	. 261

CHAPTER I

INTRODUCTION

1.1 Study Motivation and Goals

The San Fernando earthquake of 1971 resulted in a heightened concern in this country for the safety of long span highway bridges located in earthquake prone regions. In response to this concern, the study by Tseng and Penzien (1) dealing with earthquake analysis of long multispan highway bridges and the study by Abdel-Ghaffar (2) dealing with dynamic analysis of suspension bridge structures have since been conducted. Similar studies concerning arch highway bridges have not been conducted, however.

With a large share of their mass concentrated in their decks and with these decks supported on columns which in turn rest on arch ribs, "steel deck arch bridges" because of their mass distribution and geometry seem particularly vulnerable to earthquakes. Thakkar and Arya (3,4) have studied the in-plane responses of single arch ribs to seismic inputs, but these studies have limited applicability to arch bridges. Japanese studies reported in the text by Okamoto (5) have dealt with theoretical calculations for and vibration testing of a deck arch railroad bridge, but since the material composition of this bridge was not specified, the applicability of these test results to steel deck arch bridges is unknown. Therefore, this study was undertaken in an effort to answer the question, "how might actual steel

deck arch bridges respond to in-plane and out-of-plane seismic ground motions?"

The research for this study consisted of four steps. The first step was to choose a set of actual steel deck arch bridges and develop linear models of these bridges using a finite element computer program. The second step was to determine, by means of an eigenvalue-eigenvector solution, the natural frequencies and mode shapes for each bridge. The third step was to choose applicable response spectra and to use these spectra in conjunction with the natural frequencies and mode shapes of each bridge to determine maximum stresses and displacements in each bridge under different magnitudes of maximum ground acceleration in three perpendicular directions. The final step was to analyze and discuss the results of these response spectrum analyses and to highlight the locations and magnitudes of the maximum responses and their relation to the safety of the bridge.

1.2 Bridges Analyzed

Because of time limitations, only two bridges were analyzed:
South Street Bridge near Middlebury, Connecticut; and Cold Springs
Canyon Bridge near Santa Barbara, California. These two bridges were
chosen because of their differences as well as their similarities.
They are different in arch length and configuration, in column stiffnesses and end fixity, and in their number and types of deck expansion
joints. They are similar, however, in that both are steel deck arch
bridges and both have solid-ribbed arches.

1.3 Finite Element Program

The finite element program used in this study was the structural analysis program SAPV2 developed at the University of California at

Berkeley and distributed by the SAP User's Group at the University of Southern California. The program, in addition to standard truss and beam elements, also allows the user to read element stiffness matrices directly into the structure stiffness matrix. It can also perform an eigenvalue-eigenvector solution to determine the natural frequencies and mode shapes for a given structure. After the program calculates the natural frequencies and modes shapes, it can then perform response spectrum analyses on the structure utilizing a variety of solution procedures and response spectrum curve options.

CHAPTER II

BRIDGE MODELING AND PRECURSORY ANALYSES

This chapter discusses how the finite element linear models of South Street Bridge and Cold Springs Canyon Bridge were developed. The discussion for each bridge contains a description of the structure, a statement of the general goal in modeling the bridge, a sketch of the final bridge model(s), a series of descriptions on how the individual bridge components were modeled and a description of how the mass of the bridge was calculated and lumped at the various nodal points in the model(s).

The discussions of the modeling of the bridges are followed by descriptions of how the bridges were analyzed for gravity and wind load responses. Finally, this chapter concludes with presentations and discussions of the natural frequencies and mode shapes of the bridge models. Thus the groundwork is laid for the discussions of the response spectrum analyses which are contained in the next chapter.

2.1 General Modeling Notes

The following general notes apply to the modeling of both bridges:

d. All sets of local joint coordinate axes (as well as the global coordinate axes) are oriented as follows: the x axis is horizontal and parallel with the bridge centerline; the y axis is vertical; and the z axis is horizontal and perpendicular to the bridge centerline.

- 2. The geometry, member sizes and relevant details of the two bridges were obtained from design drawings supplied to us by the Connecticut State Highway Department and the California Department of Public Works. The cross-sectional areas of all members and the moments of inertia, torsional constants and shear areas of those members modeled as beams were based on the typical member cross-sections with stiffeners, splice plates, etc., neglected.
- 3. All bridge members, unless otherwise specified, were modeled as running from joint center to joint center. Thus the columns which are attached to the tops of the arch ribs were modeled as running to the centers of the arch ribs.
- 4. The weights per foot of the concrete slab, the road surfacing, the parapets and the railings for both bridges were taken directly from the "Structural Steel Designer's Handbook" by Merritt (6) which discusses South Street Bridge on pages 13-40 and 13-41, and Cold Springs Canyon Bridge on pages 13-22 and 13-23. The weights of the remaining structural members were calculated by taking the typical member cross-sectional areas times their actual lengths and then times the unit weight of steel. If these calculated weights fell short of the values given in the Handbook, then the calculated values were increased by the necessary percentages so that they would be essentially equal to the Handbook values. Thus, for example, according to the Handbook the arch ribs in South Street Bridge weigh 1070 lb/ft for a total arch rib weight of 206.51 kips. Since the total calculated

weight of the arch ribs was only 191.7 kips, the calculated weights of all arch rib members were increased by 8% so that the total arch rib weight became 207.1 kips, which is slightly greater than the Handbook weight.

5. The y axis elevations for all nodes were based on the dead load deformed shapes of the bridges as specified in the design drawings.

2.2 Modeling of South Street Bridge

2.2.1 Description of the Bridge

South Street Bridge (Figures 1 and 2) is a two lane, solid-ribbed, steel deck arch spanning Route I-84 near Middlebury, Conn. The bridge consists of 13 panels each 29 feet in length for an overall bridge length of 377 feet. The arch consists of two rectangular steel box girder ribs spaced 22 feet apart and hinged at their abutments. The arch ribs span the center 193 feet of the bridge with five panels at 29 feet in length and two panels at 24 feet in length. The arch is circular in configuration with a radius of 175 feet, an enclosed angle of 66.9° and a height of 29 feet. The ribs are connected laterally by rectangular steel box girder struts and by tubular steel diagonals, the latter forming cross-bracing between panel points.

The columns are rectangular steel tubes with their longer sides normal to the centerline of the bridge. Expansion joints located at the tops of the columns at panel points A,E,F,F,F,E, and A, prevent the transfer of x direction forces and moments about the z axis at these points.

The deck consists of a $7\frac{1}{4}$ inch two-way reinforced concrete slab supported longitudinally by wide flange floor stringers which in turn

are supported laterally by wide flange floorbeams located at each panel point. In addition, welded steel parapets consisting of three square tubes and one channel section each are fastened to the concrete slab by welded studs. The deck is divided into five continuous segments by two expansion joints located at panel points F and F', and by concrete slab splices located at panel points C and C'. The expansion joints at F and F', as well as the connections at the abutments, prevent the transfer of x direction forces and moments about the y and z axes at these points.

2.2.2 Modeling Goal and Final Bridge Model

The general goal in the modeling of South Street Bridge was to develop a finite element linear model which would be reasonably valid for earthquakes with maximum ground accelerations of 0.09g. The choice of 0.09g was based on the fact that South Street Bridge is located in Zone I of the Seismic Risk Map on page 31 of the AASHTO Specifications (7) and as such the maximum expected rock acceleration according to the Specifications would be 0.09g.

The final linear model of South Street Bridge which evolved is depicted in Figure 3. Note, for added clarity, the deck and the columns are drawn separately from the arch.

2.2.3 Arch Ribs

The arch ribs are $39\frac{1}{2}$ by 24 inch steel box girders with 3/4 inch web plates and $1\ 3/4$ inch flange plates. Between the panel points the arch ribs were modeled as straight beam elements. This created about an 8 inch offset from the true arch curve at the center of each panel. The rib connections at the arch abutments (Figure 4) were modeled as hinges with rotations about the z axis as the only degree of freedom

(dof) allowed at these points.

During construction of the bridge, a third hinge at the crown of each arch rib prevented the transfer of moments about the z axis at this point. At completion of the bridge, however, these pin connections were fully closed. Therefore at their crowns the arch ribs were modeled as continuous.

2.2.4 Arch Struts

The arch struts are 24 by 12 inch steel box girders with 9/16 inch web plates and 5/8 inch flange plates. The struts serve as lateral connections between the two arch ribs with one strut located at each panel point along the arch. The struts are oriented such that the planes of their webs are normal to the axes of the arch ribs.

Because of the rigid design of the arch rib to strut connections, it was assumed that axial forces, shear forces, torsional moments and bending moments would all be transferred through these joints. Thus the struts were modeled as three-dimensional beam elements.

2.2.5 Arch Diagonals

The arch diagonals are 12 by 4 inch steel tubes with a wall thickness of 5/16 inch. The diagonals serve as cross-bracing between the arch ribs with one pair of diagonals per panel. Because of the relatively flexible design of the arch rib to diagonal connections, it was assumed that only axial forces would be transferred from the diagonals to the arch ribs. Thus the diagonals were modeled as three-dimensional truss elements.

2.2.6 Columns

The bridge columns are 16 by 10 inch steel tubes with wall thicknesses of $\frac{1}{2}$ inch. In all, there are five different types of column end

connections in the bridge: three types of base connections and two types of top connections. Since all of the columns have at least one end connection which can be assumed to be rigid, all of the columns in the bridge were modeled as three-dimensional beam elements.

The expansion joints located at the tops of the columns at panel points A,E,F,F',E' and A' are depicted in Figure 5 and were modeled as semi-rigid connections with column end releases preventing the transfer of x axis forces and moments about the x and z axes at these points. As can be seen in Figure 5, the actual connections have curved self-lubricating bronze plates which allow large z axis rotations of the deck relative to the column. Thus it was assumed that moments about the z axis would not be transferred from the columns to the deck at these points.

The bronze plates in these expansion joints have a flat upper surface which allows x and z axis displacements of the deck relative to the columns at these points. These joints, however, have only a ±3/4 inch clearance for relative x axis displacements and a ±1/8 inch clearance for relative z axis displacements. Linear modeling of these joints, however, required that an assumption be made as to whether or not forces (or moments) are transferred from the columns to the deck at these points. Because of the large clearance for relative displacements in the x direction, it was assumed that x axis forces would not be transferred. Because of the smaller clearance for relative z axis displacements, however, it was assumed that z axis forces would be transferred. This latter assumption, because it in effect ignored the ±1/8 inch clearance for relative z axis displacements, also signified that moments about the y axis would be transferred at these

connections.

With respect to the transfer of y axis forces from the columns to the deck at these expansion joints, the actual connections allow the transfer of compressive forces only. Because of the large compressive forces on the columns due to the dead load of the deck, it was assumed that these dead loads would exceed any calculated tensile forces due to earthquake accelerations. Therefore, the assumption was made that y axis forces (both upward and downward) would be transferred at these joints.

The transfer of moments about the x axis at these expansion joints is possible only so long as the dead load compressive stresses at these points are not exceeded. Preliminary response spectrum analyses assuming full transfer of moments about the x axis were conducted. These analyses showed that at maximum z axis ground accelerations of 0.013 to 0.08g the estimated maximum combined axial and bending stresses would exceed the dead load compressive stresses at these points, i.e. the bearing plates in these expansion joints might begin to separate. Because most of these separations would begin at maximum z axis ground accelerations of 0.025g or less, which are far below the 0.09g Zone I maximum ground acceleration, the decision was made to assume in the final bridge model that moments about the x axis would not be transferred between the deck and the columns at these points.

The joints located at the tops of the columns at panel points B,C, D,D',C' and B' were modeled as fully rigid connections. This assumption was based on the rigid design of these column to deck floorbeam connections in which the columns are not only continuous to the bottom flange of the floorbeam but from the bottom to the top flange as well.

At panel points A and A' the columns are anchored to the concrete pedestals, as depicted in Figure 6, utilizing two 2 foot by $\frac{1}{2}$ inch column stiffeners, a 20 inch by $18\frac{1}{2}$ inch by $1\frac{1}{2}$ inch base plate and six 1 1/8 inch anchor bolts. At panel points B,C,C' and B' the columns are anchored to the concrete pedestals, as depicted in Figure 6, utilizing one $1\frac{1}{2}$ foot by $\frac{1}{2}$ inch column stiffener, a 20 by $18\frac{1}{2}$ by $1\frac{1}{4}$ inch base plate and four 1 1/8 inch anchor bolts. Because of their relatively rigid design, all of these column to pedestal connections were modeled as fully rigid.

At panel points D,E,E' and D' the column bases are fastened to the arch ribs utilizing 3/4 inch diaphragm stiffeners inside the arch ribs to give the columns continuity from the top of the arch ribs to the bottom. Because of their rigid design, all of these arch rib to column connections were modeled as fully rigid.

The column to floorbeam expansion joints at panel points F and F' are fastened directly to the top flange plates of the arch ribs, thus there are actually no columns at these points. In the model, however, short columns were used at these points to connect the expansion joints with the centers of the arch ribs. These columns are necessary because of the finite height of the rib cross-section. Since these columns are only about two feet in length, it was felt that modeling them as rigid links would not be necessary and that the typical column cross-section would suffice. Thus short columns with typical column cross-sections were used at panel points F and F'.

At each panel point in the model the tops of the columns were placed at the bottom of the floorbeam. Because the columns at panel points B,C,D,D',C' and B' are continuous between the top and bottom

floorbeam flanges at these points, their tops could have been placed at the same y axis elevation as the deck centroidal axis at these points. But because the distance from the deck centroidal axis to the bottom floorbeam flanges is only about 21 inches and in order to be consistent throughout the model, the decision was made to place the tops of the columns at each panel point at the same y axis elevation as the bottom flange of the floorbeam at that panel point. Thus the columns at panel points A,B,C,C'B' and A' were modeled as running from the tops of the concrete pedestals to the bottoms of the deck floorbeams and the columns at panel points D,E,F,F',E' and D' were modeled as running from the centers of the arch ribs to the bottoms of the deck floorbeams.

2.2.7 Deck

The bridge deck was modeled as a single three-dimensional beam connected to the columns at panel points A to A' by rigid links which serve to replace the floorbeams in the deck. The typical deck cross-section consists of six structural components: a reinforced concrete slab and five floor stringers. The Connecticut State Highway Department informed us that the steel parapets were not designed to contribute to the overall deck stiffnesses and our own calculations bore this out. Thus the parapets were treated in the model as contributing to dead load only.

The reinforced concrete slab is $7\frac{1}{4}$ inches thick and 34 feet wide with a 1% crown. It has both longitudinal and lateral reinforcing, only the former of which was used in the calculations of deck stiffnesses. The concrete in the slab was modeled as 50% effective, i.e. in the calculations of deck stiffnesses the area of the concrete slab was converted to steel using a modular ratio of elasticity (n) of 20. The

decision to use 50% concrete effectiveness was essentially an arbitrary compromise necessitated by the linear nature of the model.

Any cracking of the slab whether due to earthquake loads, wind loads, live loads, temperature changes or other effects would result in nonlinear behavior of the slab. Thus it was felt that while an assumption of 0% concrete effectiveness would not be correct, neither would an assumption of 100% concrete effectiveness. Therefore, a compromise value of 50% was used. In order to get some measure of the effects of this choice, an alternate bridge model assuming 100% concrete effectiveness was analyzed. The results of this analysis are discussed in section 3.8.

For each deck cross-section the areas of the concrete haunches at the floor stringers were ignored in the calculations of deck stiffnesses because they are small compared with the area of the slab as a whole.

There are four different wide flange sections which are used as stringers in the bridge. From panel points 0 to F and F' to 0' the two exterior stringers are W24x68 sections while the three interior stringers are W24x76 sections. From panel points F to F' the two exterior stringers are W24x84 sections while the three interior stringers are W24x100 sections. While the top flanges of the stringers are partially embedded in the concrete slab, the slab and the stringers were not designed to act compositely and thus in the model they were not treated as composite beams.

Because of the different wide flange sections used as stringers, there are essentially two different deck cross-sections. The various geometric properties for each deck cross-section were calculated using the same procedures. For each cross-section the area of the concrete

slab was converted to steel using n=20 and was added to the areas of the stringers and the longitudinal reinforcing to get the total cross-section area. The shear area in the y direction for each cross-section was calculated by taking the sum of the web areas of the five floor stringers. The shear area in the z direction was calculated by taking the sum of the flange areas of the five stringers and the area of the concrete slab converted to steel.

Moments of inertia about the y and z axes were calculated by taking the sum of the individual moments of inertia of the five stringers, the longitudinal reinforcing and the concrete slab converted to steel. Since the deck does not act like a composite beam and since the bulk of the moment of inertia about the z axis is contributed by the floor stringers, the centroidal axis of the deck was placed at the center of the middle floor stringer.

The deck torsion constants were calculated by taking the sum of the individual torsion constants of the five stringers and the concrete slab converted to steel. The additional torsional stiffness arising out of the bending resistance of the stringers was ignored. Response spectrum analyses (see section 3.9) indicated that under z axis acceleration the largest and most important bridge responses were virtually unaffected by the value of the torsion constants. Thus the lower and more conservative values for the torsion constants were used.

The expansion connections between the stringers and the abutments at panel points 0 and 0° are depicted in Figure 7 and were modeled as semi-fixed connections allowing displacement of the deck in the x direction and rotation of the deck about the y and z axes at these points. As can be seen in Figure 7, the actual connections have $1\frac{1}{2}$

inch elastomeric bearing pads which allow large z axis rotations of the deck. Thus it was assumed that moments about the z axis would not be transferred from the deck to the abutments.

The elastomeric pads in the stringer to abutment connections also allow x and z axis displacements of the deck at the abutments. These connections, however, have only a $\pm 3/4$ inch clearance for x axis displacements and a $\pm 1/8$ inch clearance for z axis displacements. Thus, for the same reasons as in the case of the column to floorbeam expansion connections, the assumption was made that z axis shear forces would be transferred from the deck to the abutments but that x axis axial forces would not. This latter assumption, because it allowed unlimited x axis displacements of the stringers, also signified that moments about the y axis would not be transferred from the deck to the abutments.

With respect to the transfer of y axis shear forces from the deck to the abutments, the actual connections allow the transfer of compressive forces only. Here again, for the same reasons as in the case of the column to floorbeam expansion connections, the assumption was made that y axis shear forces would be transferred from the deck to the abutments. Because this assumption prevented any y axis displacements of the floor stringers at the abutments, it also implied that torsional moments about the x axis would also be transferred from the deck to the abutments.

Between the deck abutments, the continuity of the deck is broken in four locations: at the expansion joints near panel points F and F', and at the deck slab splices at panel points C and C'. The expansion joints near panel points F and F' (Figure 8) are located $5\frac{1}{4}$ inches from

the panel points and serve to prevent the transfer of x axis axial forces and moments about the y and z axes at these points. In the model the center span was modeled from panel points F to F' with moment releases at both ends to prevent the transfer of moments about the y and z axes at these points. Axial releases could not be placed at both ends of the center span because this would have resulted in an unstable center span with respect to x axis loading. Because the mass of the center span was ignored in the x direction (see section 2.2.8), it was possible to model the center span using only one axial release without giving rise to axial forces at either end.

Panel points C and C' are the locations where the concrete slabs from 0 to F and F' to 0' respectively are spliced. At these points the concrete and the top flanges of the floor stringers are discontinuous. Also at these points the longitudinal reinforcing in the slab is doubled. While there is some continuity at C and C' with respect to rotation about the z axis, preliminary response spectrum analyses assuming full continuity at C and C' showed that under vertical (y axis) or longitudinal (x axis) acceleration the most severe bending about the z axis occurred at panel points C and C'. Thus it was assumed that under relatively low earthquake acceleration levels the moment capacities about the z axis would be exceeded. Since the deck was not designed to be continuous at C and C' with respect to rotation about the z axis, the decision was made to place moment releases about the z axis at both panel points.

These same preliminary analyses also showed that under lateral acceleration the lateral bending moments reached their largest values at panel points C and C'. The bulk of the lateral bending stiffness of

the deck is contributed by the slab. Even though the slab at C and C' is discontinuous, it can still transfer compressive forces which, when coupled with the tensile forces of the longitudinal reinforcing which is doubled at C and C', yields a connection which is comparable to the typical deck cross-section in strength. Thus no moment releases with respect to bending about the y axis were placed at these panel points.

2.2.8 Lumped Masses

The mass of South Street Bridge was lumped at 26 nodal points in the structure: at panel points 0,A,B,C,C',B',A' and 0' masses were lumped at the centroidal axis of the deck and at panel points D,E,F,F', E' and D' masses were lumped at the deck centroidal axis and at the centers of the two arch ribs.

The mass lumped at the centroidal axis of the deck at a given panel point included one-half the mass of the deck segments lying between the given panel point and the adjacent panel points plus one-half the mass of the columns at the given panel point. Because the floorbeams were replaced by rigid links, the mass moments of inertia of the various deck masses were also calculated.

The first step in the calculation of deck mass moments of inertia was to lump the masses of the various deck components at the points where they intersect the vertical planes of the floorbeams or would intersect them if they were placed at the panel points. Thus the masses of the parapets and the floor stringers were lumped at the points where they intersect the vertical planes of the floorbeams. The deck portions of the column masses were lumped as point masses at the bottoms of the floorbeams where they are fastened. The masses of the concrete slab, the intermediate and end diaphragms, the road surfacing

and the floorbeams were lumped as linear masses in the vertical planes of the floorbeams. The mass moments of inertia were then calculated for these linear and point masses with respect to x, y and z axes passing through the deck centroidal axis at each panel point.

The mass lumped at the center of one arch rib at a given panel point included one-fourth the mass of all arch members lying between the given panel point and the adjacent panel points plus one-fourth the mass of the columns at the given panel point.

Because of the expansion joints at F and F', the deck segment from F to F' can be expected to act as if supported by rollers at these points. In order to model this condition with respect to mass effect, the mass of the deck segment from F to F' was neglected in the x direction. The lumped masses and mass moments of inertia at F and F' were then calculated on this basis.

2.3 Modeling of Cold Springs Canyon Bridge

2.3.1 Description of the Bridge

Cold Springs Canyon Bridge (Figures 9 and 10) is a two lane, solid-ribbed steel deck arch spanning Cold Springs Canyon and Route 80 near Santa Barbara, California. The bridge consists of 19 panels with two at 46.5 feet in length, 13 at 63.635 feet in length and four at 74.385 feet in length for an overall bridge length of 1217.8 feet. The arch consists of two rectangular steel box girders spaced 26 feet apart and hinged at their abutments with 11 panels at 63.635 feet each for a total arch span of 700 feet.

The configuration of the arch is based on a seventh order polynomial with the northern hinges being 46.48 feet above the southern hinges and with the rise at the highest point on the arch being 144.5 feet

above the southern hinges. The ribs are connected laterally by a system of crossframes with one crossframe located at each panel point and three crossframes (labeled a, b and c) spaced equally between panel points. This crossframe configuration subdivides each panel into four subpanels. The ribs are also connected laterally by top and bottom laterals which along with the crossframes and the arch ribs creates a type of box truss configuration with the arch ribs acting in place of side trusses.

The columns located at panel points 2 to 5, 7 through 16, 18 and 19 are steel box sections with hinge connections at top and bottom.

The towers located at panel points 6 and 17 consist of steel box section columns which are rigidly fastened at their bases and are connected laterally by two steel box girder struts and by a composite steel box girder and concrete strut at the top.

The deck consists of a $7\frac{4}{7}$ inch two-way reinforced concrete slab supported longitudinally by four plate girder stringers which are in turn supported laterally by plate girder floorbeams. The parapets are in preformed reinforced concrete segments, and the assumption was made that they would not contribute to the stiffnesses of the deck. The deck is divided into three continuous segments by hinged tower connections at panel points 6 and 17 which prevent the transfer of moments about the z axis.

Between panel points 11 and 12 a system of bridge rope cables runs between the deck and the arch forming cross-bracing in the longitudinal direction and V-bracing in the lateral direction.

2.3.2 Modeling Goal and Final Bridge Models

The general goal in the modeling of Cold Springs Canyon Bridge was to develop a finite element linear model which would be reasonably valid for earthquakes with maximum ground accelerations up to 0.50g. The choice of 0.50g was based on the fact that Cold Springs Canyon Bridge is located in Zone III of AASHTO's Seismic Risk Map, and as such the maximum expected rock acceleration according to the AASHTO Specifications would be 0.50g.

The final linear models of Cold Springs Canyon Bridge which were derived are depicted in Figure 11. Note that two models evolved - one with cables and one without cables. Since these two models differ only between panel points 11 and 12, this section is drawn twice in Figure 11 - once with cables and once without cables. For added clarity the deck and the columns are drawn separately from the arch.

2.3.3 Arch Ribs

The arch ribs are 9 foot by 3 foot steel box girders with 15/16 inch webs and with flanges varying in thickness from 1.5 to 3.5 inches. Between panel and subpanel points the ribs were modeled as straight beam elements. This created a less than one inch offset from the true curve at the center of each subpanel. The arch rib stiffnesses between panel and subpanel points were based on the average flange thicknesses between these points.

As in the case of South Street Bridge, the rib connections at the arch abutments of Cold Springs Canyon Bridge (Figure 12) were modeled as hinges with rotations about the z axis as the only dof allowed at these points. Also as in the case of South Street Bridge, third hinges near the crown of each arch rib in Cold Springs Canyon Bridge were closed at the completion of the bridge and thus the arch ribs were modeled as continuous at these points.

2.3.4 Arch Crossframes

The arch crossframes (see Figure 10) are composed of five members each: continuous top and bottom HP section chords, a WT8x18 section running between the centers of the top and bottom chords, and two WT8x25 sections running between the center of the top chord and the ends of the bottom chord. The top and bottom chords are HP10x42 sections for the crossframes from panel points 8 to 15, and HP10x57 sections for the crossframes from panel point 6 to subpanel point 7c and from subpanel point 15a to panel point 17.

Due to the configuration of the crossframes, all crossframe members were modeled as three-dimensional truss elements. Each crossframe is oriented such that its plane is perpendicular to the tangents of the arch ribs at the points of connection. Figure 13 depicts a typical arch rib to crossframe to column connection at the panel points. As can be seen, the panel point crossframes are not precisely centered at the panel points but are positioned such that their planes pass through the points where the columns are fastened to the top flange plates of the arch ribs. Similarly, the three subpanel point crossframes for each panel are not centered at the subpanel points but instead they are equally spaced between the panel point crossframes.

In the models the crossframes are centered at the panel and subpanel points. These modeled positions of the crossframes hold true
near the crown of the arch but their difference from the true positions increases as one moves further away from the crown of the arch.
Therefore the largest differences from the true positions occur at the
arch hinges where in the actual structure the crossframes are 40 inches
from the hinges but in the bridge models they were placed at the hinges.

At subpanel point 11b there are two crossframes located 40 inches from and on either side of the closed third hinges (see Figure 14). Both of these crossframes were placed at their correct positions in the bridge models along with the crossframes at 11a and 11c which are located midway between the nearer of the two crossframes at 11b and the crossframe at the adjacent panel point (11 or 12 respectively).

2.3.5 Arch Laterals

The arch laterals depicted in Figure 14 are systems of HP section members which form lateral bracing between the crossframe top chords and between the crossframe bottom chords. As can be seen in Figure 14, each pair of laterals forms an inverted V which points toward the closed third hinges at subpanel point 11b. The top and bottom laterals are HP10x42 sections for those pairs of laterals between panel points 8 and 15, and HP10x57 sections between panel points 6 and 8 and between panel points 15 and 17. As in the case of the crossframe members, all of the arch laterals were modeled as three-dimensional truss elements, and as in the actual structure, the arch laterals were modeled as running from the end of one crossframe chord to the center of the next crossframe chord.

2.3.6 "Arch Elements"

With over 500 members, the arch if modeled apart from the rest of the bridge would have over 800 dof which when added to the 113 dof of the remainder of the bridge would yield a total of over 900 dof. In order to reduce this number of dof, "substructures" called "arch elements" were used. Each arch element, covering one or more subpanels, included the two arch ribs, the associated crossframes, and the top and bottom laterals. From the stiffness matrix of each arch element, the

dof of the internal nodes were condensed out. In addition, constraints were imposed at the ends of each arch element such that the x and y rotations and the z displacements of both arch ribs at these points would be the same. The condensed stiffness matrices for all of the arch elements were then assembled with the rest of the structure. The use of these arch elements resulted in a reduction of about 600 dof yielding a total of 306 dof for the final models. The condensation procedure, the configuration of the arch elements and the arch dof remaining after condensation are discussed in more detail as follows.

The 44 subpanels of the arch were divided into 22 arch elements each one being one to three subpanels in length. The configuration of the arch elements, as depicted in Figure 15, arose out of the need to recover at least some of the stresses in the arch ribs resulting from the response spectrum analyses. The SAPV2 output for a response spectrum analysis consists of two parts: maximum nodal displacements. and maximum beam and truss element stress resultants. The maximum resultants for the components of the arch elements can not be recovered because the SAPV2 program can not calculate resultants for elements whose stiffness matrices are read into the computer and because the maximum nodal displacements which are calculated have no direct relation to maximum element resultants. By modeling single subpanels as arch elements, however, the arch rib segments contained in these elements could be taken out and modeled as individual beam elements. Thus the stresses in these segments of arch rib could be calculated and recovered.

In practice, arch rib segments with one-half their actual stiffnesses remained as part of the single subpanel arch elements. The remaining one-half of the stiffnesses of these arch rib segments were represented by separate beam elements. The reason for this division of the arch rib stiffnesses was that the stiffness matrices for the single subpanel arch elements became ill-conditioned when the arch rib segments were entirely removed. Thus in the final bridge models the stresses derived from a response spectrum analysis could be recovered for 20 of the 88 arch rib segments in the bridge.

Figure 16 represents a typical panel or subpanel cross-section with the nodal points and members used in the models depicted also. The dashed lines represent pseudo-rigid links which connect the centers of the arch ribs with the ends of the top and bottom chords of the cross-frames. These pseudo-rigid links as modeled had stiffnesses approximately three times larger than the stiffnesses of the arch ribs. 1

The 193 dof remaining in the arch after condensation were two dof each at panel points 6 and 17; nine dof each at panel points 7 through 16; and nine dof each at subpanel points 6c,7c,8c,9c,10c,11b,12c,13c, 14c,15c and 16c. At panel points 6 and 17, where the arch ribs are hinged to their abutments, the dof remaining after condensation were the z rotations of the nodes at the centers of the arch ribs.

Those panel and subpanel points with nine dof remaining after condensation had all nine dof assigned to the nodes located at the centers of the arch ribs with individual x and y displacements and z rotations at each point, and common z displacements and x and y rotations. The

Stiffer links were not used because the stiffnesses of the crossframe members are small compared with the arch ribs. The use of links with stiffnesses much larger than the arch ribs would have resulted in ill-conditioned element stiffness matrices. Rigid links were not used because the program used in the condensation procedure did not have this option.

decision to make the z displacements and x and y rotations the same at both points was based on the mode shapes derived for South Street Bridge. In every South Street Bridge mode shape in which the z displacements and x and y rotations at the centers of the arch ribs were large, the values of these variables at each panel point were the same for both arch ribs.

2.3.7 Cables

There are four pair of tensioned cables which run between the deck and the arch with two pair lying in the planes of the arch ribs and two pair lying in planes normal to these planes. All of these cables were modeled as linear truss elements that resist both tensile and compressive loads.

In reality, the bridge cables could go limp under seismic compressive loads because the tensioning stresses in them are low.

However, since each pair of cables has a symmetric or nearly symmetric configuration, the changes in stress which occur within each pair of cables tend to be equal and opposite. Hence, if one cable in a pair of cables goes limp because of seismic compressive loads, the other cable in the pair must be in tension. Therefore, two linear truss elements can be used to model each pair of cables if the following assumptions are made:

- 1. No cable tensioning,
- 2. The sum of the absolute values of the calculated stresses in the two truss elements represents the actual stress which would exist in one cable.

The two pair of cables lying in vertical planes normal to the planes of the arch ribs (Figure 17) are located at panel points 11 and

12. They are composed of $1\frac{1}{9}$ inch bridge rope which is tensioned to 2000 psi and has a minimum breaking strength of 96 tons. As can be seen in Figure 17, these lateral cables run from the center of the crossframe top chord to points on the bottom of the deck floorbeam near where the columns are attached. As depicted by the dashed lines in Figure 17, however, the lateral cables were modeled as running from the center of one arch rib to the opposite column to floorbeam connection. Thus, while the lateral cables form V-bracing in the actual structure, they were modeled as cross-bracing.

The reason for modeling the lateral cables as cross-bracing was to allow the three dof each at the centers of the crossframe top chords at panel points 11 and 12 to be condensed out of the arch elements. Since the cross-sectional area of the lateral cables is only about $1\frac{1}{4}$ square inches, it was felt that changing the lateral cable configuration from V to cross-bracing would have little impact on the overall behavior of the models.

The two pair of cables lying in the same vertical planes as the arch ribs (Figure 18) are located roughly between panel points 11 and 12. These longitudinal cables are composed of 1 5/8 inch bridge rope which is tensioned to 7000 psi and has a minimum breaking strength of 162 tons. Each longitudinal cable begins at a point near where the column at one panel point is connected to the top flange of the arch rib. It then runs through a point about midway between the top and bottom flanges of the floorbeam at the other panel point, and ends at a point 98 inches from the second panel point where it is fastened to a short plate girder.

For the computer models, as depicted by the dashed lines in

Figure 18, each longitudinal cable was assumed to run from the arch rib centerline at one panel point to the column to floorbeam connection at the other panel point. Thus in the models the lower ends of the longitudinal cables were moved downward by about $4\frac{1}{2}$ feet when compared with the actual structure while the upper ends were placed about $2\frac{1}{2}$ feet lower than the point where they intersect the floorbeams in the actual structure. Modeling the longitudinal cables in this manner enabled the utilization of the existing dof at the centers of the arch ribs and at the column to floorbeam connections. Since the cross-sectional area of each longitudinal cable is only about two square inches, it was felt that this changing of the endpoints of the longitudinal cables would have little impact on the overall behavior of the models.

The response spectrum analyses of the Cold Springs Canyon Bridge model with both lateral and longitudinal cables included showed that both types of cables would reach their minimum breaking strengths at maximum ground accelerations less than 0.50g. Thus the decision was made to use two models to represent Cold Springs Canyon Bridge - one with the cables and one without the cables. Because both of these models were to represent Cold Springs Canyon Bridge, both are dealt with on an equal basis in this study. Therefore, the natural frequencies and mode shapes for both models were computed and are presented in this chapter. In addition, the results described in the next chapter include the responses of each model where applicable.

2.3.8 Columns

The columns (Figure 19) located at all panel points except 1,6,17 and 20 are $24\frac{1}{2}$ by 25 inch box shapes with $\frac{1}{2}$ inch wall thicknesses and with hinge connections at top and bottom. The column to pier

connections at panel points 2,3,4,5,18 and 19 consist of three steel plates: a 10 by 10 by $2\frac{1}{2}$ inch top plate with a concave lower surface, a 5 inch circular bearing plate with a convex upper surface and a flat lower surface, and a 10 by 10 by 2 inch bottom plate with a flat upper surface (see Figure 19). This sandwich of three plates is held together by two 1 inch bolts spaced six inches apart which run between the top and bottom plates and serve to hold the circular bearing plate in position. The same connection is used at panel points 7 through 16 to connect the bases of the columns to the top flange plates of the arch ribs. It is also used to connect the tops of all the columns to the deck floorbeams.

All the columns in the bridge were modeled as truss elements with the columns at panel points 2,3,4,5,18 and 19 being modeled as running from the tops of the concrete piers to the bottoms of the floorbeams. The columns located at panel points 7 through 16 were also modeled as ending at the bottoms of the floorbeams, but unlike the real bridge, these columns were modeled as beginning at the centers of the arch ribs rather than at the top flanges. In order to begin these columns at the top flanges, rigid links running from the centers of the arch ribs to the top flange plates would have been required. Such rigid links would have increased the complexity of the models. Since the columns are modeled as truss elements, the net result would have been somewhat smaller axial deformations. The change in axial deformation due to a $4\frac{1}{2}$ foot reduction in column length at each of these points would be small and its effects negligible. Thus the columns at panel points 6 through 17 were modeled as beginning at the centers of the arch ribs.

2.3.9 Towers

The towers (Figure 20) located at panel points 6 and 17 are each composed of five members: two columns having 48 by $52\frac{1}{2}$ inch box shapes with $1\frac{1}{4}$ inch wall thicknesses and with their longer sides normal to the centerline of the bridge, two $73\frac{1}{2}$ by 30 inch intermediate box girder struts with $1\frac{1}{4}$ inch flange plates and $\frac{1}{2}$ inch webs, and a single composite top strut composed of a 61 3/4 inch by 30 inch box girder with 7/8 inch flange plates and 5/8 inch webs and topped by a short segment of concrete slab which varies in thickness from $7\frac{1}{4}$ to 12 11/16 inches.

In modeling the towers (see Figure 21), all dof except the six dof each at the deck centroidal axis at panel points 6 and 17 were condensed out thus eliminating 24 dof from each tower. The remaining six by six stiffness matrix for each tower was then read into the SAPV2 program using the Read-in Stiffness Matrix Element.

The column to skewback connections are very rigid in design with 29 prestressed 1 3/8 inch rods used to anchor the columns to the skewbacks. Thus the columns were modeled as three-dimensional beam elements fixed at their bases and running from the tops of the skewbacks to the elevation of the deck centroidal axis. The intermediate strut to column connections are also very rigid and thus the intermediate struts were modeled as three-dimensional beam elements rigidly connected to the tower columns.

In the models, the tower columns were connected to the deck centroidal axis by pseudo-rigid links which served to replace the top tower struts. These pseudo-rigid links ran from the tops of the tower columns horizontally to the deck centroidal axis. The stiffnesses of

these pseudo-rigid links were roughly three times larger than the corresponding stiffnesses of the intermediate tower struts. 1

2.3.10 Deck

As in the case of South Street Bridge, the deck in Cold Springs Canyon Bridge was modeled as a single three-dimensional beam connected to the columns at panel points 2 through 5, 7 through 16, 18 and 19 by rigid links which serve to take the place of the deck floorbeams. The typical deck cross-section consists of six components: a reinforced concrete slab, four floor stringers and a deck lateral.

The concrete slab is $7\frac{1}{4}$ inches thick and 34 feet wide with a 1.56 tilt for water runoff and with both longitudinal and lateral reinforcing, only the former of which was used in the calculations of deck stiffnesses. For the same reasons as discussed with respect to the South Street Bridge deck, the concrete in the Cold Springs Canyon Bridge deck was modeled as 50% effective. Thus, in the calculations of deck stiffness constants, the area of concrete was converted to steel using a modular ratio of 20. In order to get some measure of the effects of this choice, an alternate version of the model with cables assuming 100% concrete effectiveness was analyzed. The results of this analysis are discussed in section 3.8.

Two additional items should also be mentioned with regard to the concrete slab. First, because the slab is fastened to each floor stringer by trios of 7/8 inch shear connectors spaced every 6 to 18 inches, the assumption was made that the slab and the stringers would

¹ While rigid links were used to replace the deck floorbeams (see section 2.3.10), they could not be used in place of the top tower struts because the computer program used for the condensation of the tower dof had no rigid link element.

act as a composite beam. Second, for each deck cross-section the areas of the concrete haunches at the floor stringers were ignored in the calculations of deck stiffness constants because they are small compared with the area of the slab as a whole.

All of the floor stringers are plate girders with 52 by 5/16 inch web plates, 10 inch wide top flange plates and 12 inch wide bottom flange plates. The two dimensions which vary along the length of the floor stringers are the thicknesses of the top and bottom flange plates. The top flange plate varies from 5/8 inch to 1 inch in thickness while the bottom flange plate varies from 5/8 inch to 1 1/8 inch in thickness. Because of these various changes in flange thicknesses, there are basically four different panel point to panel point plate girders which are used as stringers with all four stringers at any deck cross-section being the same. In the bridge models the average top and bottom flange thicknesses between panel points were used in the calculations of deck stiffness constants for each panel.

The deck laterals (Figure 22) are WT8x18 sections which run in a zig-zag fashion between the two outer floor stringers and which lie in a plane 11 inches above the bottom of the stringer web plates. In the models the cross-sectional area of the laterals was divided into x and z components both of which were used in the calculations of deck stiffnesses.

Based on the assumptions made above, there were four deck cross-sections used in the models. The first ran from panel points 1 to 2 and 19 to 20; the second from panel points 2 to 4 and 8 to 15; the third from panel points 4 to 5, 7 to 8, 15 to 16 and 18 to 19; and the fourth from panel points 5 to 7 and 16 to 18.

The various geometric stiffness constants for each deck crosssection were calculated using the same basic procedures. For each
cross-section the area of concrete was first converted to steel using
n=20 and was used along with the areas of the longitudinal reinforcing,
the stringers and the x axis component of the deck lateral to calculate
the total cross-sectional area, the vertical (y axis) location of the
deck centroidal axis and the moment of inertia about the z axis. The
moment of inertia about the y axis was based on the areas of the
concrete slab converted to steel, the longitudinal reinforcing and the
stringers.

The shear area in the y direction for each deck cross-section was calculated by taking the sum of the web areas of the stringers. The shear area in the z direction was calculated by taking the sum of the area of the concrete slab converted to steel, the flange areas of the stringers and the z component of the area of the deck lateral.

The torsional constant for each deck cross-section was calculated by summing the individual torsional constants of the concrete slab converted to steel and the four stringers. As in the case of South Street Bridge and for the same reasons discussed in section 2.2.7, the deck torsional constants for Cold Springs Canyon Bridge did not include the additional torsional stiffness due to the bending resistance of the stringers.

The expansion connections between the floor stringers and the abutment at panel point 1 are depicted in Figure 23 and were modeled as semi-fixed connections allowing x axis deck displacements and rotations of the deck about the y and z axes at panel point 1. As can be seen in Figure 23, the actual connections have curved,

self-lubricating, bronze bearing plates which allow large z axis rotations. Thus it was assumed that no moments about the z axis would be transferred from the deck to the abutment at panel point 1. In addition, these bronze bearing plates have a flat side which allows x and z axis displacements of the stringers. These connections have $+8\frac{1}{2}$ inch and $-6\frac{1}{2}$ inch clearances for x axis displacements but only a $\pm 1/16$ inch clearance for z axis displacements. Thus, for the same reasons as in the case of the South Street Bridge deck to abutment connections, the assumption was made that z axis shear forces would be transferred from the deck to the abutment at panel point 1 in Cold Springs Canyon Bridge but that there would be no transfer of x axis axial forces or moments about the y axis at this point.

The bearing connections between the stringers and the abutment at panel point 20 are depicted in Figure 24 and were modeled as semi-fixed connections allowing rotations of the deck about the y and z axes at this point. As can be seen in Figure 24, the actual connections have 2 inch elastomeric bearing pads which allow large z axis rotations. Thus it was assumed that no moments about the z axis would be transferred from the deck to the abutment at panel point 20. In addition, these pads allow some motion of the floor stringers in the x and z directions. The system of deck laterals ends at panel point 20, however, with a pin connection at the center of the deck (see Figure 22) which prevents any x or z axis motion of the deck at this point. This pin connection does allow rotation about the y axis. Thus it was assumed that z axis shear forces and x axis axial forces would be transferred at panel point 20 but that bending moments about the y axis would not be.

The stringer to abutment connections at panel points 1 and 20 allow the transfer of compressive forces only. Here again, for the same reasons as in the case of the South Street Bridge deck to abutment connections, the assumption was made that both y axis shear forces and torsional moments about the x axis would be transferred from the deck to the abutments at panel points 1 and 20 of Cold Springs Canyon Bridge.

at the two towers located at panel points 6 and 17. At these points the deck floor stringers are connected to the towers by pins located 33 inches from and on either side of the panel points. In the models it was assumed that bending moments about the z axis would not be transferred at these points and thus moment releases were used at the ends of the deck segments connected to the towers. In order to simplify the modeling of these deck to tower connections, the deck segments ending at the towers were modeled as running to the towers rather than to points 33 inches from them.

2.3.11 Lumped Masses

The mass of Cold Springs Canyon Bridge was lumped at 40 nodal points in each model: at panel points 1 through 6 and 17 through 20, masses were lumped at the deck centroidal axis; and at panel points 7 through 16, masses were lumped at the deck centroidal axis and at the centers of the arch ribs.

All of the procedures used in lumping deck and arch masses and in calculating deck mass moments of inertia for Cold Springs Canyon

Bridge were the same procedures used for South Street Bridge. In the mass moment of inertia calculations for Cold Springs Canyon Bridge the

towers, cables and deck laterals were dealt with as follows:

- 1. The various deck masses were lumped in the vertical planes of the top tower struts as well as in the vertical planes of the deck floorbeams;
- 2. The masses of the top tower struts were lumped as linear masses in their own vertical planes;
- 3. One-fourth of the mass of each tower, excluding the top tower strut, was lumped at each end of the top tower strut;
- 4. The masses of the deck laterals and the bridge cables were neglected in the mass moment of inertia calculations.

2.4 Gravity and Wind Load Responses

The purpose of this section of the text is to describe the procedures which were used in calculating gravity and wind load responses for comparison with seismic responses. The responses chosen for these comparisons were dead load displacements, dead load stresses, live load stresses, wind load displacements and wind load stresses.

2.4.1 Dead Load Responses

The dead load displacements of both bridges were taken directly from the design drawings. The dead load stresses were calculated by applying the dead loads to the bridge models (the model with cables for Cold Springs Canyon Bridge). For the arch in each model the dead load was lumped at the mass points. For the deck in each model, however, the dead load was applied as a uniformly distributed load across each panel.

2.4.2 Live Load Stresses

In designing South Street Bridge and Cold Springs Canyon Bridge, equivalent live plus impact loads on each arch rib of 1498 lb/ft and

904 lb/ft respectively were used (6). Therefore, in calculating live load stresses, a maximum live load of 3 kips per foot of bridge was assumed for South Street Bridge and a maximum live load of 1.8 kips per foot of bridge was assumed for Cold Springs Canyon Bridge.

In calculating arch rib live load stresses, models of the South Street Bridge and Cold Springs Canyon Bridge arch ribs were utilized. The South Street Bridge arch rib model was the same as the arch ribs in the overall bridge model. The Cold Springs Canyon Bridge arch rib model, however, was a simplified version of the arch ribs in the overall models with only 11 panel segments as opposed to 44 subpanel segments.

Utilizing the maximum live loads assumed above, maximum column loads at each panel point were calculated. The estimated maximum live load stress in each arch rib element was then based on the worst combination of these maximum column live loads. As an example, for panel CD in South Street Bridge the largest live load stress occurs when maximum column live loads are placed at panel points F,F',E' and D'. Thus, this is the stress which was taken to be the estimated maximum live load stress in panel CD of South Street Bridge.

Deck live load stresses were calculated by applying the full live loads to the bridge models (the model with cables for Cold Springs Canyon Bridge). For each bridge the live load was applied as a uniformly distributed load across the full length of the deck. The results of these deck live load analyses should be regarded as estimates only, because partial deck loading was not considered.

2.4.3 Wind Load Responses

An assumed maximum wind load pressure of 75 pounds per square foot was applied to each bridge profile in the z direction. The resulting z direction loads were then applied to the bridge models (the model with cables for Cold Springs Canyon Bridge) thus yielding estimated values for maximum wind load stresses and displacements.

2.5 Natural Frequencies and Mode Shapes

2.5.1 General Comments

The first 36 natural frequencies and mode shapes for the South Street Bridge model and the first 26 natural frequencies and mode shapes for each of the Cold Springs Canyon Bridge models were calculated and are presented in this section. All of the mode shapes obtained can be categorized in one of two groups. The modes in the first group are characterized by z axis displacements and/or x axis rotations and thus represent out-of-plane or space motion. The modes in the second group represent in-plane motion and are characterized by x axis displacements and/or y axis displacements. In presenting the mode shapes for each bridge model, two tables are used - one for each group of mode shapes. These tables, in addition to listing the modes, also list the period of vibration for each mode along with descriptions of the primary displacements or rotations.

Those figures containing the plots of out-of-plane modes each show the x, y and z axis displacement of the deck and each arch rib. In these figures, the top two plots are for the x and y displacements of the deck and the arch ribs, while the bottom two plots represent the z displacements of the deck and the arch ribs. Because the displacements of the deck are plotted for the centroidal axis only, any

x axis rotations of the deck are not depicted in these figures. The x axis deck rotations are noted, however, in the tabular listings of the mode shapes. For the section of the deck above the arch ribs (panel points C to C' in South Street Bridge and panel points 6 to 17 in Cold Springs Canyon Bridge), the x axis deck rotations are virtually the same as the x axis rotations of the arch as a whole. The latter rotations can be seen by comparing the displacements of the east arch rib (e) and the west arch rib (w). Large x axis deck rotations for the approach spans of South Street Bridge (panel points 0 to C and C' to O') are noted in the figures as well as in the tables.

The figures which contain the plots of those mode shapes characterized by x axis and/or y axis displacements each show the x and y displacements of the deck and the arch ribs. Because the displacements of both arch ribs at each panel point are identical in these mode shapes, there is only one curve representing arch rib displacements in each figure.

Note that in all of the mode shape figures the deck and the arch ribs are not drawn to scale.

2.5.2 South Street Bridge Mode Shapes

Figures 25 to 60 represent the first 36 modes of vibration for the South Street Bridge model. Table 1 lists the 22 out-of-plane modes while Table 2 lists the 14 in-plane modes.

The first five modes can be described as follows. The fundamental mode (period = 1.565 seconds) consists mainly of a longitudinal translation of the south half of the deck. The second mode (period = 1.124 seconds) consists mainly of a longitudinal translation of the north half of the deck. The third mode (period = 0.6206 seconds) represents

a single in-plane wave with both deck and arch in phase. The fourth mode (period = 0.6125 seconds) consists of an out-of-plane half wave translation in the z direction accompanied by a $1\frac{1}{2}$ wave longitudinal rotation. The fifth mode (period = 0.3920 seconds) represents an out-of-plane full wave translation in the z direction accompanied by a full wave longitudinal rotation.

2.5.3 Cold Springs Canyon Bridge Mode Shapes With Cables

Figures 61 to 86 represent the first 26 modes of vibration for the Cold Springs Canyon Bridge model with cables. Table 3 lists the 18 out-of-plane modes while Table 4 lists the 8 in-plane modes.

Because one end of the deck is pinned, the lower modes of both Cold Springs Canyon Bridge models are not characterized by longitudinal deck translation (in contrast to South Street Bridge which has no direct longitudinal deck restraints). The fundamental mode (period = 2.732 seconds) represents an out-of-plane half wave translation in the z direction (analogous to mode 4 of South Street Bridge). The second mode (period = 2.117 seconds) consists of a single in-plane wave (analogous to mode 3 of South Street Bridge). The third mode (period = 1.561 seconds) represents an out-of-plane full wave translation of the deck in the z direction (similar to mode 5 of South Street Bridge). The fourth mode (period = 1.182 seconds) consists of an out-of-plane 1½ wave translation of the deck in the z direction (similar to mode 7 of South Street Bridge). The fifth mode (period = 1.167 seconds) represents an in-plane 1½ wave translation (analogous to mode 6 of South Street Bridge).

2.5.4 Cold Springs Canyon Bridge Mode Shapes Without Cables

Figures 87 to 112 represent the first 26 modes of vibration for the Cold Springs Canyon Bridge model without cables. Table 5 lists the 18 out-of-plane modes while Table 6 lists the 8 in-plane modes.

Because of the absence of the cables which tie the deck to the arch ribs, the fundamental mode (period = 3.535 seconds) consists of an out-of plane half wave translation in the z direction which involves only the deck. The second mode (period = 2.469 seconds) represents a single in-plane wave (analogous to mode 3 of South Street Bridge). The third mode (period = 1.854 seconds) consists of an out-of-plane half wave translation of the arch in the z direction. The fourth mode (period = 1.603 seconds) represents an out-of-plane full wave translation of the deck in the z direction (similar to mode 5 of South Street Bridge). The fifth mode (period = 1.167 seconds) represents an in-plane 1½ wave translation (analogous to mode 6 of South Street Bridge).

CHAPTER III

RESPONSE SPECTRUM ANALYSES

This chapter discusses the assumptions and calculations made in and the results of the response spectrum analyses which were conducted on the two bridges. In the first section of this chapter, the method of analysis and the response spectra which were chosen for use in the response spectrum analyses are discussed along with the definitions of frequently used terms and abbreviations. The second through fifth parts of this chapter present and discuss the following types of maximum responses: arch rib stresses, arch rib displacements, deck stresses and deck displacements. In sections two through five, specific arch rib and deck stresses and displacements are discussed in terms of where and under which direction of maximum ground acceleration they reach their largest values, how these largest values compare with gravity and/or wind load responses, why these largest response values occur where they do and why they may differ between the two bridges.

Part six of this chapter discusses the responses of other items in the South Street Bridge and Cold Springs Canyon Bridge models, namely, deck expansion joints, arch rib hinges, column to floorbeam connections, column base connections and bridge cables. Sections seven, eight and nine discuss how the results may have been affected by the following: the lumping of the deck masses at panel points only,

the neglecting of stringer bending resistance in the calculations of deck torsion constants and the assumption that only 50% of the deck concrete slab cross-sectional area would be acting at any given time.

3.1 General Notes

3.1.1 Method of Analysis

A complete time-history "load-displacement" dynamic analysis is usually quite expensive to perform. As an alternative, the response spectrum method, which is well known (8), has the attractive feature of lower computation cost. It consists of choosing a response spectrum which indicates the maximum response corresponding to a given normal mode and natural frequency. One issue with the method is how the maximum responses for the different normal modes should be combined to produce a "representative" maximum response.

The following formula was chosen for combining the various modal responses to a given spectrum:

$$R = \left(\sum_{k=1}^{N} R_{k}^{2} + 2\sum_{k=1}^{N} R_{j}^{2}\right)^{\frac{1}{2}}$$

where:

R = representative maximum value of a particular response;

R_k = peak value of the particular response due to the kth mode;

N = total number of modes;

R_j & R_j = peak value of the particular response due to the ith and jth modes, respectively;

i & j = all pairs of modes such that $(F_j - F_i)/F_i = 0.1$ and 1 = i < j = N:

 F_i & F_j = frequencies of vibration of the ith and jth modes, respectively.

This formula is taken from the Nuclear Regulatory Commission (NRC) Regulatory Guide 1.92, page 3, section 1.2.2 entitled "Ten Percent Method" (9).

The first summation in the formula is the well known square root of the sum of the squares (SRSS) of the modal responses. The second summation is used only for those pairs of modes with frequencies of vibration within 10% of one another and is the cross-product term of the square of the sum of the two modal responses R_i and R_i .

Because closely spaced modes tend to be additive rather than independent and because many of the modes of the two bridges considered here are closely spaced, it was felt that the Ten Percent Method would be an appropriate procedure to use.

As discussed in section 2.3.6, SAPV2 output for response spectrum analyses consists of maximum nodal displacements and maximum element forces and moments. It does not include maximum combined axial and bending stresses, however. Thus, in order to obtain some estimates of combined stresses, it was necessary to find ways of combining maximum axial stresses and maximum bending stresses. The two methods used were the SRSS of these maximum stresses and the summation of these maximum stresses.

3.1.2 Response Spectra

The response spectra chosen for use in the response spectrum analyses were the Normalized Rock Spectra depicted in Figure 113 and

¹ Note that since these maximum stresses are SRSS values themselves, they are always positive.

taken from the report by Gates (10). These spectra are based on accelerograms from five California sites. Three of these accelerograms correspond to the San Fernando Earthquake of 1971, one to the Parkfield Earthquake of 1966 and one to the San Francisco Earthquake of 1957. In deriving the Normalized Rock Spectra, each accelerogram response spectrum for 36 damping was first normalized and then all five were averaged and smoothed for three ranges of maximum ground acceleration: 0.00g to 0.15g, 0.15g to 0.30g and 0.30g to 0.70g.

The Normalized Rock Spectra are the basis for AASHTO's Response Coefficient "C" Curves, figure 1.2.20A, page 29 of the AASHTO Specifications (7). The AASHTO Specifications state that these Response Coefficient "C" Curves can be used as design response spectra. In deriving the AASHTO curves, the Normalized Rock Spectra were first smoothed to remove the abrupt changes in slope at periods of 0.20, 0.41, 0.51 and 0.60 seconds. These "smoother" versions of the Normalized Rock Spectra were then reduced by factors of 4 for ductility and 1 to 2 for risk. Thus the AASHTO curves are about 4 to 8 times lower than the Normalized Rock Spectra.

The paper by Imbsen, Nutt and Penzien (11) states that "the response spectra currently used in the AASHTO Specifications should be revised so as not to include the reduction for ductility" and that "ductility reductions should be made on an individual component basis". In addition, the reductions for risk, which vary with the period of vibration, are meant for modifying the coefficient "C" in the equivalent static force method of earthquake analysis and are not necessarily meant for application to each mode shape in a response spectrum analysis. Therefore, the decision was made to use the Normalized Rock

Spectra with no modifications for ductility or risk and with no additional smoothing.

Two additional notes should also be mentioned at this time.

First, the final component results in this study were not reduced by factors for ductility because it was felt that any consideration of the complex topic of ductility would be beyond the scope of this study. Second, the abutments, skewbacks and column piers in South Street Bridge and Cold Springs Canyon Bridge were all assumed to rest on or within ten feet of bedrock and thus no soil amplification factors were applied to the Normalized Rock Spectra.

The Normalized Rock Spectra are similar to the NRC's Horizontal and Vertical Design Response Spectra for % damping depicted in Figure 114 (12). The NRC spectra were considered for use in this study, but because they are similar to the Normalized Rock Spectra, the decision was made to use only the latter. Therefore, all remaining uses of the words "normalized spectra" in this study will refer to the Normalized Rock Spectra.

Input spectra for maximum ground accelerations of 0.09g and 0.30g were applied to the South Street Bridge model in the x, y and z directions. Input spectra for maximum ground accelerations of 0.30g and 0.50g were applied to the Cold Springs Canyon Bridge model in the x, y and z directions. A maximum ground acceleration of 0.09g was chosen for South Street Bridge because, as discussed earlier, this is the AASHTO Zone I maximum ground acceleration which is specified for the bridge site. In order to provide a common acceleration level for comparisons between the two bridges, a maximum ground acceleration of 0.30g was used for both bridges. A maximum ground acceleration of

0.50g was chosen for Cold Springs Canyon Bridge because this is the acceleration specified by AASHTO for the bridge site.

It should be noted that the input spectra for these three different maximum ground accelerations (0.09g, 0.30g and 0.50g) were derived from the three different normalized spectra depicted in Figure 113. The input spectrum for a maximum ground acceleration, A, of 0.09g was derived from the normalized spectrum for A = 0.00g to 0.15g. The input spectrum for A = 0.30g was derived from the normalized spectrum for A = 0.15g to 0.30g. Finally, the input spectrum for A = 0.50g was derived from the normalized spectrum for A = 0.30g to 0.70g. While the input spectrum for A = 0.30g could have been derived from the normalized spectrum for A = 0.30g to 0.70g, because this spectrum is less than or equal to the one for A = 0.15g to 0.30g, the latter was chosen in order to be conservative.

If input spectra for several values of A from 0.00g to 0.70g were derived and then used to calculate bridge responses versus A, the results would be discontinuous at A = 0.15g and 0.30g because the normalized spectra change at these points. But since only the input spectra for A = 0.09g, 0.30g and 0.50g were derived and since the calculated bridge responses to these spectra are only approximate, it was felt that the use of straight line interpolation between these calculated values would provide reasonable estimates of the responses for intermediate values of A. Thus the curves of maximum stress or displacement versus A, which are presented in sections 3.3 to 3.6, were plotted using straight line segments between the responses at A = 0.00g, 0.09g and 0.30g for South Street Bridge, and A = 0.00g, 0.30g and 0.50g for Cold Springs Canyon Bridge.

3.1.3 Definitions

In the course of the following discussions many terms and phrases are used quite frequently. For the sake of brevity the following shortened versions of these terms or phrases will be used:

- 1. "SSB" will refer to South Street Bridge;
- 2. "CSCB" will refer to Cold Springs Canyon Bridge;
- 3. "Stress" or "displacement" unless otherwise specified will refer to representative maximum seismic stress or displacement, respectively, as calculated by response spectrum analyses;
- 4. "Acceleration" or "A" unless otherwise specified will refer to maximum ground acceleration;
- 5. "Vertical bending" will refer to deck bending arising out of y axis displacements of the deck;
- 6. "Lateral bending" will refer to deck bending arising out of z axis displacements of the deck;
- 7. "Minor axis bending" will refer to arch rib bending in the weaker direction:
- 8. "Major axis bending" will refer to arch rib bending in the stronger direction;
- 9. "SRSS" will refer to square root of the sum of the squares;
- 10. "Reserve strength after dead load" will refer to the strength remaining in a deck, arch rib or other element after the estimated dead load stress in the element is subtracted from the yield stress of 33 ksi;
- 11. "Reserve strength after dead plus live load" will refer to the strength remaining in a deck, arch rib or other element

after the estimated dead and live load stresses in the element are subtracted from the yield stress of 33 ksi.

3.2 Arch Rib Stresses

Figures 115 to 120 are plots of arch rib stresses versus acceleration for SSB and CSCB. These figures include plots of the following arch rib stresses where applicable:

- Axial stress (f₁);
- 2. Minor axis bending stress (f₂);
- Major axis bending stress (f₃);
- 4. Combined stress by SRSS (f_{srss});
- 5. Combined stress by summation (f_{sum}).

The figures also include the following where applicable:

- Yield stress (f_v);
- 2. Yield stress minus dead load stress (f_y f_d) or reserve strength after dead load;
- 3. Yield stress minus dead load stress minus one-half live load stress ($f_v f_d f_1/2$);
- 4. Yield stress minus dead load stress minus live load stress $(f_y f_d f_l)$ or reserve strength after dead plus live loads;
- Wind load stress (f_y).

Figures 115, 116 and 117 each contain plots of arch rib stresses versus acceleration for the SSB arch rib element deemed to be the most critical under x, y and z axis acceleration, respectively. Similar plots for CSCB arch rib elements are contained in Figures 118, 119 and 120.

In deriving the figures, all arch rib elements in the SSB model

were checked and compared, and the following arch rib subpanel elements were checked and compared for both CSCB models: 6c-7, 7c-8, 8c-9, 9c-10, 10c-11, 12c-13, 13c-14, 14c-15, 15c-16 and 16c-17. While stresses in these arch rib elements were calculated for both CSCB models, because the values in the model with cables were larger than the corresponding values in the model without cables, all the results depicted in Figures 118, 119 and 120 represent arch rib stresses for the CSCB model with cables.

Note that in Figures 115 to 120 and in the plots of other bridge responses versus acceleration contained in sections 3.3, 3.4 and 3.5, any underlined response represents the largest calculated value of that response for the specified bridge in the specified direction of acceleration.

3.2.1 Axial Stresses

In the SSB model the largest arch rib axial stresses occur in elements CD under z axis acceleration. These stresses, under accelerations of 0.09g, reach 2.45 ksi which is only 8.8% of the elements' reserve strength after dead load and only 11% of the elements' reserve strength after dead plus live loads (see Figure 117).

The arch rib axial stresses reach their largest values in the CSCB model with cables in elements 16c-17 under y axis acceleration. At accelerations of 0.50g, these values reach 10.8 ksi which is 46% of the elements' reserve strength after dead load and 54% of the elements' reserve strength after dead loads.

For both bridges the largest axial stresses in the arch ribs occur near an abutment. The axial stresses in the two arch ribs of SSB are large under z axis acceleration because they act as a couple

and provide moment resistance against lateral displacements of the bridge. If one assumes that under z axis acceleration the arch as a whole will act in a manner similar to a uniformly loaded fixed-ended beam, then one would expect the moment in the arch to be largest near the abutments and hence the axial stresses to be largest near the abutments. For CSCB, the axial stresses in the arch ribs are large under y axis acceleration because arch bridges are designed to resist vertical loads by converting them into arch rib axial forces.

The deck and arch ribs in SSB and CSCB tend to act as a unit under y axis acceleration, and under z axis acceleration the deck and the arch ribs in SSB also tend to act as a unit. In CSCB under z axis acceleration, however, the deck and the arch ribs are more independent because between panel points 6 and 17 they are connected only by the lateral cables at panel points 11 and 12. Since there is less transfer of stresses from the deck to the arch ribs under z axis acceleration in CSCB, the axial stresses in the arch ribs due to z axis acceleration are less than those due to y axis acceleration. But in SSB where there is greater transfer of stresses from the deck to the arch ribs under z axis acceleration, the axial stresses due to z axis acceleration are larger than those due to y axis acceleration.

3.2.2 Major Axis Bending Stresses

The largest arch rib major axis bending stresses in the SSB model occur in elements DE under x axis acceleration. With accelerations of 0.0%, these bending stresses reach 2.21 ksi which is only 7.8% of the elements' reserve strength after dead load and only 11% of the elements' reserve strength after dead plus live loads (see Figure 115).

In the CSCB model with cables, the arch rib major axis bending

stresses reach their largest values in elements 15c-16 under x axis acceleration. These bending stresses, under accelerations of 0.50g, reach 14.3 ksi which is 60% of the elements' reserve strength after dead load and 10% greater than the elements' reserve strength after dead plus live loads (see Figure 118).

In the SSB model under x axis acceleration, large arch rib major axis bending stresses occur in elements E'D' as well as elements DE. One way of explaining this is to assume that the response of the arch ribs to x axis acceleration is analogous to the static response of the single SSB arch rib depicted in Figure 121 to its own weight applied in the positive x rather than the negative y direction. As can be seen in the figure, the moment in the arch rib under this loading is largest at the quarter points much the same as the arch rib major axis bending stresses in the SSB model under x axis acceleration.

For the CSCB model with cables under x axis acceleration, large arch rib major axis bending stresses occur in elements 6c-7, 9c-10 and 12c-13 as well as elements 15c-16. For the model without cables, the distribution of arch rib major axis bending stresses follows very closely the distribution of moments for the single SSB arch rib depicted in Figure 121. Thus, the unusual distribution of arch rib major axis bending stresses in the CSCB model with cables under x axis acceleration can be attributed to the influence of the longitudinal cables.

That the largest arch rib major axis bending stresses do not occur under y axis (vertical) acceleration can best be explained by the uniformity of the vertical load which arises from the uniform y axis acceleration of all bridge supports. Uniform vertical loads can be efficiently resisted by arch rib compression (or tension) with minimal

bending. Horizontal loads however, such as those due to x axis acceleration, can only be resisted by combined compression (or tension) and bending of the arch ribs.

3.2.3 Minor Axis Bending Stresses

In the SSB model the largest arch rib minor axis bending stresses occur in elements CD under z axis acceleration. These bending stresses, at accelerations of 0.09g, reach 2.63 ksi which is only 9.4% of the elements' reserve strength after dead load and only 12% of the elements' reserve strength after dead plus live loads, but is 8.0% greater than the elements' wind load stress (see Figure 117).

The arch rib minor axis bending stresses reach their largest values for the CSCB model with cables in elements 6c-7 under z axis acceleration. With accelerations of 0.50g, these bending stresses reach 11.7 ksi which is 48% of the elements' reserve strength after dead load, 87% of the elements' reserve strength after dead plus live loads and 82% of the elements' wind load stress (see Figure 120).

For both bridges the largest minor axis bending stresses occur near arch abutments under z axis acceleration. Arch rib minor axis bending stresses occur only under z axis acceleration. If one assumes that under z axis acceleration the arch ribs act in a manner similar to a uniformly loaded fixed-ended beam, then one would expect the minor axis bending stresses in the arch ribs to be largest at or near the arch abutments.

3.2.4 Combined Stresses

The largest arch rib combined stresses by SRSS and by summation in the SSB model occur in elements CD under z axis acceleration. At accelerations of 0.0%, these combined stresses by summation reach

6.96 ksi which is 25% of the elements' reserve strength after dead load and 35% of the elements' reserve strength after dead plus live loads, but is more than 2.8 times the elements' wind load stress (see Figure 117).

In the CSCB model with cables, the arch rib combined stresses by SRSS and by summation reach their largest values in elements 6c-7 under z axis acceleration. These combined stresses by summation, under accelerations of 0.50g, reach 20.2 ksi which is 83% of the elements reserve strength after dead load, 50% greater than the elements reserve strength after dead plus live loads and 42% greater than the elements wind load stress (see Figure 120).

3.3 Arch Rib Displacements

Figures 122 to 133 are plots of arch rib displacements for the SSB and CSCB models. These figures include plots of x displacements (Δx) , y displacements (Δy) and z displacements (Δz) due to seismic effects. These figures also include the following where applicable:

- 1. Dead load displacements (Δy_d) ;
- 2. Wind load displacements $(\Delta x_w \text{ and } \Delta z_w)$;
- 3. Dead load plus wind load displacements (Δy_{d+w}) .

Figures 122, 123 and 124 contain plots of SSB arch rib displacements at panel points C to C' under accelerations of 0.09g in the x, y and z directions, respectively. Similar plots for the CSCB arch ribs at panel points 6 to 17 under accelerations of 0.50g are depicted in Figures 125, 126 and 127.

Figures 128, 129 and 130 each contain plots of arch rib displacements versus acceleration for the two SSB arch rib nodal points deemed to be the most critical under x, y and z axis acceleration. Similar

plots for CSCB arch rib nodes are depicted in Figures 131, 132 and 133.

In deriving Figures 122 to 133, all arch rib panel point nodes were checked and compared in the SSB model and in the CSCB models. As in the case of arch rib stresses, arch rib displacements were larger in the CSCB model with cables rather than in the model without cables. Thus the results in Figures 125 to 127 and Figures 131 to 133 represent the arch rib displacements for the CSCB model with cables.

3.3.1 X Axis Displacements

In the SSB model the largest x axis displacements of the arch ribs occur at panel point E under x axis acceleration. With accelerations of 0.09g, these x axis displacements reach 0.019 feet (see Figures 122 and 128).

The arch rib x axis displacements reach their largest value in the CSCB model with cables at panel point 15 under x axis acceleration. These x axis displacements, at accelerations of 0.50g, reach 0.27 feet (see Figures 125 and 131).

For both bridges the largest x axis displacements of the arch ribs occur near quarter points under x axis acceleration. One way of explaining this phenomenon is to assume, as was done in the case of the SSB arch rib major axis bending stresses, that the responses of the arch ribs to x axis acceleration are analogous to the static responses of the SSB arch rib depicted in Figure 121 to its own self weight applied in the positive x rather than the negative y direction. As can be seen in Figure 121, the x axis displacements of the arch rib are largest under this loading at the quarter points much the same as the x axis displacements of the arch ribs in the SSB and CSCB models under x axis acceleration.

3.3.2 Y Axis Displacements

The largest arch rib y axis displacements in the SSB model occur at panel point E under x axis acceleration. At accelerations of 0.09g, these y axis displacements reach 0.037 feet which is 48% greater than the arch rib dead load displacements at panel point E (see Figures 122 and 128).

In the CSCB model with cables, the y axis displacements of the arch ribs reach their largest values at panel point 10 under x axis acceleration. These y axis displacements, under accelerations of 0.50g, reach 0.45 feet which is more than 3.0 times the arch rib dead load displacements at panel point 10 (see Figures 125 and 131).

As in the case of x axis arch rib displacements, the y axis arch rib displacements in both bridges are largest near quarter points under x axis acceleration. One way of explaining this is to once again assume, as was done in the case of the SSB arch rib major axis bending stresses, that the responses of the arch ribs to x axis acceleration are analogous to the static responses of the SSB arch rib depicted in Figure 121 to its own weight applied in the positive x direction rather than the negative y direction. As can be seen in the figure, the y axis displacements of the arch rib under this loading are largest at the quarter points much the same as the y axis displacements of the SSB and CSCB arch ribs under x axis acceleration.

3.3.3 Z Axis Displacements

In the SSB model the largest arch rib z axis displacements occur at panel point F under z axis acceleration. These z axis displacements, at accelerations of 0.09g, reach 0.081 feet which is more than 2.3 times the arch rib wind load displacements at panel point F (see

Figures 124 and 130).

The arch rib z axis displacements reach their largest values in the CSCB model with cables at panel point 12 under z axis acceleration. With accelerations of 0.50g, these z axis displacements reach 1.49 feet which is 53% larger than the arch rib wind load displacements at panel point 12 (see Figures 127 and 133).

The largest z axis displacements of the arch ribs in both bridges occur near the middle of the arch ribs under z axis acceleration. If one assumes that the responses of the arch ribs to z axis acceleration are comparable to the responses of a fixed ended beam under uniform loading, then one would expect the z axis displacements of the arch ribs under z axis acceleration to be largest near midspan.

3.4 Deck Stresses

Figures 134 to 139 are plots of deck stresses versus acceleration for SSB and CSCB. These figures include plots of the following deck stresses where applicable:

- Axial stress (f₁);
- 2. Lateral bending stress in the concrete slab (f_{c2}) ;
- Vertical bending stress (f₃);
- 4. Combined axial and vertical bending stress by SRSS (f_{srss});
- 5. Combined axial and vertical bending stress by summation (f_{sum}).

All of the stresses listed above represent stresses in the stringers except for lateral bending stress which represents stress in the concrete slab. The concrete slab lateral bending stresses were calculated by taking the lateral bending stresses of the deck beam elements and dividing by the modular ratio "n". In order to distinguish

between steel and concrete stresses, a postscript "c" was added to the symbol for lateral bending stress.

Figures 134 to 139 also include the following where applicable:

- Yield stress for steel (f_y);
- 2. Allowable stress for concrete (fca);
- 3. Yield stress minus dead load stress for steel (f_y f_d) or reserve strength after dead load;
- 4. Yield stress minus dead load stress minus one-half live load stress for steel $(f_y f_d f_1/2)$;
- 5. Yield stress minus dead load stress minus live load stress for steel (f_y f_d f₁) or reserve strength after dead plus live loads;
- 6. Wind load stress for concrete (f_{cw}).

Figures 134, 135 and 136 each contain plots of deck stresses versus acceleration for the SSB deck element deemed to be the most critical under x, y and z axis acceleration, respectively. Similar plots for the CSCB deck elements are depicted in Figures 137, 138 and 139.

Analysis of the CSCB model with cables showed that at accelerations of 0.333g in the x direction and 0.316g in the z direction, the longitudinal and lateral cables respectively might reach their minimum breaking strengths. Because none of the cables reach their minimum breaking strengths under y axis accelerations of 0.50g or less, the results depicted in Figure 138 represent deck stresses in element 15-16 for the CSCB model with cables.

Comparisons of the CSCB models with and without cables show that under x axis acceleration some elements exhibit greater axial stresses

if the cables are removed but that vertical bending stresses in all elements decrease if the cables are removed. The net result is that the combined axial and vertical bending stresses are larger for the model with cables as opposed to the model without cables. Thus the results in Figure 137 represent deck stresses in element 15-16 for the CSCB model with cables.

Comparisons of the CSCB models with and without cables also show that under z axis acceleration most deck elements exhibit increases in lateral bending stresses if the cables are removed. The bending stresses in element 10-11 for both CSCB models are plotted in Figure 139. The solid curve labelled " f_{c2} " and plotted from 0.00g to 0.50g represents the stress in the model with cables. The dashed line labelled " f_{c2} " and plotted from 0.331g to 0.50g represents the stress in the model without cables. In addition, a dashed transition curve is drawn from the lateral bending stress at 0.316g for the model without cables to the lateral bending stress at 0.331g for the model without cables. Note that 0.316g and 0.331g are the z axis accelerations at which the first and last longitudinal cables, respectively, reach their minimum breaking strengths.

3.4.1 Axial Stresses

The largest deck axial stresses in the SSB model occur in element E'D' under x axis acceleration. At accelerations of 0.09g, these axial stresses reach 0.10 ksi which is only 0.38% of the element's reserve strength after dead load and only 0.44% of the element's reserve strength after dead plus live loads.

In the CSCB model without cables the deck axial stresses reach their largest values in element 19-20 under x axis acceleration. These axial stresses, under accelerations of 0.50g, reach 15.8 ksi which is 57% of the element's reserve strength after dead load and 61% of the element's reserve strength after dead plus live loads.

Because the SSB deck is unrestrained with respect to x axis displacements at the deck abutments and is discontinuous with respect to x axis displacements at panel points F and F', the north and south sections of the deck (panel points F' to 0' and 0 to F) tend to act as rigid bodies with respect to x axis displacements. Thus there is very little differential displacement within each SSB deck section and hence very little axial stress.

In CSCB the deck is restrained with respect to x axis displacements at the deck abutment at panel point 20, but is unrestrained with respect to x axis displacements at the deck abutment at panel point 1. In addition, the deck is continuous with respect to x axis displacements between panel points 1 and 20. Thus, any x axis displacements of the deck (relative to panel point 20) require axial deformation of the deck. Since panel point 20 is the point where x axis displacements of the deck are prevented, one might expect the largest axial stress under x axis acceleration to occur in element 19-20.

3.4.2 Vertical Bending Stresses

In the SSB model the largest vertical deck bending stresses occur in element DE under x axis acceleration. These bending stresses, at accelerations of 0.09g, reach 4.00 ksi which is only 15% of the element's reserve strength after dead load and only 18% of the element's reserve strength after dead plus live loads (see Figure 134).

The vertical bending stresses in the deck reach their largest values for the CSCB model with cables in element 15-16 under x axis

acceleration. With accelerations of 0.50g, these bending stresses reach 12.7 ksi which is 52% of the element's reserve strength after dead load and 60% of the element's reserve strength after dead plus live loads (see Figure 137).

For both bridges the largest vertical bending stress in the deck occurs above an arch rib quarter point under x axis acceleration. In SSB and CSCB, as discussed in section 3.2.1, the deck and the arch ribs tend to act as a unit with respect to vertical motion. Thus, since the largest arch rib major axis bending stresses occur between panel points D and E in SSB and between subpanel point 15c and panel point 16 in CSCB, one might expect the largest vertical bending stresses in the decks to occur at the corresponding locations.

3.4.3 Lateral Bending Stresses

The largest lateral bending stresses in the deck concrete slab of the SSB model occur in element CD under z axis acceleration. At accelerations of 0.09g, these bending stresses reach 98 psi which is only 7.3% of the allowable concrete stress of 1350 psi (assuming an ultimate concrete stress of 3000 psi), but is over 2.3 times the element's wind load stress (see Figure 136).

In the CSCB model without cables the lateral bending stresses of the deck concrete slab reach their largest values in element 10-11 under z axis acceleration. These bending stresses, under accelerations of 0.50g, reach 1089 psi which is 91% of the allowable concrete stress of 1200 psi (as specified in the design drawings), but is over 3.1 times the element's wind load stress (see Figure 139).

For both bridges the only direction of acceleration which gives rise to lateral deck bending stresses is the z direction. If one

assumes that the responses of the bridge decks to z axis acceleration are analogous to the responses of the decks to wind loads, then because the wind load stresses in the SSB deck are largest at panel point C, one would expect the lateral deck bending stresses in SSB under z axis acceleration to be largest in elements BC or CD.

For the CSCB model without cables this wind load analysis comparison is not applicable because the CSCB model with cables was used to calculate the wind load responses. If one assumes, however, that the responses of the CSCB deck to z axis acceleration are analogous to the responses of a simply supported beam to uniform loading, then one would expect the lateral deck bending stresses to be largest in element 10-11.

3.4.4 Combined Stresses

In the SSB model the largest combined deck stresses by SRSS or by summation occur in element DE under x axis acceleration. These combined stresses by summation, at accelerations of 0.09g, reach 4.09 ksi which is only 15% of the element's reserve strength after dead load and only 18% of the element's reserve strength after dead plus live loads (see Figure 134).

The combined deck stresses by SRSS and by summation reach their largest values for the CSCB model with cables in element 15-16 under x axis acceleration. With accelerations of 0.50g, these combined stresses by summation reach 24.8 ksi which is 1.4% greater than the element's reserve strength after dead load and 16% greater than the element's reserve strength after dead plus live loads (see Figure 137).

3.5 Deck Displacements

Figures 140 to 151 are plots of deck centroidal axis displacements for the SSB and CSCB models. These figures include plots of x displacements (Δx), y displacements (Δy) and z displacements (Δz) due to seismic effects. They also include dead load displacements (Δy) and wind load displacements (Δz) where applicable.

Figures 140, 141 and 142 contain plots of SSB deck centroidal axis displacements at all panel points under accelerations of 0.09g in the x, y and z directions, respectively. Similar plots for the CSCB deck under accelerations of 0.50g are contained in Figures 143, 144 and 145.

Figures 146, 147 and 148 each contain plots of deck centroidal axis displacements versus acceleration for the two SSB deck nodes deemed to be the most critical under x, y and z axis acceleration, respectively. Similar plots for CSCB deck nodes are depicted in Figures 149, 150 and 151.

As discussed with respect to deck stresses, none of the cables in CSCB reach their minimum breaking strengths under y axis accelerations of 0.50g or less. Thus the results depicted in Figures 144 and 150 represent deck centroidal axis displacements for the CSCB model with cables.

Comparisons of the CSCB models with and without cables show that under x axis acceleration the x axis displacements of the deck will increase if the cables are removed but that the y axis displacements will decrease. The results in Figures 143 and 149 depict two curves for x axis displacement but only one curve for y axis displacement. The solid curves labelled Δx and Δy which are plotted from 0.00g to

0.50g in Figure 149 represent the x and y displacements, respectively, of the model with cables. The dashed curves labelled $\Delta x'$ which are plotted from 0.333g to 0.50g in Figure 149 represent the x axis displacements of the model without cables. As was stated in the discussion of deck stresses, 0.333g is the x axis acceleration at which the longitudinal cables in the model with cables may reach their minimum breaking strengths.

Comparisons of the CSCB models with and without cables also show that under z axis acceleration the deck z axis displacements increase if the cables are removed. The z axis deck centroidal axis displacements are plotted for both models in Figures 145 and 151. The solid curves labelled Δz which are plotted from 0.00g to 0.50g in Figure 151 represent the z axis displacements of the model with cables. The dashed curves labelled Δz which are plotted from 0.331g to 0.50g in Figure 151 represent the z axis displacements of the model without cables. A dashed transition curve is also depicted in Figure 151 between 0.316g and 0.331g, the previously mentioned critical acceleration levels for the lateral cables.

3.5.1 X Axis Displacements

The largest x axis deck displacements in the SSB model occur in the segment from panel points 0 to F under x axis acceleration. At accelerations of 0.09g, these x axis displacements reach 0.205 feet (see Figures 140 and 146).

In the CSCB model without cables the x axis deck displacements reach their largest values at panel point 1 under x axis acceleration. These x axis displacements, under accelerations of 0.50g, reach 0.40 feet (see Figures 143 and 149).

As discussed earlier with respect to deck axial stress, the north and south sections of the SSB deck tend to act as rigid bodies with respect to x axis displacements. Thus, at any given time there are basically only two values for x axis displacement of the deck: one for the south section and one for the north section. Since the columns at panel points B, C and D which resist x axis displacements of the south section of the deck are longer and thus more flexible than the columns at panel points D', C' and B' which resist x axis displacements of the north section of the deck, the larger x axis displacement of the deck under x axis acceleration occurs in the south section.

Also as discussed earlier with respect to axial stress, in CSCB the x axis displacements of the deck depend on axial elastic deformation between the free end at panel point 1 and the pinned end at panel point 20. Thus, under x axis acceleration, the largest x axis deck displacement occurs at panel point 1.

3.5.2 Y Axis Displacements

In the SSB model the largest y axis deck displacements occur at panel point E under x axis acceleration. These y axis displacements, at accelerations of 0.09g, reach 0.037 feet which is 48% greater than the dead load displacements at panel point E (see Figures 140 and 146).

The y axis deck displacements reach their largest values in the CSCB model with cables at panel point 10 under x axis acceleration. With accelerations of 0.50g, these y axis displacements reach 0.45 feet which is more than 3.0 times the dead load displacement at panel point 10 (see Figures 143 and 149).

For both bridges the largest y axis deck displacement occurs above an arch rib quarter point under x axis acceleration. As

discussed earlier with respect to vertical deck bending stress, the deck and the arch ribs in SSB and CSCB tend to act as a unit with respect to vertical displacements. Thus, since the y axis displacements of the arch ribs are largest at panel point E in SSB and panel point 10 in CSCB both under x axis acceleration, so too are the y axis displacements of the decks largest at these points under x axis acceleration.

3.5.3 Z Axis Displacements

The largest z axis displacements of the deck in the SSB model occur at panel point F under z axis acceleration. At accelerations of 0.09g, these z axis displacements reach 0.095 feet which is more than 2.5 times the wind load displacement of the deck at panel point F (see Figures 142 and 148).

In the CSCB model without cables the z axis deck displacements reach their largest values at panel points 11 and 12 under z axis acceleration. These z axis displacements, under accelerations of 0.50g, reach 2.20 feet which is 91% greater than the deck wind load displacements at panel points 11 and 12 (see Figures 145 and 151).

The largest z axis deck displacements for both bridges occur above the middle of the arch ribs under z axis acceleration. Utilizing the simply supported beam analogy which was discussed under the topic of lateral deck bending stresses, one would expect the z axis deck displacements under z axis acceleration to be largest near the middle of each bridge.

3.6 Other Member or Connection Responses

Figures 152 to 157 are plots depicting the levels and directions of acceleration at which various SSB and CSCB member and connection

modeling assumptions may no longer be valid.

Figures 152 and 153 depict the x and z axis acceleration levels, respectively, at which the following SSB modeling assumptions may no longer be valid:

- The calculated x axis deck displacements at the deck abutments will not exceed the ±3/4 inch clearance for such displacements at these points;
- 2. The calculated x axis deck displacements at the column to floorbeam expansion connections will not exceed the ±3/4 inch clearance for differential column to floorbeam x axis displacement at these points;
- 3. The calculated column combined stresses by SRSS will not exceed the reserve strength after dead load for the columns;
- 4. The calculated arch rib combined stresses by SRSS will not exceed the arch rib dead load prestresses at the arch abutments.

A similar figure for y axis acceleration is not presented for SSB because none of the assumptions made in the modeling of SSB became invalid until y axis accelerations well above 0.09g were reached.

Figures 154, 155 and 156 depict the x, y and z axis accelerations, respectively, at which the following modeling assumptions for the CSCB model with cables may no longer be valid:

- 1. The sum of the absolute values of the calculated axial stresses in each pair of cable elements will not exceed the minimum breaking strength for one of these cables;
- 2. The calculated column axial stresses will not exceed the dead load compressive stresses in the columns;

- 3. The calculated arch rib axial stresses will not exceed the arch rib dead load prestresses at the arch abutment at panel point 17;
- 4. The calculated arch rib combined stresses by SRSS will not exceed the arch rib dead load prestresses at the arch abutment at panel point 17;
- 5. The calculated z axis displacements at the tops of the towers will not exceed the z axis displacement required to cause the stresses in the tower columns to exceed the yield stress of 33 ksi.

Figure 157 depicts the z axis acceleration levels at which the following modeling assumptions for the CSCB model without cables may no longer be valid:

- The calculated arch rib combined stresses by SRSS will not exceed the arch rib dead load prestresses at the arch abutment at panel point 17;
- 2. The calculated z axis displacements at the tops of the towers will not exceed the z axis displacement required to cause the stresses in the tower columns to exceed the yield stress of 33 ksi.

Similar figures for x and y axis acceleration were not presented for the CSCB model without cables because none of the assumptions made in the modeling process became invalid until x axis accelerations well above 0.50g were reached and because the model without cables is not valid under y axis accelerations of 0.50g or less.

The discussion which follows is divided into the following five parts: deck expansion joint responses, arch rib hinge responses,

column to floorbeam connection responses, column base connection responses and CSCB responses with cables versus without cables. Each one of these sections deals with one or more of the SSB and CSCB modeling assumptions listed above.

3.6.1 Deck Expansion Joint Responses

The response spectrum analysis results depicted in Figures 115, 122, 128, 134, 140 and 146 are based on the SSB model which assumes unlimited x axis deck displacements at the abutments and independent x axis displacements of the deck and the columns at panel points A, E, F, F', E' and A'. Thus the results are not totally correct for x axis accelerations of 0.027g or more as indicated in Figure 152. The true results would depend on the system responses to the cyclical impact loads which may occur at x axis accelerations of 0.027g or more for the south deck section and 0.047g or more for the north deck section. Determination of such responses would, however, require nonlinear analysis which was beyond the scope of this study.

In the CSCB model without cables the response spectrum analyses showed that the $+8\frac{1}{2}$ and $-6\frac{1}{2}$ inch clearances for x axis displacements of the deck at the abutment at panel point 1 would not be exceeded until an x axis acceleration of approximately 0.82g was reached. Thus the modeling assumption specifying unlimited x axis deck displacements at panel point 1 is valid for both models under x axis accelerations up to 0.50g.

3.6.2 Arch Rib Hinge Responses

At z axis accelerations of 0.076g the response spectrum analyses of SSB showed that the dead load compressive stresses transferred through the arch rib hinges are exceeded by the SRSS of the calculated

axial and minor axis bending stresses (see Figure 153). Thus, partial separation of the pin and one of the arch rib hinge shoes in each arch rib to abutment connection might occur at accelerations of 0.0% in the z direction. Such a separation, even if it were complete, would probably not cause bridge failure because only one of the two shoes in each connection would be separated from the connecting pin at any given time thus leaving the other shoe to maintain arch rib to pin alignment.

Response spectrum analyses for CSCB with cables showed that at a y axis acceleration of 0.416g the dead load compressive stresses transferred through the arch rib hinges at panel point 17 are exceeded by calculated axial stresses (see Figure 155). At a z axis acceleration of 0.276g these same dead load stresses are exceeded by the SRSS of the calculated axial and minor axis bending stresses (see Figure 156). At an acceleration of 0.531g in the z direction these dead load stresses are exceeded by calculated axial stresses alone (see Figure 156). Thus the retaining caps in the arch rib to abutment connections may begin to act at a y axis acceleration of 0.416g and at a z axis acceleration of 0.276g.

Calculations concerning when the CSCB retaining caps might yield under y and z axis accelerations were performed. These calculations were based on the response spectrum analysis results and on the assumption that all tensile forces between the arch ribs and the abutments would be transmitted through the pin caps. The calculations showed that yielding due to axial stresses alone might occur in the caps under y axis accelerations of 0.59g and z axis accelerations of 0.84g. Calculations concerning the SRSS of the axial and minor axis

because of the complexity involved. Therefore, the possibility remains that yielding could occur in the caps at panel point 17 under accelerations of 0.50g in the z direction and possibly in the y direction. Note that the responses of the arch hinges at panel point 6 were not determined by this study but they should be similar to those at panel point 17.

3.6.3 Column to Floorbeam Connection Responses

The response spectrum analyses for the CSCB model with cables showed that computed axial stresses in the columns might exceed dead load compressive stresses at panel point 10 under an x axis acceleration of 0.525g (see Figure 154) and at panel points 9, 14, 8, 15, 10, 13, 12, 11, 7 and 16 at y axis accelerations of 0.249g, 0.254g, 0.321g, 0.349g, 0.356g, 0.399g, 0.401g, 0.403g, 0.417g and 0.453g, respectively (see Figure 155). Any higher acceleration levels would require the two bolts in the respective column to floorbeam connections to resist tensile forces. Calculations showed that the stresses in the connecting bolts at panel point 9 could reach 109.2 ksi at y axis accelerations of 0.50g.

In the case of SSB the response spectrum analyses showed that the dead load compressive stresses transferred through the column to floorbeam expansion joints would not be exceeded until x and y axis accelerations well above 0.0% are reached. Thus, x and y axis accelerations pose no threat to these expansion connections. The responses of these joints to z axis acceleration were not precisely determined by the response spectrum analyses because, as discussed in section 2.2.6, these joints were modeled as hinges with respect to

rotation about the x axis. As stated in section 2.2.6, however, preliminary response spectrum analyses did indicate that partial separations of the floorbeam and the columns at these expansion joints could occur at low levels of z axis acceleration.

3.6.4 Column Base Connections

Calculations of SSB column to pedestal joint capacities were performed based on the geometry of the joints as depicted in Figure 6 and also based on the following six assumptions:

- 1. A linear stress distribution as depicted in Figure 158;
- 2. Full dead load;
- 3. An ultimate concrete stress of 3000 psi;
- 4. No anchor bolt prestresses:
- 5. No column buckling;
- 6. A column base plate yield stress of 46 ksi.

These calculations showed that the column base plates at panel points B and B' might yield at 24% of the column yield moments under x axis acceleration. Utilizing this result and the calculated column moments by response spectrum analysis, it was estimated that yielding might occur in these base plates at x axis accelerations of 0.025g.

This 0.025g acceleration level is slightly below the 0.027g level at which the ±3/4 inch clearance for x axis displacements of the deck at the south abutment (panel point 0) might be exceeded. This 0.025g acceleration level, however, is well below the 0.047g level at which the ±3/4 inch clearance for x axis displacements of the deck at the north abutment (panel point 0') might be exceeded. Thus, while it is possible that yielding could occur in the column base plates at panel point B prior to the south abutment x axis restraints coming into play,

it seems more likely to be reached in the column base plates at panel point B' prior to the north abutment x axis restraints coming into play.

In CSCB the columns are truss members and thus there is very little if any transfer of moments from the columns to the concrete pedestals at panel points 2, 3, 4, 18 and 19. Moments are, however, transferred from the tower columns to the concrete skewbacks at panel points 6 and 17. The response spectrum analyses of the CSCB model without cables indicated that z axis accelerations of 0.526g and 0.585g could cause the z axis displacements at the tops of the towers at panel points 17 and 6, respectively, to exceed the value required for yielding in the tower columns. Thus, at the prescribed maximum acceleration of 0.50g in the z direction, it is possible, but not likely, that yielding could occur in the tower columns. Because of the complexity of the CSCB tower to column skewback connections, calculations aimed at determining when the ultimate concrete stress might be reached at these connections were not attempted. However, considering the relationship which exists for SSB between the stresses in the columns and the corresponding stresses in the concrete pedestals, it appears that there is a distinct possibility that in the tower column to skewback connections at panel points 6 and 17 of CSCB the ultimate concrete stress could be reached at z axis accelerations of 0.50g or less.

3.6.5 CSCB Responses With and Without Cables

As discussed in section 3.4, the longitudinal and lateral cables between and at panel points 11 and 12 of CSCB may reach their minimum breaking strengths well below accelerations of 0.50g in the x and z

directions, respectively. The breaking of these cables would (as discussed in sections 3.2 to 3.5) cause increases in some deck stresses and displacements but decreases in all arch rib stresses and displacements.

In addition to reductions in arch rib stresses and displacements, the removal of the cables from CSCB would result in other beneficial effects as well. One example is that the x axis acceleration required to cause the dead load prestresses in the columns at panel point 10 to be fully relieved would change from 0.525g (see Figure 154) to over 1g if the longitudinal cables were removed. Another example is that (as indicated in Figures 156 and 157) if the lateral cables were removed the z axis accelerations required to cause the arch rib dead load prestresses at panel point 17 to be exceeded by SRSS combined stresses and by axial stresses alone would change from 0.276g to 0.343g and from 0.531g to over 0.71g, respectively.

The removal of the cables from CSCB would result in the bridge being less safe because of the increases in some deck stresses and displacements and because of other changes as well. For example, Figures 156 and 157 illustrate that the z axis acceleration required to cause yielding in the tower columns at panel points 6 and 17 might change from over 0.63g to 0.585g and from 0.531g to 0.526g, respectively, if the lateral cables were removed.

3.7 Deck Lumped Masses

The deck masses, as discussed in sections 2.2.8 and 2.3.11, were lumped at the panel points with no masses lumped between these points. As a way of determining the effects of this mass distribution, response spectrum analyses were conducted on the SSB model utilizing

deck masses lumped at panel and midpanel points. The largest responses from the original response spectrum analyses and the corresponding responses with deck masses lumped at panel and midpanel points are listed in Tables 7, 8 and 9 for x, y and z axis accelerations, respectively. The changes in the responses are also listed in the tables as percentages.

The only major changes in bridge responses occurred under y axis acceleration with decreases of about 25% in the y axis displacements at panel points F and F' and with increases in vertical deck bending stresses of 150% for segment D'C'. Vertical deck bending stresses in other segments increased to as much as 1.86 ksi under y axis accelerations of 0.09g. For segments EF, FF' and F'E' the vertical deck bending stresses became largest under y axis acceleration as opposed to x axis acceleration. But for the deck as a whole the largest vertical bending stress under x axis acceleration was more than twice the largest value under y axis acceleration, as is the case in the original model.

For SSB, midpanel deck mass points were utilized between panel points C and C only. Storage limitations in the SAPV2 program prevented the use of additional midpanel points. These same limitations prevented any redistribution of deck masses in the CSCB models. Such a redistribution for CSCB would probably have resulted in bridge response changes similar to those for SSB, because the greater panel lengths in CSCB tend to be balanced by the greater deck stiffnesses.

3.8 Deck Torsion Constants

As discussed in sections 2.2.7 and 2.3.10, the bending resistance of the stringers was neglected in the calculations of deck torsion

constants. In order to determine the effects of this decision, response spectrum analyses were conducted utilizing the higher torsion constants derived by including the stringer bending resistance. Tables 10 and 11 contain the largest responses calculated by the original response spectrum analyses and the corresponding responses with the higher torsion constants for z axis accelerations of the SSB model and the CSCB model without cables, respectively. Also listed in the tables are the changes in the responses as percentages.

Both bridges exhibited substantial decreases in their largest arch rib major axis bending stresses, but their largest arch rib combined stresses, which are of more interest, were little changed.

While the largest y axis displacements for both bridges did decrease marginally, the more important z axis displacements were virtually unchanged. Overall therefore, the changes for both bridges are negligible.

3.9 Deck Concrete Effectiveness

The concrete deck slabs, as discussed in sections 2.2.7 and 2.3.10, were assumed to be 50% effective, i.e. the modular ratio was assumed to be 20. As a means of determining the effects of this assumption, response spectrum analyses assuming 100% concrete effectiveness were conducted. Tables 12, 13 and 14 contain the largest responses calculated by the original response spectrum analyses and the corresponding responses assuming 100% concrete effectiveness for the SSB model under x, y and z axis accelerations, respectively. Similar lists for the CSCB model with cables are contained in Tables 15, 16 and 17. The changes in the responses as percentages are also listed in the tables.

For SSB the changes in the largest bridge responses were

negligible under all directions of acceleration. The changes in the largest CSCB responses under y and z axis accelerations are also negligible. Under x axis acceleration, however, all of the largest CSCB responses decreased markedly.

Note that lateral deck bending moments rather than stresses are presented in Tables 14 and 17. This is because the calculation of stresses in the deck concrete slab is directly dependent upon the modular ratio (as well as the moment of inertia). Thus, while the moments in the deck change by less than 20% when the modular ratio is changed from 20 to 10, the procedures used in this study to approximate the stresses in the slab yield values of stress which differ by as much as 64%.

The greater influence of concrete effectiveness on the CSCB responses to x axis acceleration as opposed to the SSB responses to x axis acceleration is due to three major reasons. First, the longitudinal cables are the only means by which longitudinal forces can be transferred from the deck to the arch ribs in CSCB. The deck in SSB, on the other hand, is connected to the arch ribs longitudinally by moment resisting columns at panel points D and D.

The second major reason is the greater continuity of the CSCB deck. With respect to vertical deck bending, the CSCB deck is discontinuous at panel points 6 and 17 while the SSB deck is discontinuous at panel points C, F, F' and C'. With respect to axial forces, the CSCB deck is continuous and is pinned at one abutment while the SSB deck is discontinuous at panel points F and F' and is free at both abutments.

Finally, the third reason is that the CSCB deck has a composite

cross-section while the SSB deck does not. Thus, increasing the concrete effectiveness from 50 to 100% caused about a 16% increase in the vertical deck moments of inertia in CSCB, but only a 6% increase in SSB.

CHAPTER IV

SUMMARY AND CONCLUSION

4.1 Summary

In order to assess the potentially damaging effects of earthquakes on arch bridges, South Street Bridge (SSB) in Connecticut and Cold Springs Canyon Bridge (CSCB) in California were chosen for study. Both bridges are steel deck arches with solid ribs (see Figures 1, 2, 9 and 10). Their major geometric and design features are summarized in Table 18.

The study was based on computer modeling utilizing the response spectrum method. For each bridge the two arch ribs were modeled individually, as were the tower members (for CSCB), the columns over the ribs, the columns in the approach spans and the arch bracing members. However, the deck system - which includes the floorbeams, stringers and reinforced concrete slab - was modeled as a series of beam elements connected laterally on each side to the columns by rigid or virtually rigid elements.

The bridge masses were essentially lumped at the panel points.

Certain parametric and comparative studies were made on the procedure for lumping the masses and on the computation of the torsion constants for the deck and the choice of the value of the steel to concrete modular ratio for the deck. The results of these studies generally supported the validity of the models which were used.

The support and connection details were carefully considered and modeled within the limits of linear elasticity. The only exceptions were the cables in CSCB, the low minimum breaking strengths of which necessitated the use of two bridge models - one with cables and one without cables.

The first 36 natural frequencies and mode shapes of SSB and the first 26 natural frequencies and mode shapes for each CSCB model were computed. The fundamental frequencies which were calculated are 0.64 cps for SSB, 0.37 cps for CSCB with cables and 0.28 cps for CSCB without cables. The fundamental mode of SSB consists mainly of a longitudinal translation of the south half of the deck (Figure 25). For CSCB with cables the fundamental mode represents an out-of-plane half wave translation of the deck and the arch in the z direction (Figure 61). The fundamental mode of CSCB without cables consists of an out-of-plane half wave z axis translation of the deck only (Figure 87).

The "Normalized Rock Spectra" were used as input for the response spectrum analyses, with maximum ground accelerations of 0.09g for SSB and 0.50g for CSCB. The large difference in the input levels is due to the differences (as recognized by AASHTO) in the seismicity of the structure sites. The input spectra were applied in each of three orthogonal directions with no reductions for ductility.

The resulting seismic responses of the bridges to the input motions are summarized in Tables 19, 20 and 21. Table 19 gives the maximum responses of the arch ribs. In general, these maximum responses occurred at the same relative locations in both bridges and in the same directions of ground acceleration. As expected, however, due mainly to the difference in the intensities of ground motion, the

maximum responses of SSB are relatively mild while those of CSCB are quite substantial. For the latter, if the absolute values of the axial and bending stresses are added, the arch ribs would be stressed somewhat beyond their yield points (assuming full dead and live loads).

It appears that the most injurious direction of ground motion is the z direction which is the horizontal direction normal to the bridge axis. The next most injurious direction of ground motion appears to be the x direction which is the horizontal direction parallel to the axis of the bridge. Finally, the y direction, which is the vertical direction, appears least damaging.

Responses of the decks, summarized in Table 20, are qualitatively similar to those of the arch ribs. However, the maximum deck displacements under z axis acceleration were appreciably larger than those for the arch ribs (26.4 inches versus 17.9 inches for CSCB).

In modeling the bridges as linearly elastic systems, a number of assumptions were necessary, such as the clearance of the expansion joints would not be exceeded by the relative movements of the deck. The effects of this assumption and certain other assumptions involving the arch rib hinges, the column to floorbeam connections and the column base connections were investigated. These investigations involved determining the ground accelerations required to cause these assumptions to become invalid. The results are summarized in Table 21 and also include the responses of the CSCB cables. These results would seem to indicate that the structures might experience distress at some of these connections (and in the CSCB cables) at ground accelerations considerably below the specified maximum levels (i.e. 0.09g for SSB and 0.50g for CSCB).

4.2 Concluding Remarks

Based on the response spectrum curves used, it seems that at 0.09g the overall responses of SSB should be quite acceptable. The overall responses of CSCB at 0.50g are much larger and, as pointed out earlier, in several instances the maximum stresses (dead plus live plus seismic stresses) exceed the yield stresses of the deck and/or the arch ribs. However, it must be borne in mind that:

- No attenuation of the response spectrum values was allowed for ductility although such allowances seem warranted by experience;
- 2. The probability of simultaneous occurrence of full live loads and maximum seismic loads is low;
- 3. The exceedence of the deck or arch rib stresses over nominal yield stress is limited in magnitude and duration.

Therefore, the results presented here probably should not be viewed with undue concern.

On the other hand, the possibility that some connections might experience distress at levels of ground motion substantially lower than 0.09g for SSB or 0.50g for CSCB may well justify closer examinations of these connections. This is probably not surprising, as experience with earthquake effects seems to indicate that it is often the structural details that require more attention.

The most serious limitation of the work reported here is perhaps the assumption of linear elasticity. A maximum displacement of 26.4 inches may well result in appreciable geometric nonlinear effects. Of course, exceedence of yield stress would call for an analysis that would take material nonlinearity into account. Future research should

consider these nonlinear effects.

Another limitation of the work presented here is the use of the response spectrum method which assumes that the motions of all bridge supports are the same. The validity of this assumption decreases with longer spans. Thus, the effects of non-uniform motion of the supports also appears to be a significant topic for future studies.

Finally, it would be a worthwhile and interesting project to conduct field testing of deck arch bridges and/or to install recording systems on a bridge such as CSCB so that nature can supply the input excitation.

TABLES

Table 1 SSB Mode Shapes Characterized by Z Axis Displacements and/or X Axis Rotations

Primary Deck and Arch X Axis Rotations	Full Wave Rotations 1½ Wave Rotations 2 Wave Rotations In-Phase Rotations	2 Wave Rotations 2½ Wave Rotations 3 Wave Rotations	Rotation @ C Rotation @ C'	Rotation @ B Rotation @ B'
Primary Arch Z Axis Displacements	Half Wave Displacements		Full Wave Displacements Full Wave Displacements In-Phase Displ. @ D & E In-Phase Displ. @ D' & E'	Out-Of-Phase Displ. @ D & E Out-Of-Phase Displ. @ D' & E'
Primary Deck Z Axis Displacements	Half Wave Displacements Full Wave Displacements 1½ Wave Displacements	2 Wave Displacements	2½ Wave Displacements 3 Wave Displacements	3½ Wave Displacements 4 Wave Displacements
Period, seconds	0.6125 0.3920 0.2706 0.2363 0.2103 0.1710	0.1476 0.1258 0.1032	0.0960 0.0917 0.0789 0.0655 0.0666	0.0539 0.0533 0.0506 0.0476 0.0455
Mode No.	4 2 C 8 Q 2 E	14 16 18	\$828888	2433884

Table 2 SSB Mode Shapes Characterized by X Axis Displacements and/or Y Axis Displacements

	84		
Primary Arch Y Axis Displacements	Full Wave Displacements 1½ Wave Displacements 2 Wave Displacements In-Phase Displacements	2½ Wave Displacements 3 Wave Displacements	
Primary Deck Y Axis Displacements	Full Wave Displacements 1½ Wave Displacements 2 Wave Displacements Tn-Phase Displacements	2½ Wave Displacements 3 Wave Displacements Displacement @ C Displacement @ C	Displacement @ B Displacement @ B*
Primary Deck X Axis Displacements	In-Phase Displ South Half In-Phase Displ North Half		Half Wave Displ South Half Half Wave Displ North Half
Period, seconds	1.565 1.124 0.6206 0.3487 0.1885	0.1293 0.1060 0.0648 0.0600	0.0504 0.0503 0.0499 0.0432
Mode No.	4 4 6 9 9 5	32548	፠፠፠፠

CSCB Mode Shapes Characterized by Z Axis Displacements and/or X Axis Rotations for the Model with Cables Table 3

Mode	Period,	Primary Deck Z Axis	Primary Arch Z Axis	Primary Deck and Arch
No.	seconds	Displacements	Displacements	X Axis Rotations
+1	2,732	Half Wave Displacements	Half Wave Displacements	
3	1,561	Full Wave Displacements		
4	1,182	$1\frac{1}{2}$ Wave Displacements		
9	0.8967	•	Full Wave Displacements	
۷	0,8398		Full Wave Displacements	
ω	0.7234	2 Wave Displacements	1	
11	\$15.0	$2\frac{1}{2}$ Wave Displacements		
13	0,4269	1	$1\frac{1}{2}$ Wave Displacements	Half Wave Rotations
14	0,4117			Full Wave Rotations
16	0,3855	3 Wave Displacements		1½ Wave Rotations
17	0.3648		2 Wave Displacements	2 Wave Rotations
18	0.3542			1½ Wave Rotations
19	0.3383		$2\frac{1}{2}$ Wave Displacements	1½ Wave Rotations
80	0,3030		2 Wave Displacements	2 Wave Rotations
22	0.2787	$3\frac{1}{2}$ Wave Displacements		
83	0,2521		$2\frac{1}{2}$ Wave Displacements	,
₹2	0,2428			$2\frac{1}{2}$ Wave Rotations
25	0,2263		3 Wave Displacements	

Table 4 CSCB Mode Shapes Characterized by X Axis Displacements and/or Y Axis Displacements for the Model with Cables

Primary Arch Y Axis Displacements	Full Wave Displacements $\%$ 1½ Wave Displacements	2 Wave Displacements In-Phase Displacements	2½ Wave Displacements 3 Wave Displacements	4
Primary Deck Y Axis Displacements	Full Wave Displacements 1½ Wave Displacements	2 Wave Displacements In-Phase Displacements	2½ Wave Displacements 3 Wave Displacements	4
Primary Deck X Axis Displacements	charmond frankt and Afrit	nati waye bispiacements		Full Wave Displacements
Period, seconds	2.117 1.167	0.6106 0.4269	0,3980	0.21%
Mode No.	0 N	10,	12	%

Table 5 GSCB Mode Shapes Characterized by Z Axis Displacements and/or X Axis Rotations for the Model without Cables

Z Axis Primary Deck and Arch Displacements X Axis Rotations	placements		placements		acements $1\frac{1}{2}$ Wave Rotations		Full Wave Rotations	12 Wave Rotations	cements 2 Wave Rotations		12 Wave Rotations	cements 2 Wave Rotations	acements		$2\frac{1}{2}$ Wave Rotations	A TABLE OF THE PARTY OF THE PAR
Primary Arch Z Axis Disp	Half Wave Displacements		Full Wave Displacements	•	$1\frac{1}{2}$ Wave Displacements				2 Wave Displacements			2 Wave Displacements	$2\frac{1}{2}$ Wave Displacements			3 Wave Displacements
Primary Deck Z Axis Displacements	Half Wave Displacements	Full Wave Displacements		2 Wave Displacements		$2\frac{1}{2}$ Wave Displacements				3 Wave Displacements				$3\frac{1}{2}$ Wave Displacements	•	
Period, seconds	3.535	1,603	0.9567	0.7717	0,5807	0.5199	0,4209	0,4018	0.3807	0.3731	0.3533	0,3038	0.2906	0.2813	0.2486	0.2331
Mode No.	ى ب	, 14 (~	œ	Ħ	12	14	15	17	18	19	80	21	ಐ	₹	25

CSCB Mode Shapes Characterized by X Axis Displacements and/or Y Axis Displacements for the Model without Cables Table 6

s ents	ments & nts	ts ents	nts +s	3
Primary Arch Y Axis Displacements	Full Wave Displacements 1½ Wave Displacements	2 Wave Displacements Tn-Phase Displacements	22 Wave Displacements) wave propracements
Primary Deck Y Axis Displacements	Full Wave Displacements 1½ Wave Displacements	2 Wave Displacements Tn-Phase Displacements	2½ Wave Displacements	Maye Displacements
Primary Deck X Axis Displacements	Holf Warre Dian accoments	mert was tradement		Full Wave Displacements
Period, seconds	2.469 1.167 0.6220	0.6227	0.3981	0.2230
Mode No.	0 N	10,	3 12	3%

Table 7 SSB Responses as a Function of Deck Mass Distribution Under X Axis Accelerations of 0.09g

	Response	Maximum Value With Mass Lumped at Panel Points Only	Corresponding Value With Mass Lumped at Panel and Mid- panel Points	Percent Change in Response
Arch	Rib			
	Major Axis Bending Stress	2.21 ksi	2.33 ksi	+5.4%
	X Axis Displacement	0.019 ft	0.019 ft	N. C.
	Y Axis Displacement	0.037 ft	0.038 ft	+2.7%
Deck				
	Vertical Bending Stress	4.00 ksi	4.25 ksi	+6.2%
	X Axis Displacement	0.205 ft	0.219 ft	+6.8%
	Y Axis Displacement	0.037 ft	0.038 ft	+2.7%

Table 8 SSB Responses as a Function of Deck Mass Distribution Under Y Axis Accelerations of 0.09g

	Response	Maximum Value With Mass Lumped at Panel Points	Corresponding Value With Mass Lumped at Panel and Mid- panel Points	Percent Change in Response
Arch	Rib			
	Axial Stress	0.79 ksi	0.82 ksi	+3.8%
	Major Axis Bending Stress	0.70 ksi	0.70 ksi	N. C.
	Combined Stress (by summation)	1.47 ksi	1.49 ksi	+1.4%
	X Axis Displacement	0.003 ft	0.003 ft	N. C.
	Y Axis Displacement	0.008 ft	0.006 ft	-25%
Deck				
	Vertical Bending Stress	0.48 ksi	1.19 ksi	+150%
	Y Axis Displacement	0.008 ft	0.006 ft	-25%

Table 9 SSB Responses as a Function of Deck Mass Distribution Under Z Axis Accelerations of 0.09g

Response	Maximum Value With Mass Lumped at Panel Points	Corresponding Value With Mass Lumped at Panel and Mid- panel Points	Percent Change in Response
Arch Rib			
Axial Stress	2.45 ksi	2.39 ksi	-2.4%
Major Axis Bending Stress	1.88 ksi	1.70 ksi	-9.6%
Minor Axis Bending stress	2.63 ksi	2.68 ksi	+1.9%
Combined Stress (by summation)	6.96 ksi	6.76 ksi	-2.%
X Axis Displacement	0.007 ft	0.006 ft	-14%
Y Axis Displacement	0.029 ft	0.026 ft	-10%
Z Axis Displacement	0.081 ft	0.081 ft	N. C.
Deck			
Lateral Bending Stress	98 psi	99 psi	+1.0%
Z Axis Displacement	0.095 ft	0.094 ft	-1.1%

Table 10 SSB Responses as a Function of Deck Torsion Constant Under Z Axis Accelerations of 0.09g

Response	Maximum Value With Low Torsion Constant	Corresponding Value With High Torsion Constant	Percent Change in Response
Arch Rib		•	
Axial Stress	2.45 ksi	2.45 ksi	N. C.
Major Axis Bending Stress	1.88 ksi	1.52 ksi	-1%
Minor Axis Bending Stress	2.63 ksi	2.67 ksi	+1.5%
Combined Stress (by summation)	6.96 ksi	6.64 ksi	-4.6%
X Axis Displacement	0.007 ft	0.006 ft	-14%
Y Axis Displacement	0.029 ft	0.027 ft	-6.%
Z Axis Displacement	0.081 ft	0.081 ft	N. C.
Deck			
Lateral Bending Stress	98 psi	101 psi	+3.1%
Z Axis Displacement	0.095 ft	0.094 ft	-1.1%

Table 11 CSCB Responses as a Function of Deck Torsion Constant Under Z Axis Accelerations of 0.50g (Model Without Cables)

Response	Maximum Value With Low Torsion Constant	Corresponding Value With High Torsion Constant	Percent Change in Response
Arch Rib			
Axial Stress	7.0 ksi	7.1 ksi	+1.4%
Major Axis Bending Stress	2.4 ksi	1.8 ksi	- 2 <i>5</i> %
Minor Axis Bending Stress	9.6 ksi	9.8 ksi	+2.1%
Combined Stress (by summation)	16.1 ksi	16.1 ksi	N. C.
X Axis Displacement	0.05 ft	0.05 ft	N. C.
Y Axis Displacement	0.16 ft	0.14 ft	-12%
Z Axis Displacement	1.15 ft	1.13 ft	-1.7%
Deck			
Lateral Bending Stress	1090 psi	1090 psi	N. C.
Z Axis Displacement	2.20 ft	2.20 ft	N. C.

Table 12 SSB Responses as a Function of Concrete Effectiveness Under X Axis Accelerations of $0.09 \mathrm{g}$

	Response	Maximum Value With 50% Effec- tiveness	Corresponding Value With 100% Effec- tiveness	Percent Change in Response
Arch	n Rib			
	Major Axis Bending Stress	2.21 ksi	2.20 ksi	-0.5%
	X Axis Displacement	0.019 ft	0.018 ft	-5.3%
	Y Axis Displacement	0.037 ft	0.036 ft	-2.7%
Deck	c			
	Vertical Bending Stress	4.00 ksi	3.80 ksi	-5.0%
	X Axis Displacement	0.205 ft	0.204 ft	-0.5%
	Y Axis Displacement	0.037 ft	0.036 ft	-2.7%

Table 13 SSB Responses as a Function of Concrete Effectiveness Under Y Axis Accelerations of 0.0%

	Response	Maximum Value With 50% Effec- tiveness	Corresponding Value With 100% Effec- tiveness	Percent Change in Response
Arch	Rib			
	Axial Stress	0.79 ksi	0.79 ksi	N. C.
	Major Axis Bending Stress	0.70 ksi	0.69 ksi	-1.4%
	Combined Stress (by summation	1.47 ksi	1.46 ksi	-0.7%
	X Axis Displacement	0.003 ft	0.003 ft	N. C.
	Y Axis Displacement	0.008 ft	0.008 ft	N. C.
Deck				
	Vertical Bending Stress	0.48 ksi	0.47 ksi	-2.1%
	Y Axis Displacement	0.008 ft	0.008 ft	N. C.

Table 14 SSB Responses as a Function of Concrete Effectiveness Under Z Axis Accelerations of 0.09g

	Response	Maximum Value With 50% Effec- tiveness	Corresponding Value With 100% Effec- tiveness	Percent Change in Response
Arch	Rib			
	Axial Stress	2.45 ksi	2.42 ksi	-1.2%
	Major Axis Bending Stress	1.88 ksi	1.89 ksi	+0.5%
	Minor Axis Bending Stress	2.63 ksi	2.60 ksi	-1.1%
	Combined Stress (by summation)	6.% ksi	6.91 ksi	-0.7%
	X Axis Displacement	0.007 ft	0.006 ft	-14%
	Y Axis Displacement	0.029 ft	0.029 ft	N. C.
	Z Axis Displacement	0.081 ft	0.081 ft	N. C.
Deck				
	Z Axis Displacement	0.095 ft	0.095 ft	N. C.
	Lateral Bending Moment	1608 k-ft	1836 k-f t	+14%

Table 15 CSCB Responses as a Function of Concrete Effectiveness Under X Axis Accelerations of 0.50g (Model With Cables)

	Response	Maximum Value With 50% Effec- tiveness	Corresponding Value With 100% Effec- tiveness	Percent Change in Response
Arch	Rib			
	Major Axis Bending Stress	14.3 ksi	4.7 ksi	-67%
	X Axis Displacement	0.27 ft	0.22 ft	-1%
	Y Axis Displacement	0.45 ft	0.29 ft	-36%
Deck				
	Axial Stress	14.0 ksi	11.1 ksi	-21%
	Vertical Bending Stress	12.7 ksi	4.2 ksi	-67%
	Combined Stress (by summation)	24.8 ksi	14.1 ksi	-43%
	X Axis Displacement	0.38 ft	0.30 ft	-21%
	Y Axis Displacement	0.45 ft	0.29 ft	- 36%

Table 16 CSCB Responses as a Function of Concrete Effectiveness Under Y Axis Accelerations of 0.50g (Model With Cables)

	Response	Maximum Value With 50% Effec- tiveness	Corresponding Value With 100% Effec- tiveness	Percent Change in Response
Arch	Rib			
	Axial Stress	10.8 ksi	10.8 ksi	N. C.
	Major Axis Bending Stress	11.5 ksi	11.0 ksi	-4.3%
	Combined Stress (by summation)	18.2 ksi	17.6 ksi	- 3.3%
	X Axis Displacement	0.09 ft	0.09 ft	N. C.
	Y Axis Displacement	0.30 ft	0.30 ft	N. C.
Deck				
	Vertical Bending Stress	9.7 ksi	9.9 ksi	+2.1%
	X Axis Displacement	0.02 ft	0.02 ft	N. C.
	Y Axis Displacement	0.32 ft	0.32 ft	N. C.

Table 17 CSCB Responses as a Function of Concrete Effectiveness Under Z Axis Accelerations of 0.50g (Model With Cables)

Response	Maximum Value With 50% Effec- tiveness	Corresponding Value With 100% Effec- tiveness	Percent Change in Response
Arch Rib			
Axial Stress	8.7 ksi	8.4 ksi	-3.4%
Major Axis Bending Stress	4.4 ksi	4.7 ksi	+6.8%
Minor Axis Bending Stress	11.7 ksi	13.5 ksi	+15%
Combined Stress (by summation)	20.2 ksi	21.8 ksi	+7.9%
X Axis Displacement	0.07 ft	0.07 ft	N. C.
Y Axis Displacement	0.24 ft	0.24 ft	N. C.
Z Axis Displacement	1.49 ft	1.44 ft	-3.4%
Deck			
Z Axis Displacement	1.84 ft	1.77 ft	-3.8%
Lateral Bending Moment	29070 k-ft	34420 k-ft	+18%

Table 18 SSB and CSCB Geometric and Design Characteristics

Item	South Street Bridge	Cold Springs Canyon Bridge
Fundamental Frequency	0.64 cps	0.37 cps
Overall Length	377 ft	1218 ft
Arch Span	193 ft	700 ft
Arch Rib Panel Lengths	2 @ 24 (ends) 5 @ 29 (middle)	11 @ 63.635'
Arch Configuration	Circular with 175' Radius	Seventh Order Polynomial
Arch Rise to Span Ratio	1:6.66	1:4.84 for South Hinge 1:7.14 for North Hinge
Rib Spacing to Span Ratio	1:8.77	1: 26.9
Rib Depth to Span Ratio	1: 58.6	1:73.0 to 1:75.7
Rib to Total Dead Load Ratio	1: 6.01	1:2.79
Expansion Joints in Deck	4 @ Panel Points A, F, F' and A'	1 @ Panel Point 1
Deck Hinges	6 @ Panel Points A, C, F, F', C' and A'	4 @ Panel Points 1, 6, 17 and 20
Wind Load Transfer	Deck to Arch via Columns	Deck to Arch via Cables and/or Deck to Foundation via Towers

Table 19 Largest SSB and CSCB Arch Rib Responses

Response	Lan	Largest SSB Responses		Lare	Largest CSCB Responses	ses
	Response @A=0.09g	Element or Panel Point	Direction	Response @A=0. 50g	Element or Panel Point	Direction
Arch Rib Stresses						٠
Axial	2.45 ks1	СD	23	10.8 ks1	16c-17	>
Major Axis Bending	2.21 ks1	DE	×	14.3 ks1	15c-16	101 ×
Minor Axis Bending	2.63 ks1	GD	23	11.7 ks1	6c-7	23
Combined (by sum.)	6.96 ks1	αD	23	20.2 ks1	6c-7	23
Arch Rib Displacements						
X Axis	0.23 fn.	臼	×	3.24 in.	15	×.
Y Axis	0.44 in.	臼	×	5.40 in.	10	×
Z Axis	0.97 in.	٤ų	83	17.9 in.	12	Ø

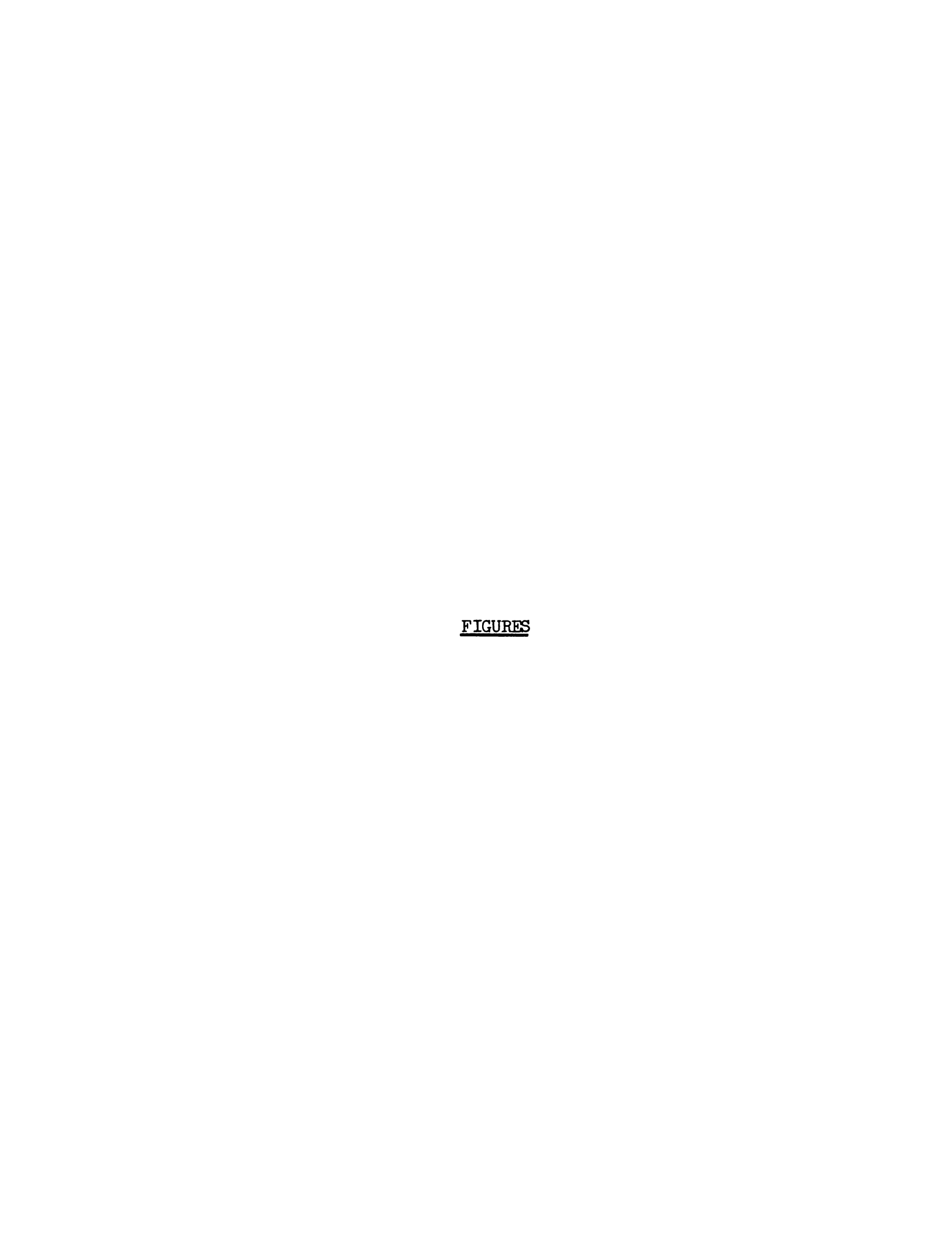
Table 20 Largest SSB and CSCB Deck Responses

S	Direction		×	×	Ŋ	×		×	×	83
Largest CSCB Responses	Element or Panel Point		19-20	15-16	10-11	15-16		1	10	11 & 12
Large	Response @A=0,50g		15.8 ksi ⁺	12.7 ksi	1089 psi [†]	24.8 ksi		4.81 in.	5.40 in.	26.4 in. ⁺
ŭ	Direction		×	*	Ŋ	×		×	×	23
Largest SSB Responses	Element or Panel Point		E'D'	DE	CD	DE		0 to F	ы	ſΞŧ
Larg	Response @A=0.09g		0.10 ks1	4.00 ksi	98.2 psi	4.09 ksi		2.46 in.	0.44 in.	1.14 in.
Response		Deck Stresses	Axial	Vertical Bending	Lateral Bending*	Combined (by sum.)	Deck Displacements	X Axis	Y Axis	Z Axis

* stress in concrete slab + model without cables

Table 21 Other Key SSB and CSCB Responses

Key CSCB Responses	Sufficient clearances under x axis accelerations up to 0.82g.	Retaining rings could begin acting at y and z axis accelerations of 0.416g and 0.276g respectively.	Connecting bolts could begin acting at ∞ x and y axis accelerations of 0.525g and 0.249g respectively.	Ultimate concrete stress in the tower to skewback connections could be reached at z axis accelerations of 0.50g.	Longitudinal cables could break at x axis accelerations of 0.333g and lateral cables could break at z axis accelerations of 0.316g.
Key SSB Responses	Insufficient clearances under x axis accelerations of 0.027g or more.	Partial separations of arch rib shoes and connecting pins could begin at z axis accelerations of 0.076g.	Total separations of the column to floorbeam expansion joints are not likely until x and y axis accelerations well above 0.09g occur.	Yielding in some column base plates might occur at x axis accelerations of 0.025 g.	None
Item	Deck Expansion Joints	Arch Rib Hinges	Column to Floorbeam Connections	Column Base Connections	Cables



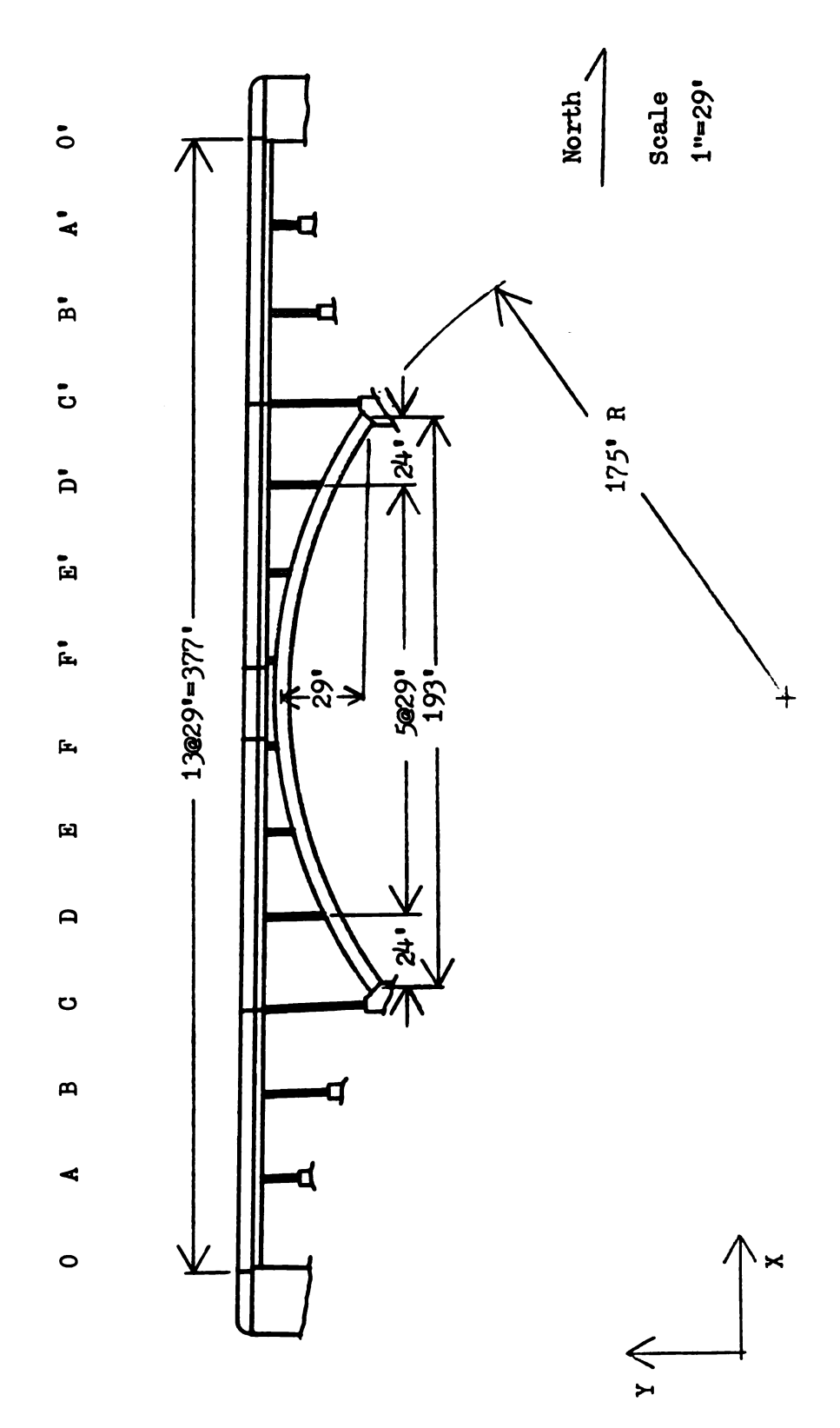


Figure 1 South Street Bridge Profile

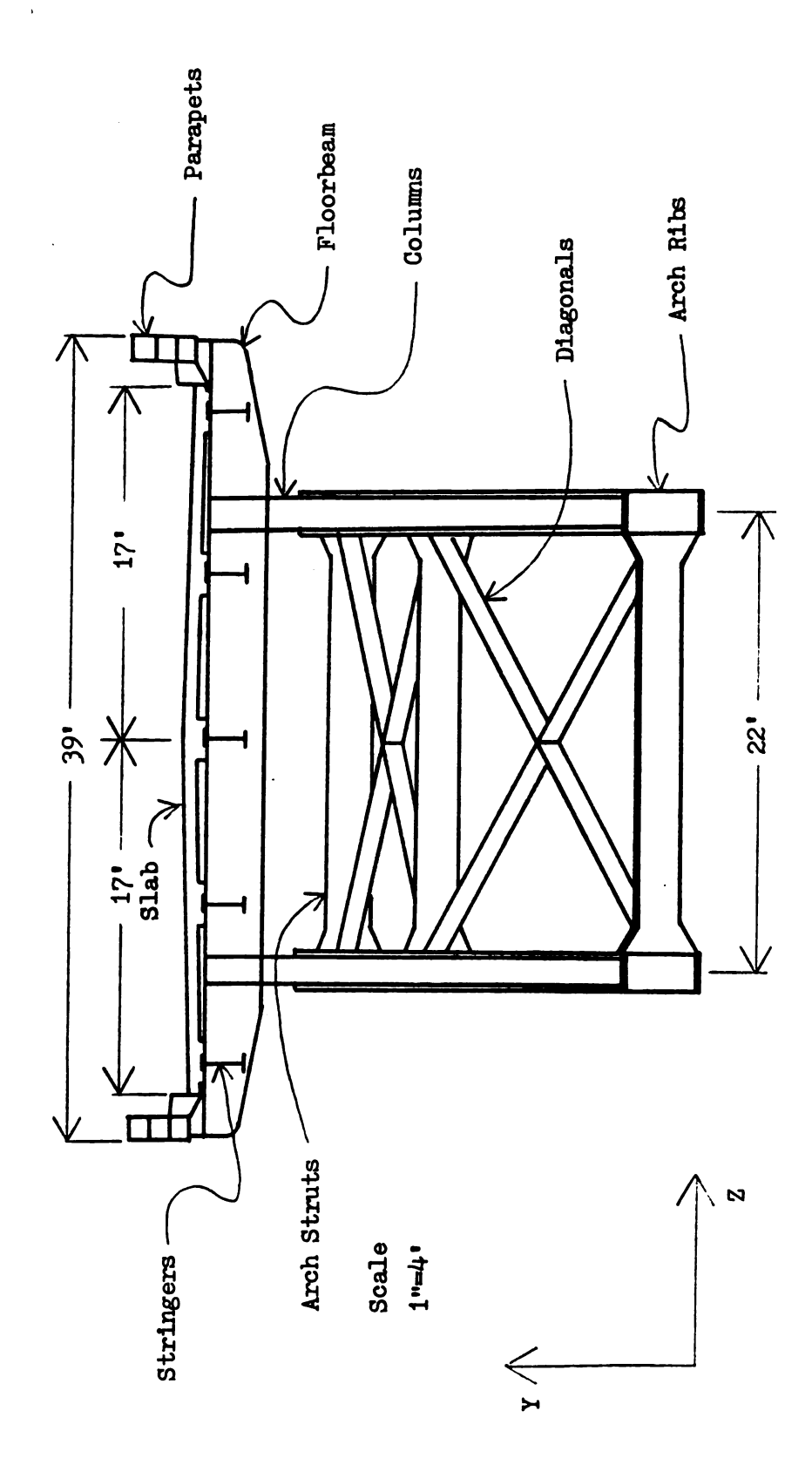


Figure 2 South Street Bridge Gross-section

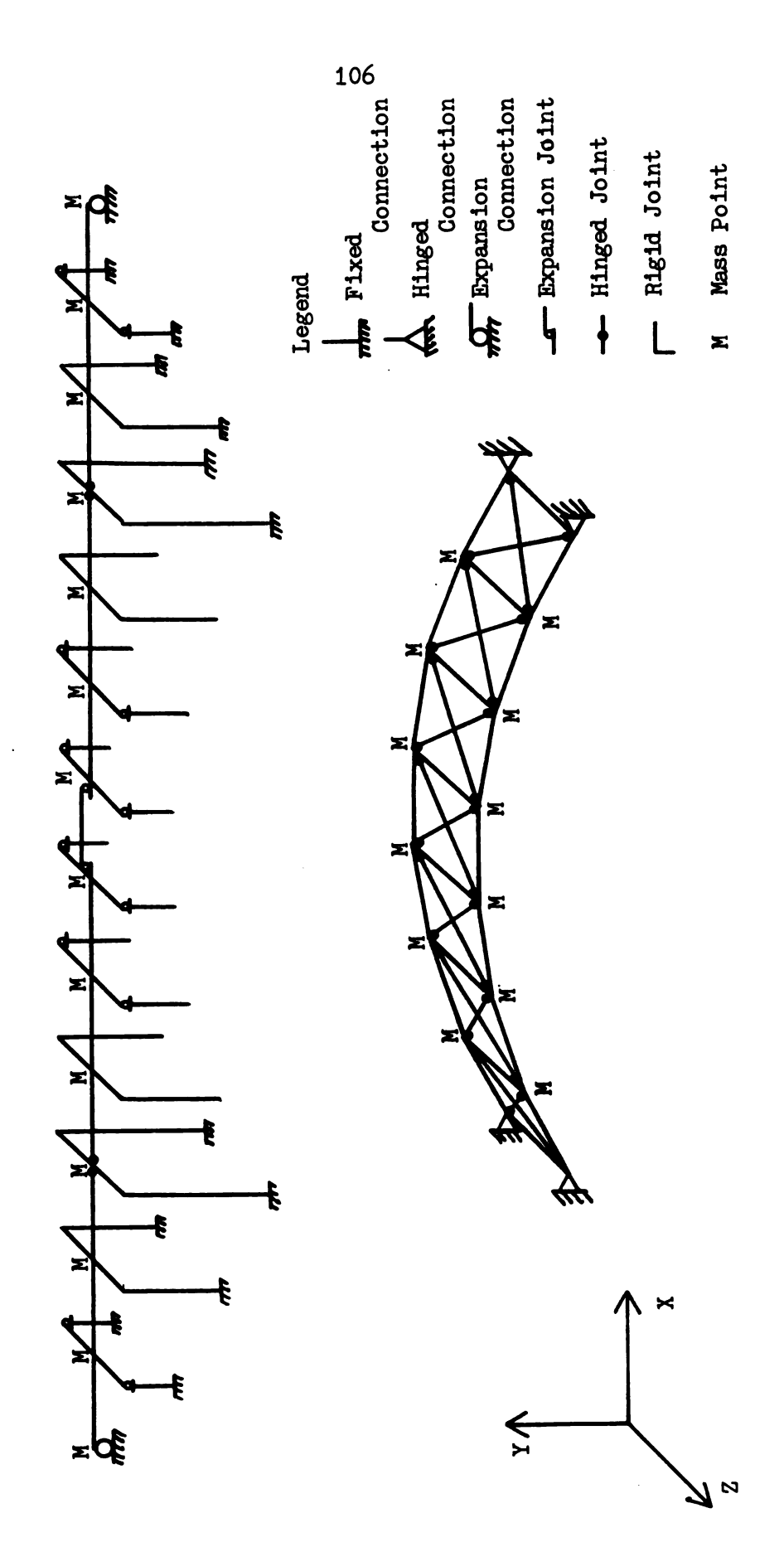


Figure 3 Final South Street Bridge Model

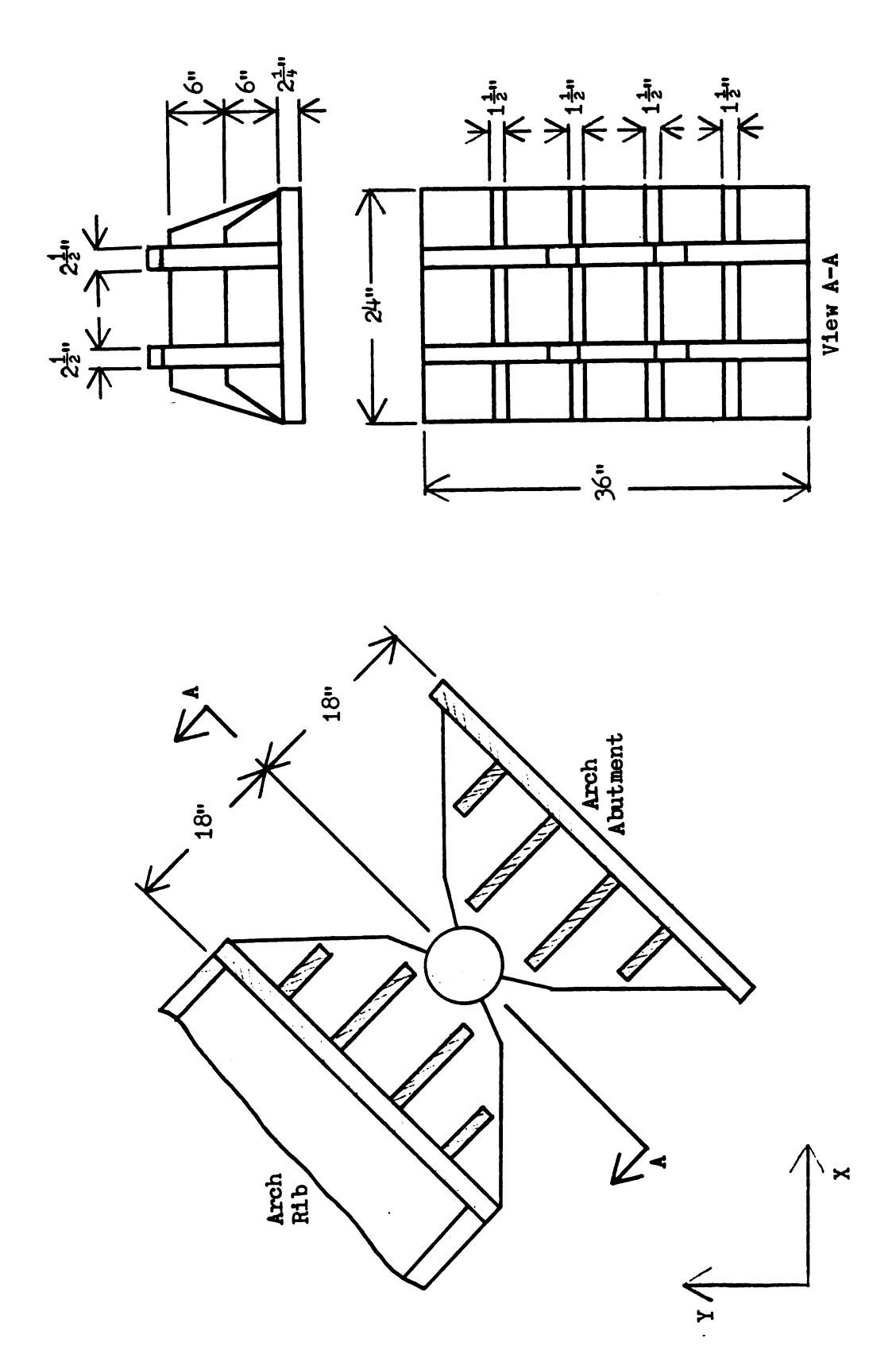


Figure 4 Arch Abutment Hinge Connection

Section B-B

Figure 5 Column to Floorbeam Expansion Joints

View A-A

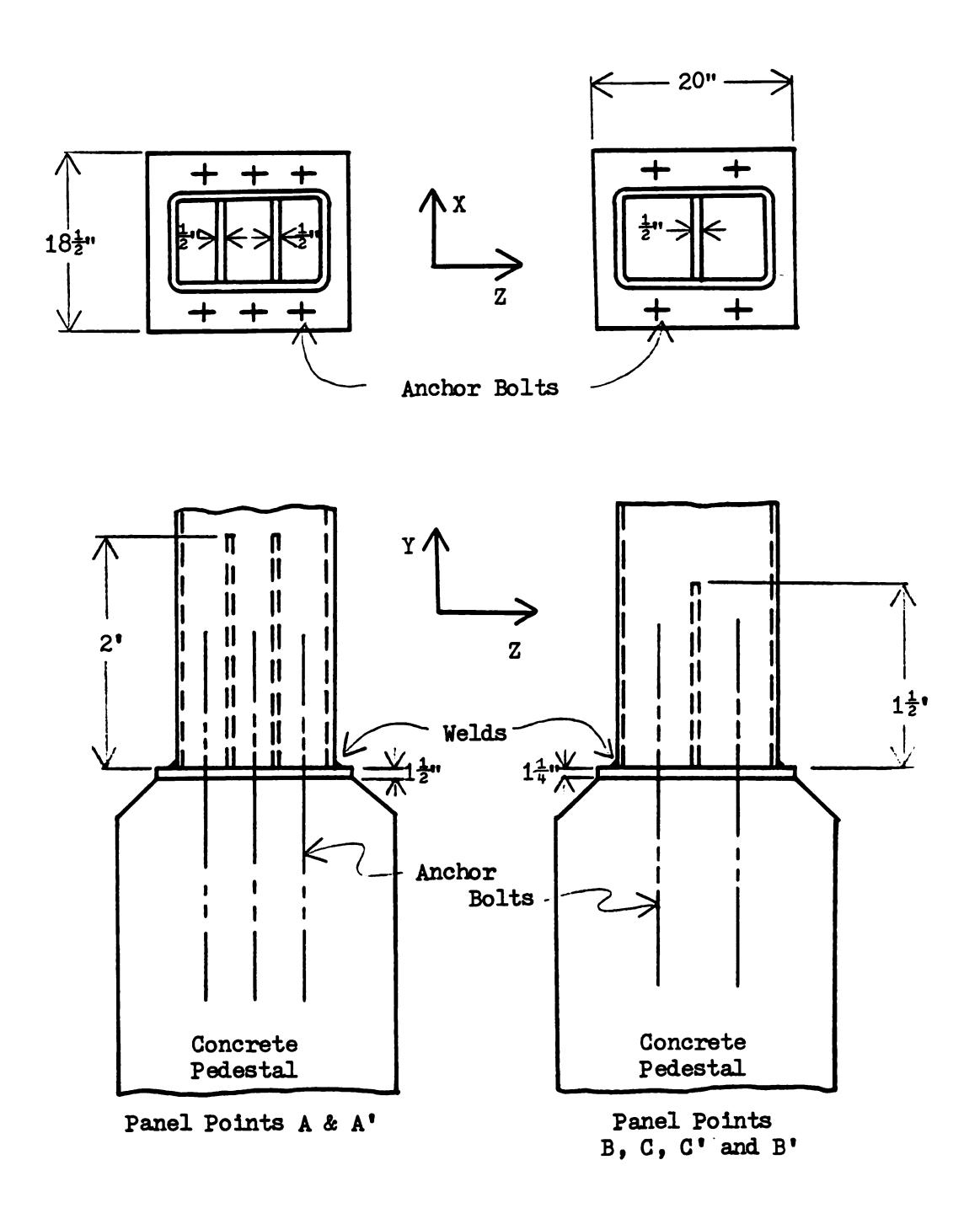


Figure 6 Column Base Connections

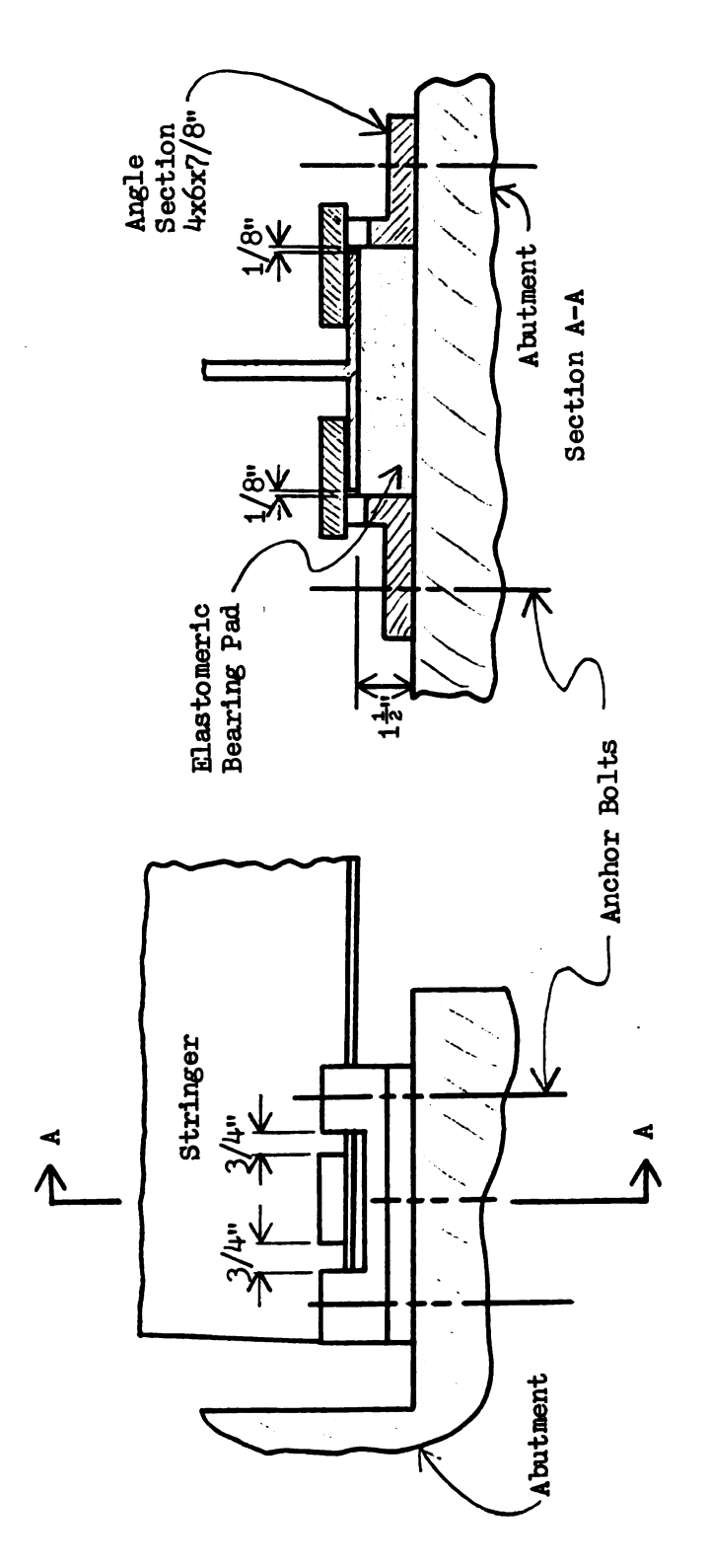


Figure ? Deck Abutment Connections

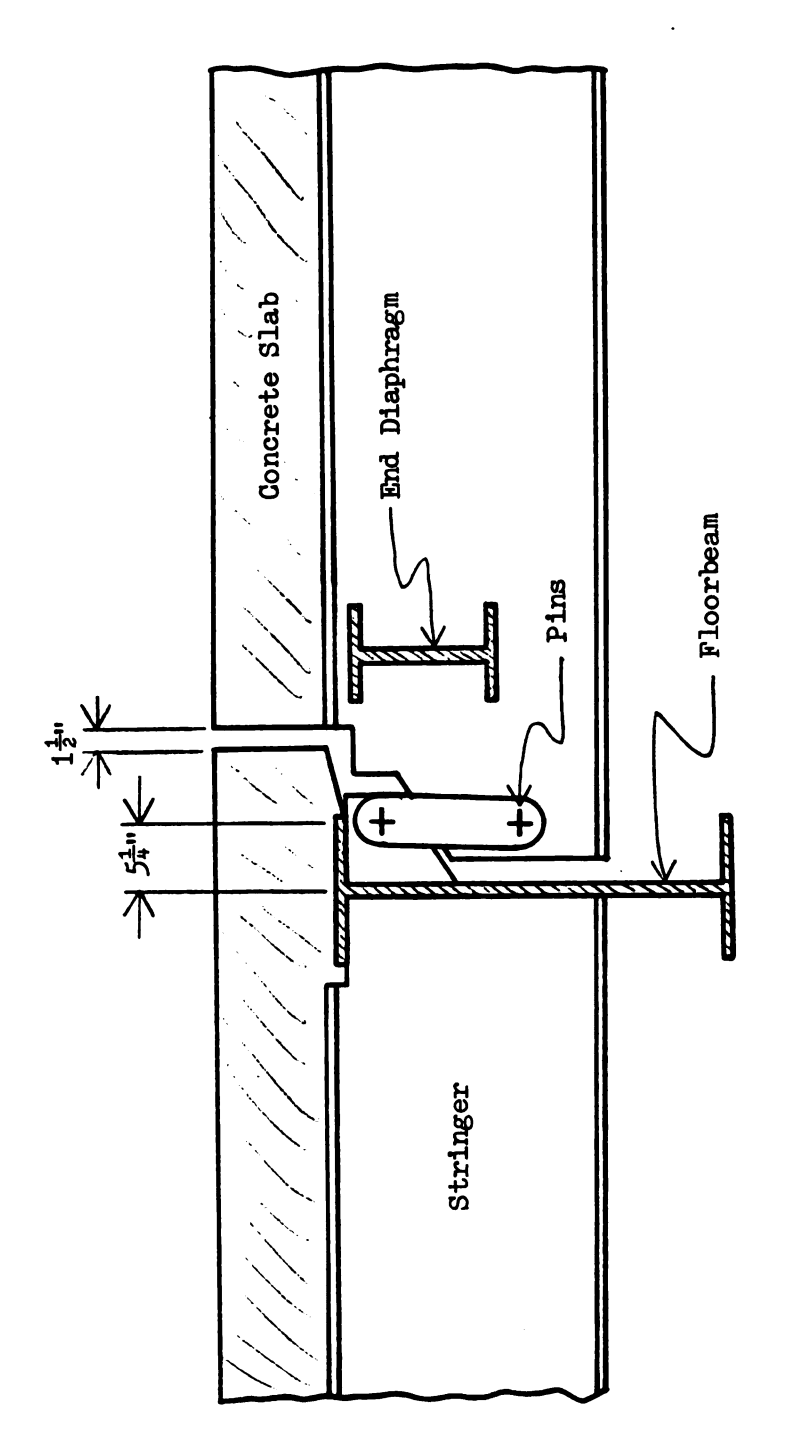


Figure 8 Deck Expansion Joints at F and F'

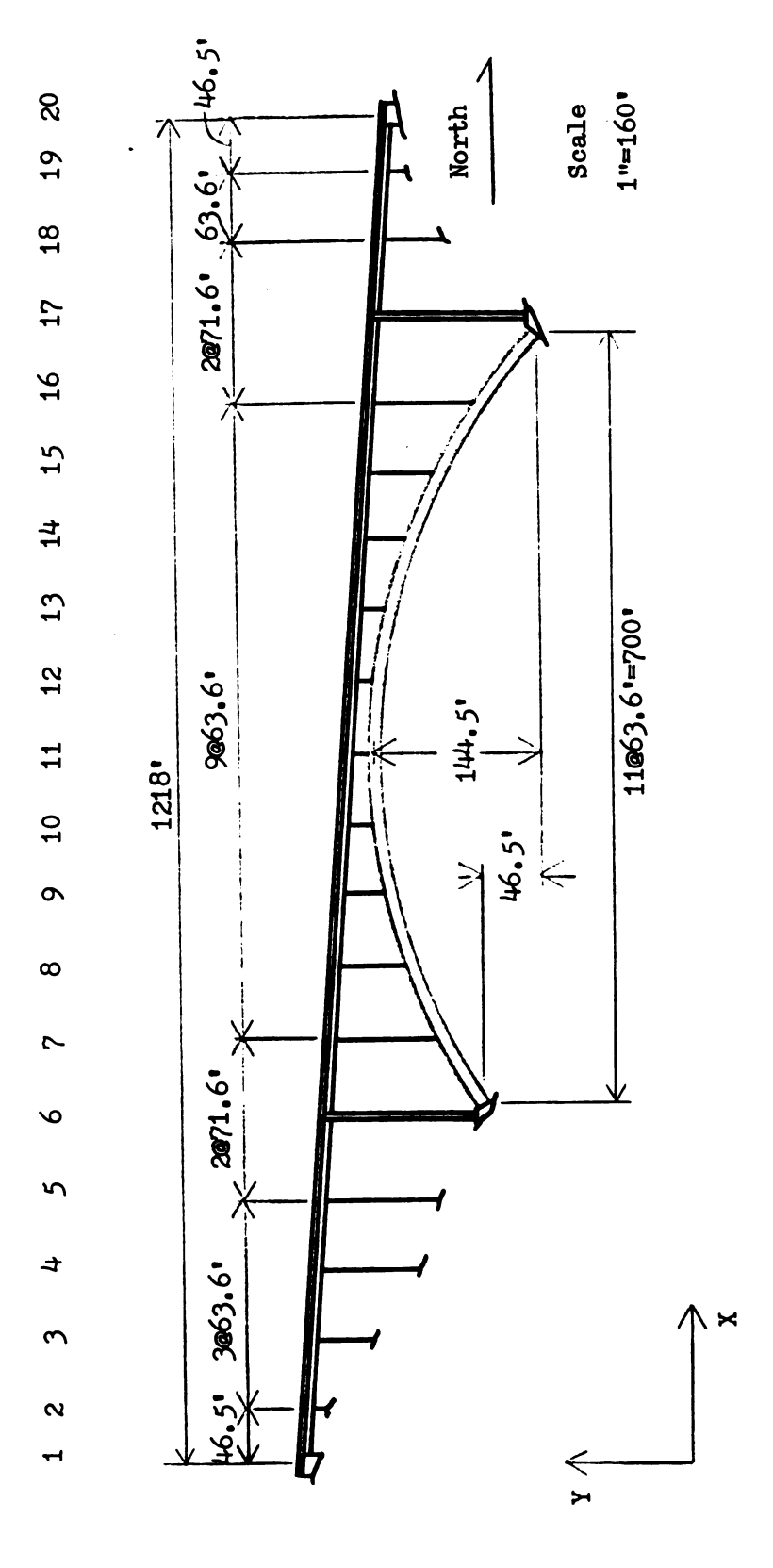


Figure 9 Cold Springs Canyon Bridge Profile

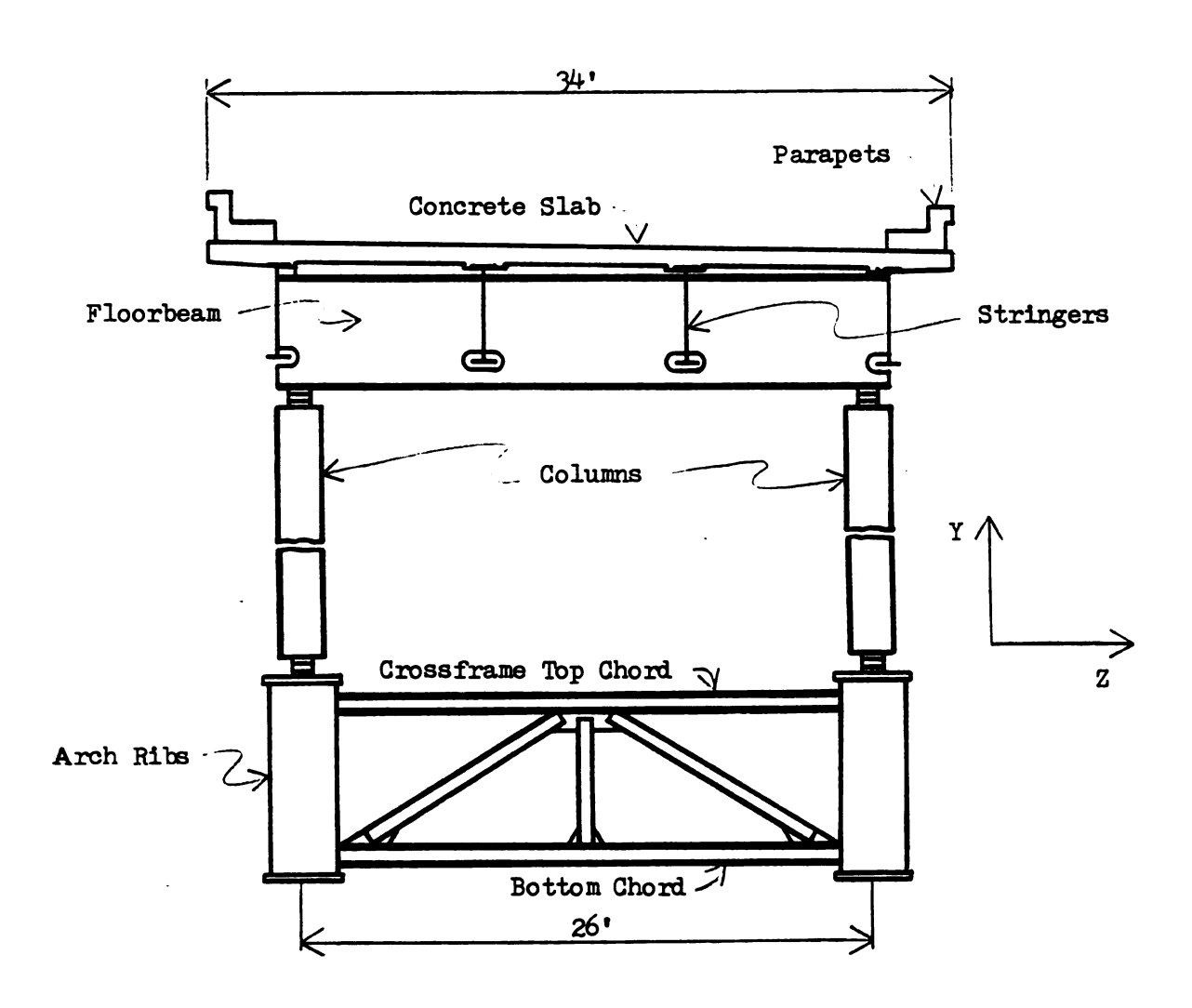


Figure 10 Cold Springs Canyon Bridge Cross-section

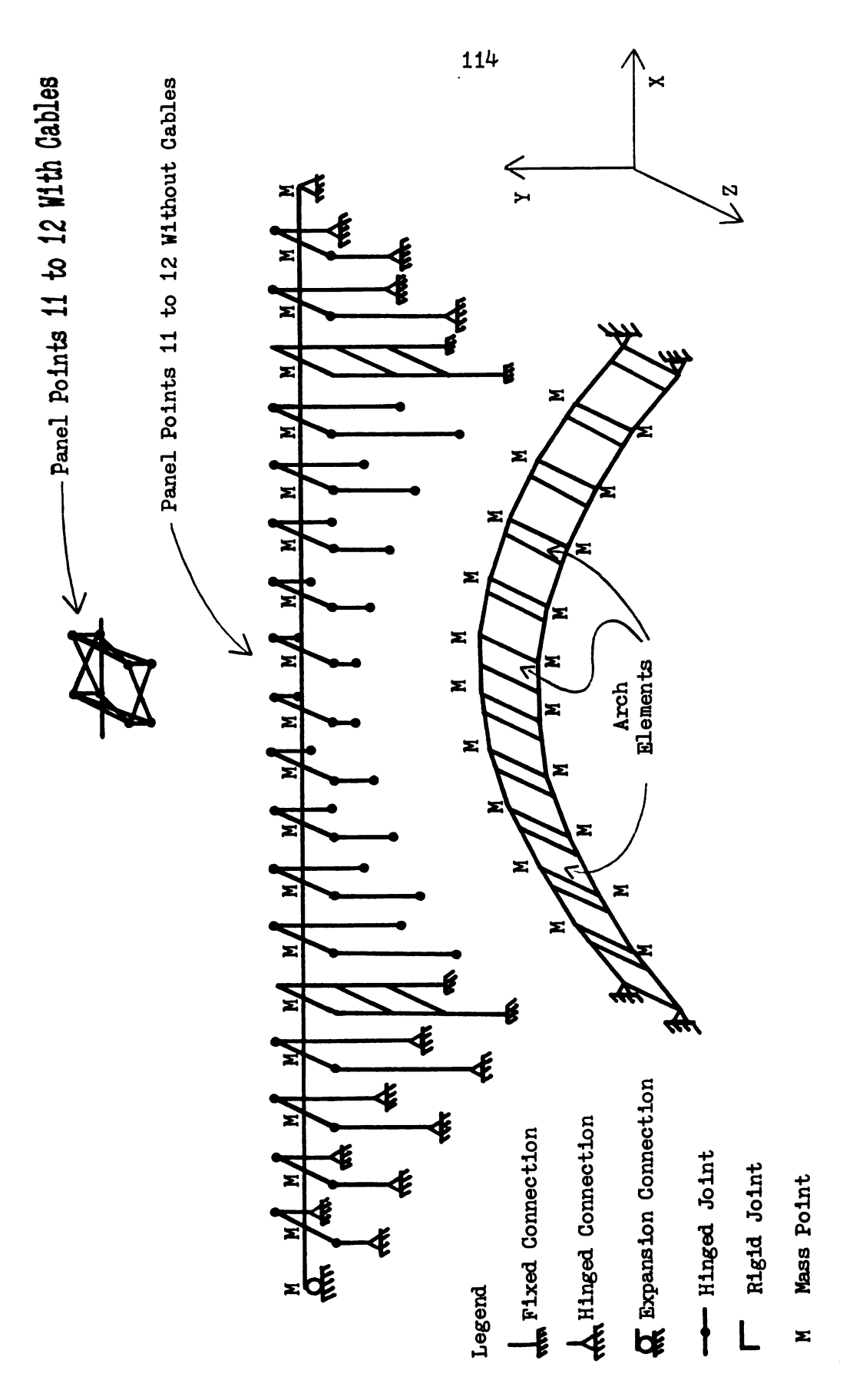


Figure 11 Cold Springs Canyon Bridge Models

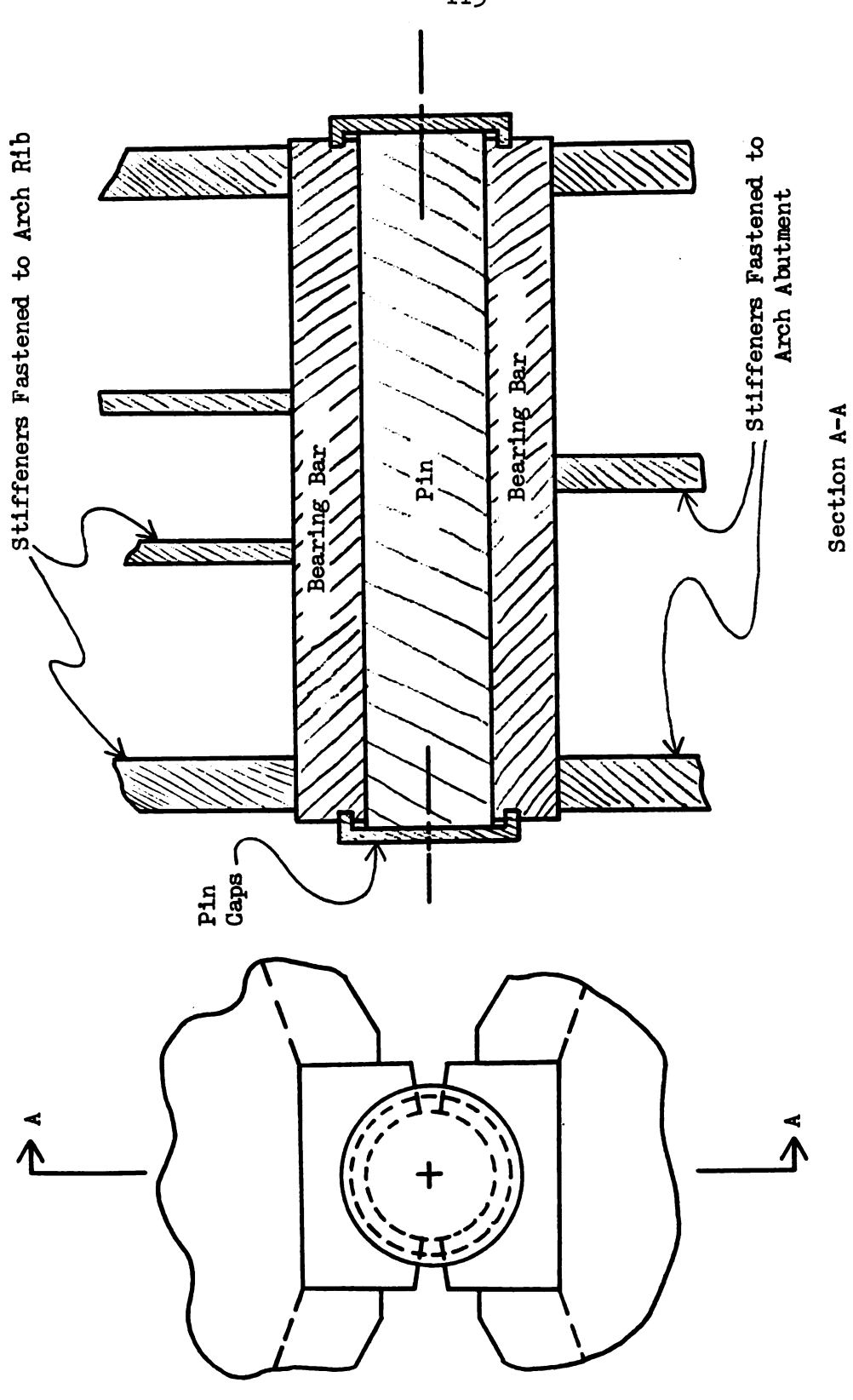


Figure 12 Arch Rib Abutment Connection

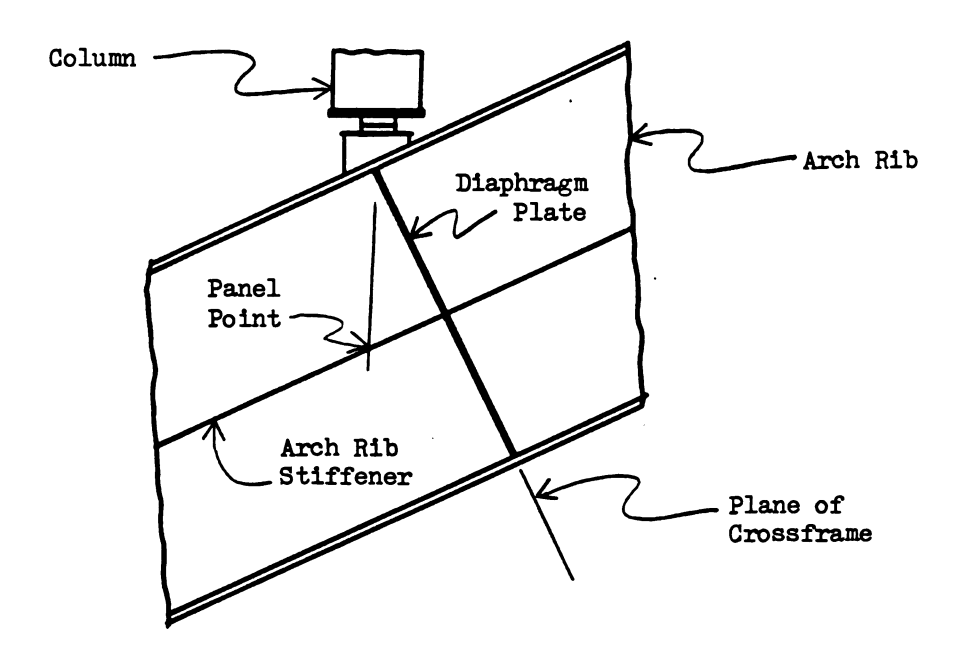


Figure 13 Arch Rib to Column to Crossframe Connection

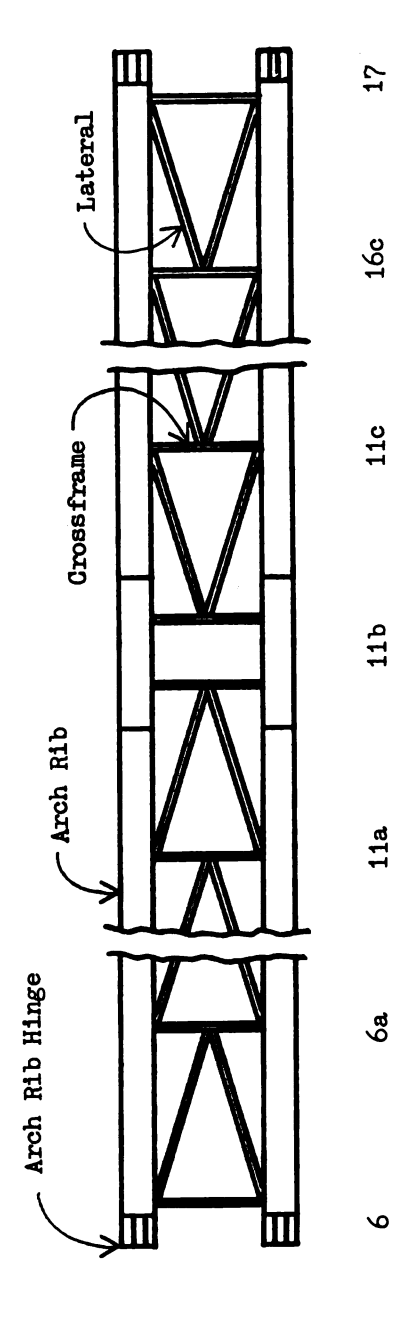
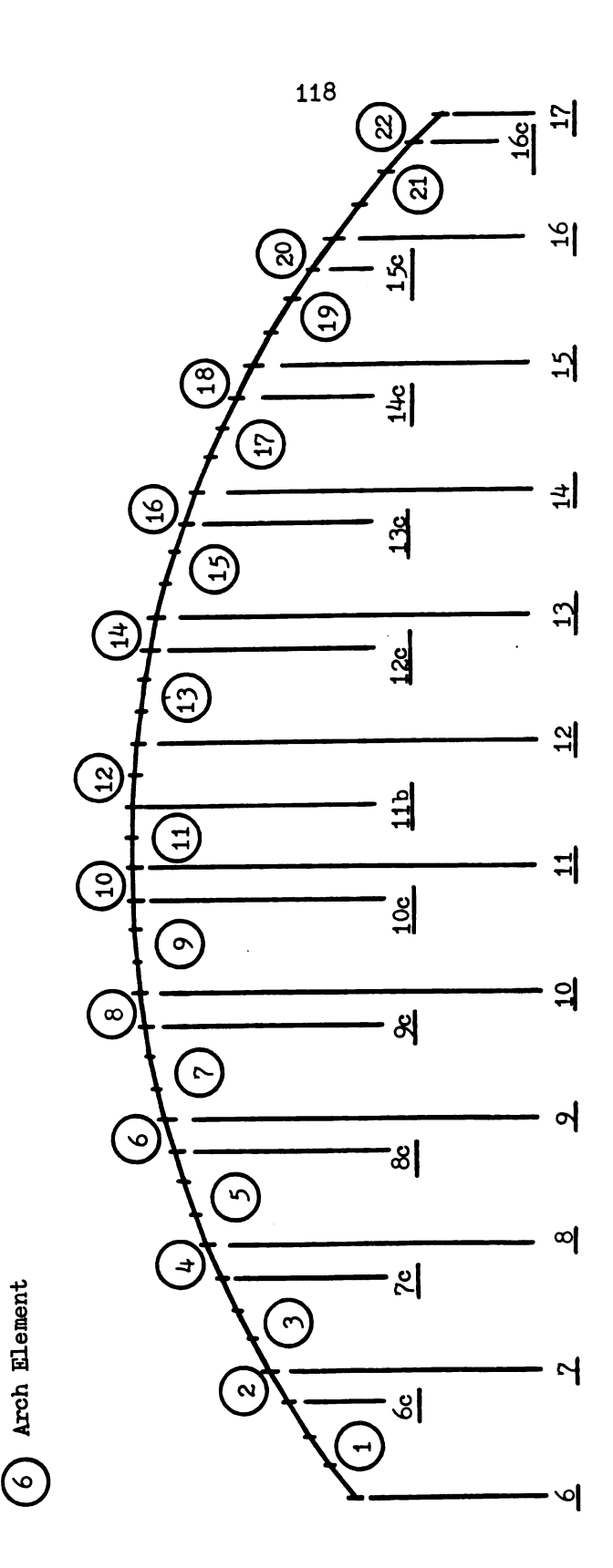


Figure 14 Arch Laterals Plan View



2 Subpanel or Panel Point

Legend

Figure 15 Arch Element Configuration

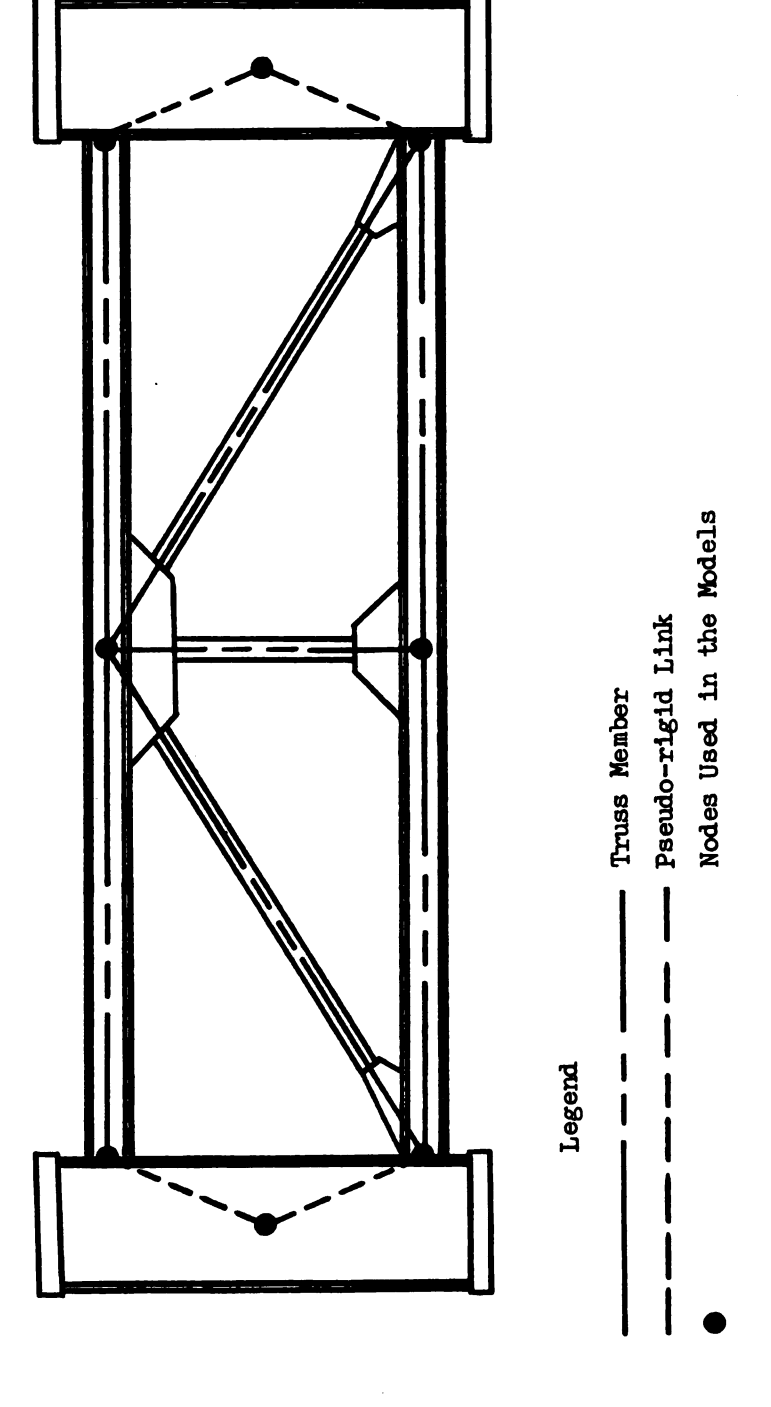


Figure 16 Arch Cross-section as Modeled

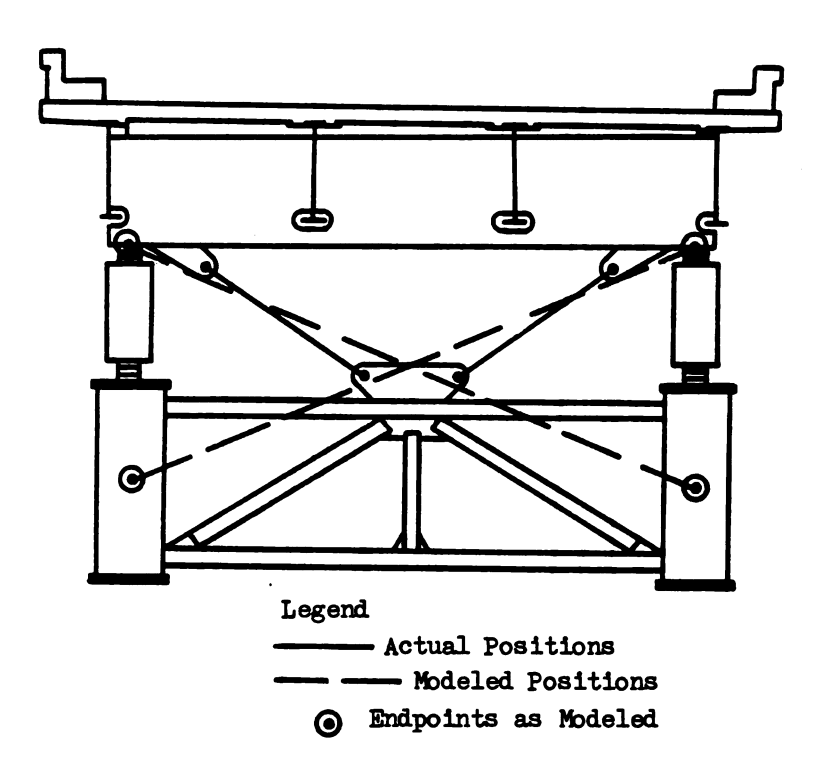
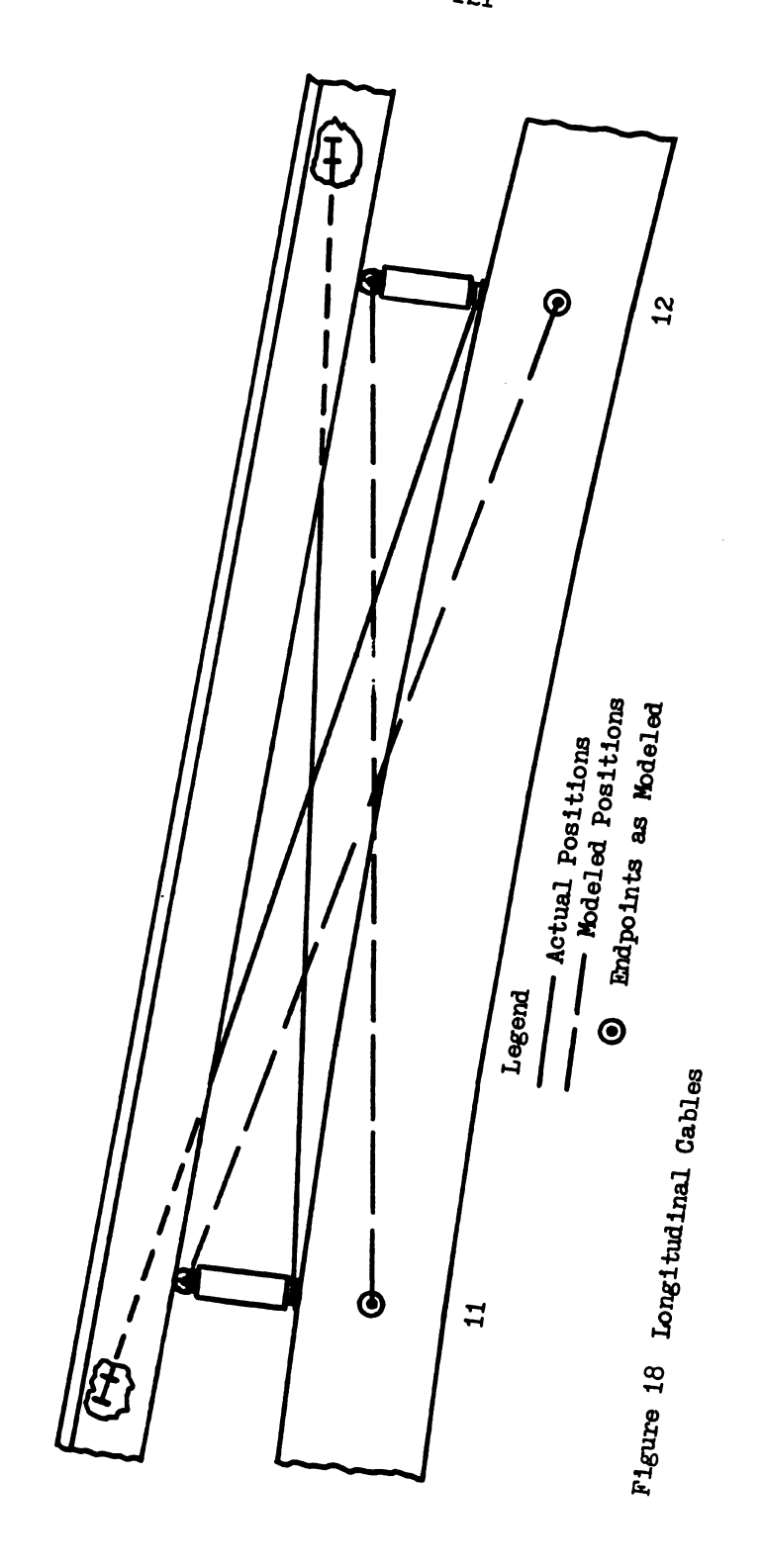


Figure 17 Lateral Cables



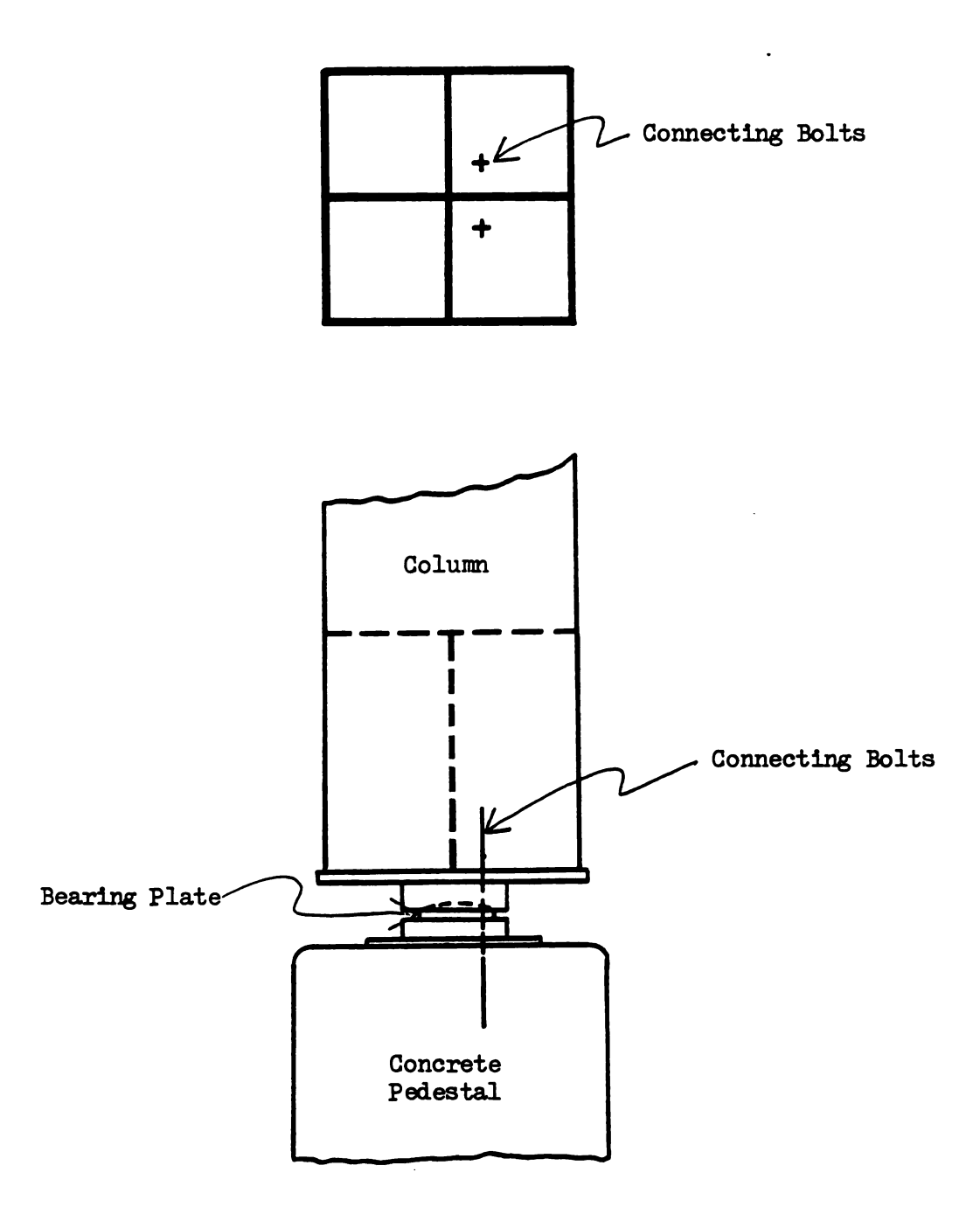


Figure 19 Column Cross-section and Pedestal Connection

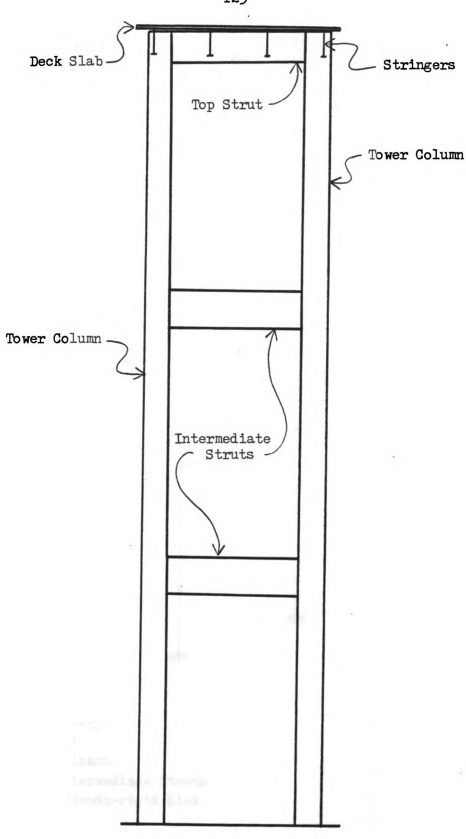
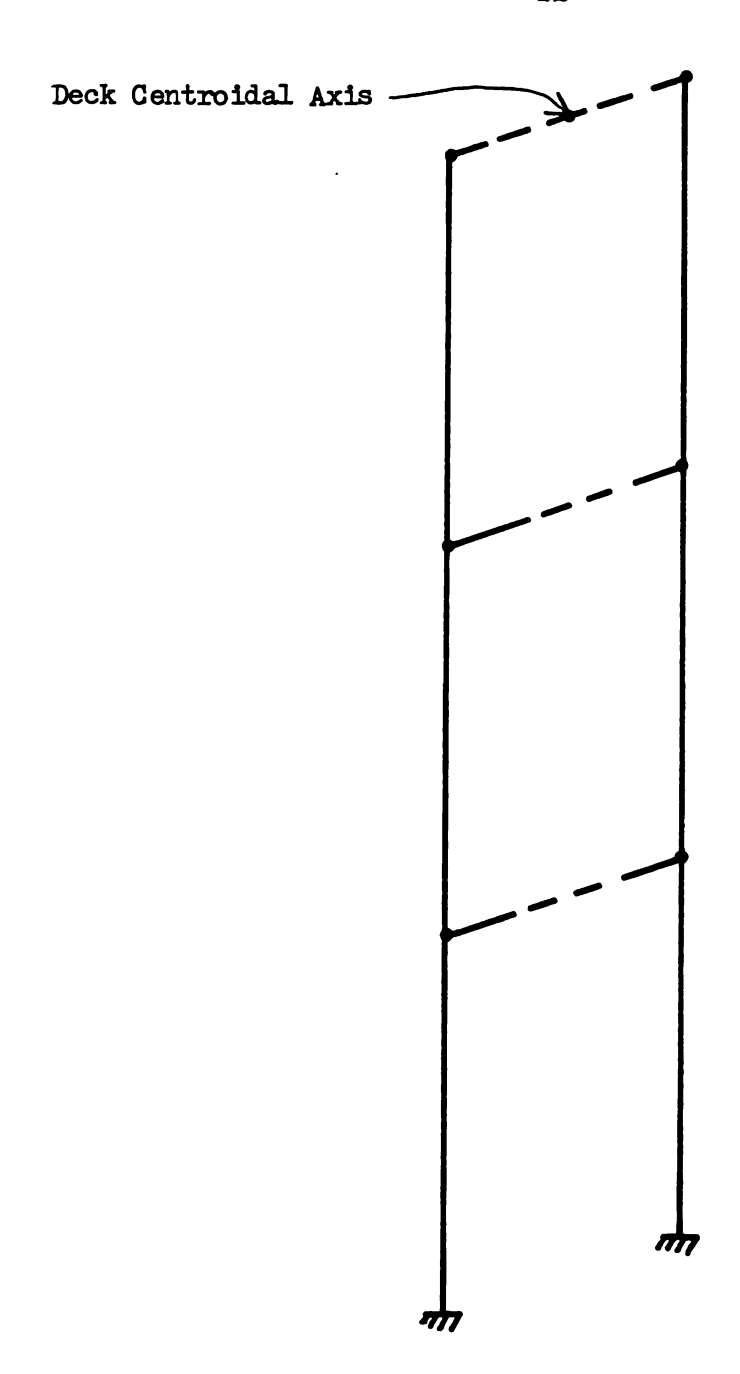


Figure 20 Tower Elevation View



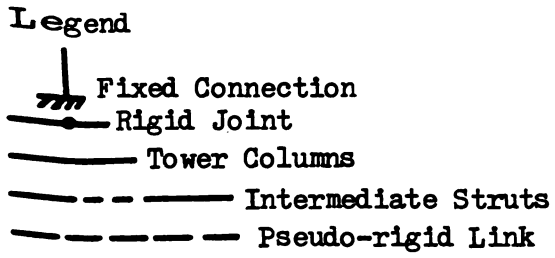


Figure 21 Tower Model

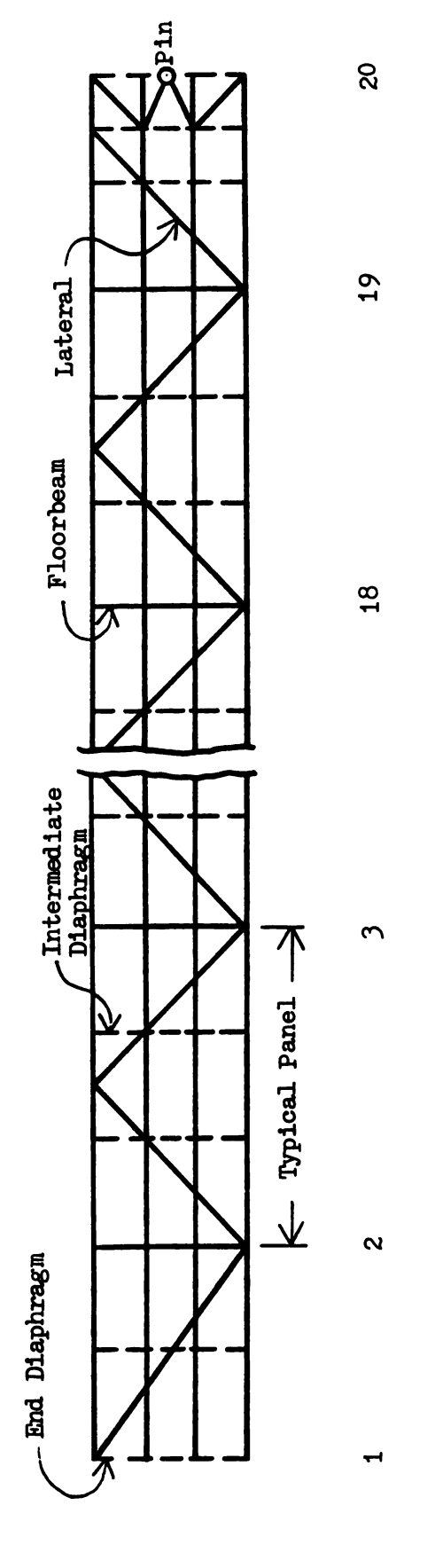


Figure 22 Deck Laterals

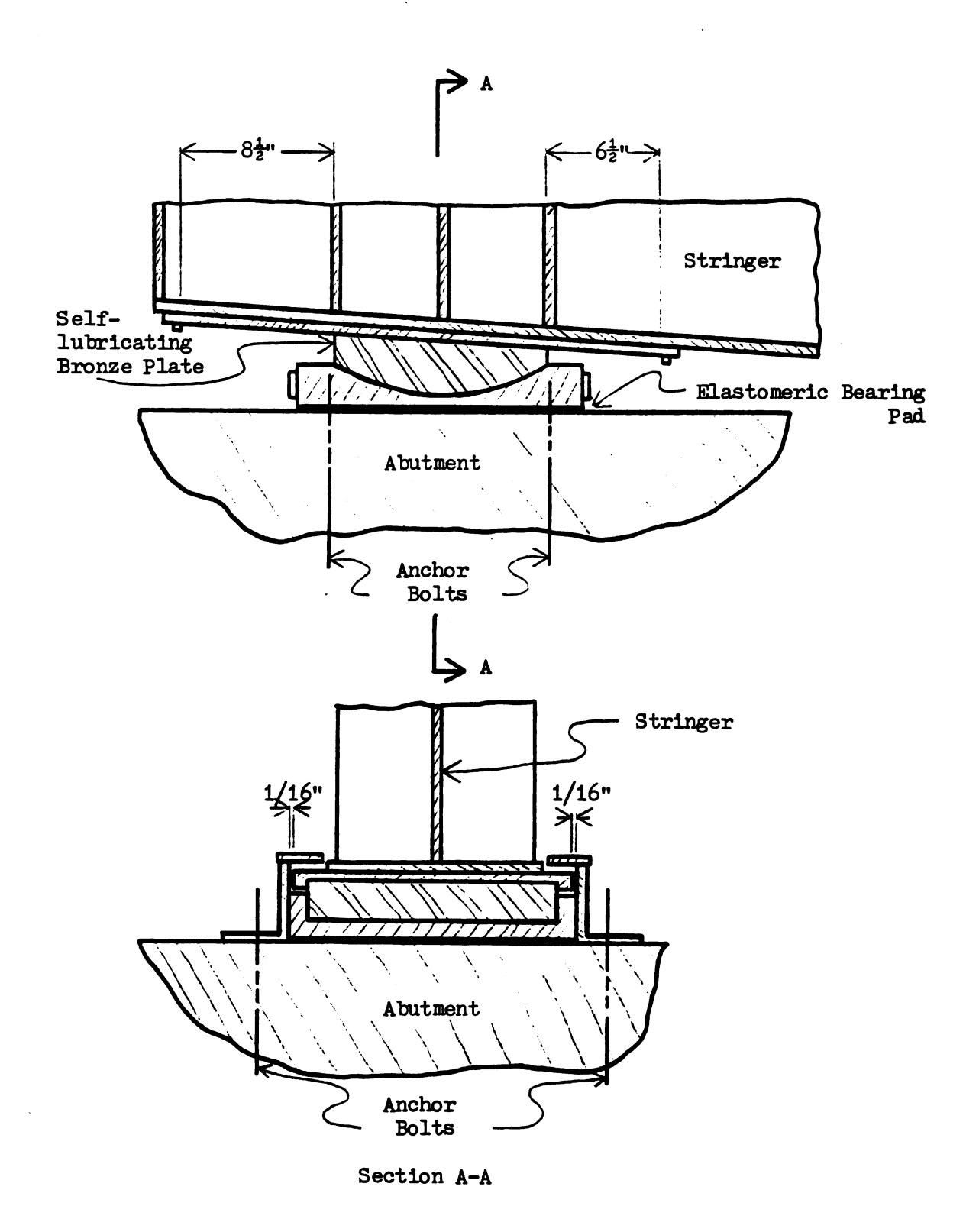
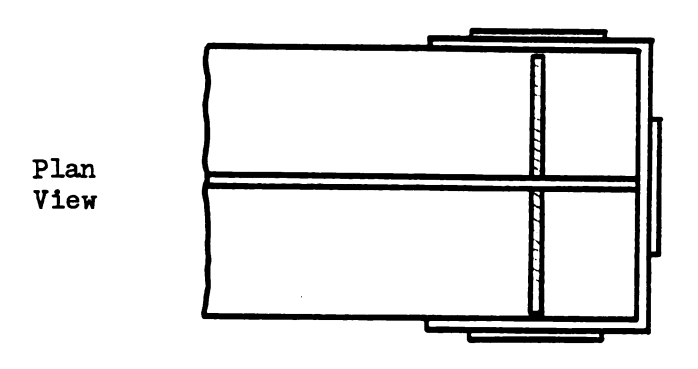


Figure 23 Deck Expansion Connections at Panel Point 1



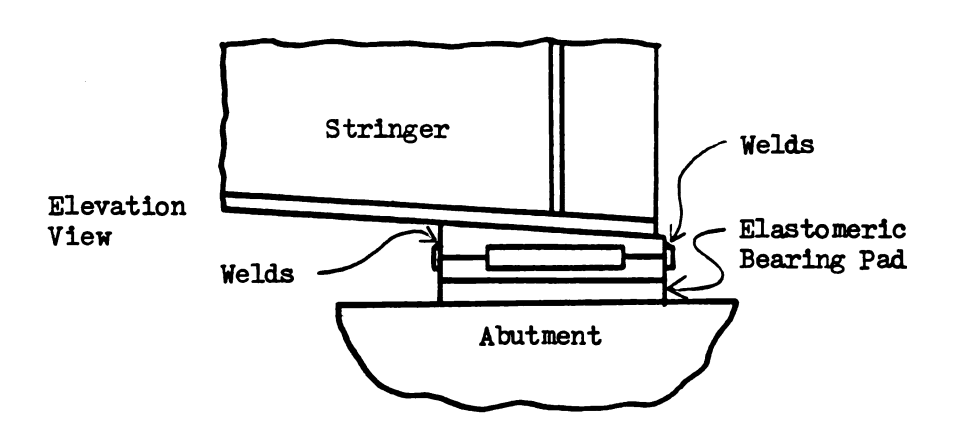


Figure 24 Deck Bearing Connections at Panel Point 20



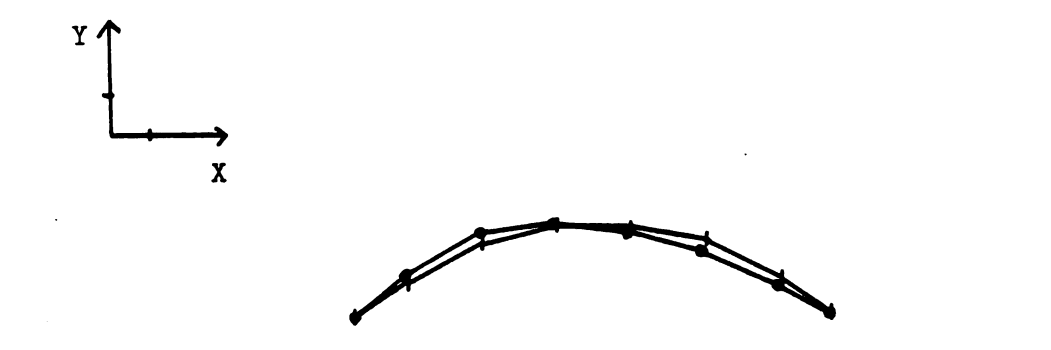


Figure 25 SSB Mode 1



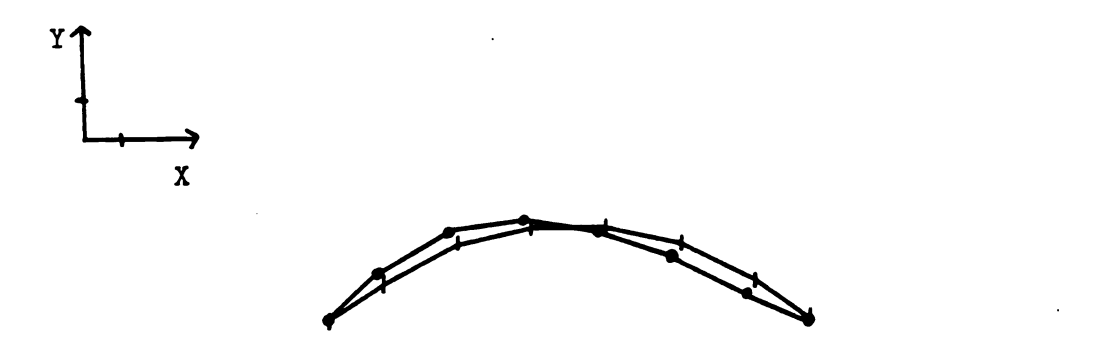


Figure 26 SSB Mode 2

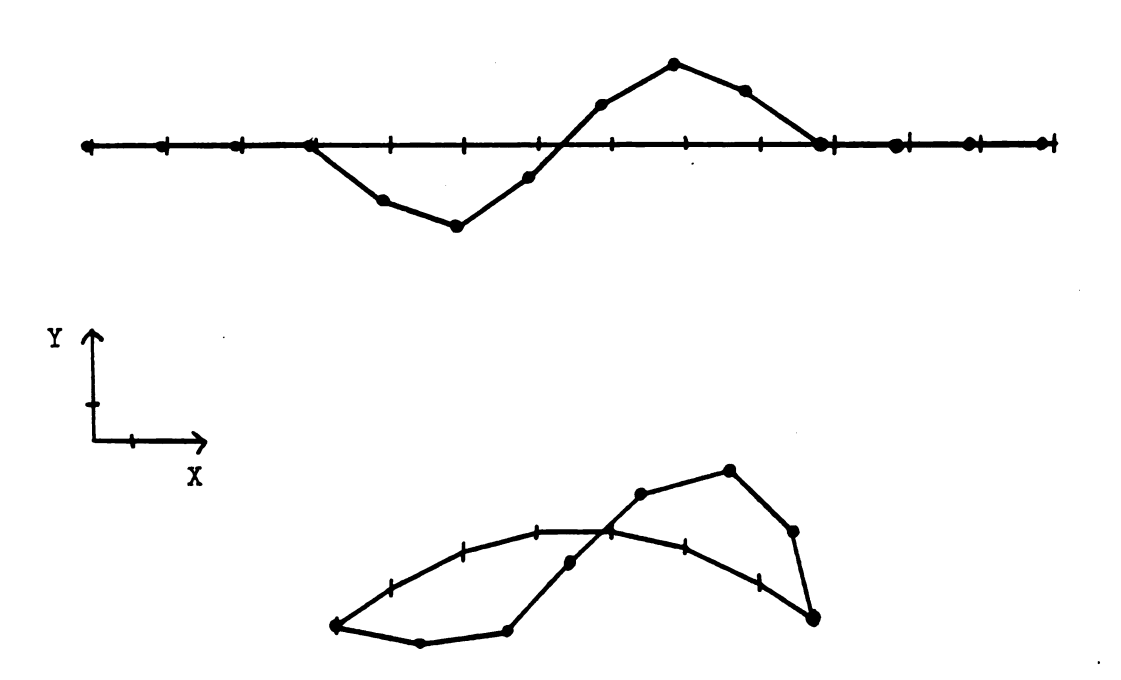


Figure 27 SSB Mode 3

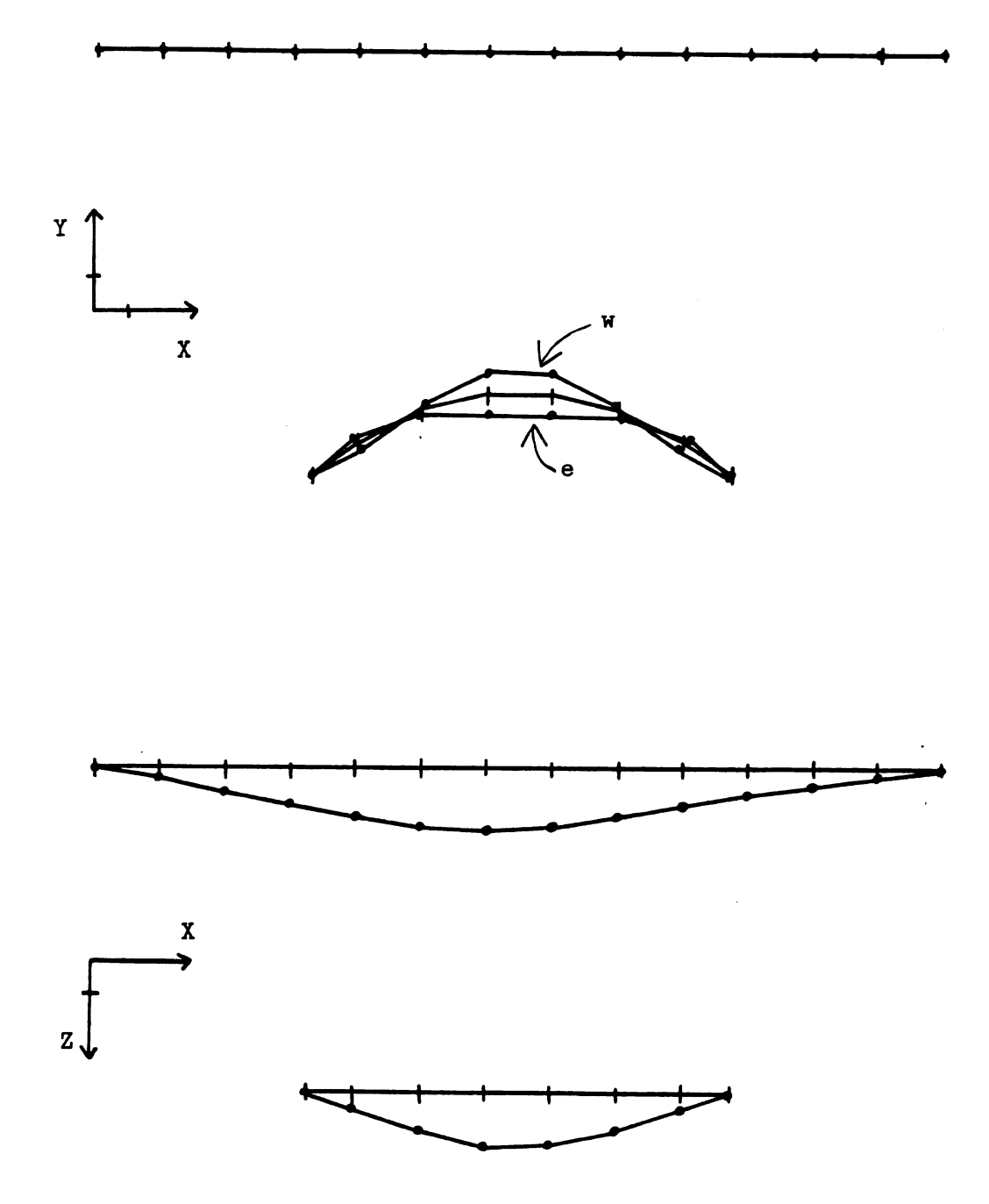


Figure 28 SSB Mode 4

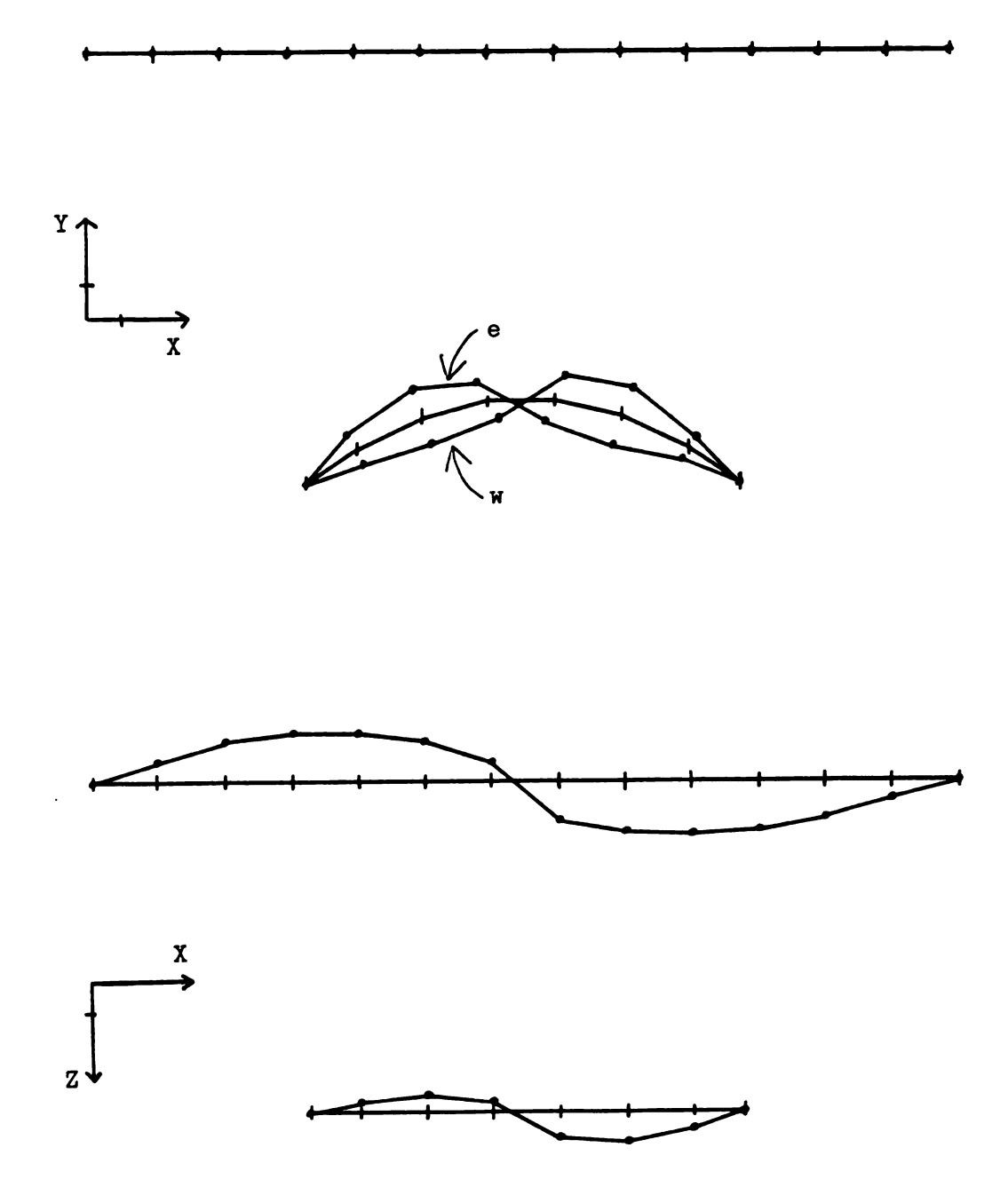


Figure 29 SSB Mode 5

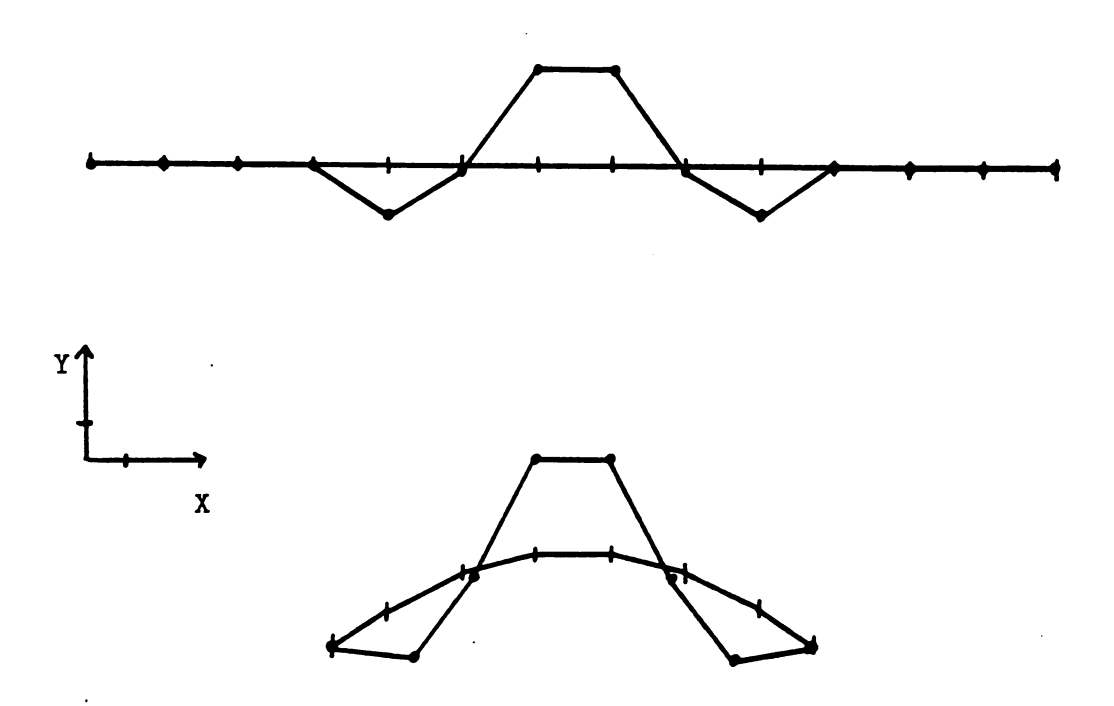


Figure 30 SSB Mode 6

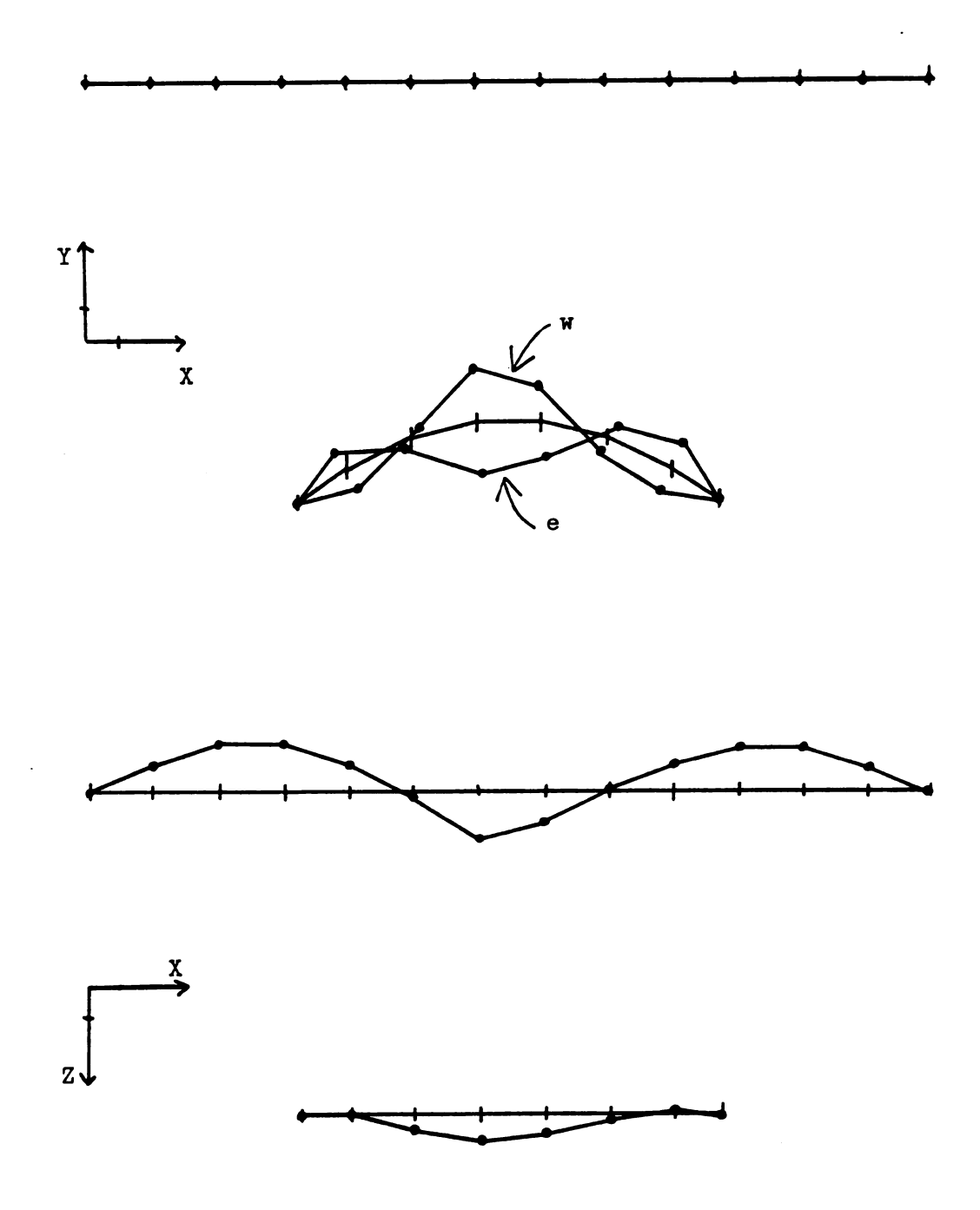


Figure 31 SSB Mode 7

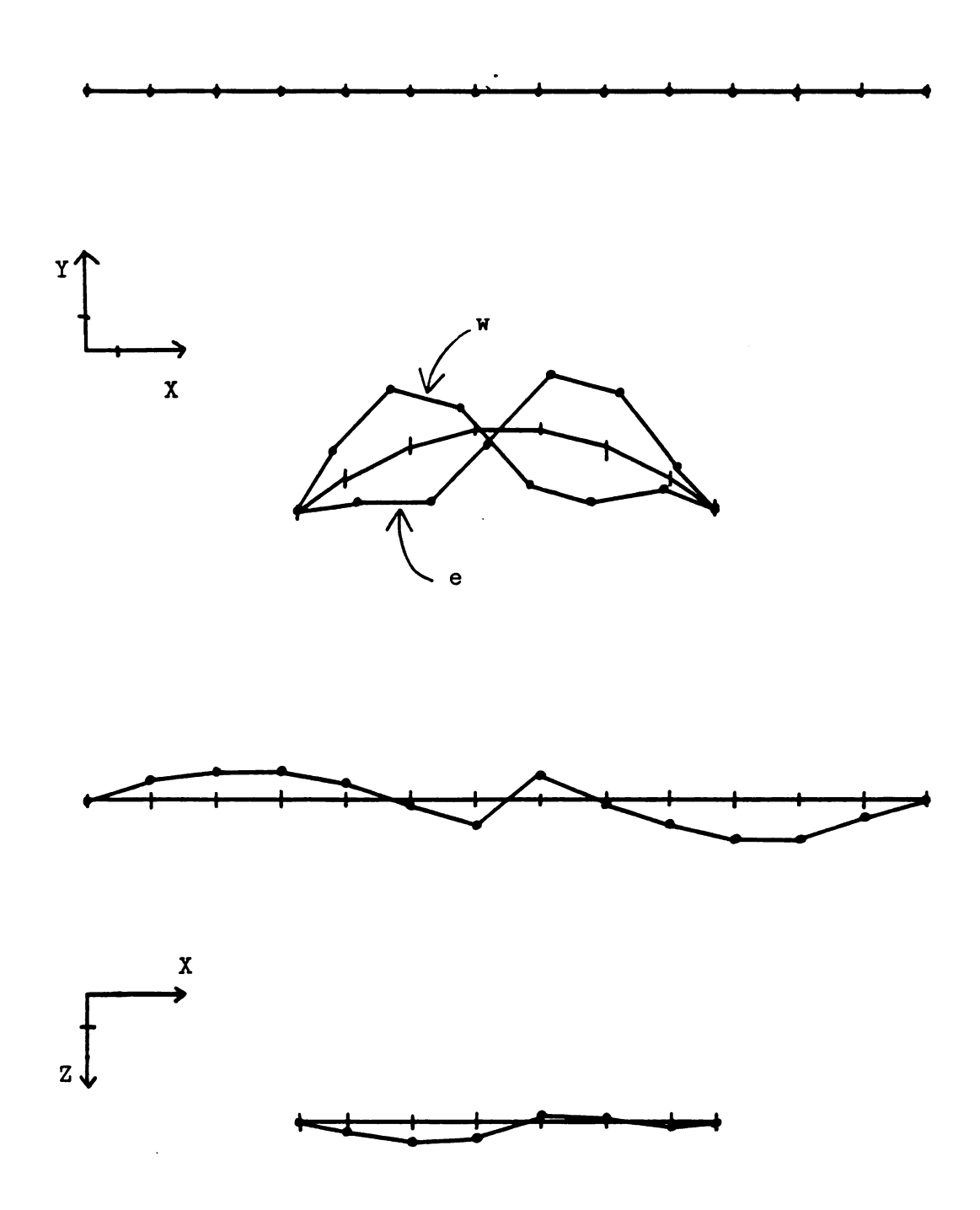


Figure 32 SSB Mode 8

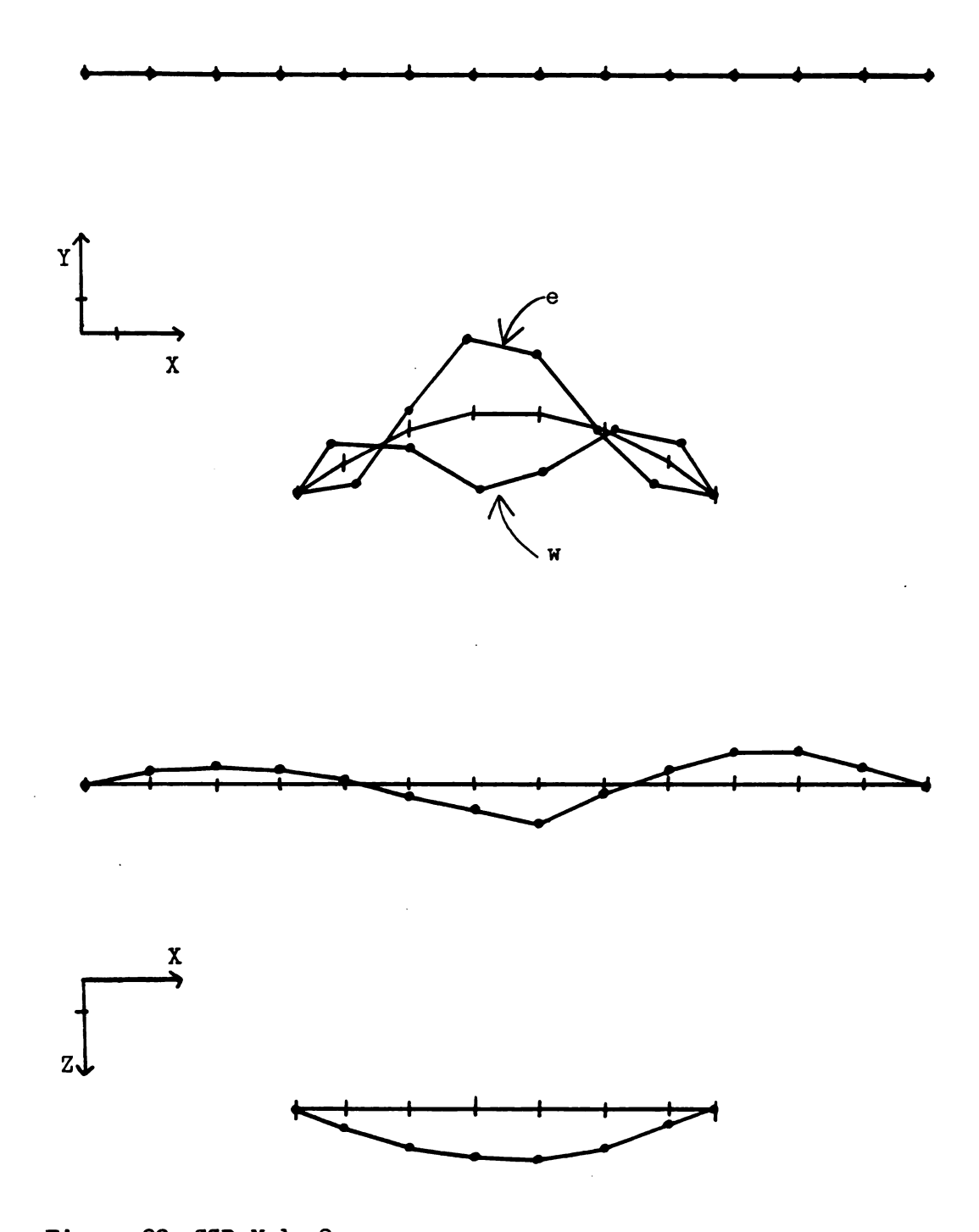


Figure 33 SSB Mode 9

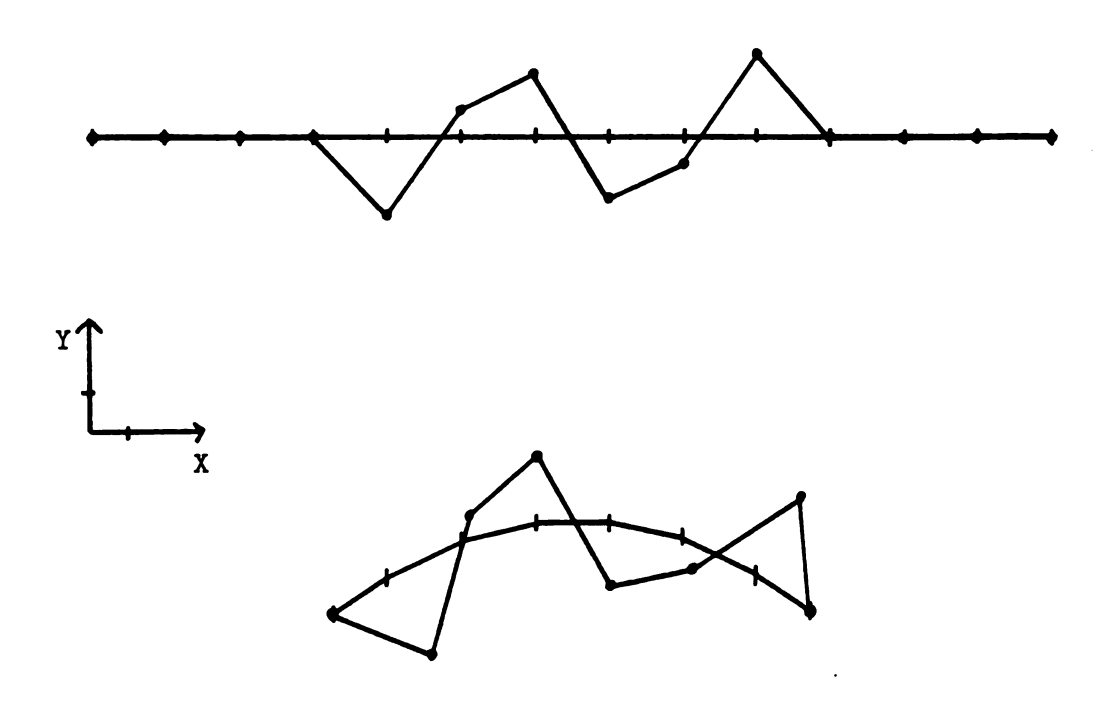


Figure 34 SSB Mode 10

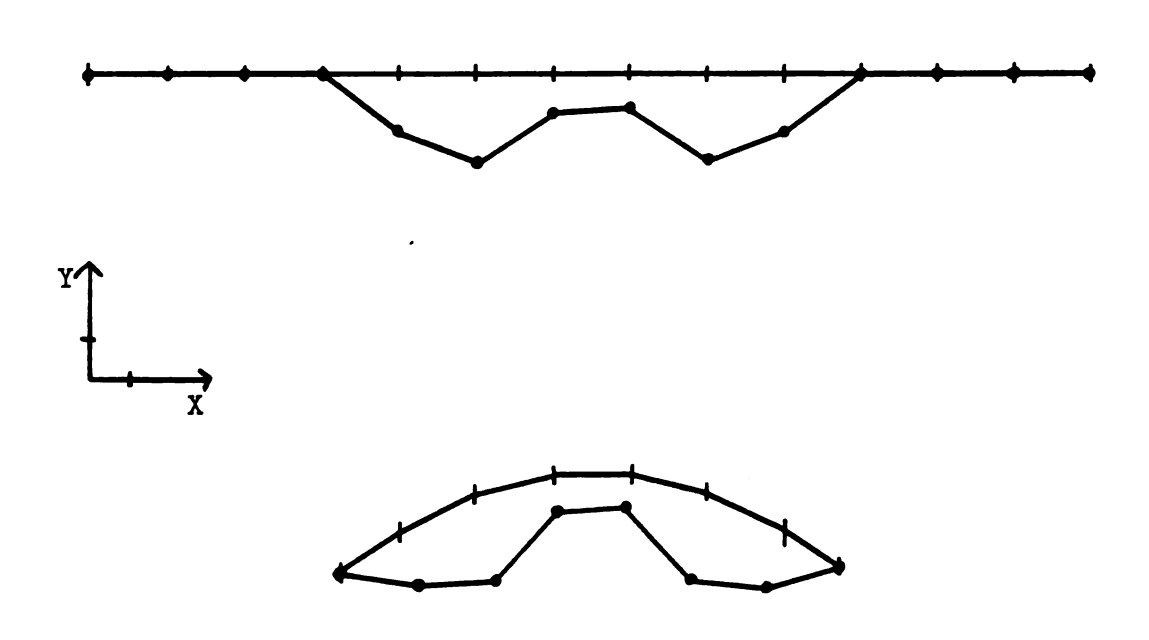


Figure 35 SSB Mode 11

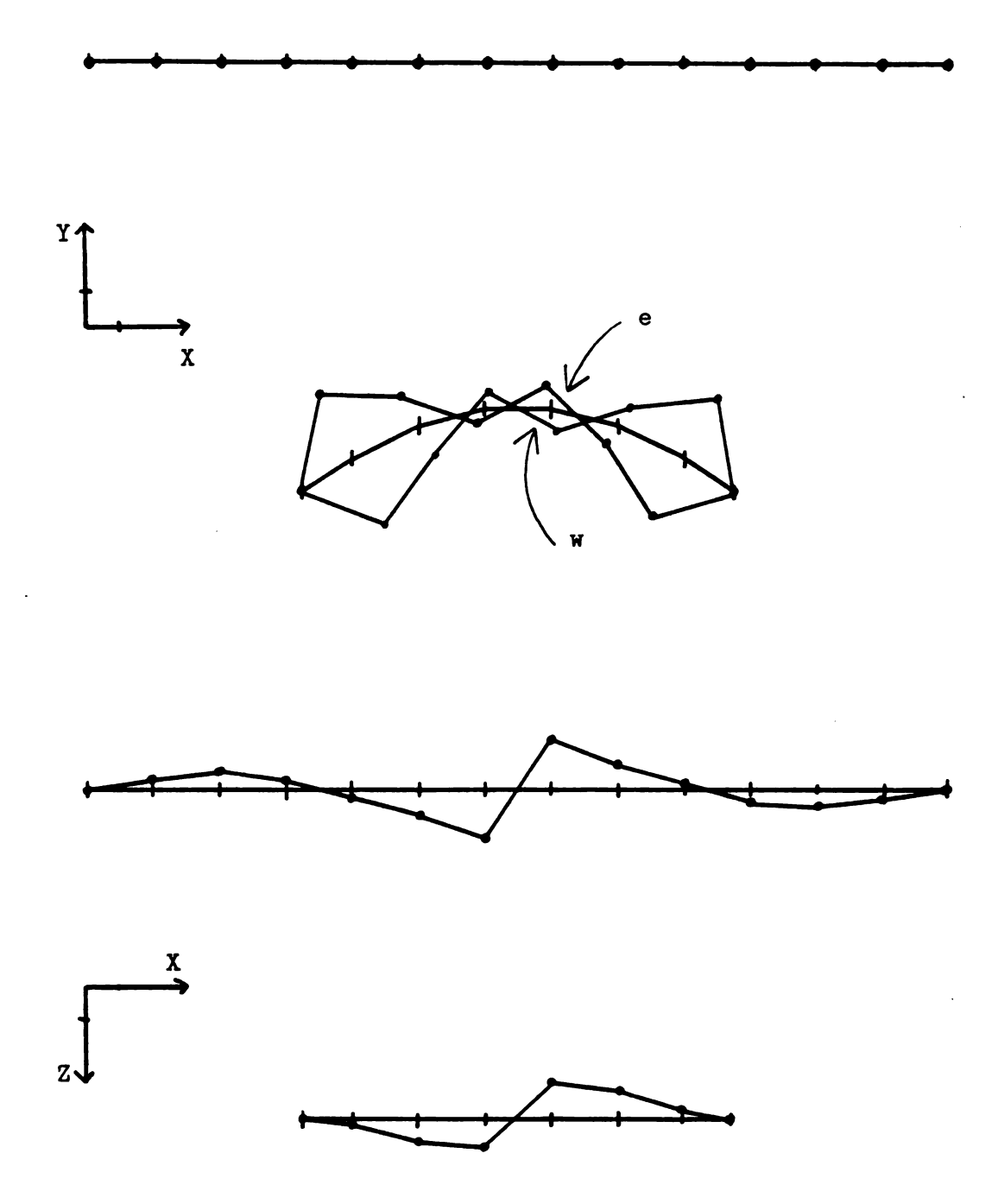


Figure 36 SSB Mode 12

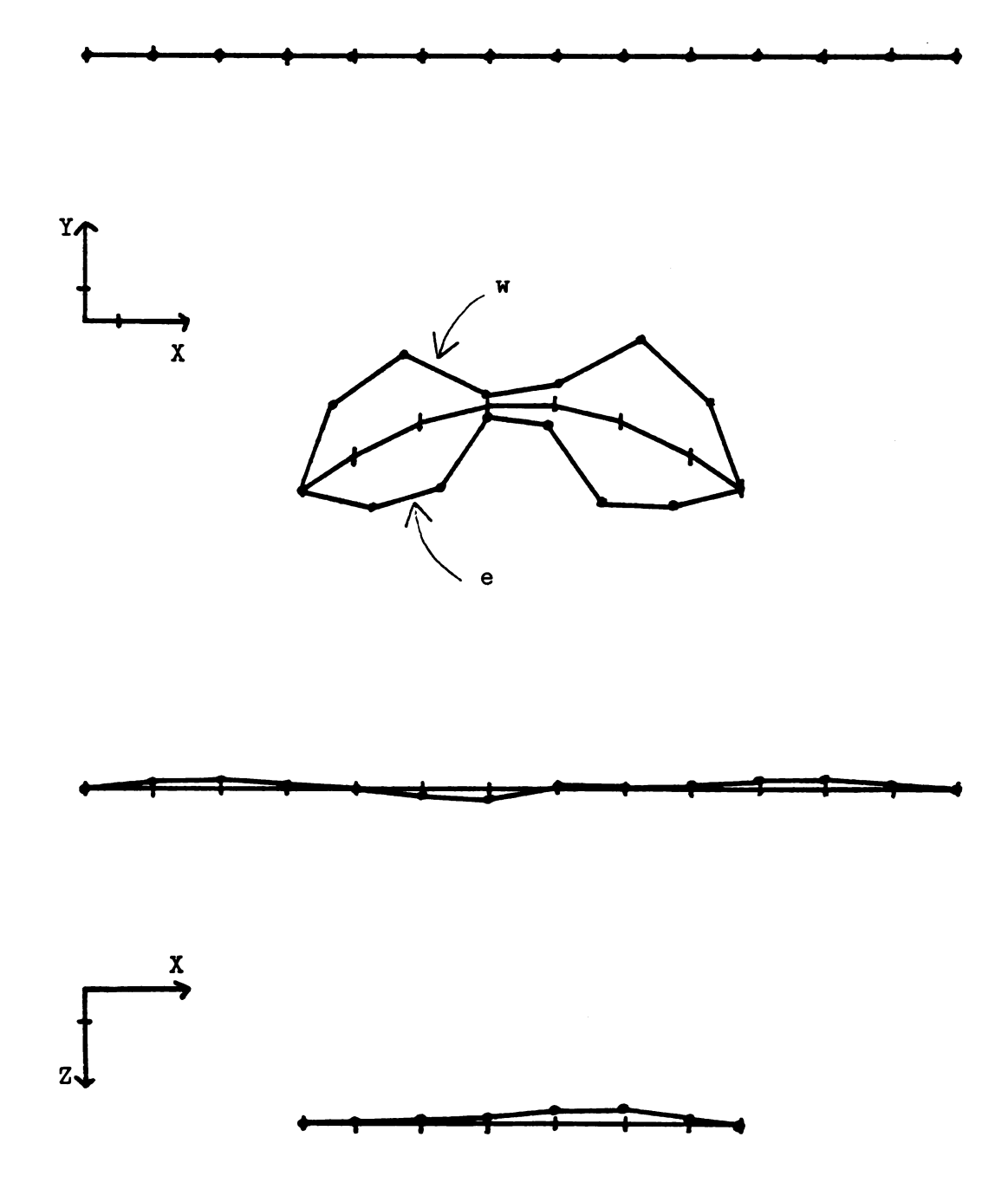


Figure 37 SSB Mode 13



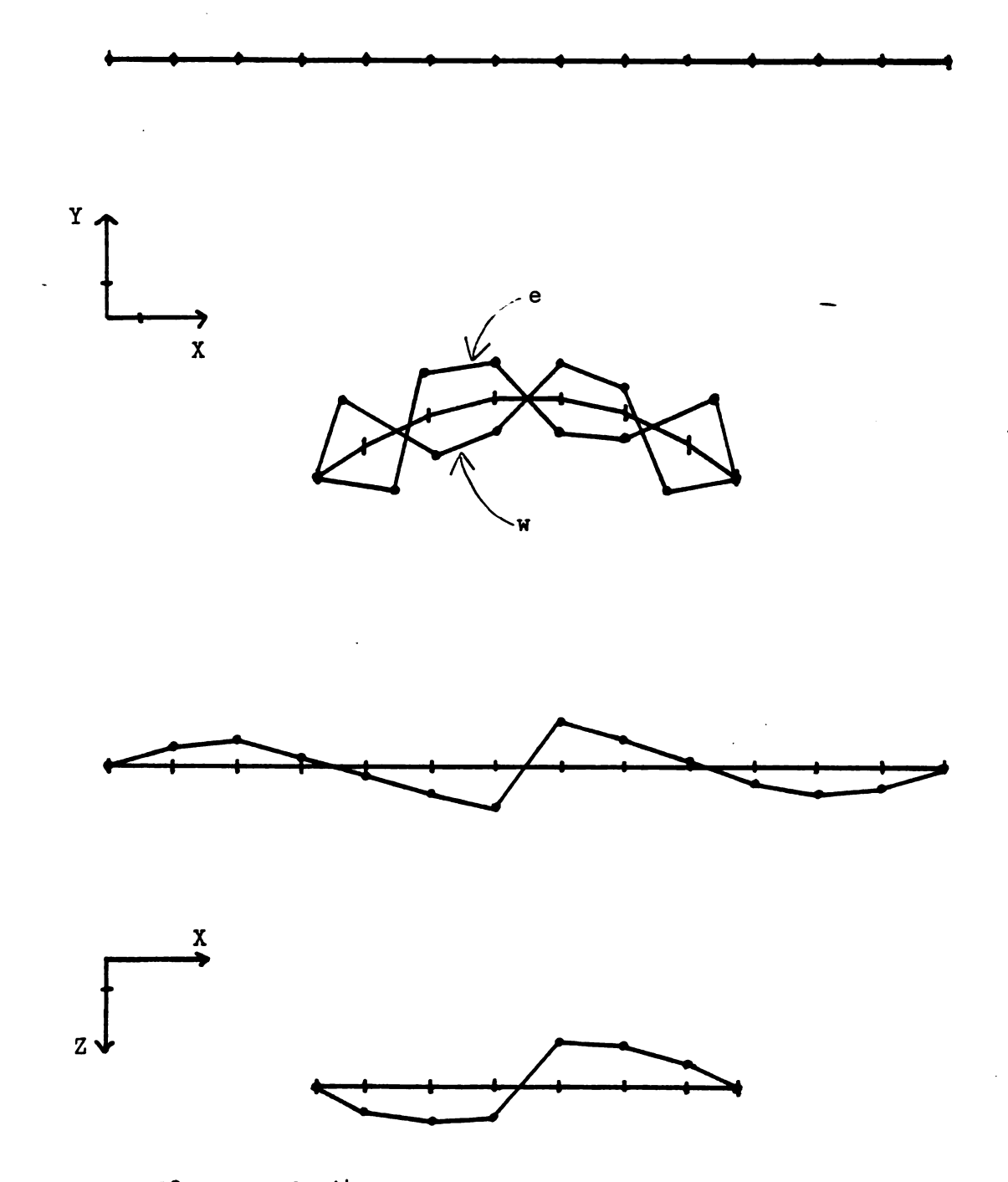


Figure 38 SSB Mode 14

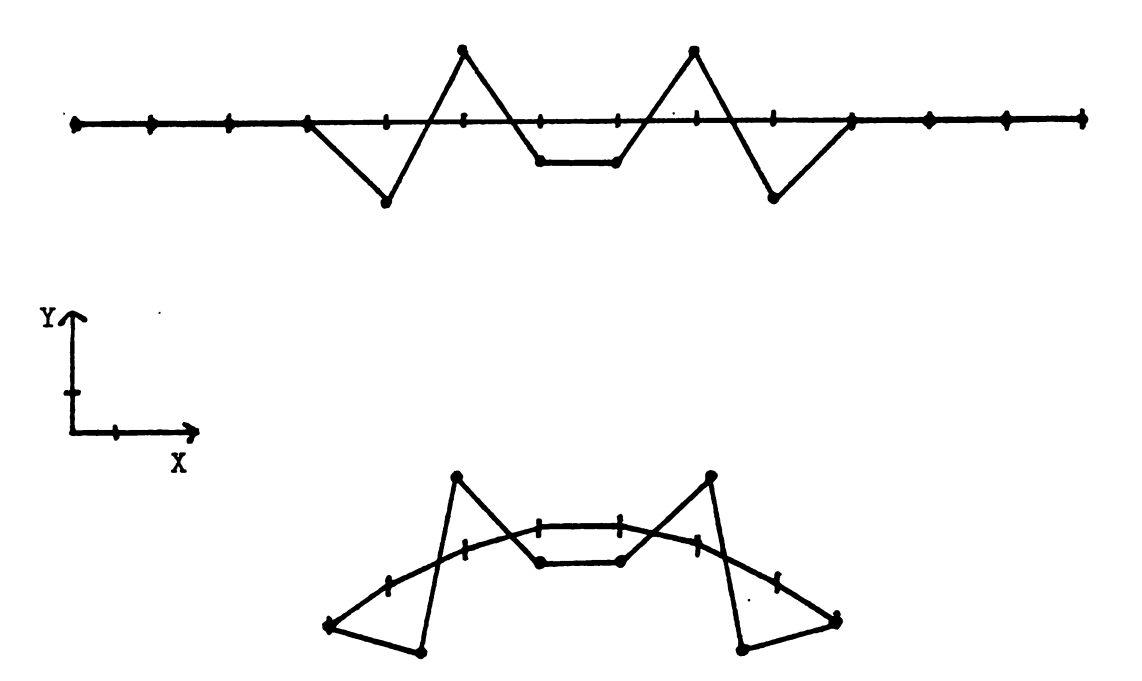


Figure 39 SSB Mode 15

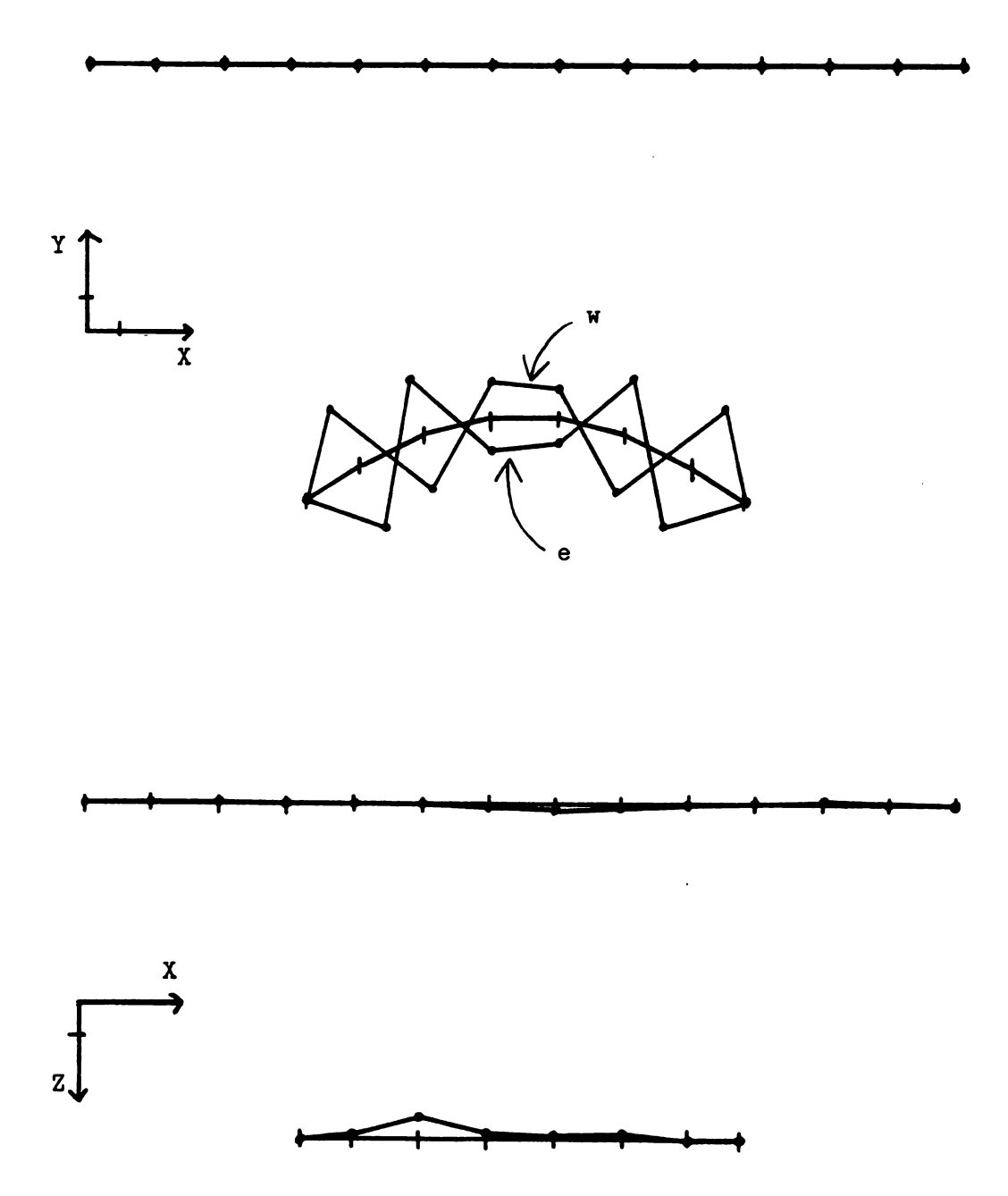


Figure 40 SSB Mode 16

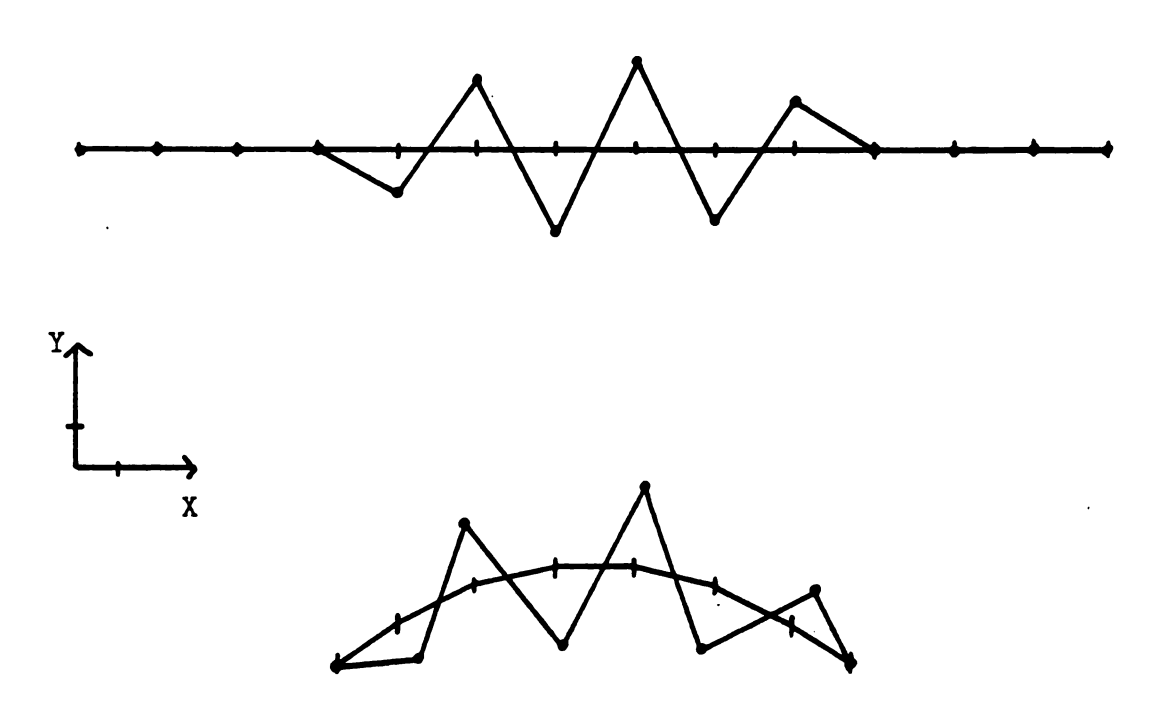


Figure 41 SSB Mode 17

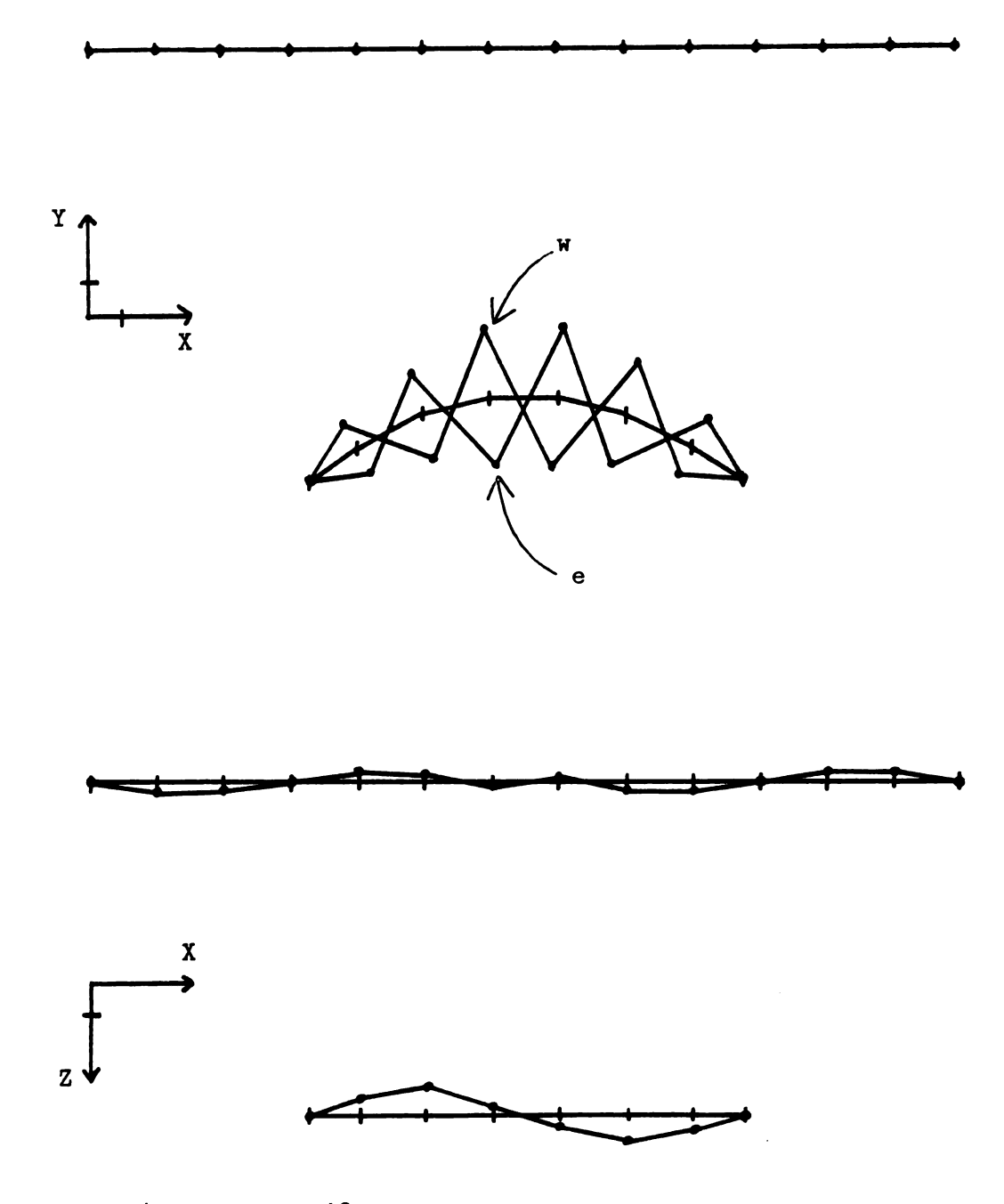


Figure 42 SSB Mode 18

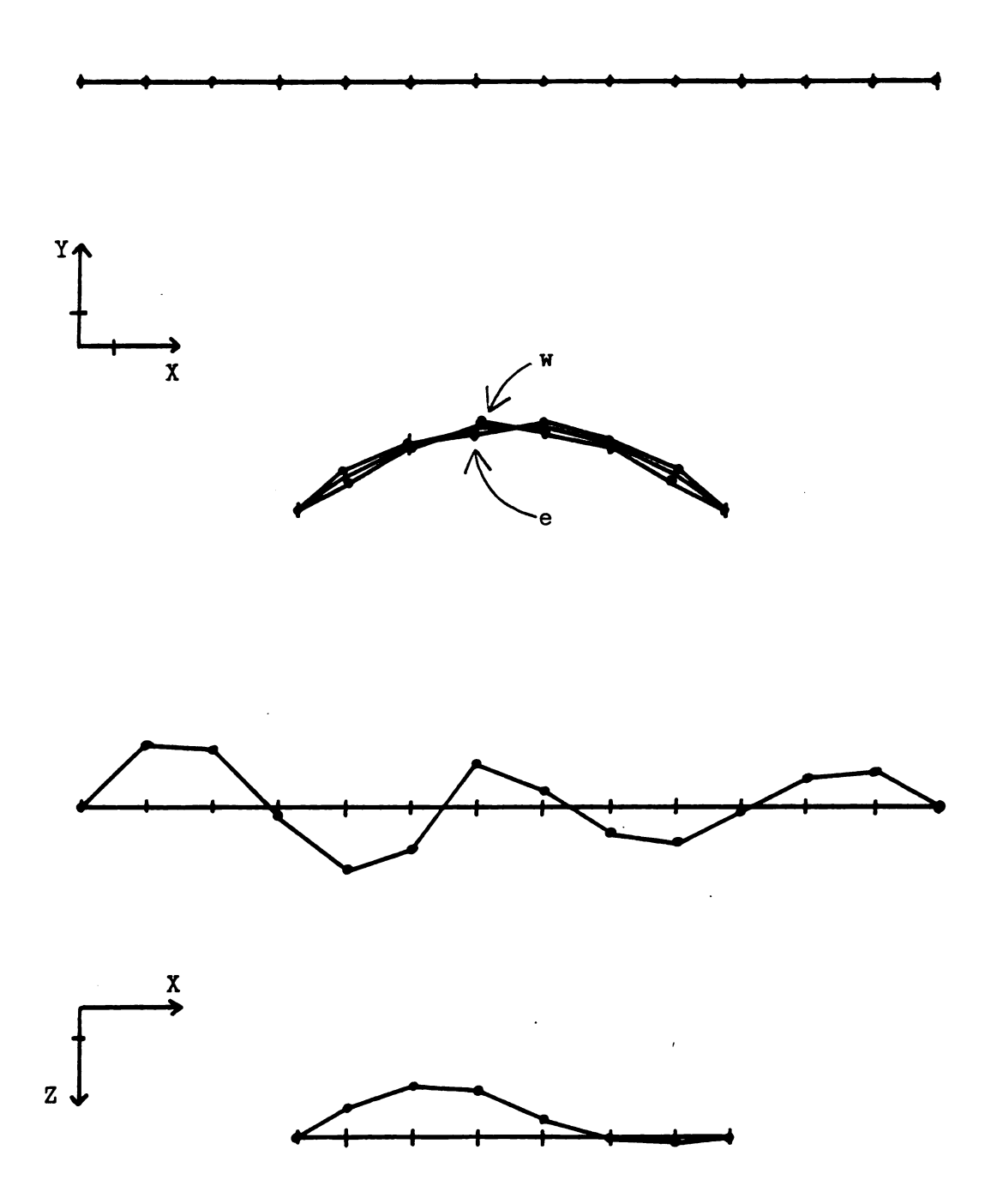


Figure 43 SSB Mode 19

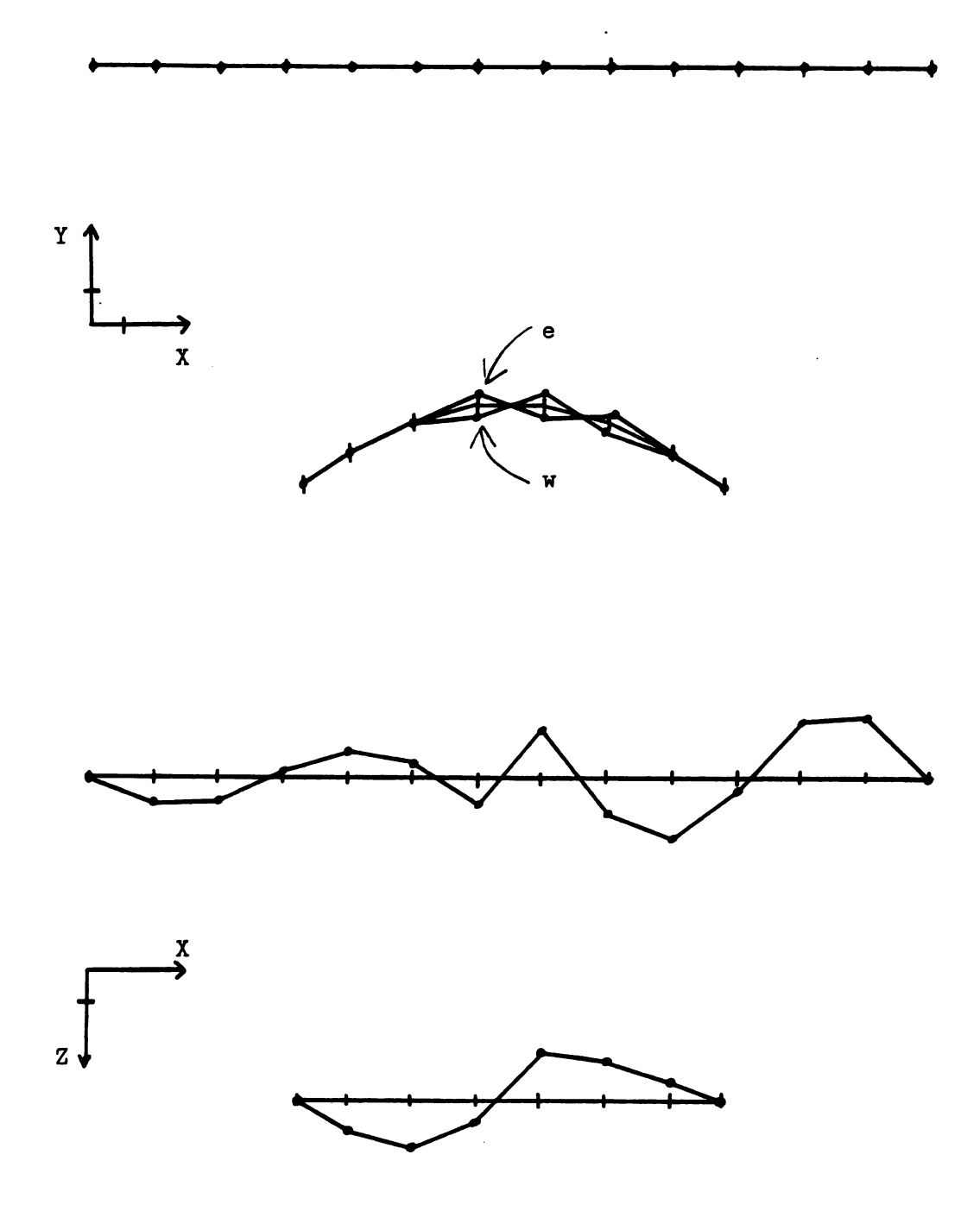
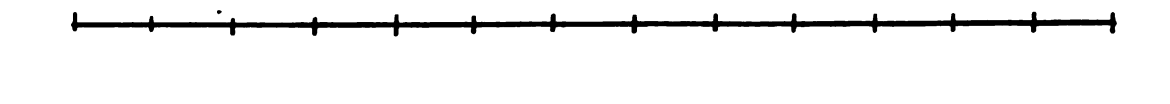
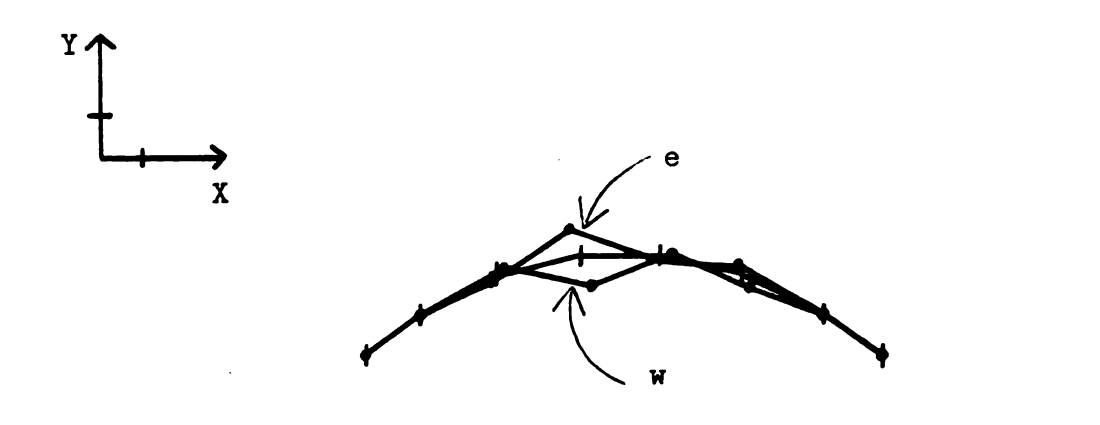


Figure 44 SSB Mode 20





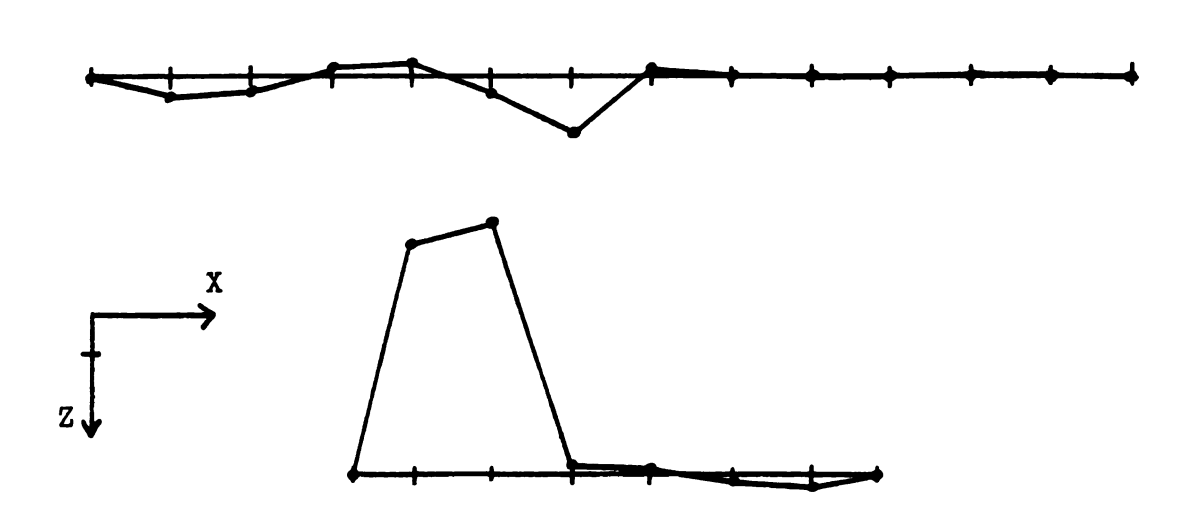


Figure 45 SSB Mode 21

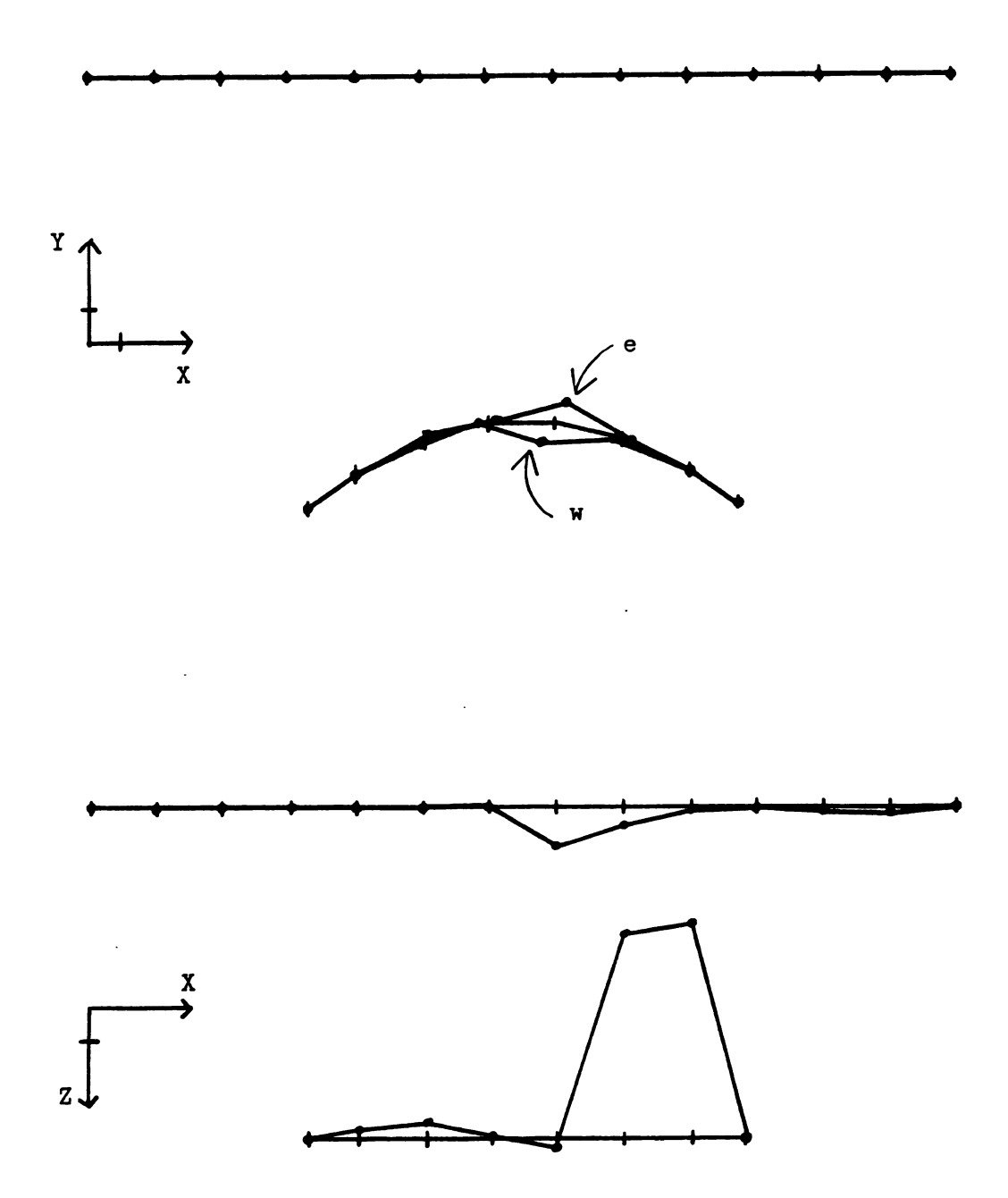
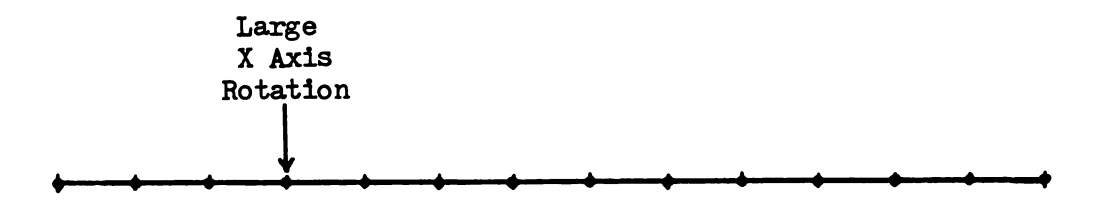


Figure 46 SSB Mode 22



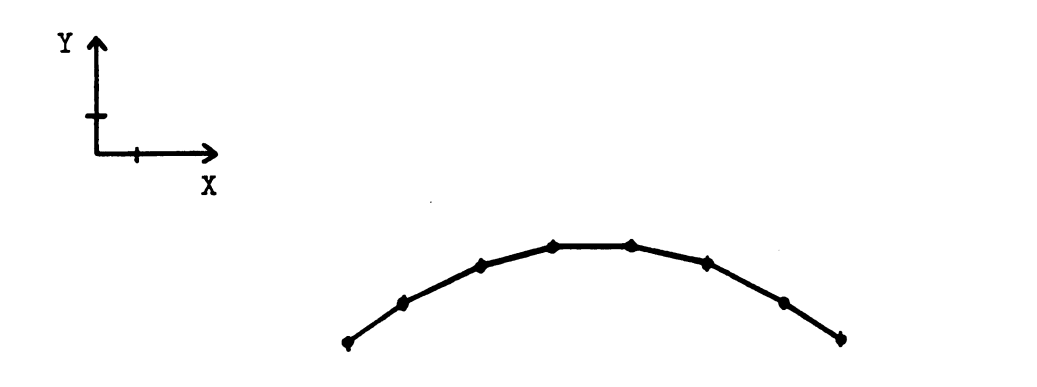
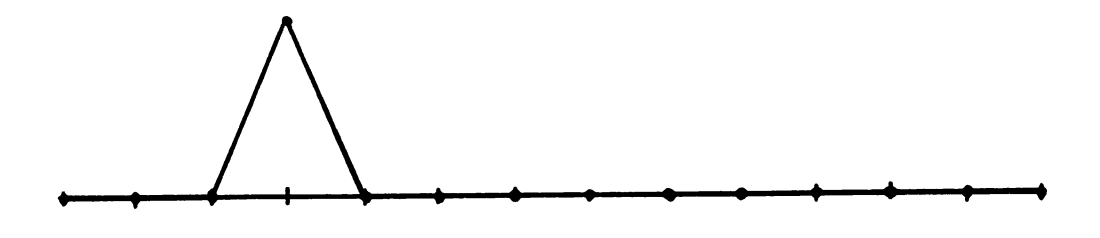






Figure 47 SSB Mode 23



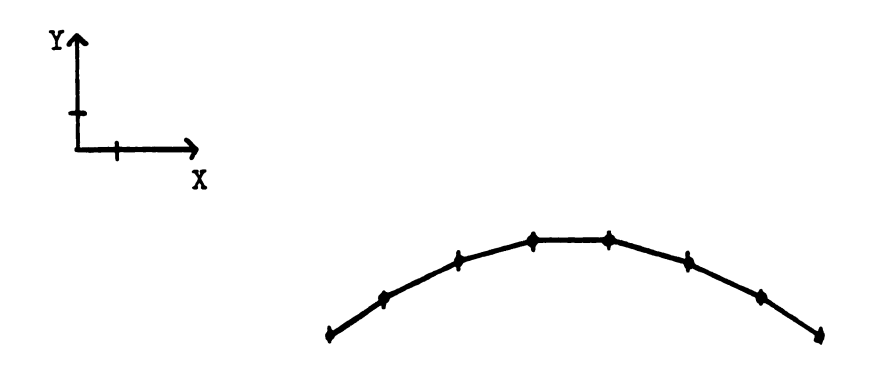


Figure 48 SSB Mode 24

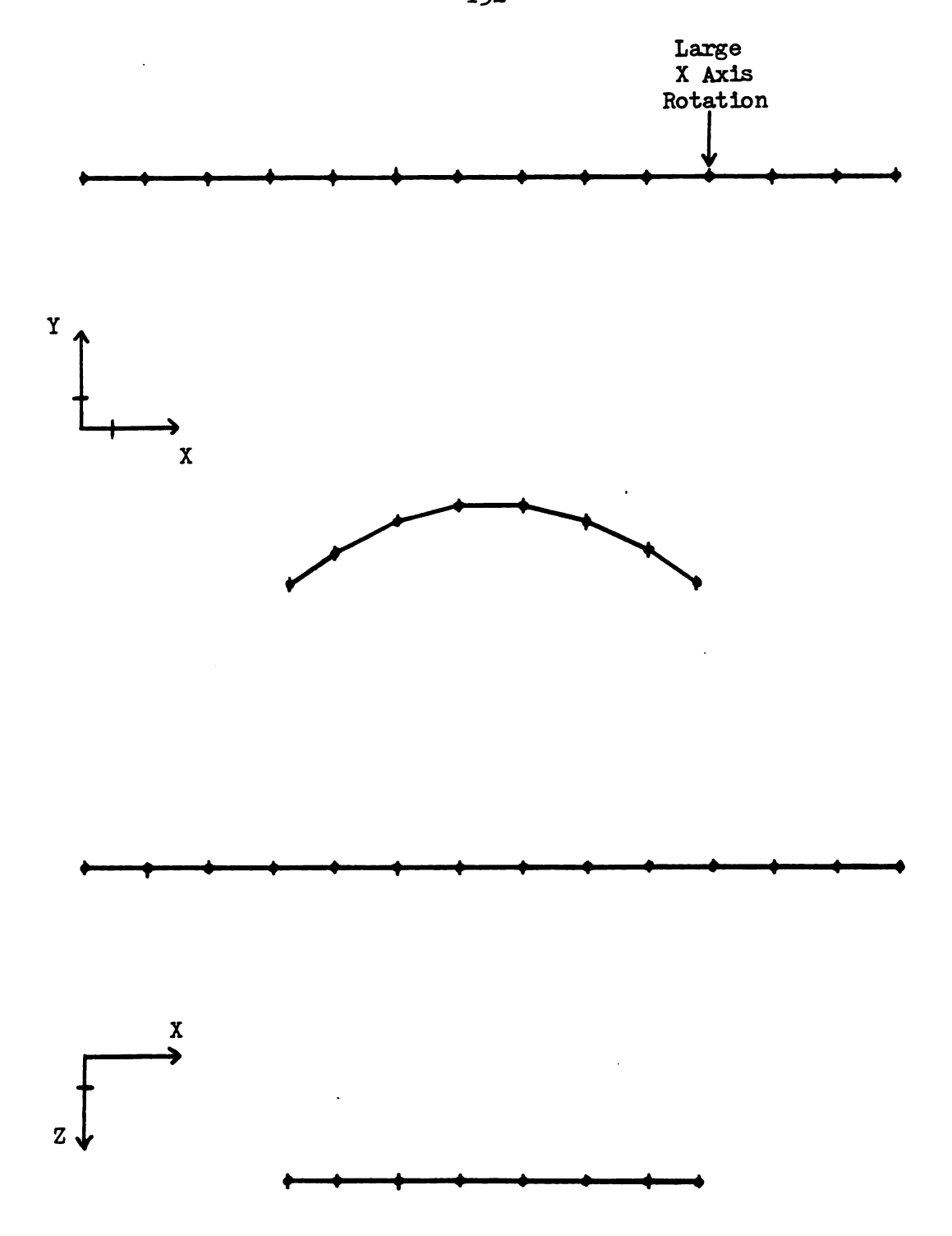


Figure 49 SSB Mode 25

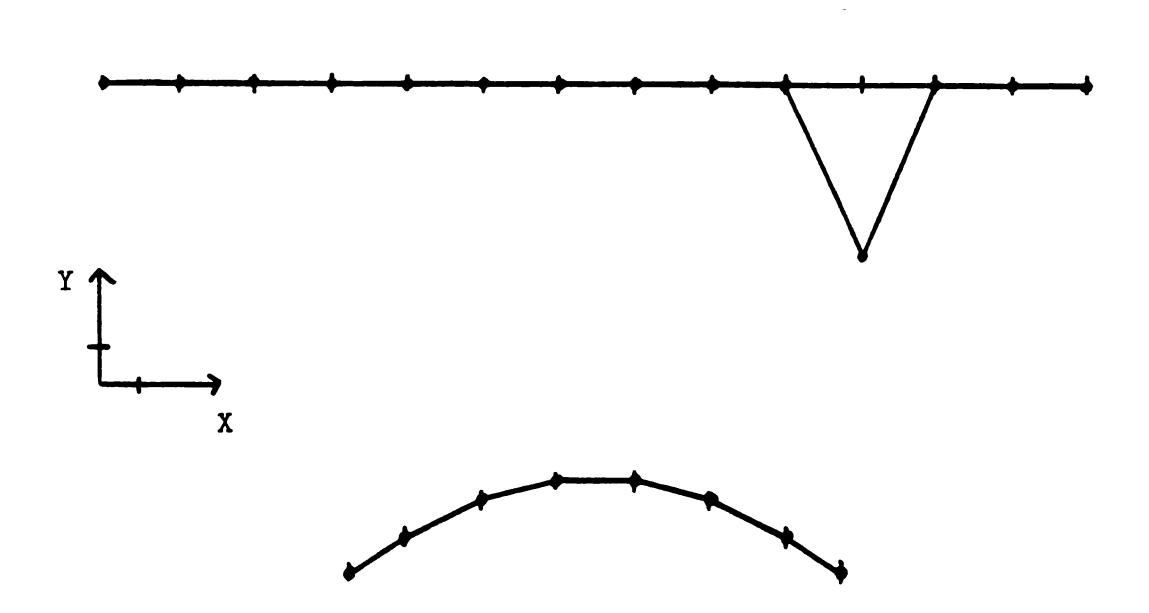


Figure 50 SSB Mode 26

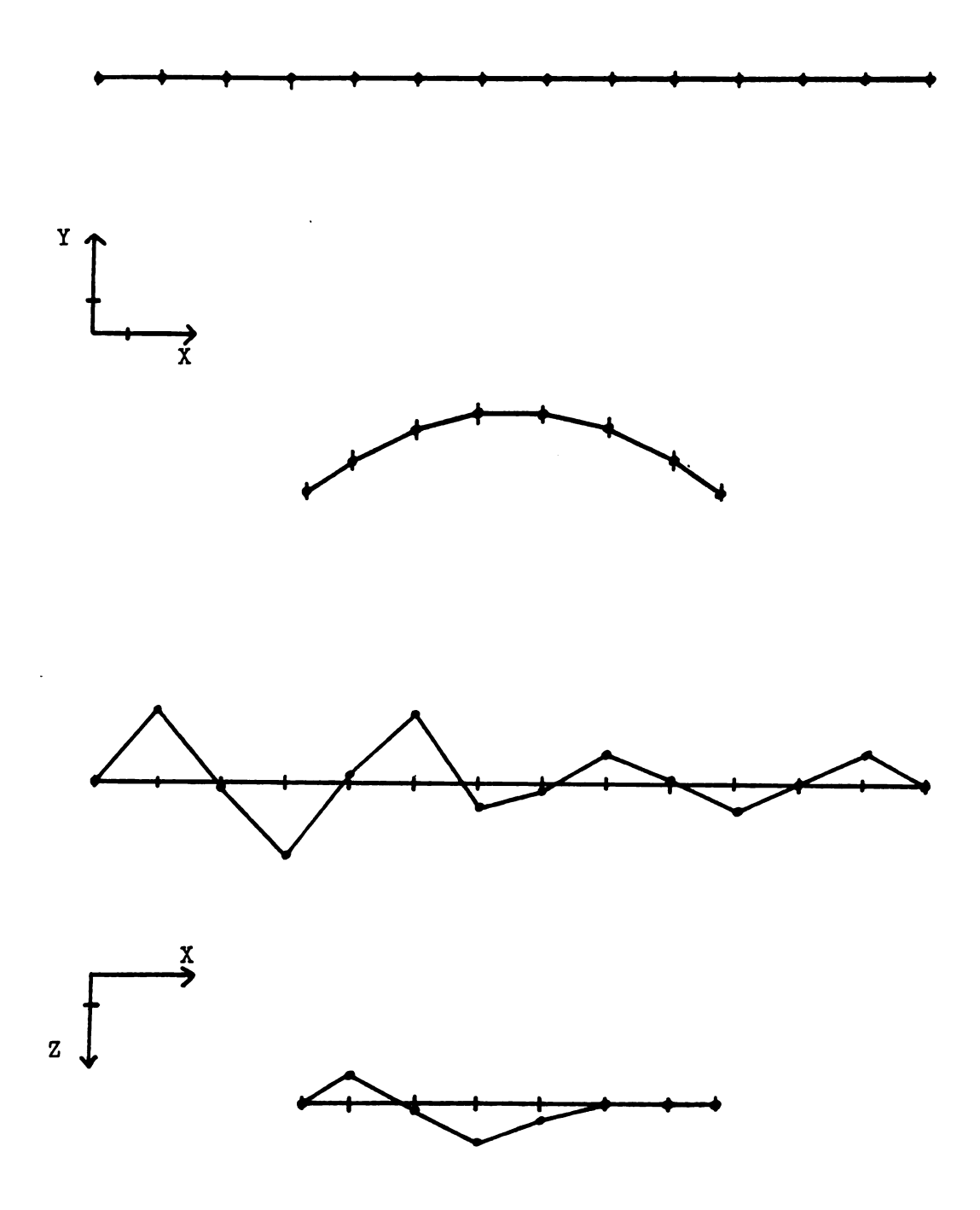


Figure 51 SSB Mode 27

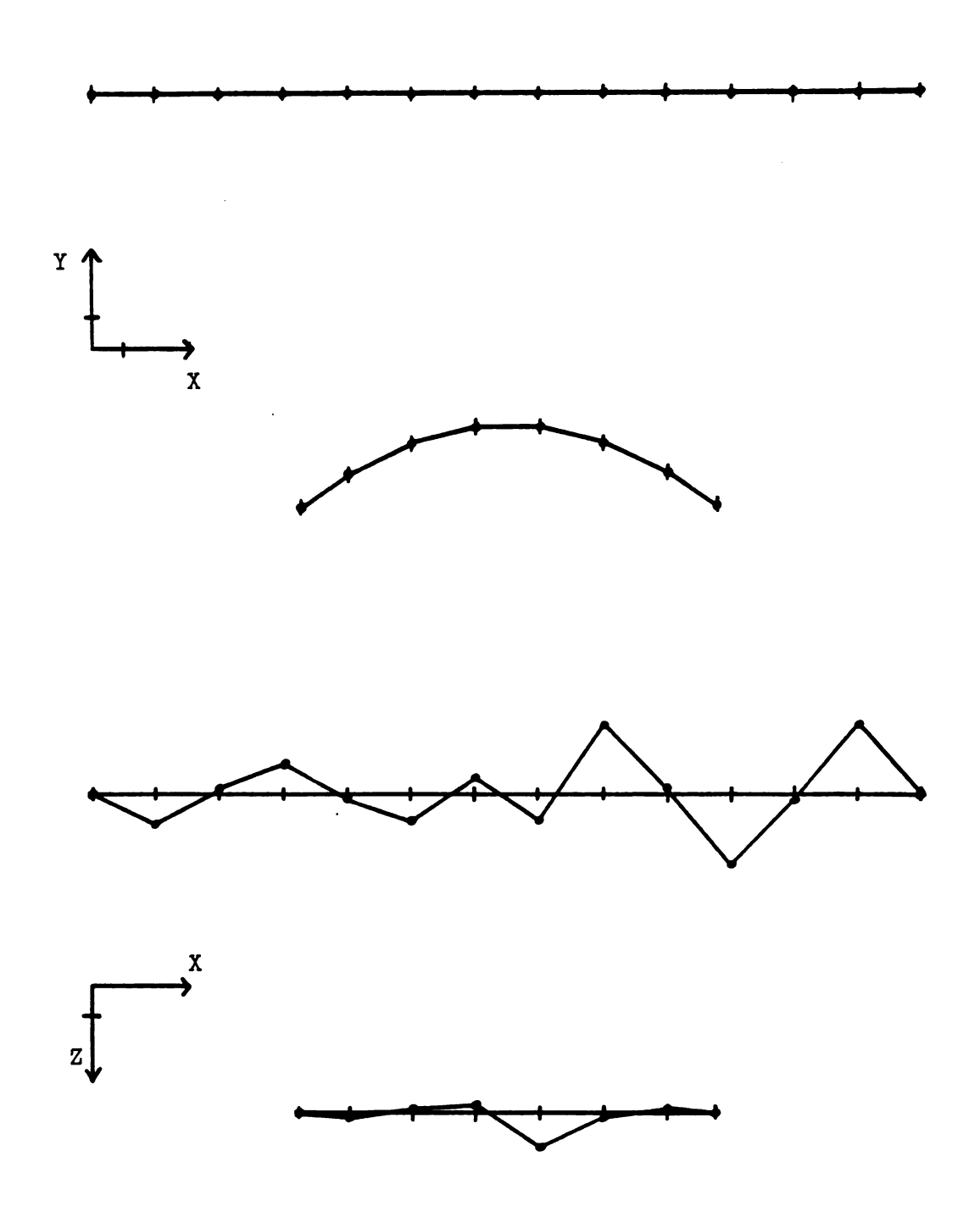
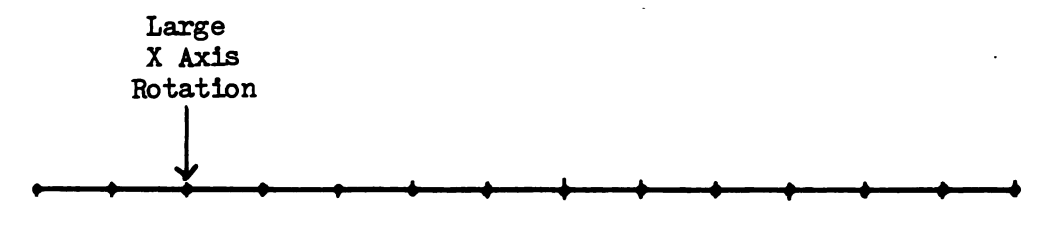
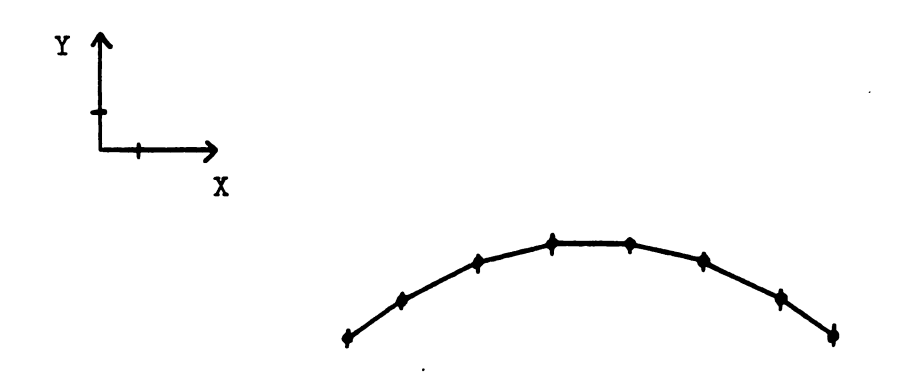


Figure 52 SSB Mode 28





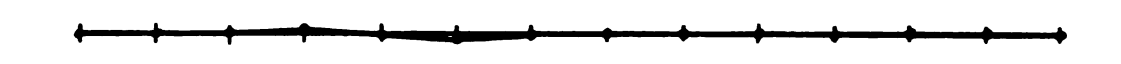




Figure 53 SSB Mode 29

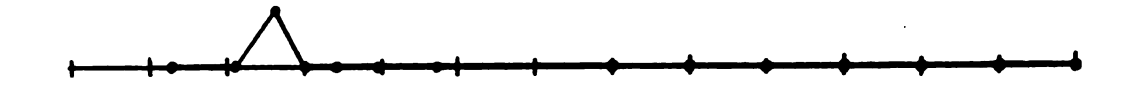




Figure 54 SSB Mode 30



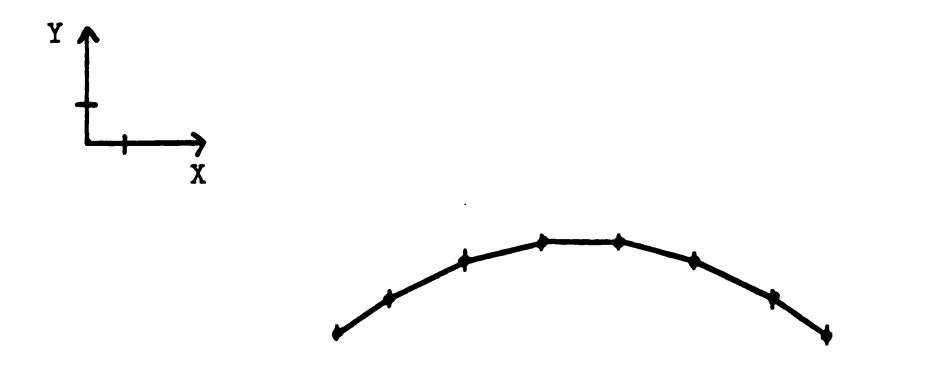
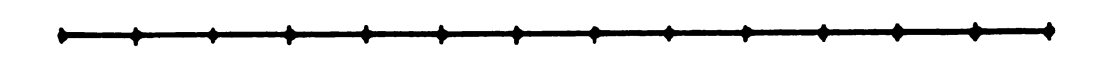


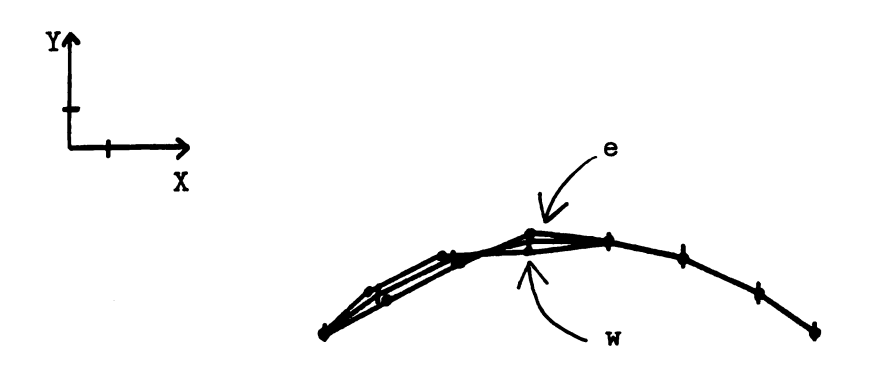
Figure 55 SSB Mode 31





Figure 56 SSB Mode 32







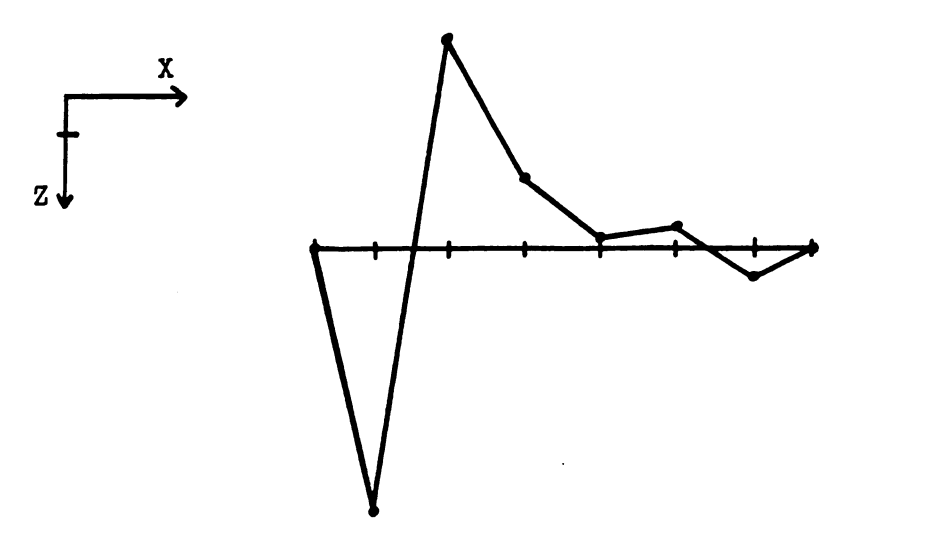
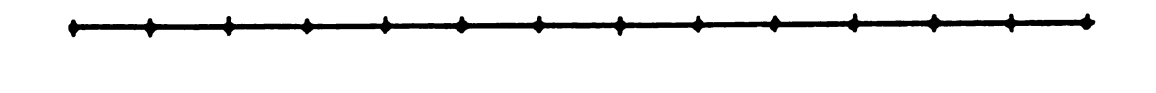
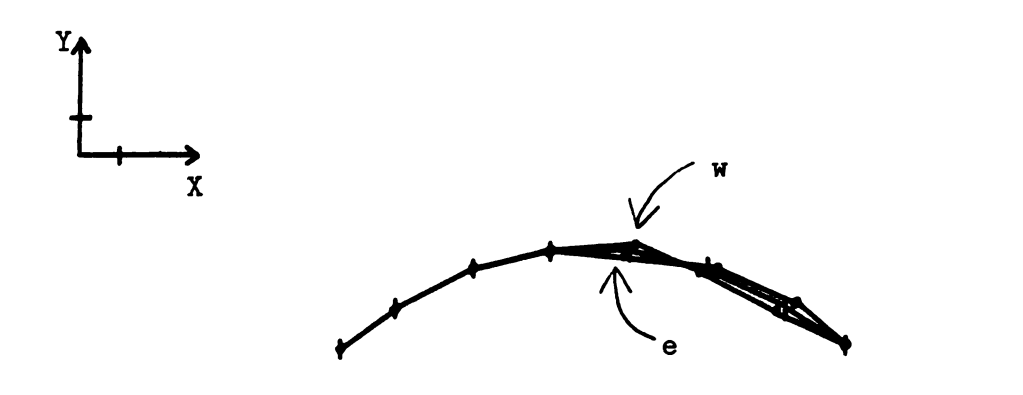


Figure 57 SSB Mode 33







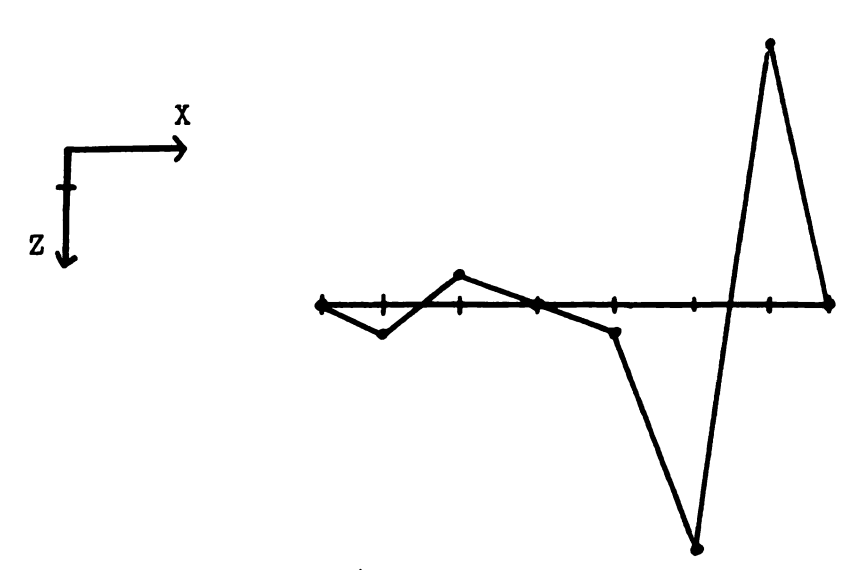


Figure 58 SSB Mode 34

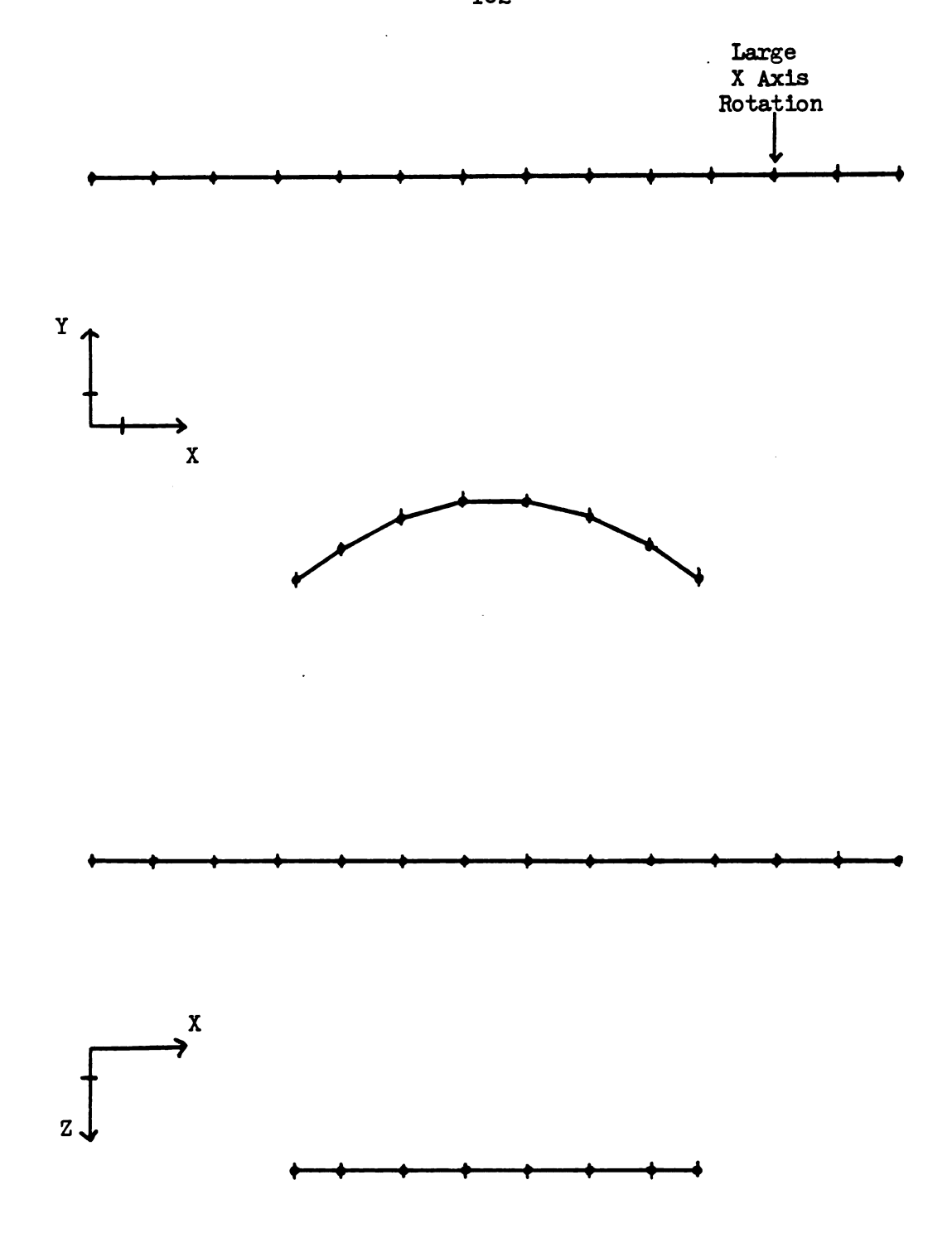
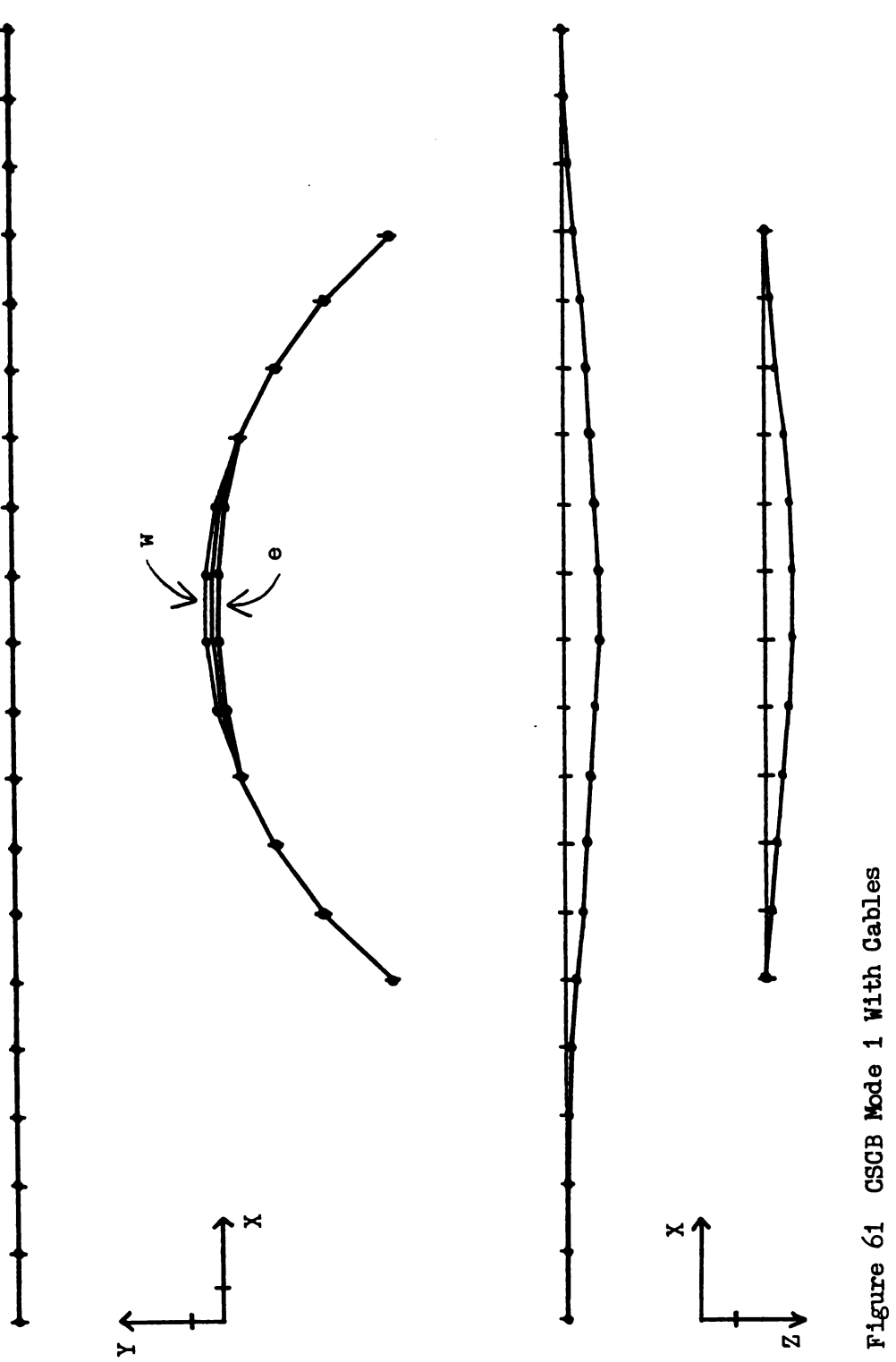


Figure 59 SSB Mode 35





Figure 60 SSB Mode 36



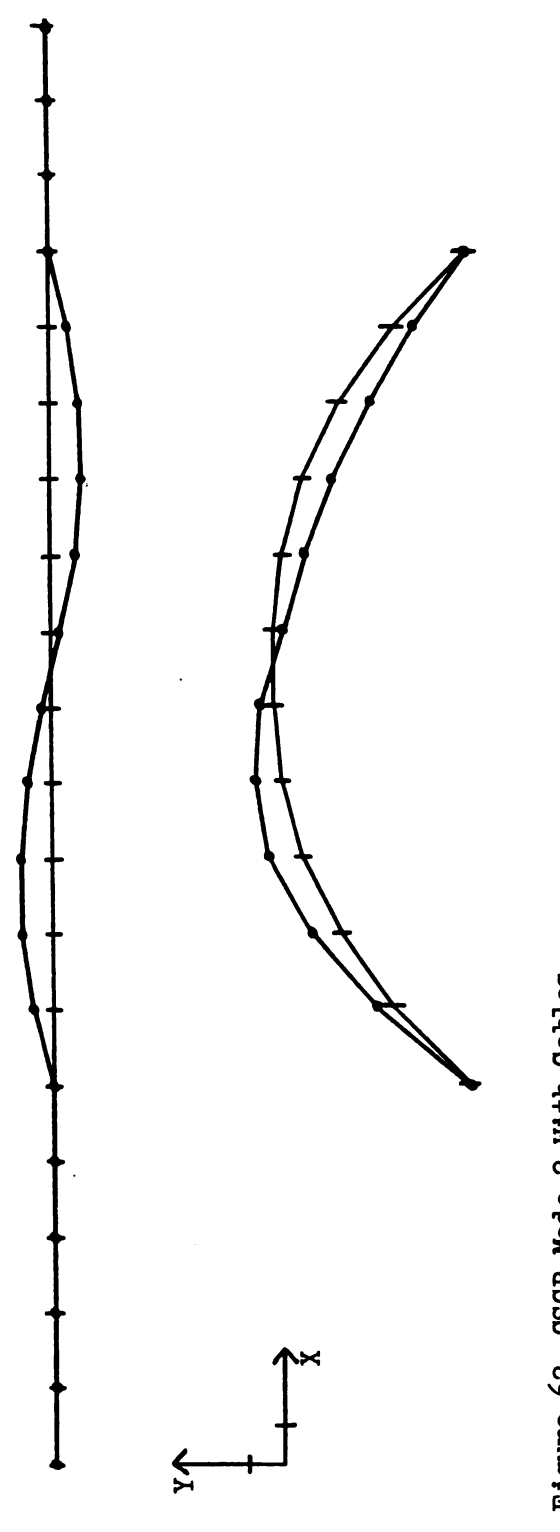
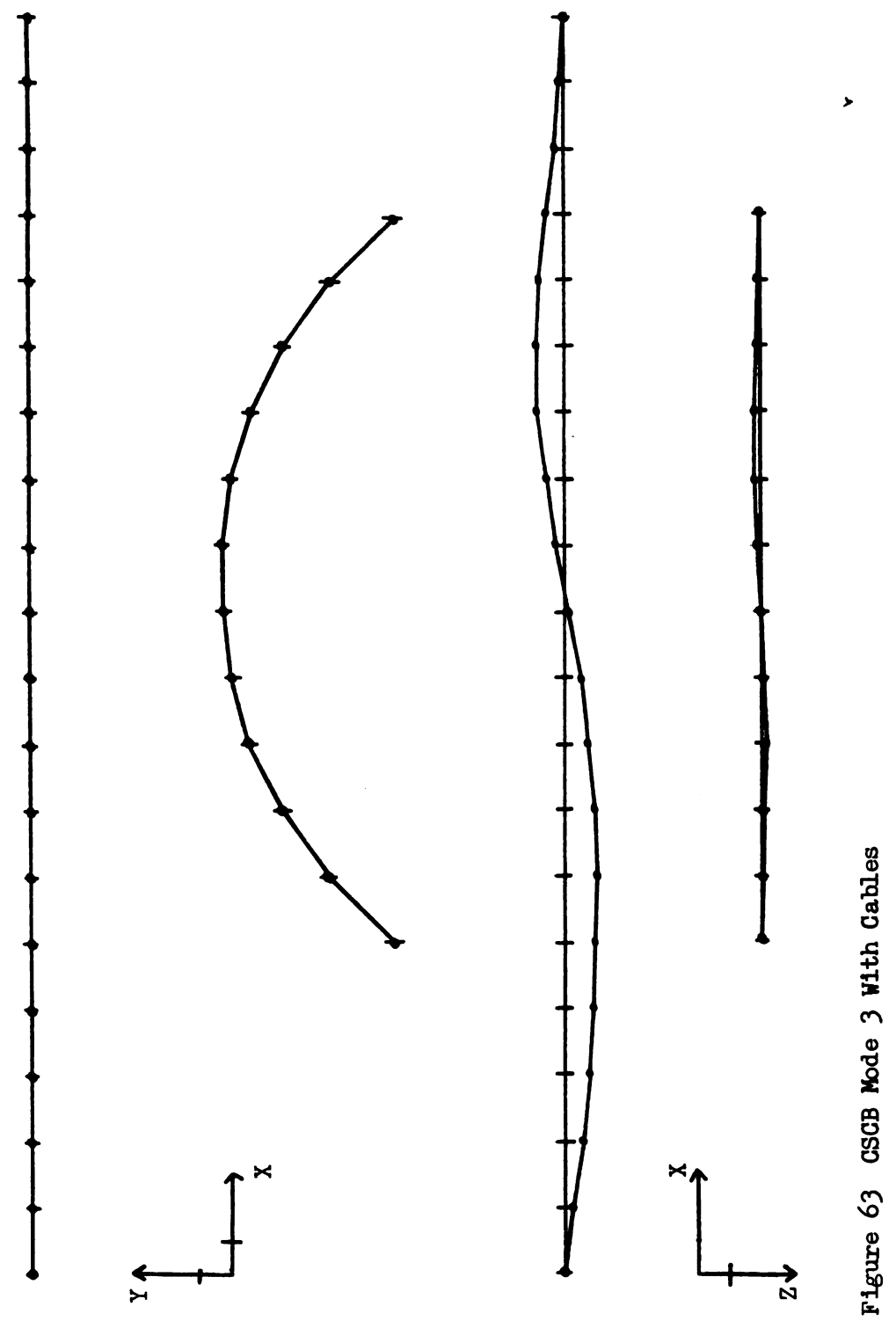


Figure 62 GSCB Mode 2 With Cables



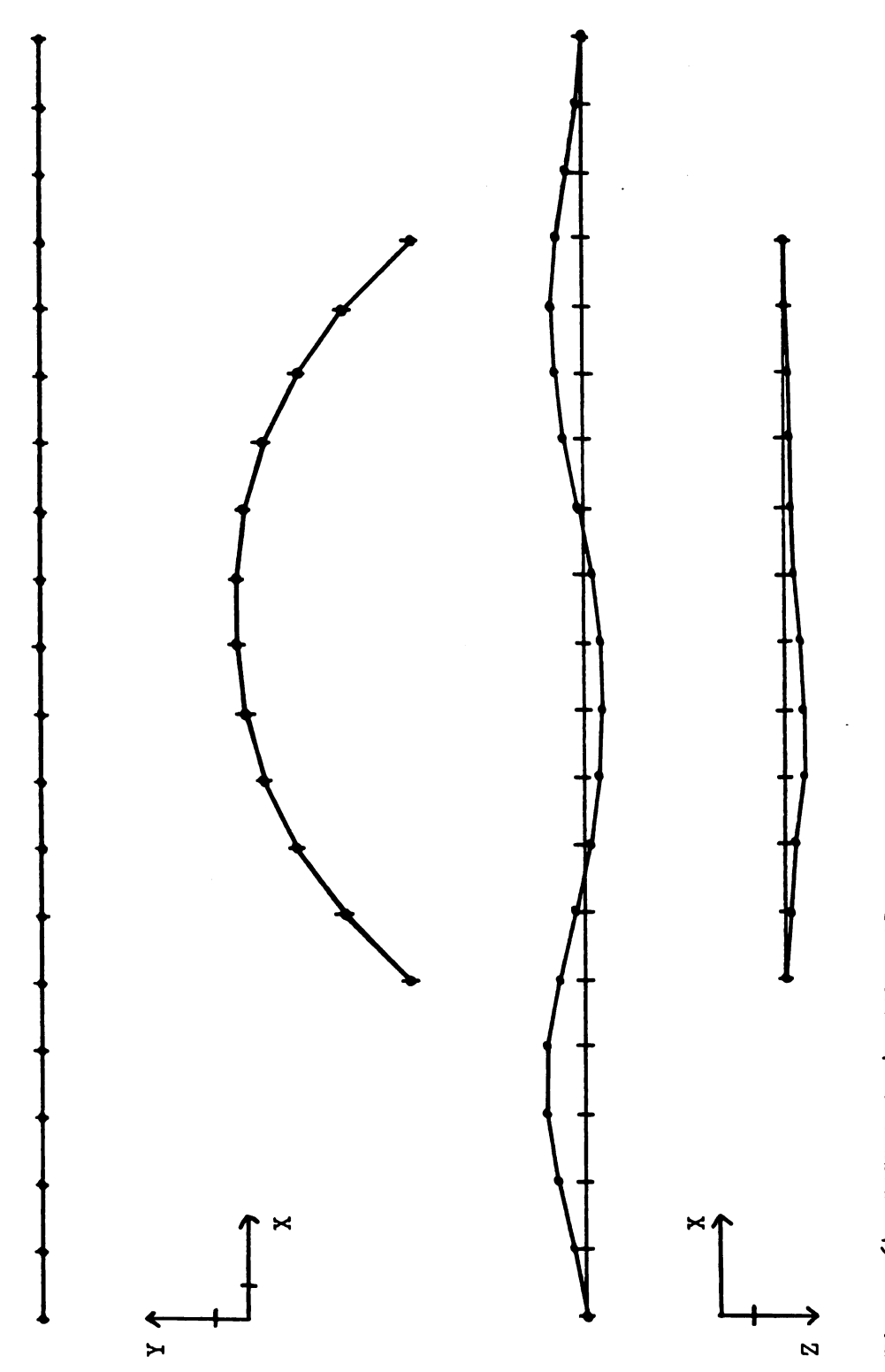
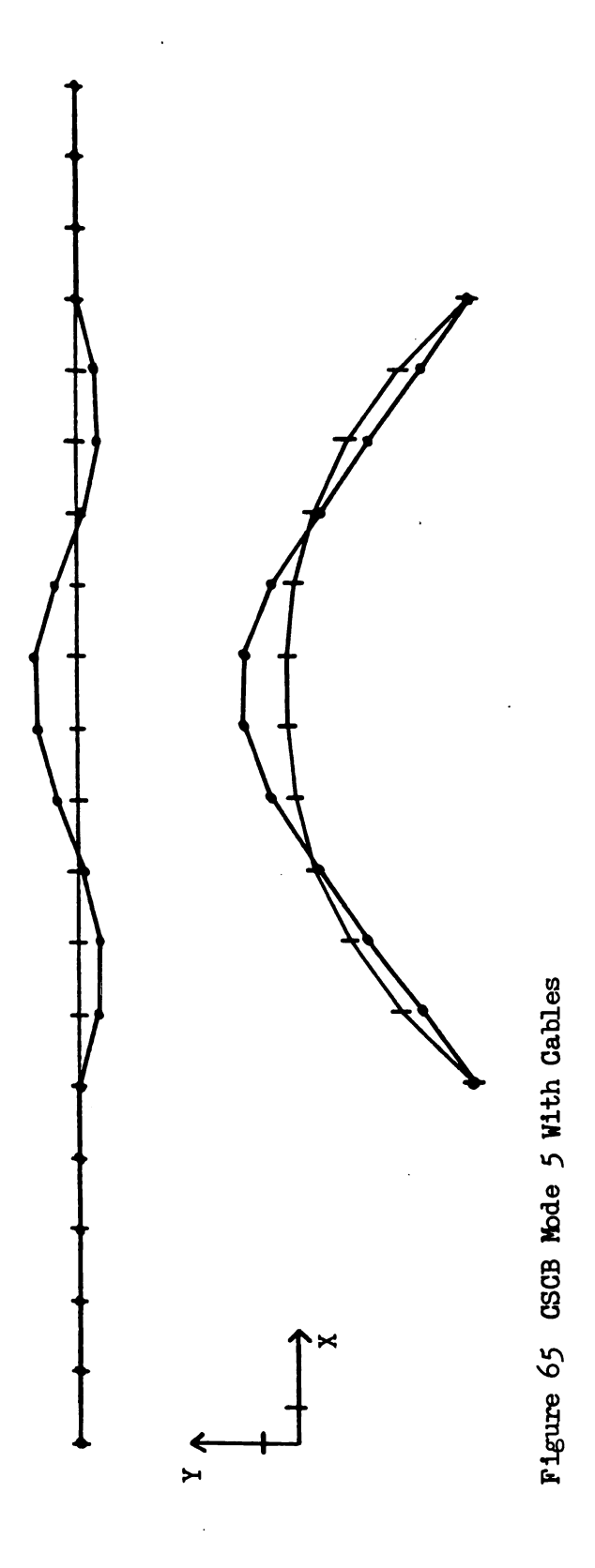


Figure 64 GSCB Mode 4 With Cables



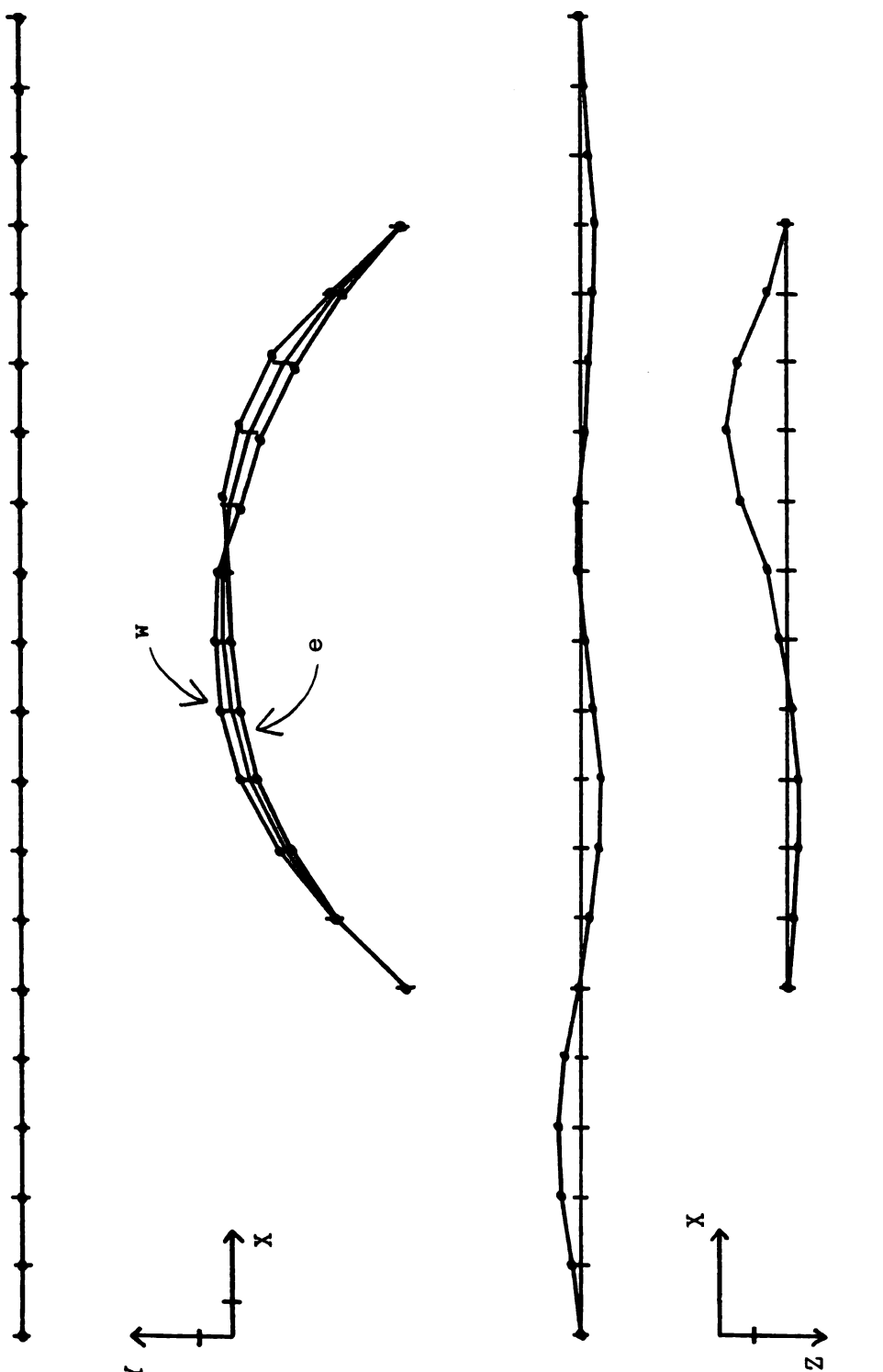


Figure 66 CSCB Mode 6 With Cables

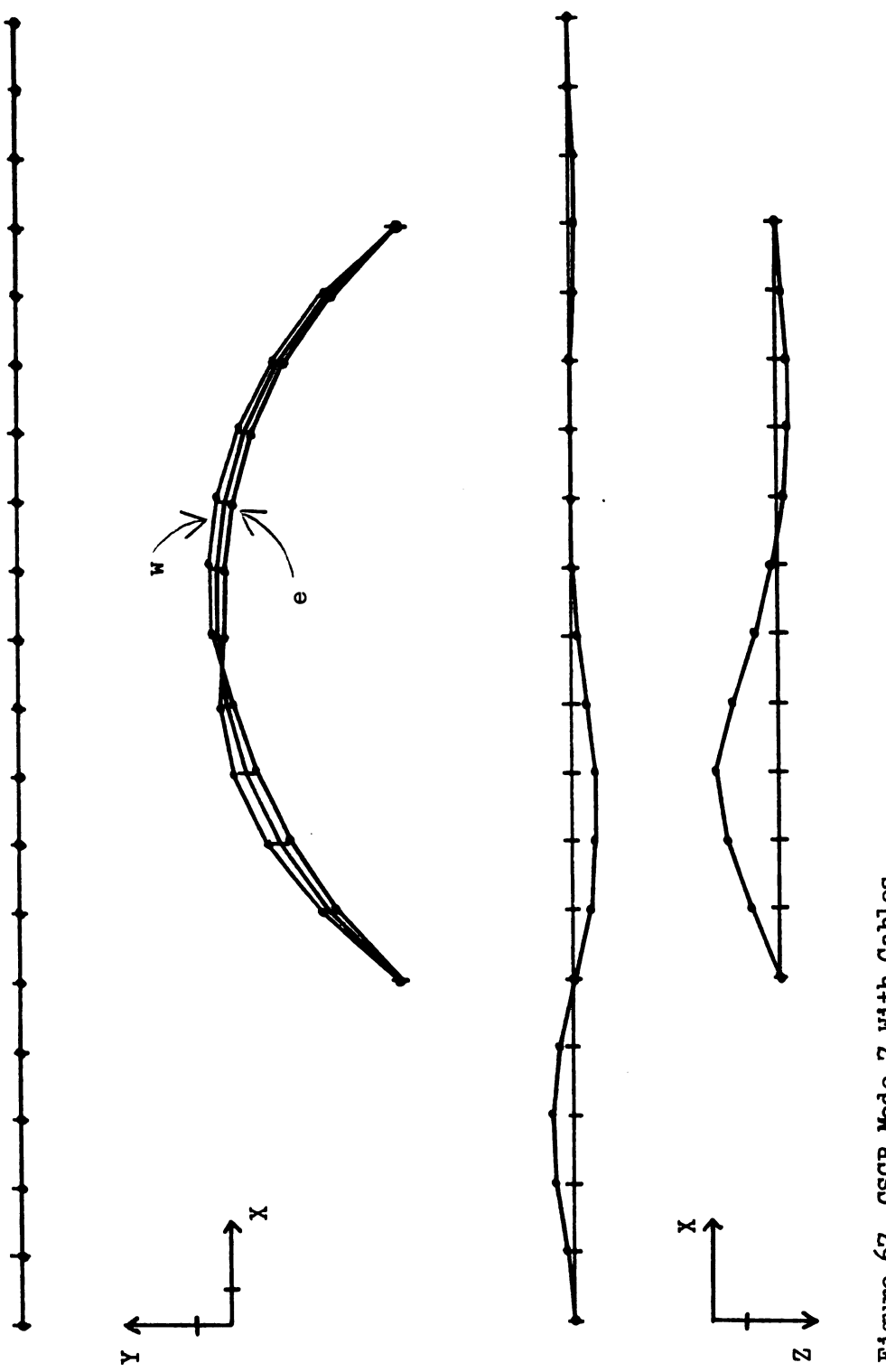


Figure 67 CSCB Mode 7 With Cables

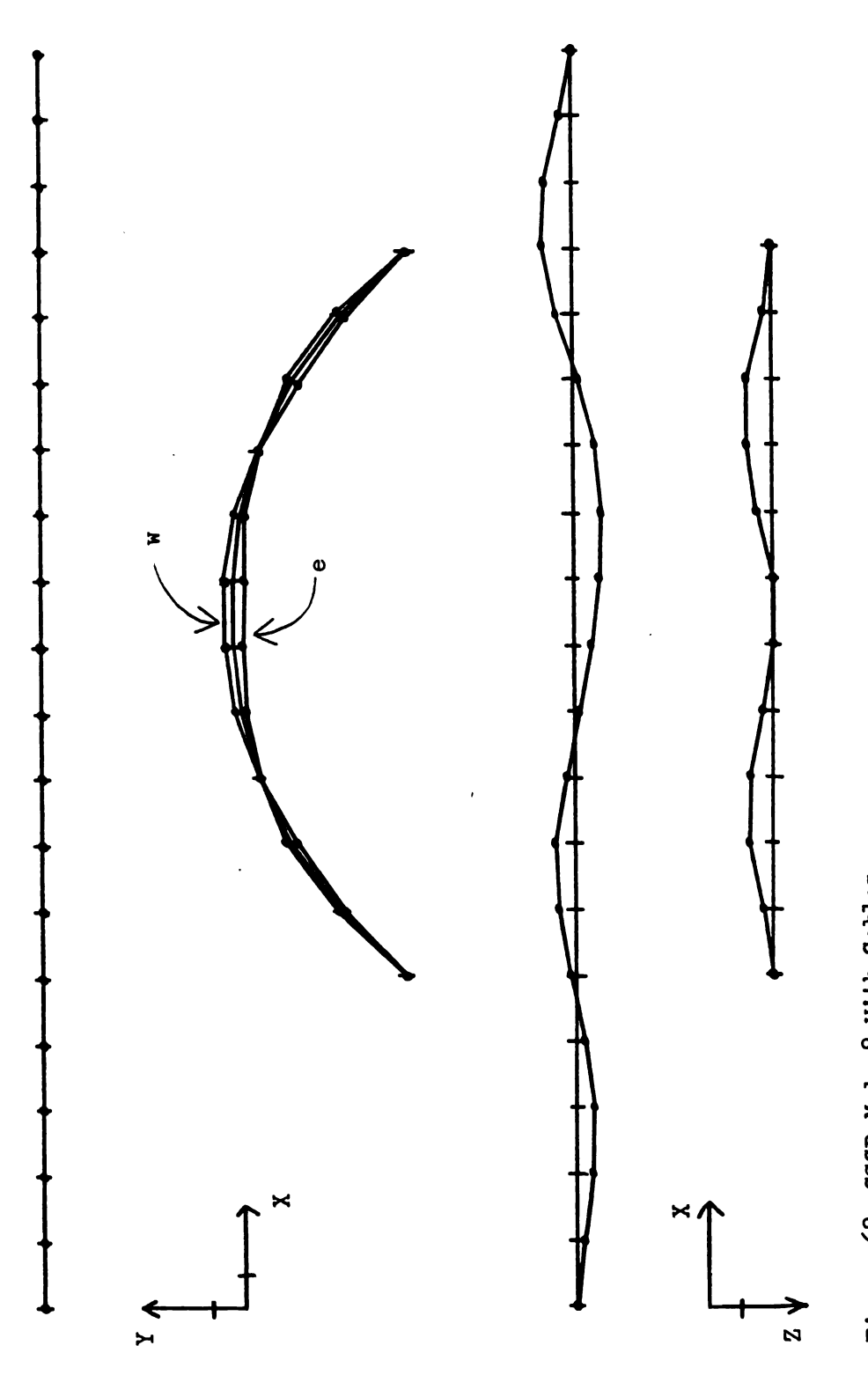


Figure 68 CSCB Mode 8 With Cables

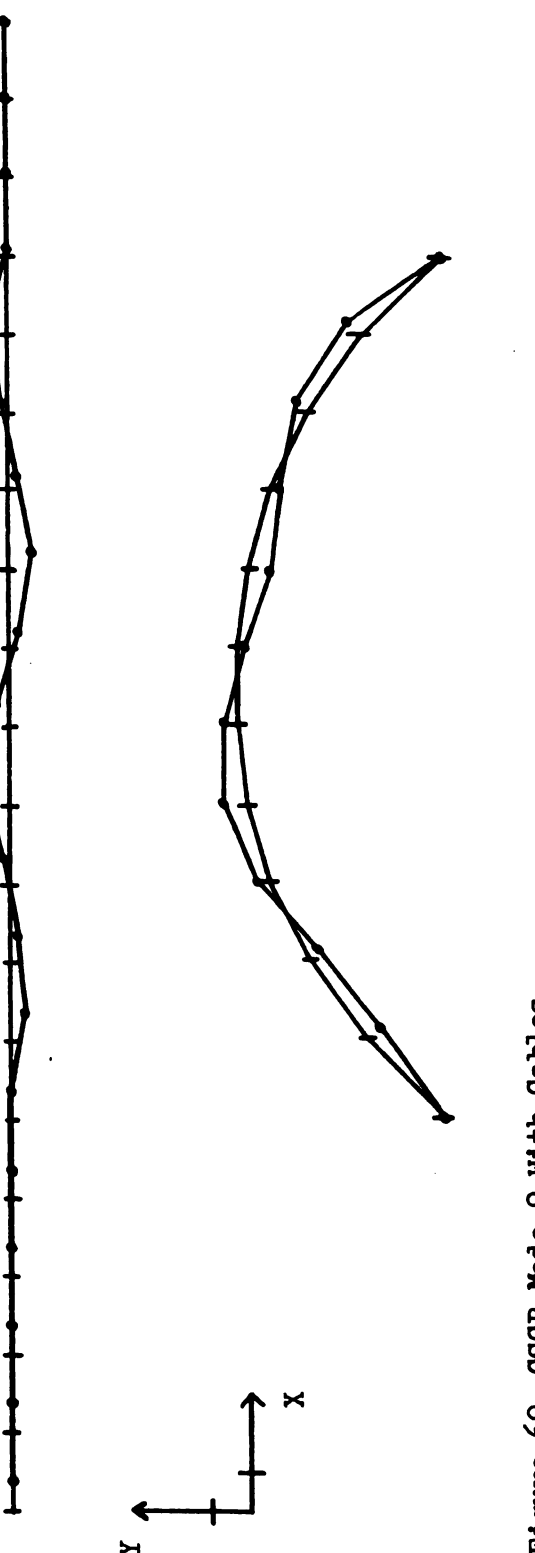


Figure 69 GSCB Mode 9 With Cables

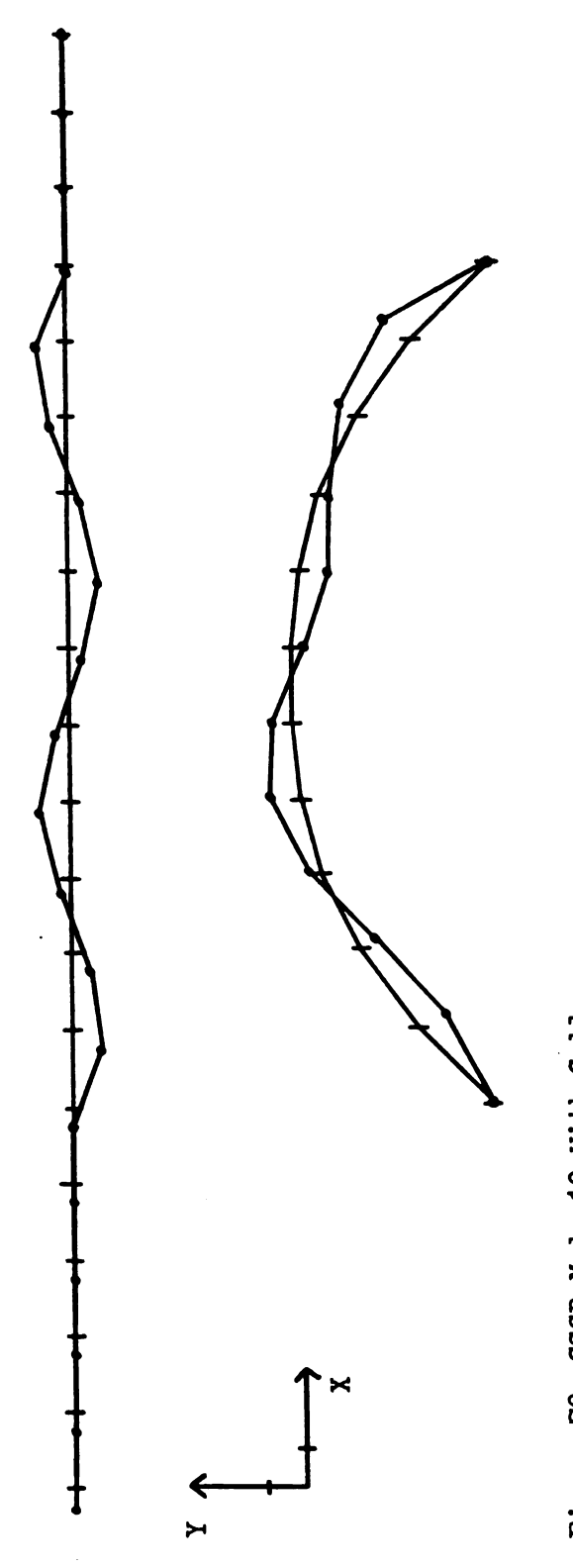
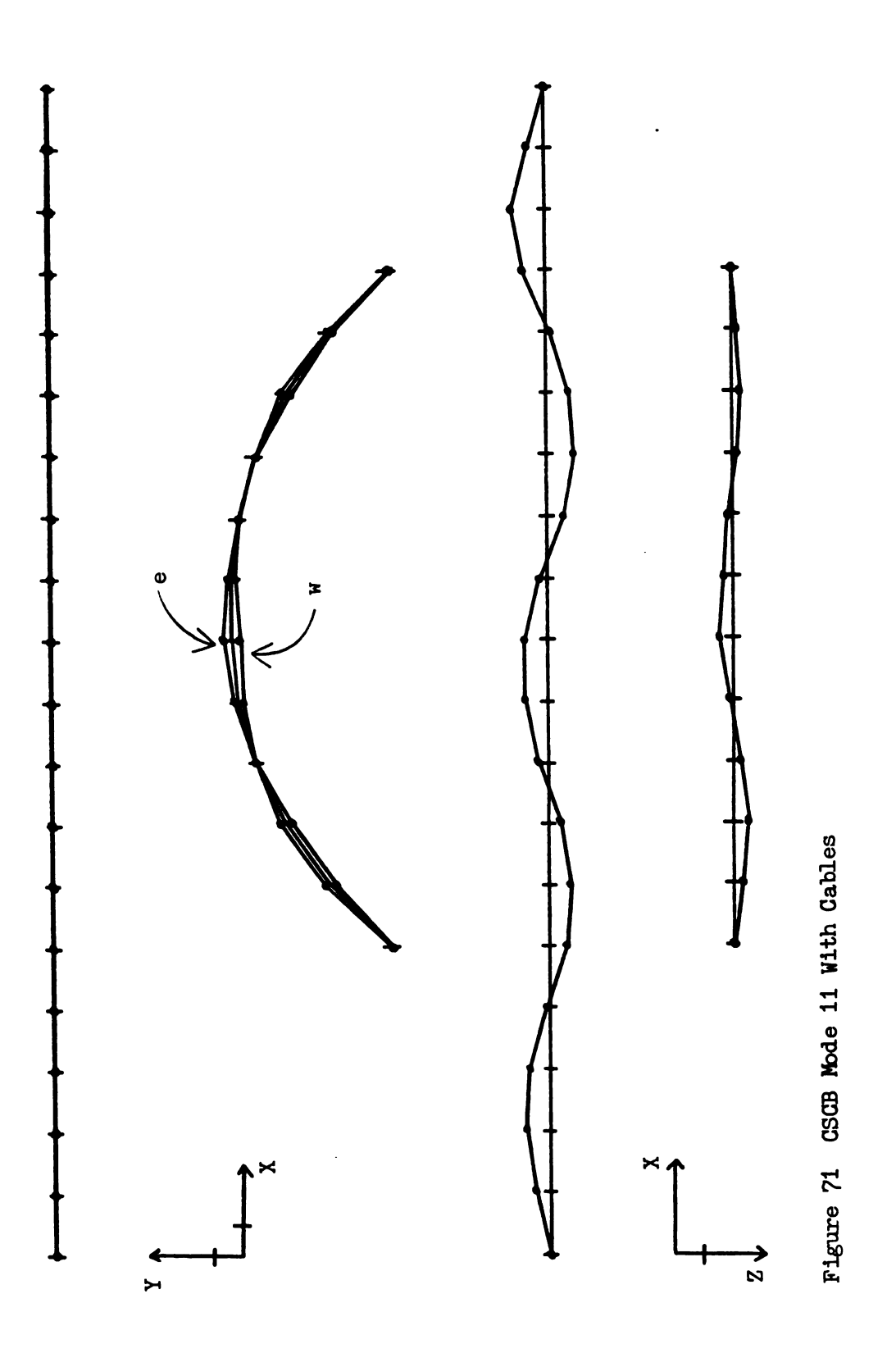


Figure 70 CSCB Mode 10 With Cables



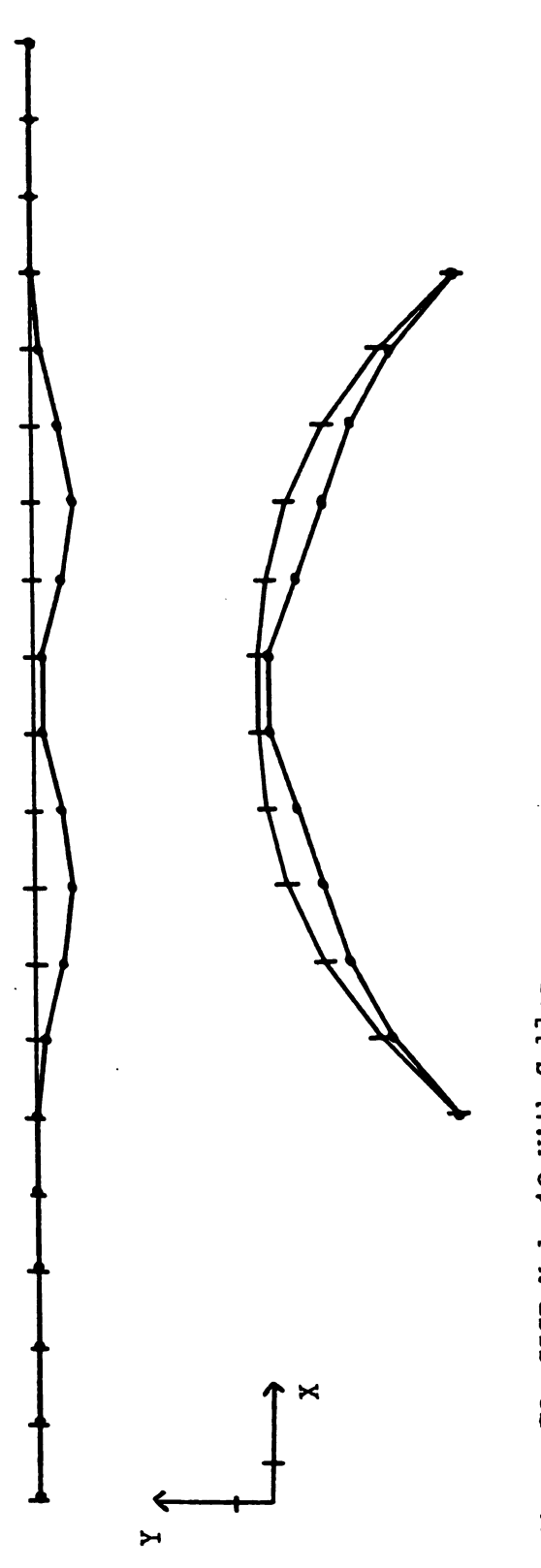


Figure 72 CSCB Mode 12 With Gables

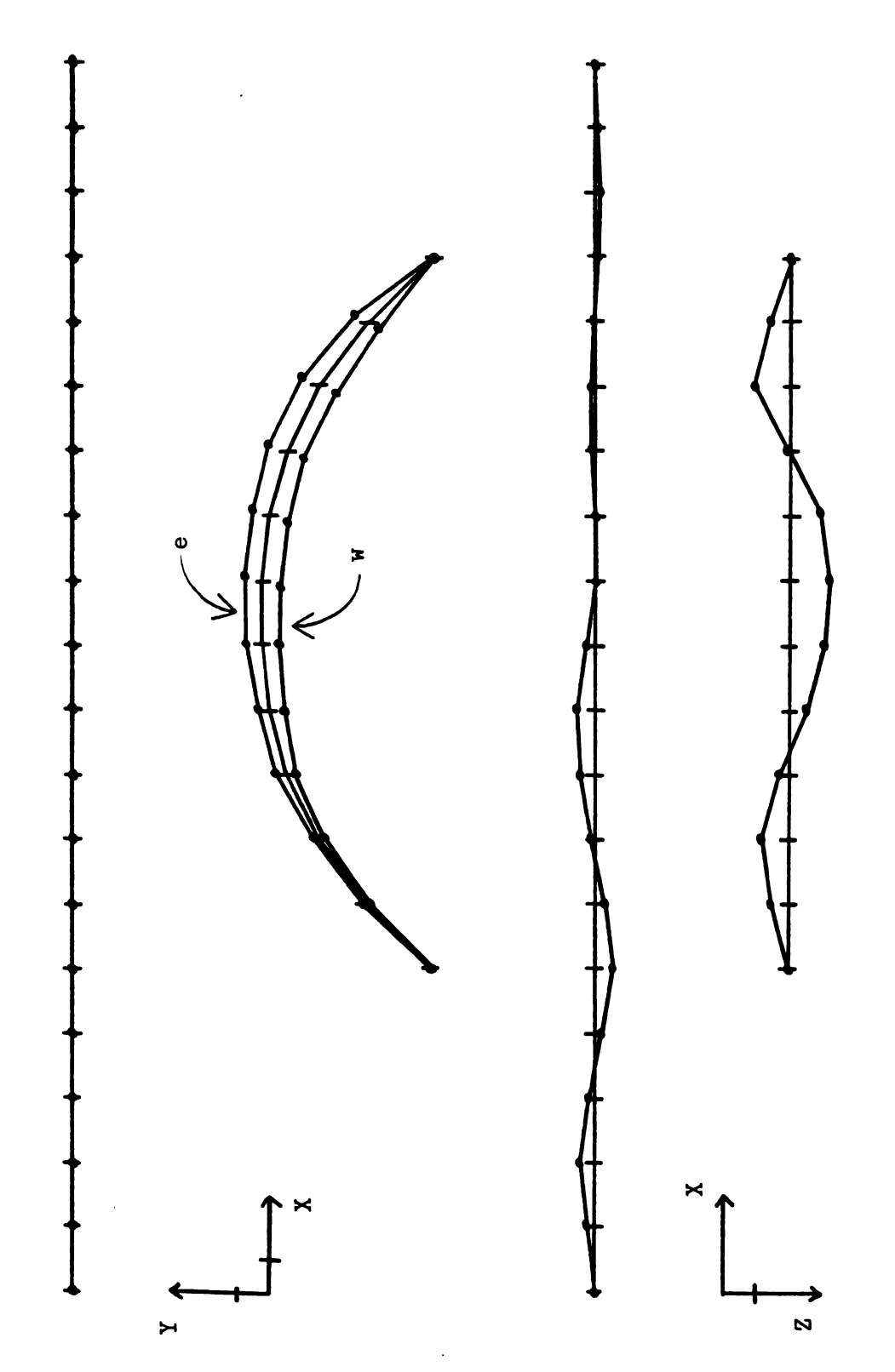
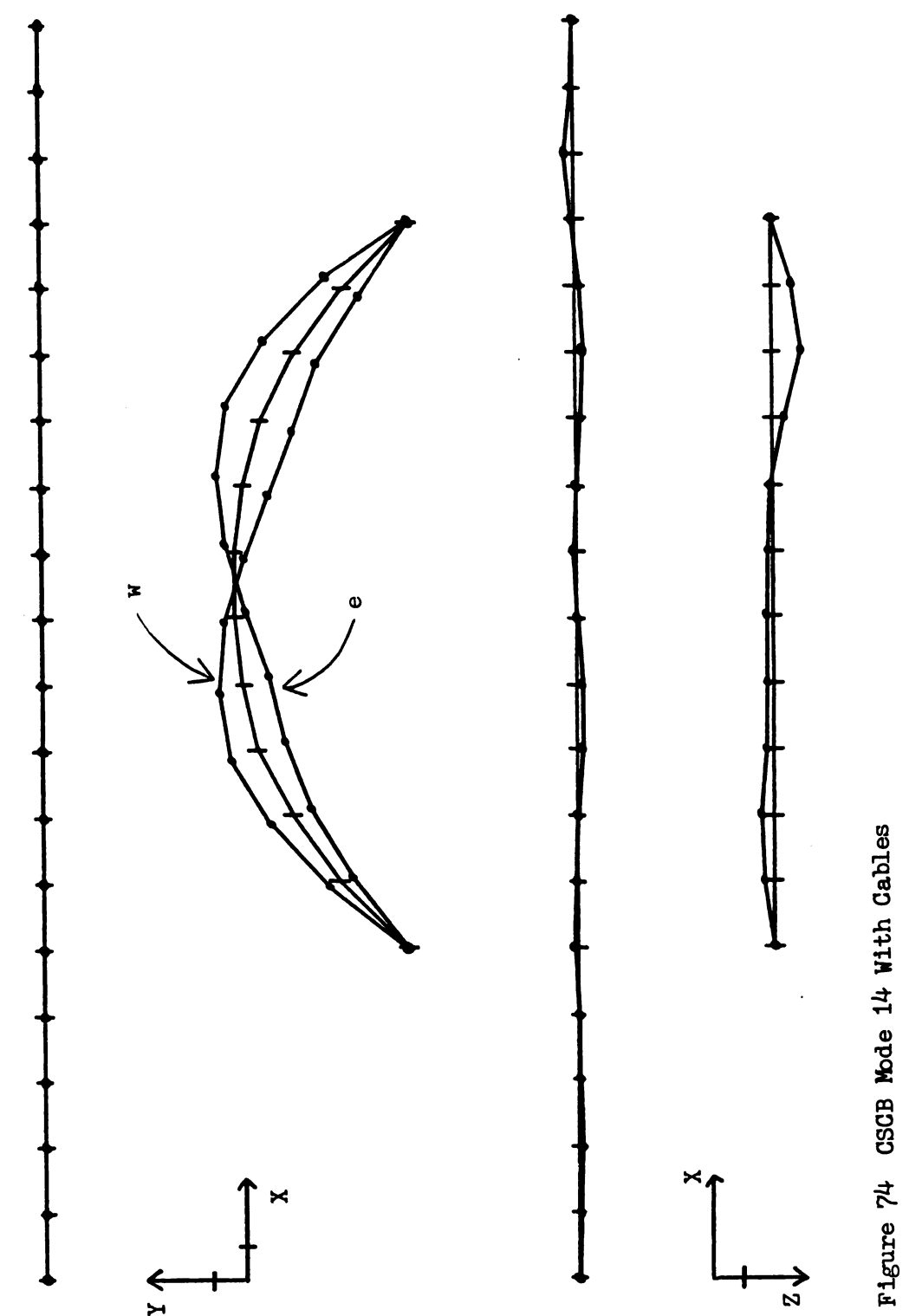


Figure 73 GSCB Mode 13 With Cables



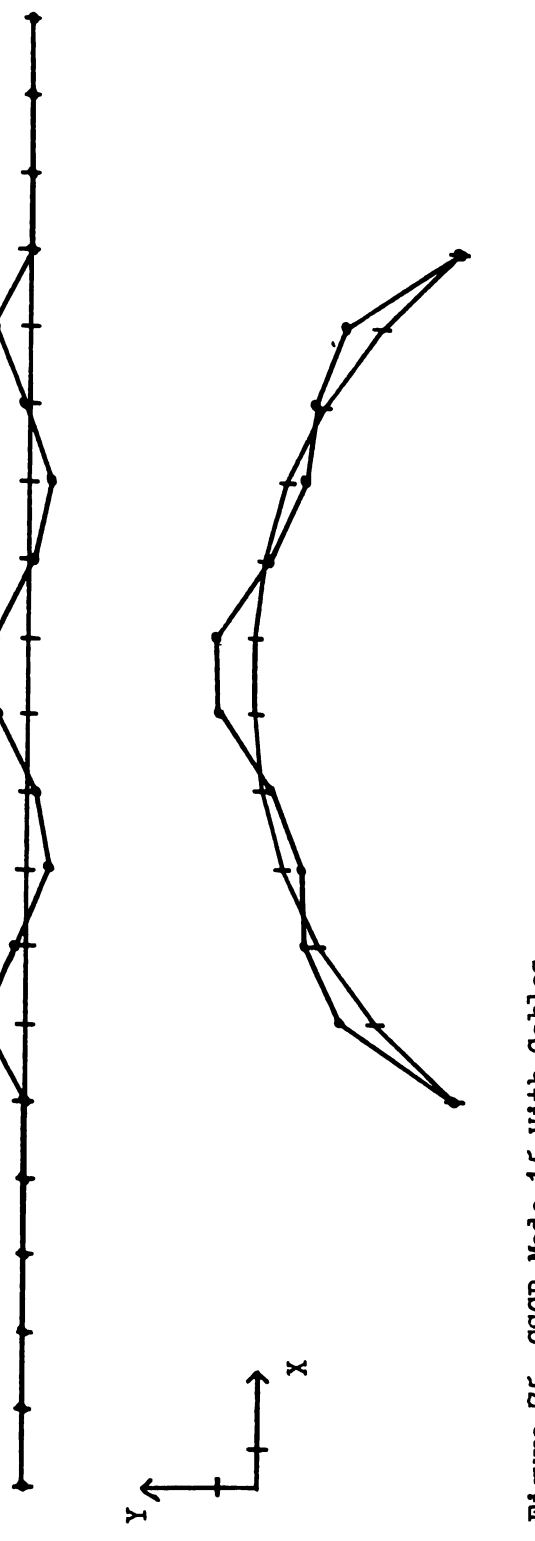


Figure 75 CSCB Mode 15 With Cables

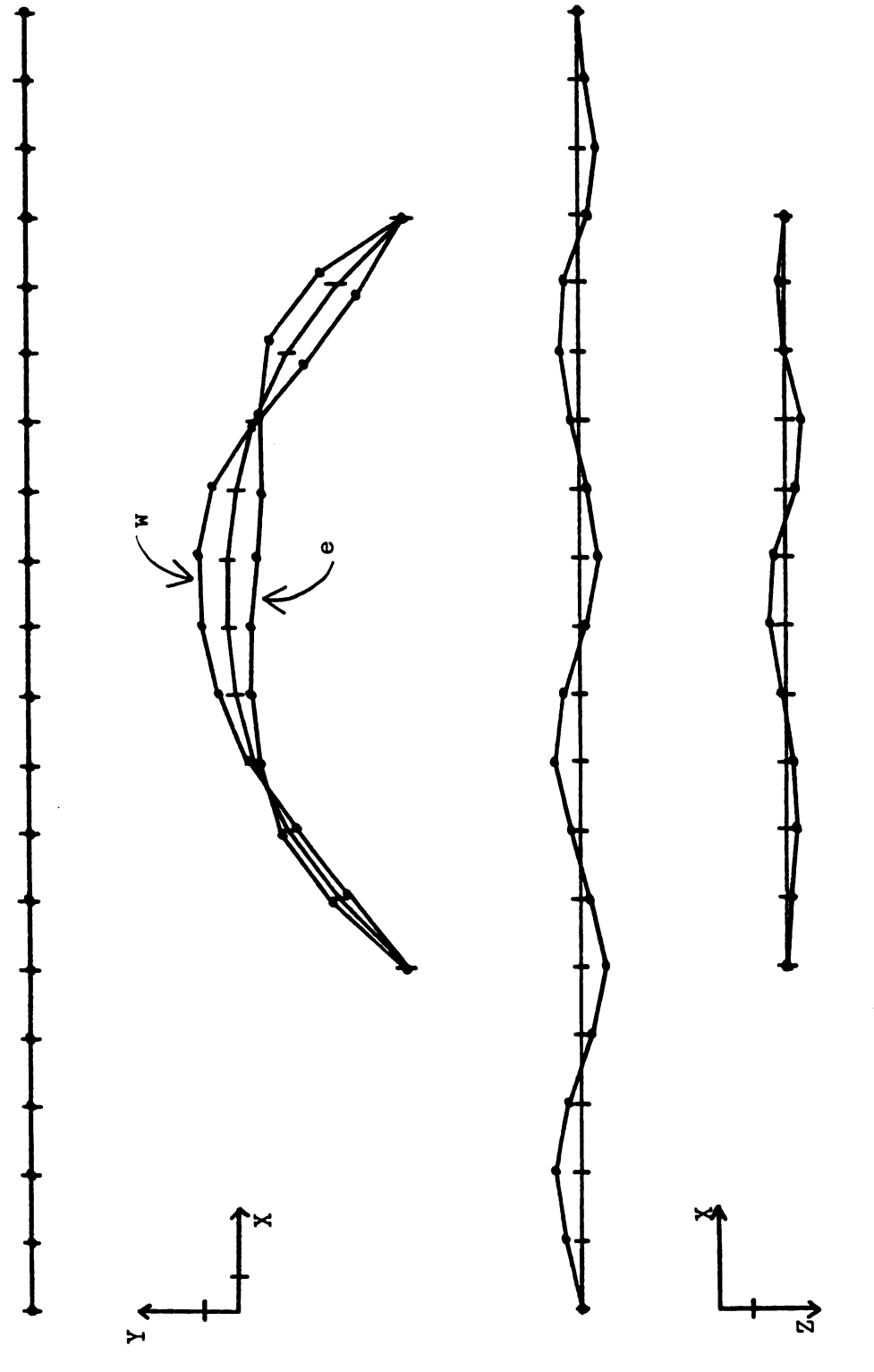


Figure 76 CSCB Mode 16 With Cables

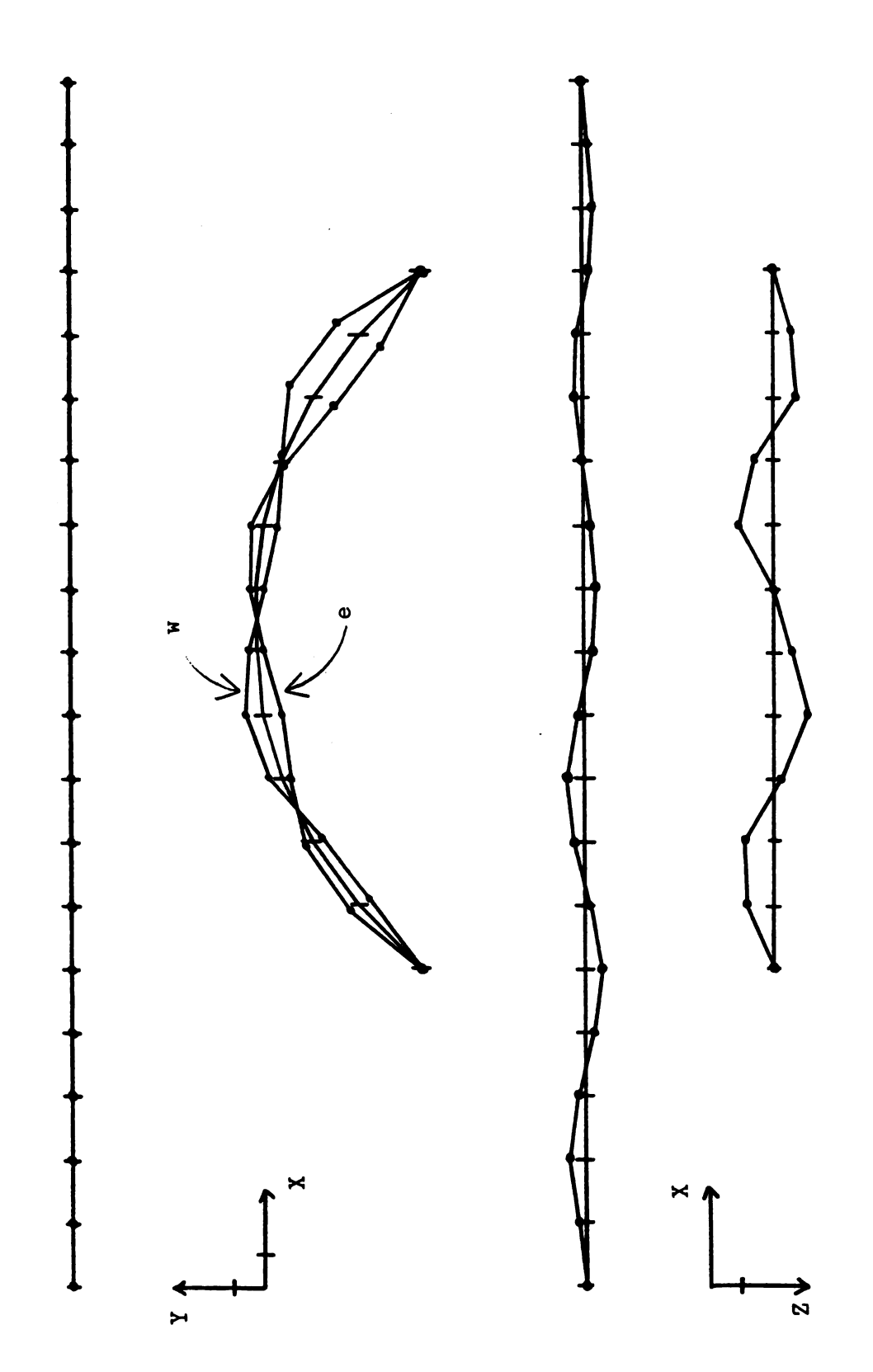


Figure 77 CSCB Mode 17 With Cables

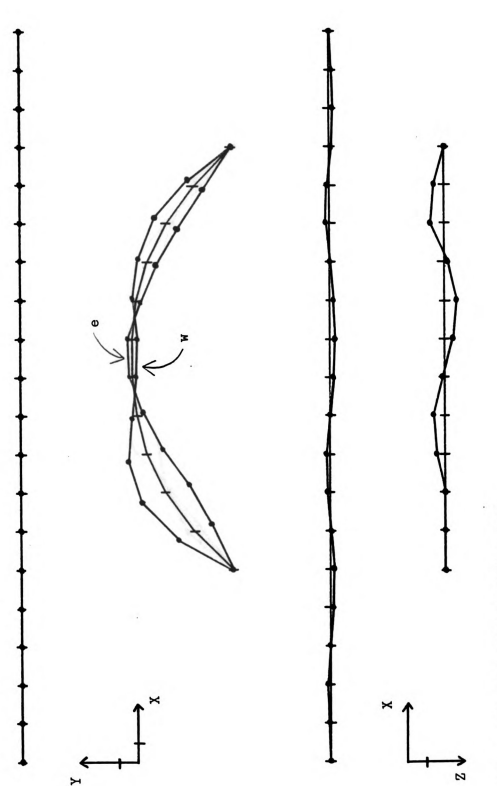


Figure 78 GSGB Mode 18 With Gables

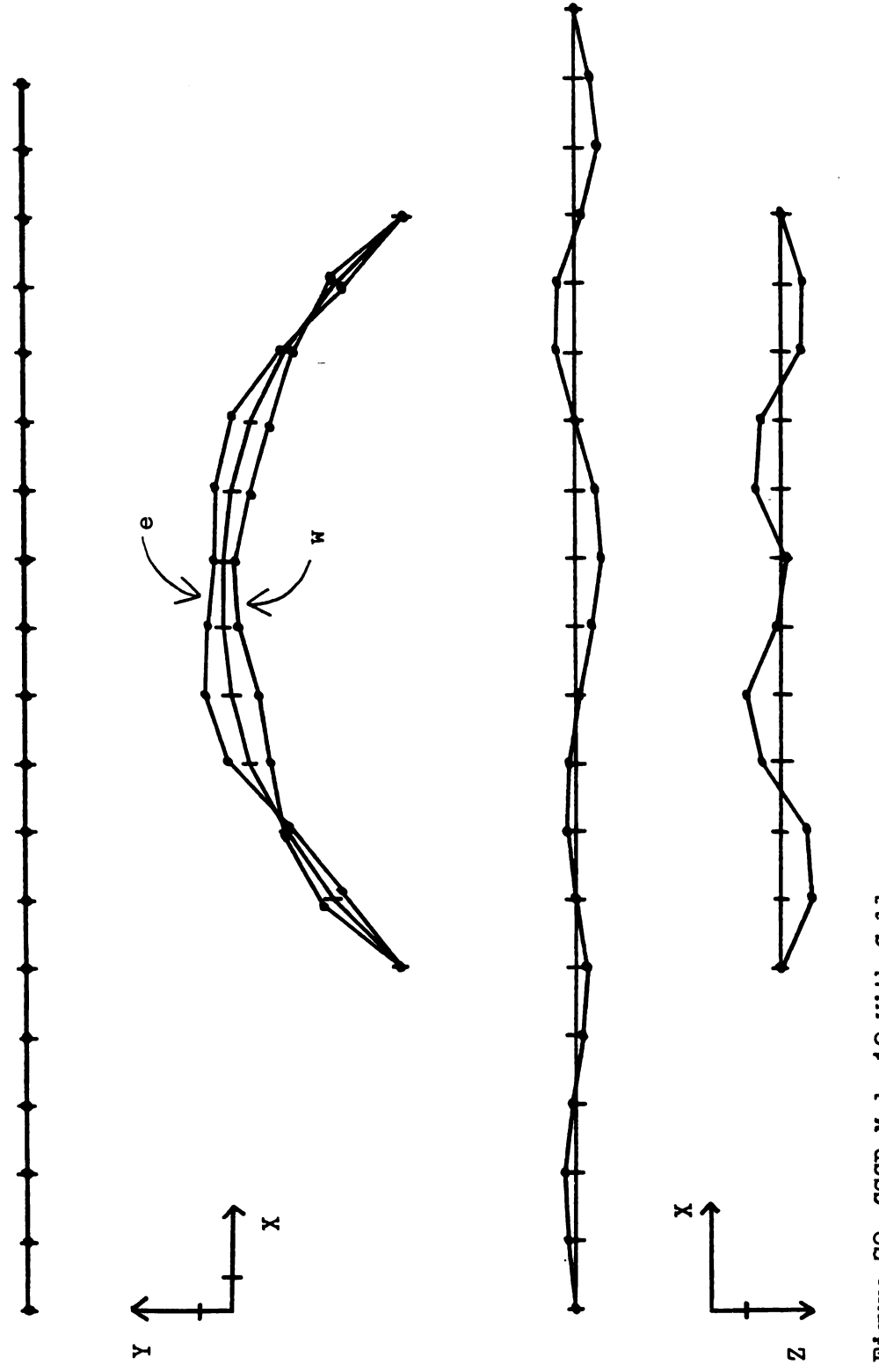


Figure 79 GSCB Mode 19 With Cables

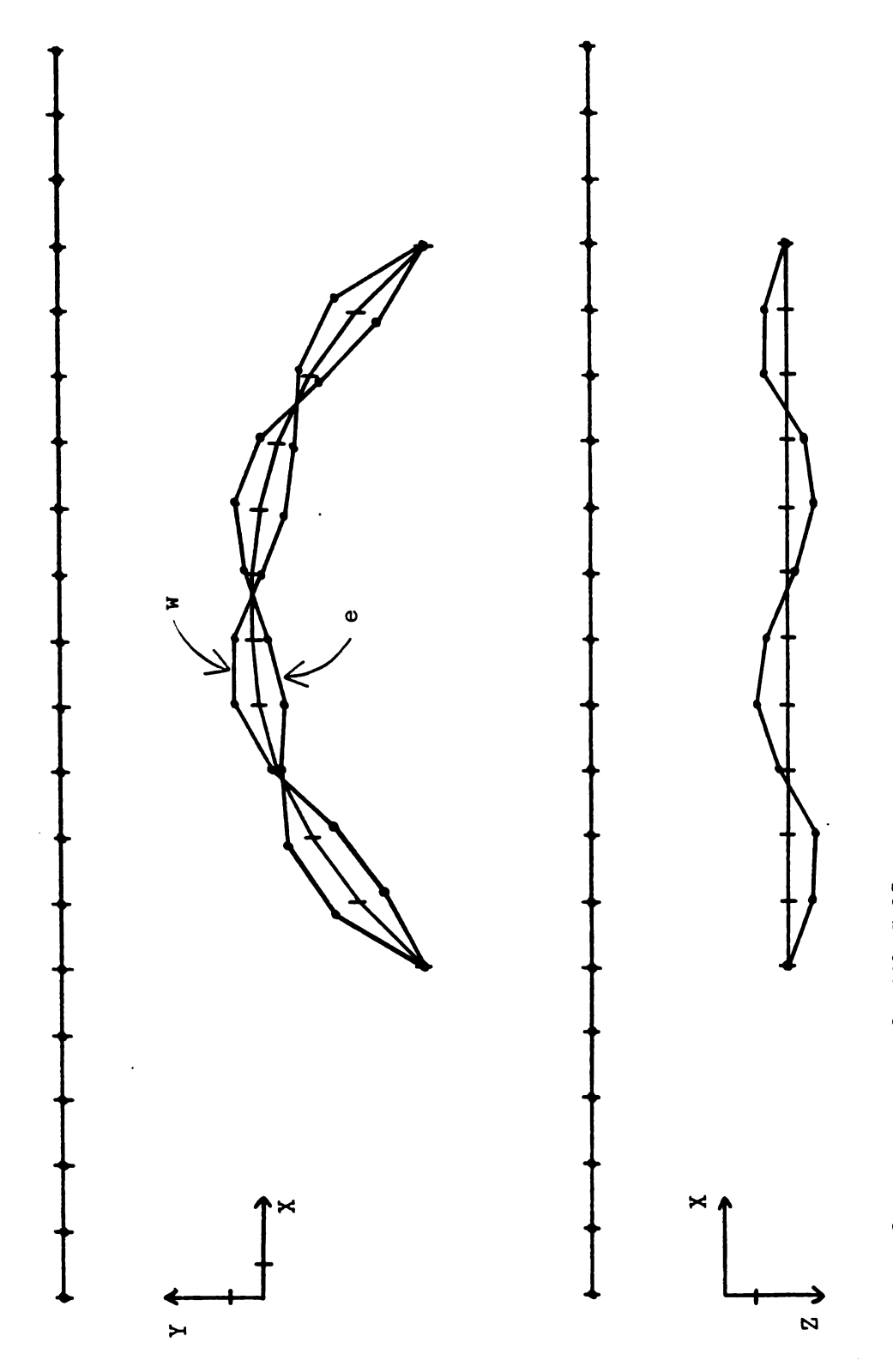


Figure 80 CSCB Mode 20 With Cables

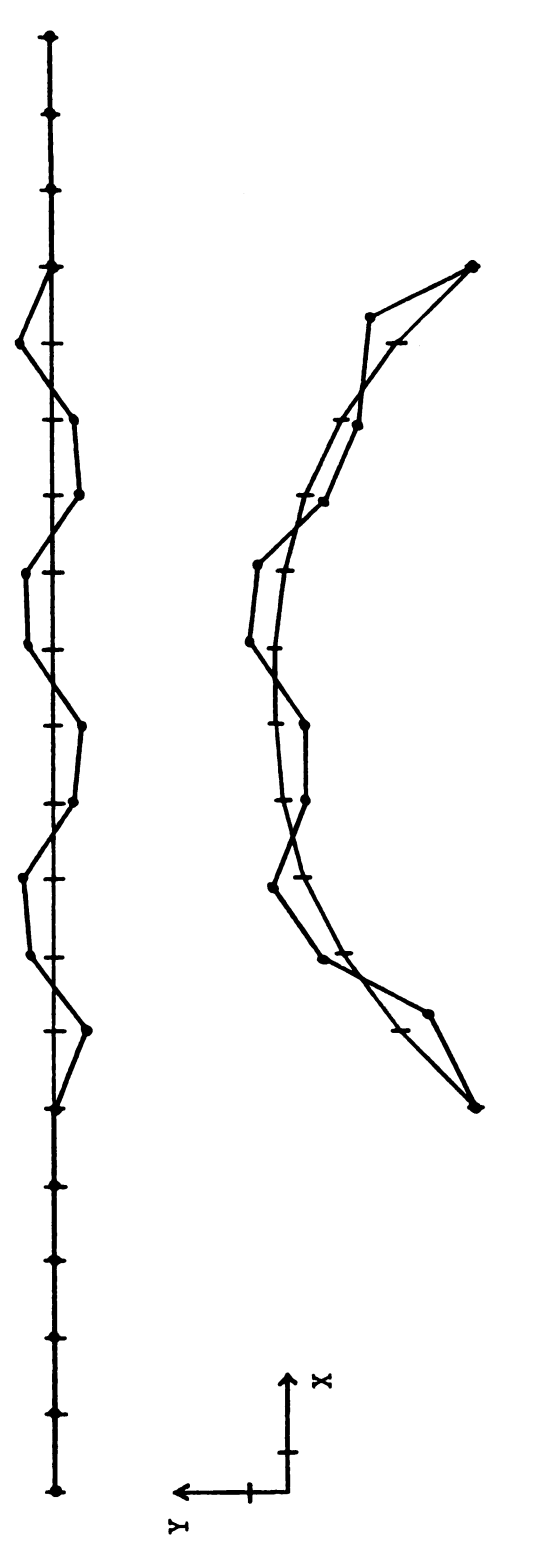
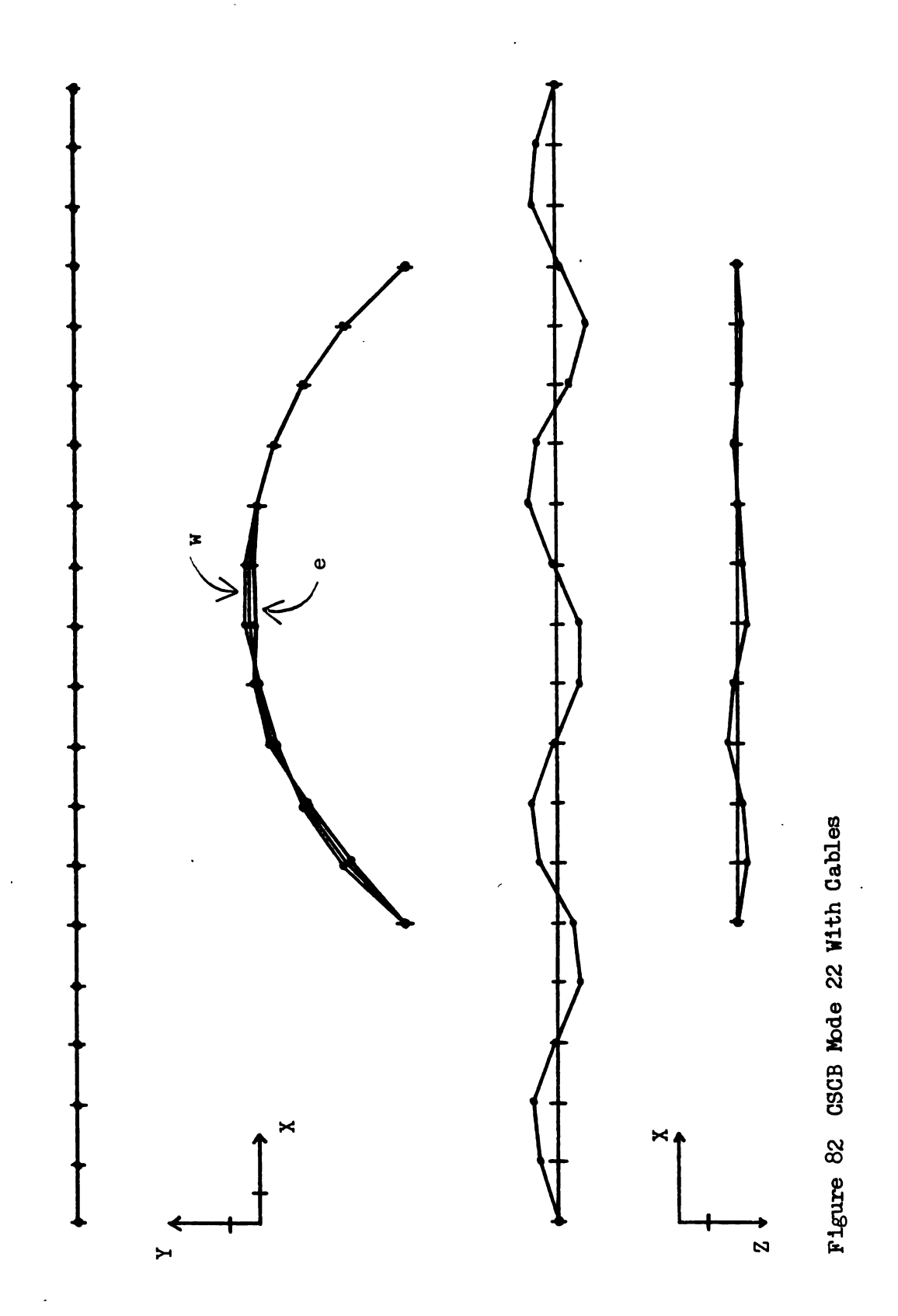


Figure 81 CSCB Mode 21 With Cables



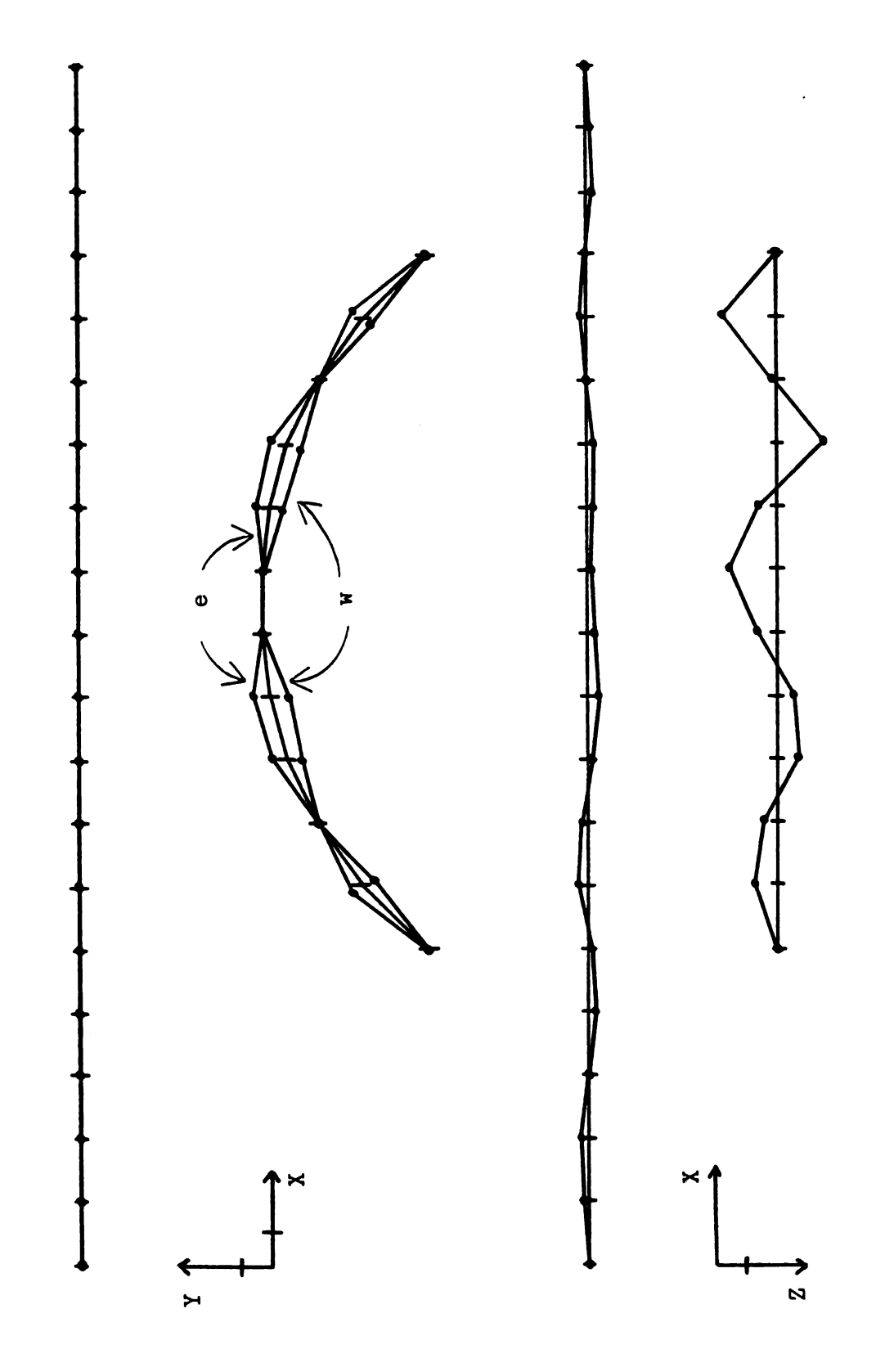
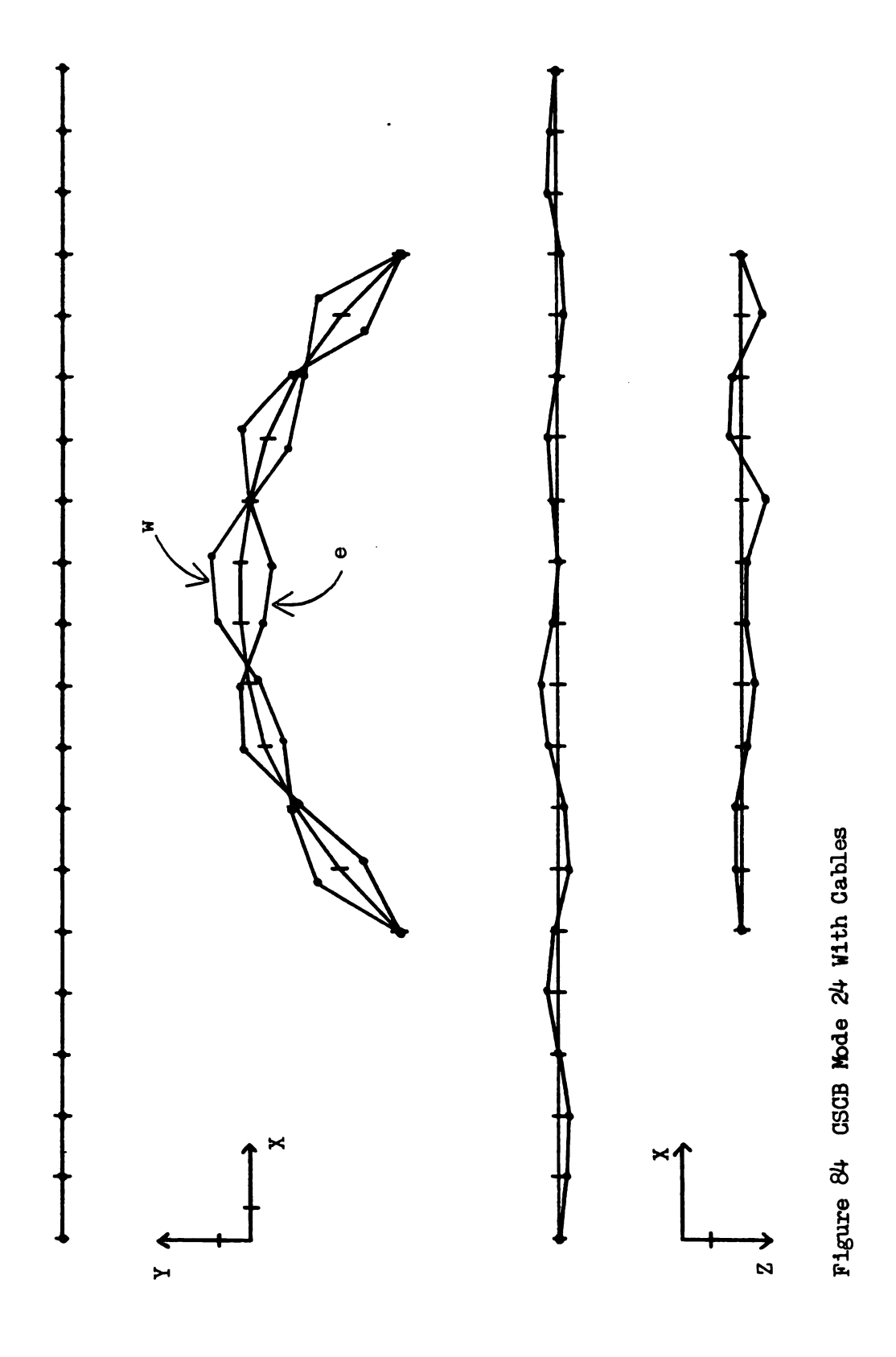
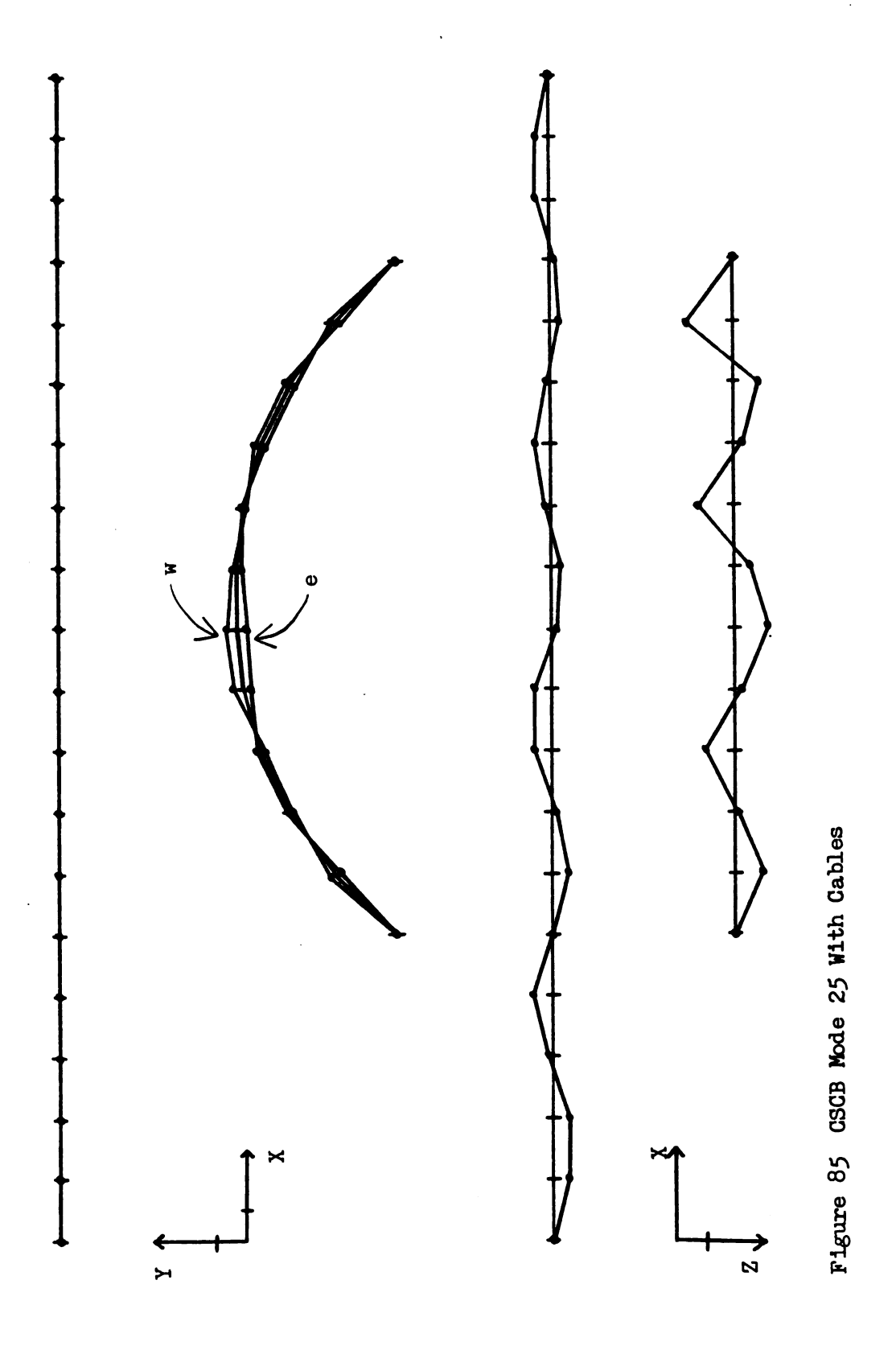
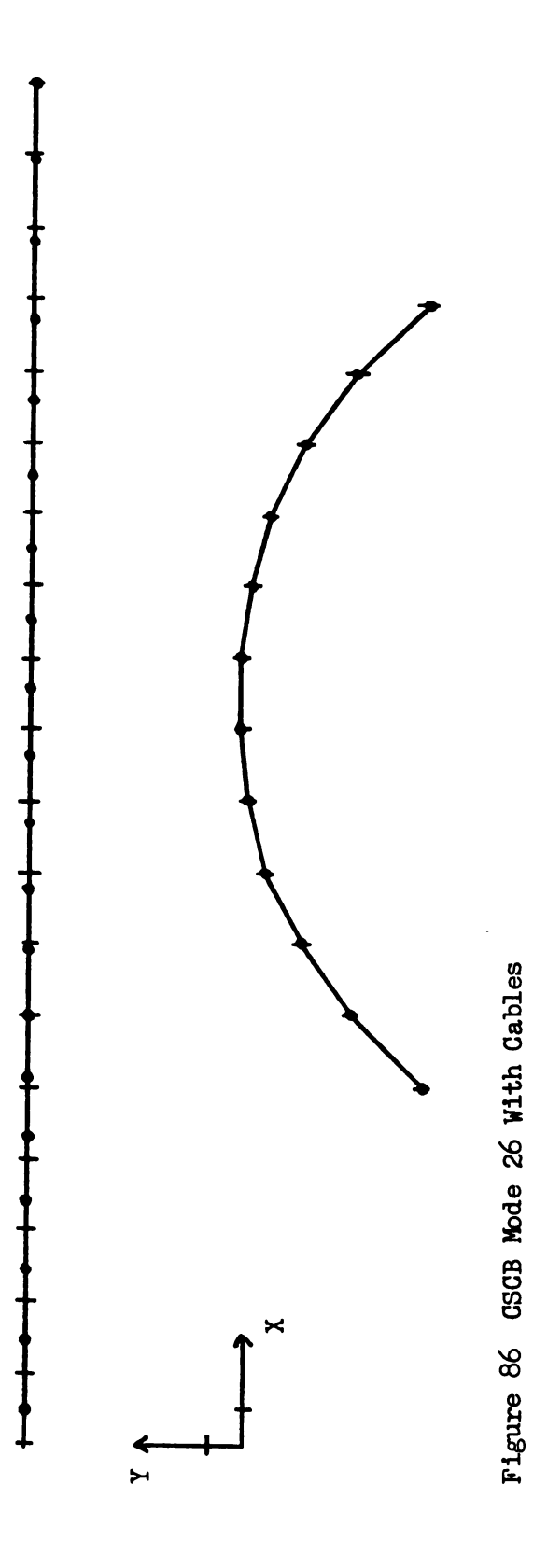


Figure 83 CSCB Mode 23 With Cables







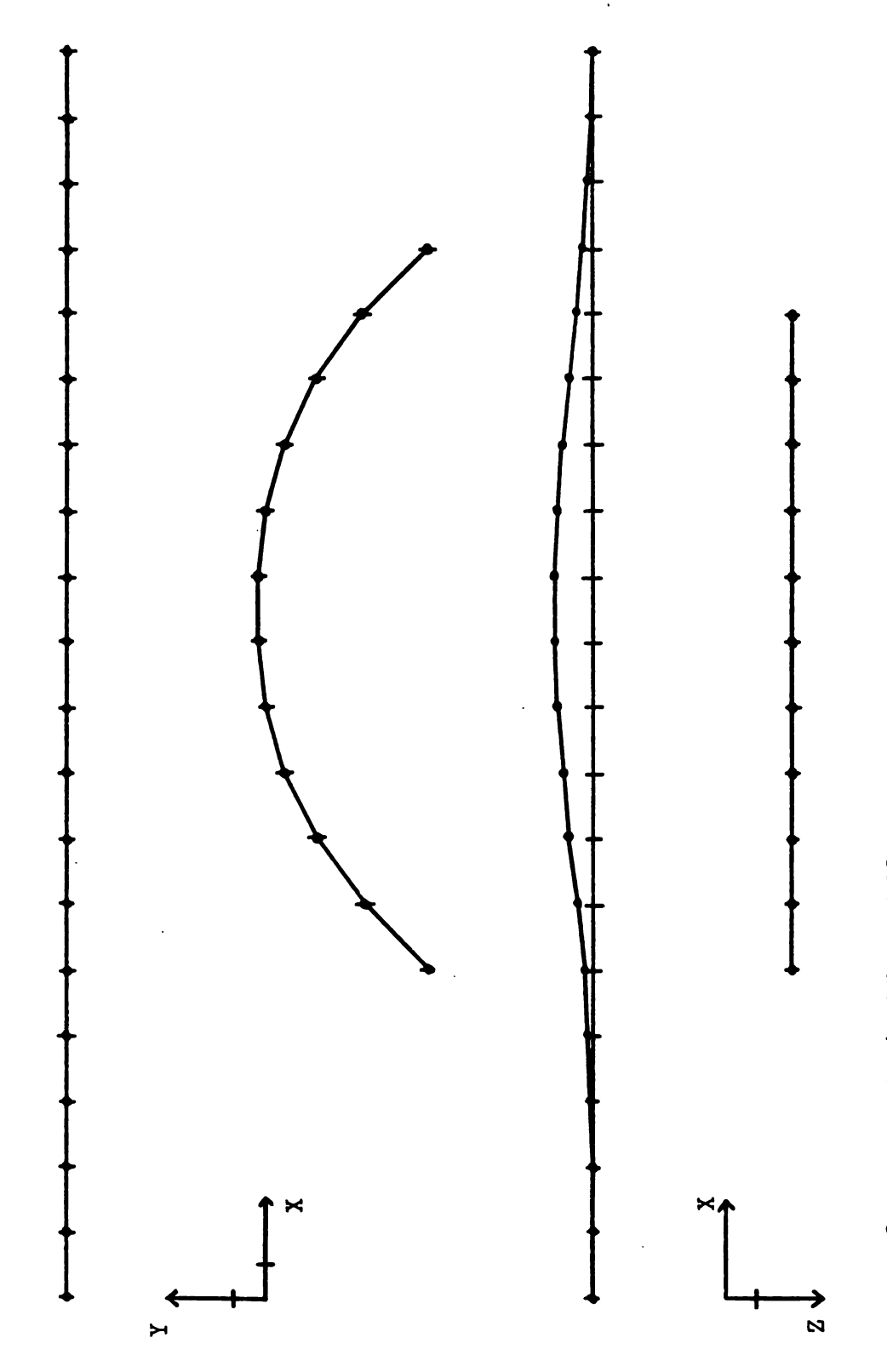


Figure 87 CSCB Mode 1 Without Cables

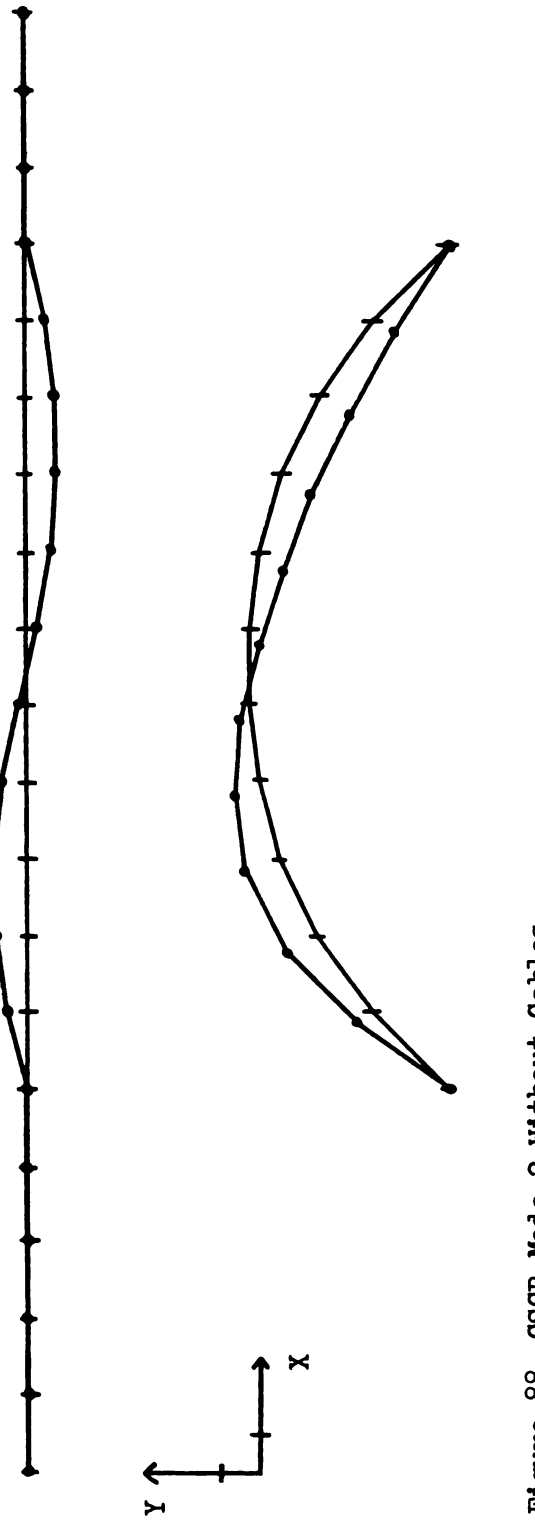


Figure 88 CSCB Mode 2 Without Cables

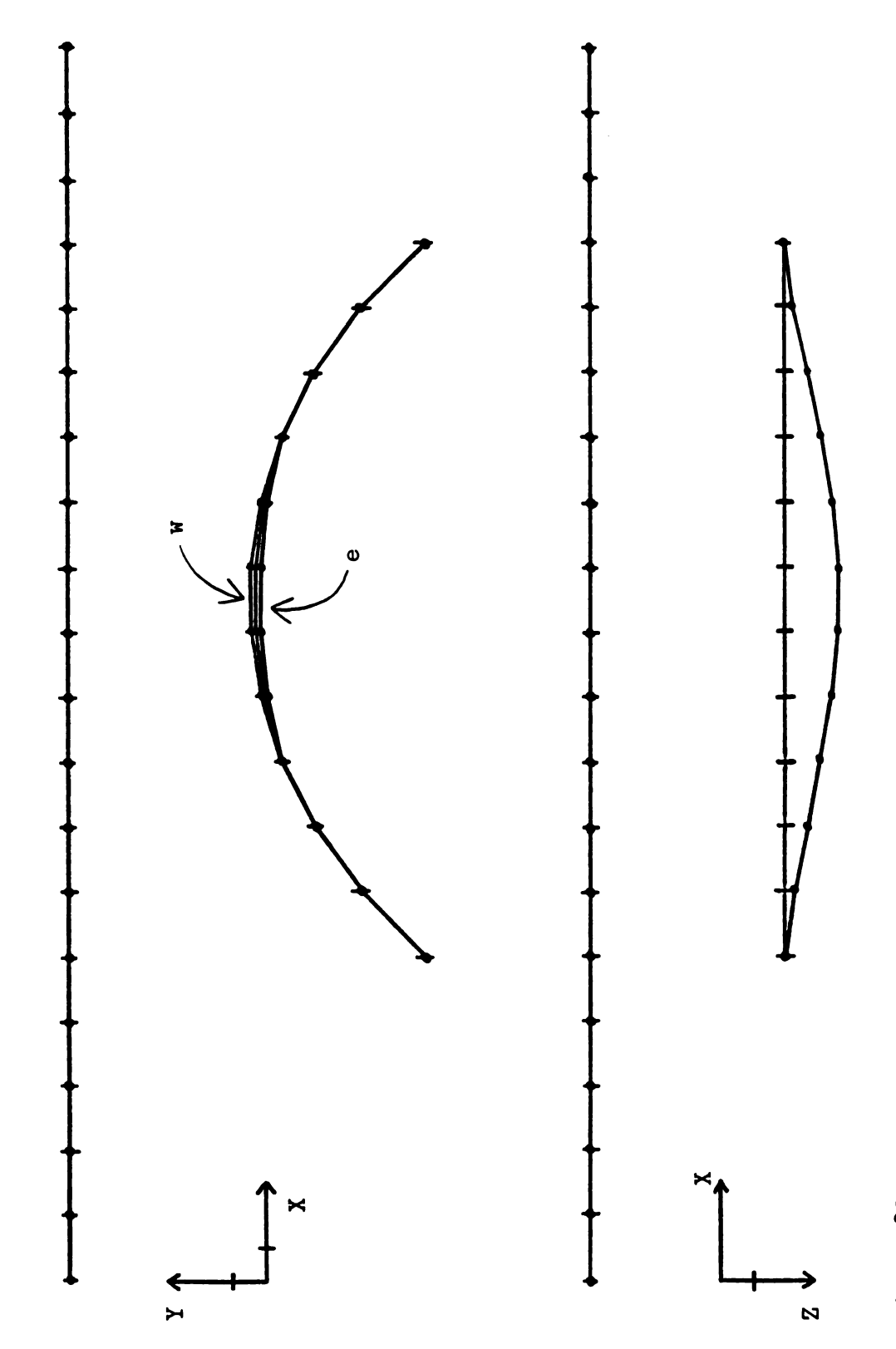
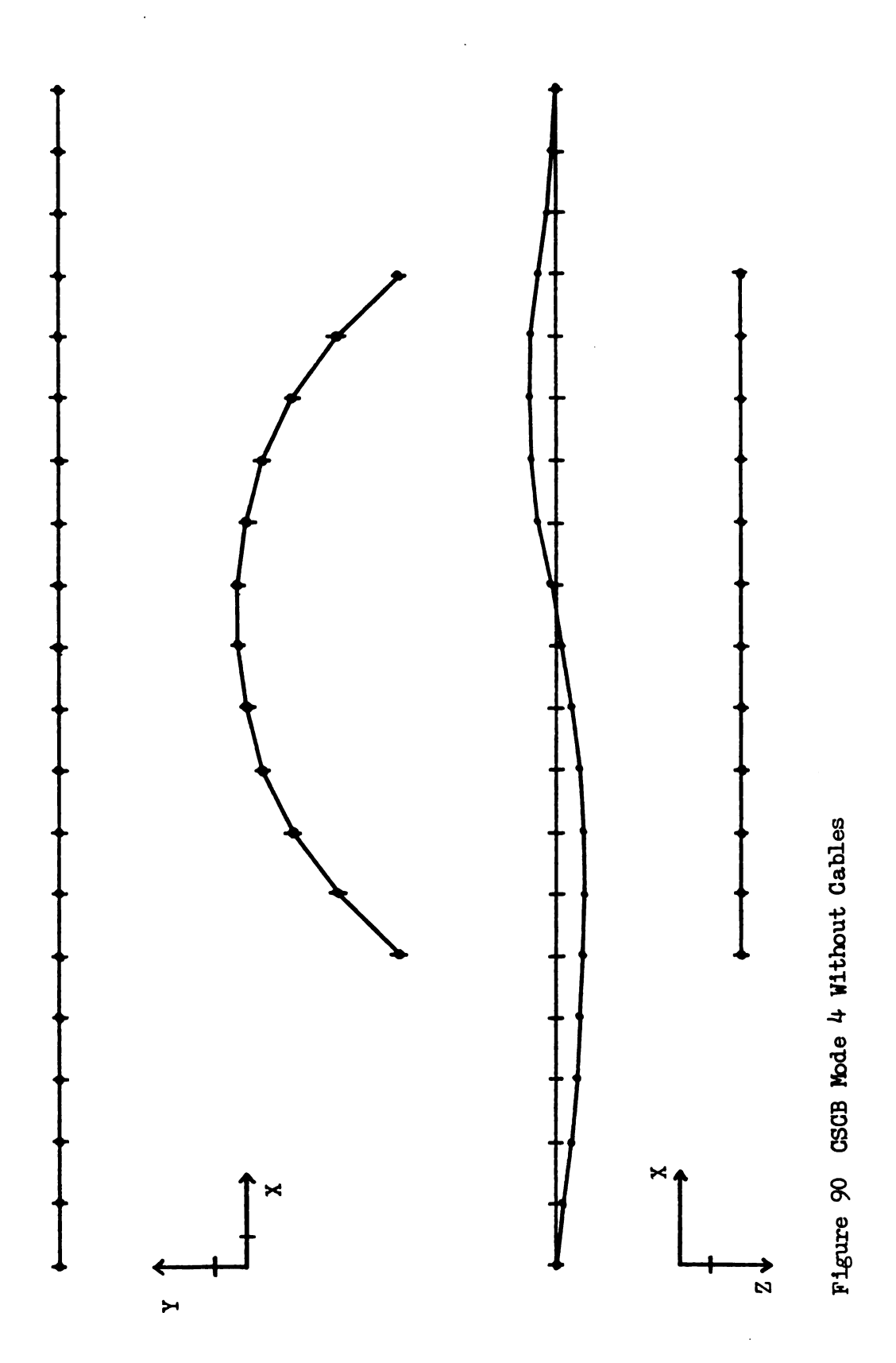


Figure 89 CSCB Mode 3 Without Cables



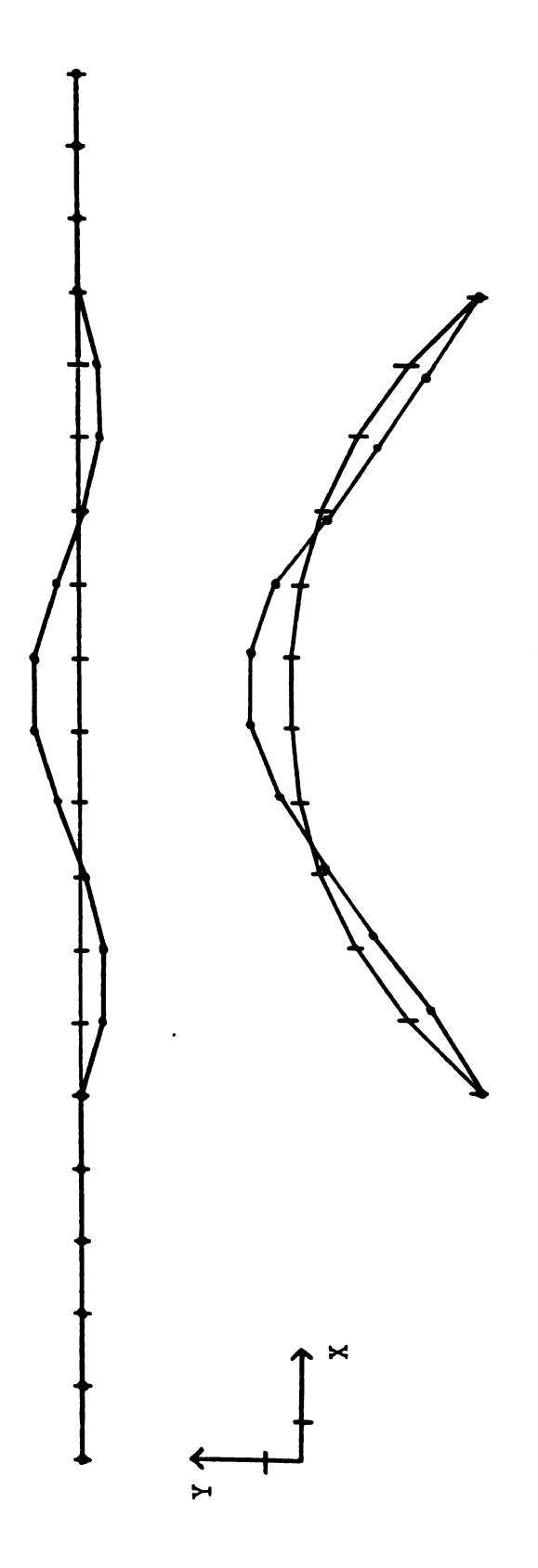
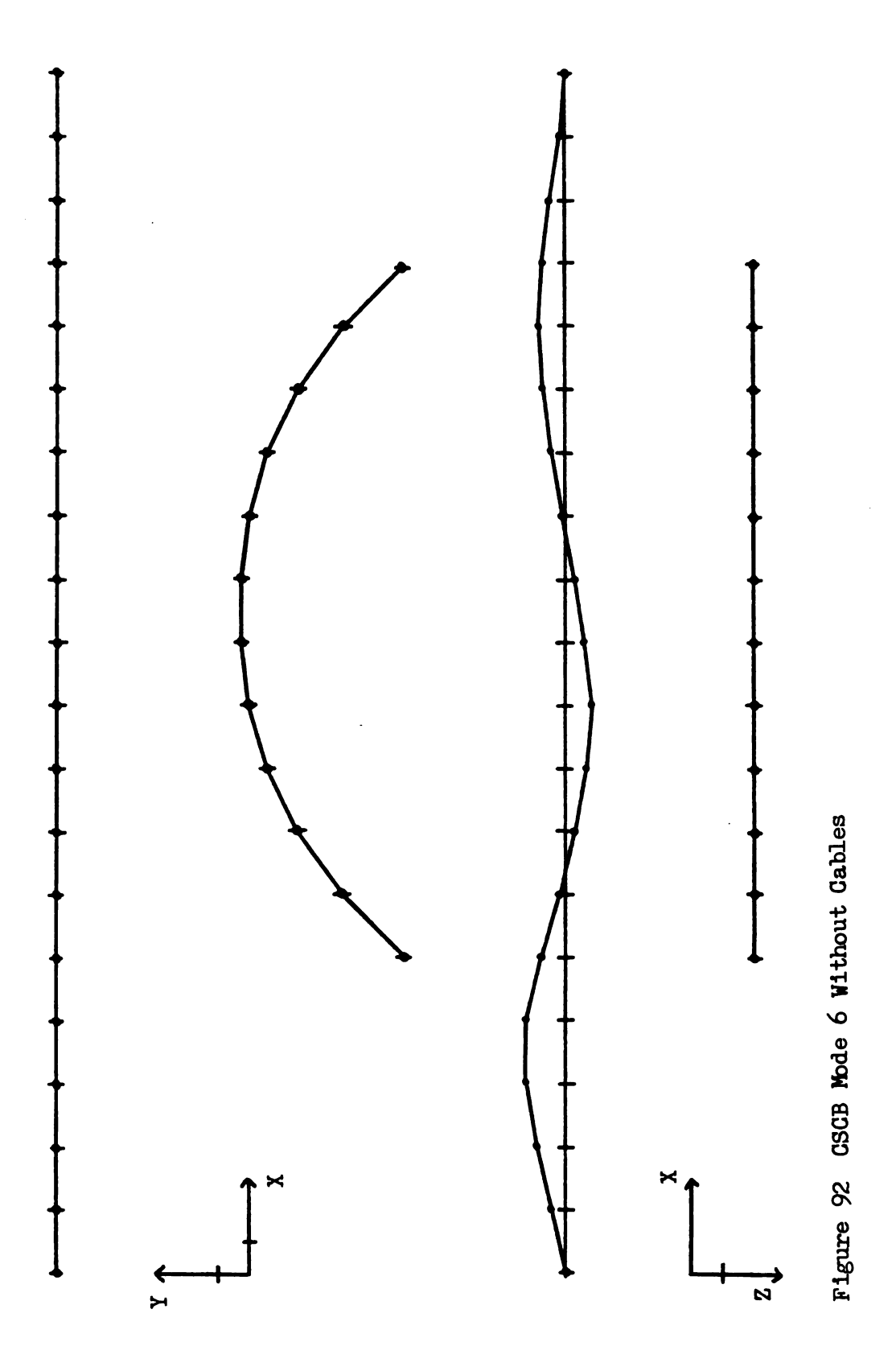


Figure 91 CSCB Mode 5 Without Cables



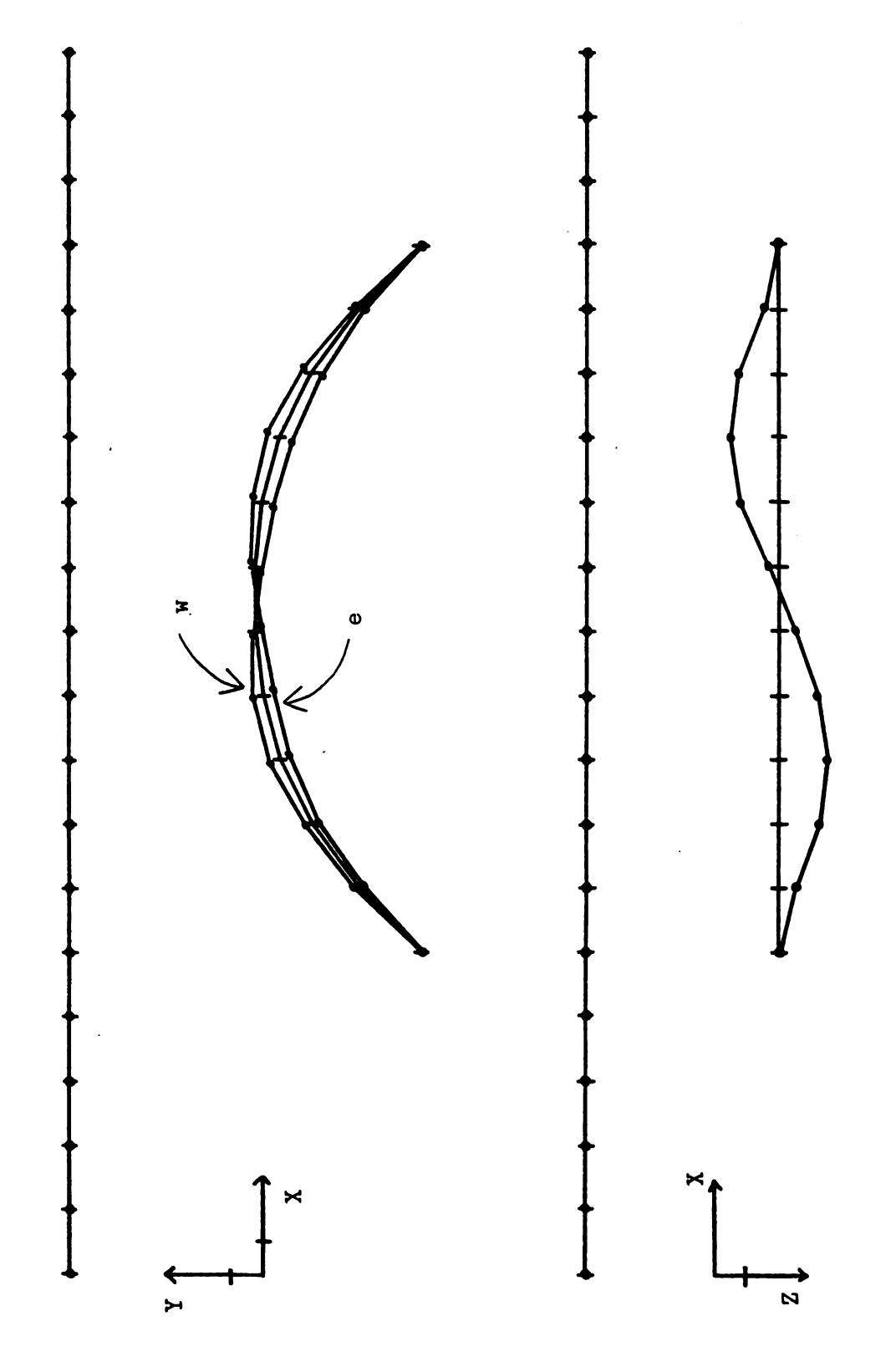
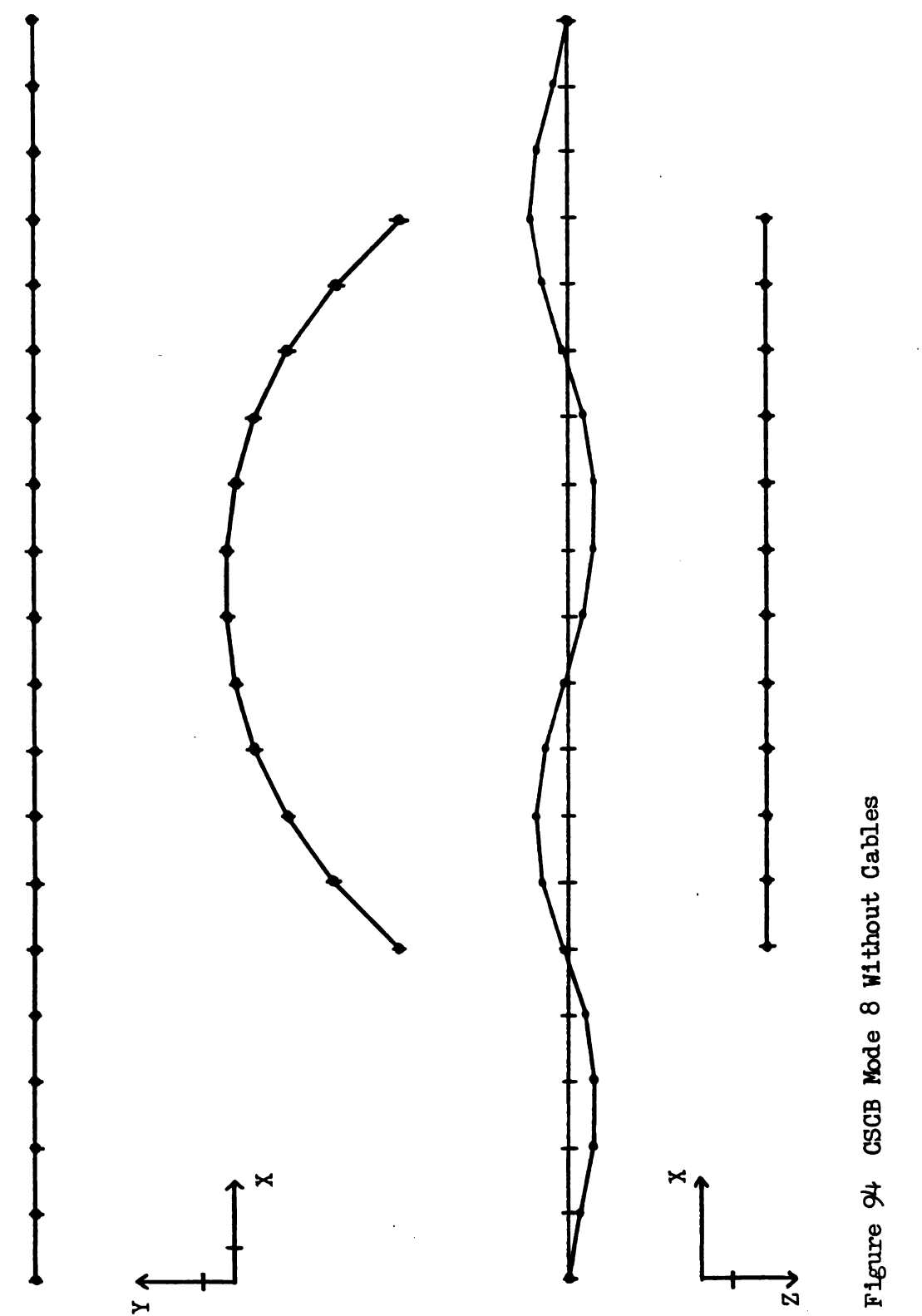


Figure 93 CSCB Mode 7 Without Cables



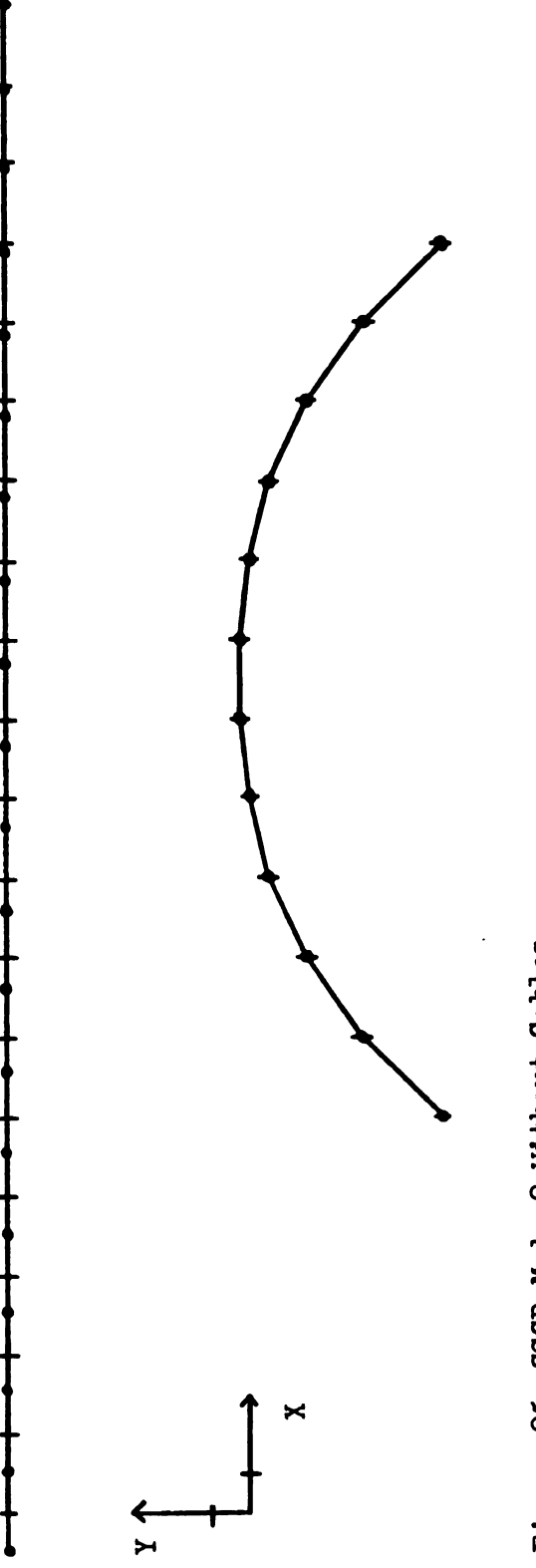


Figure 95 GSCB Mode 9 Without Gables

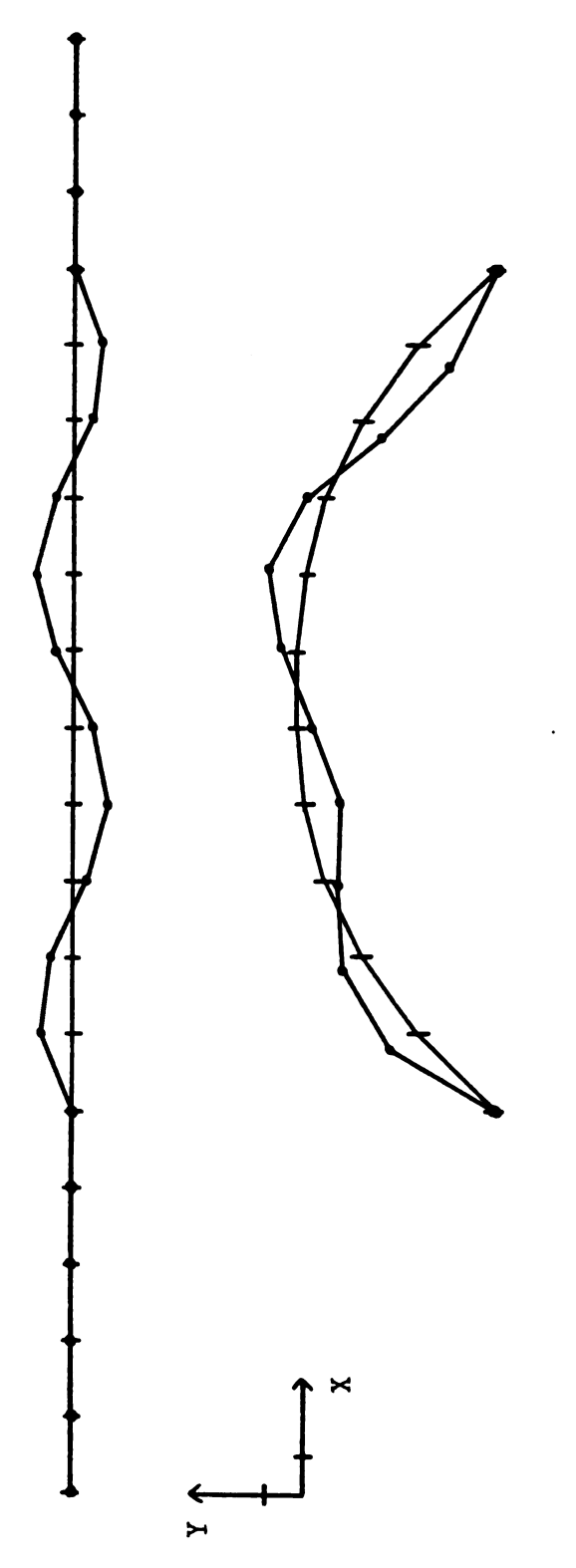


Figure 96 GSCB Mode 10 Without Gables

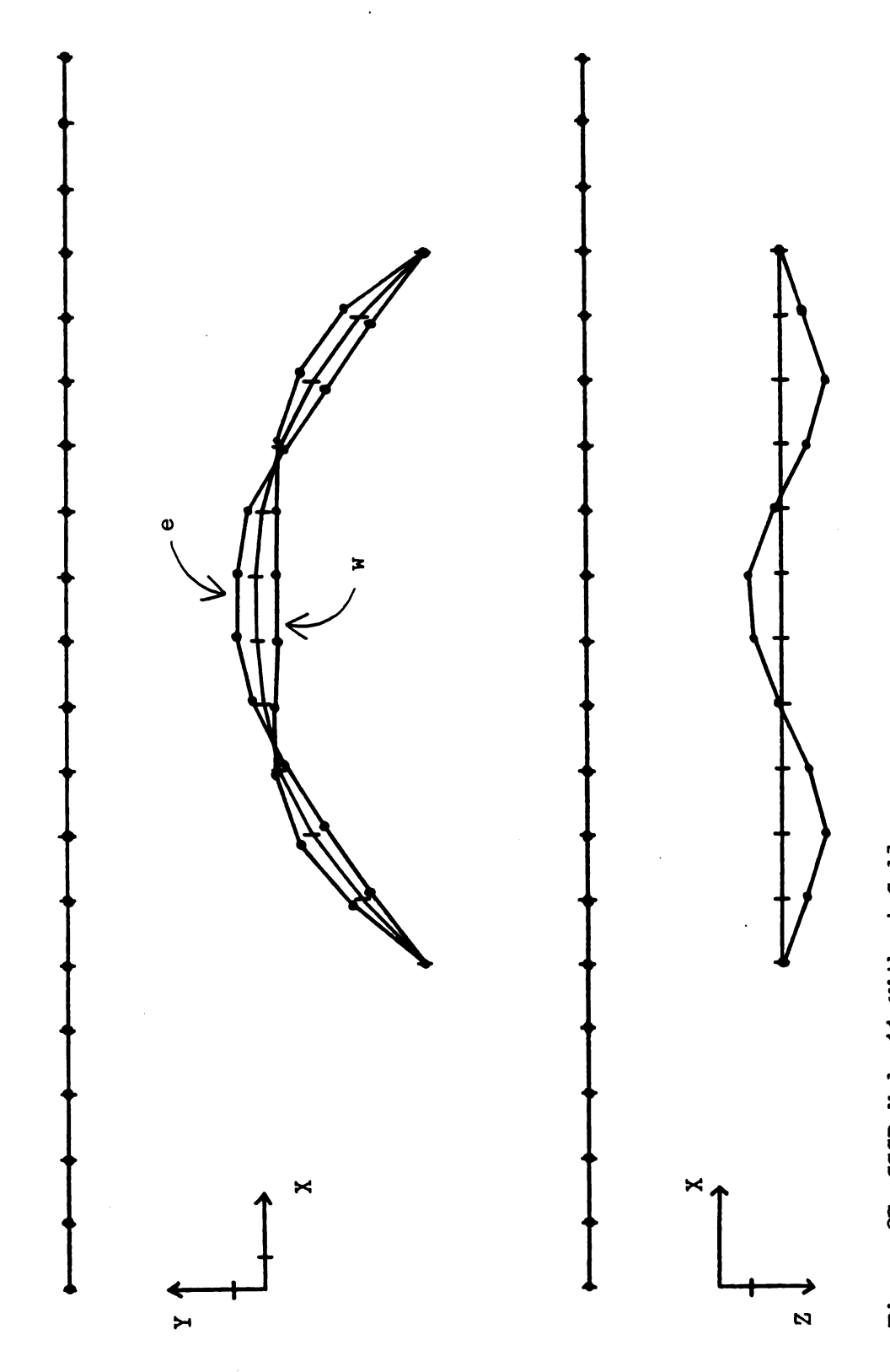


Figure 97 GSCB Mode 11 Without Cables

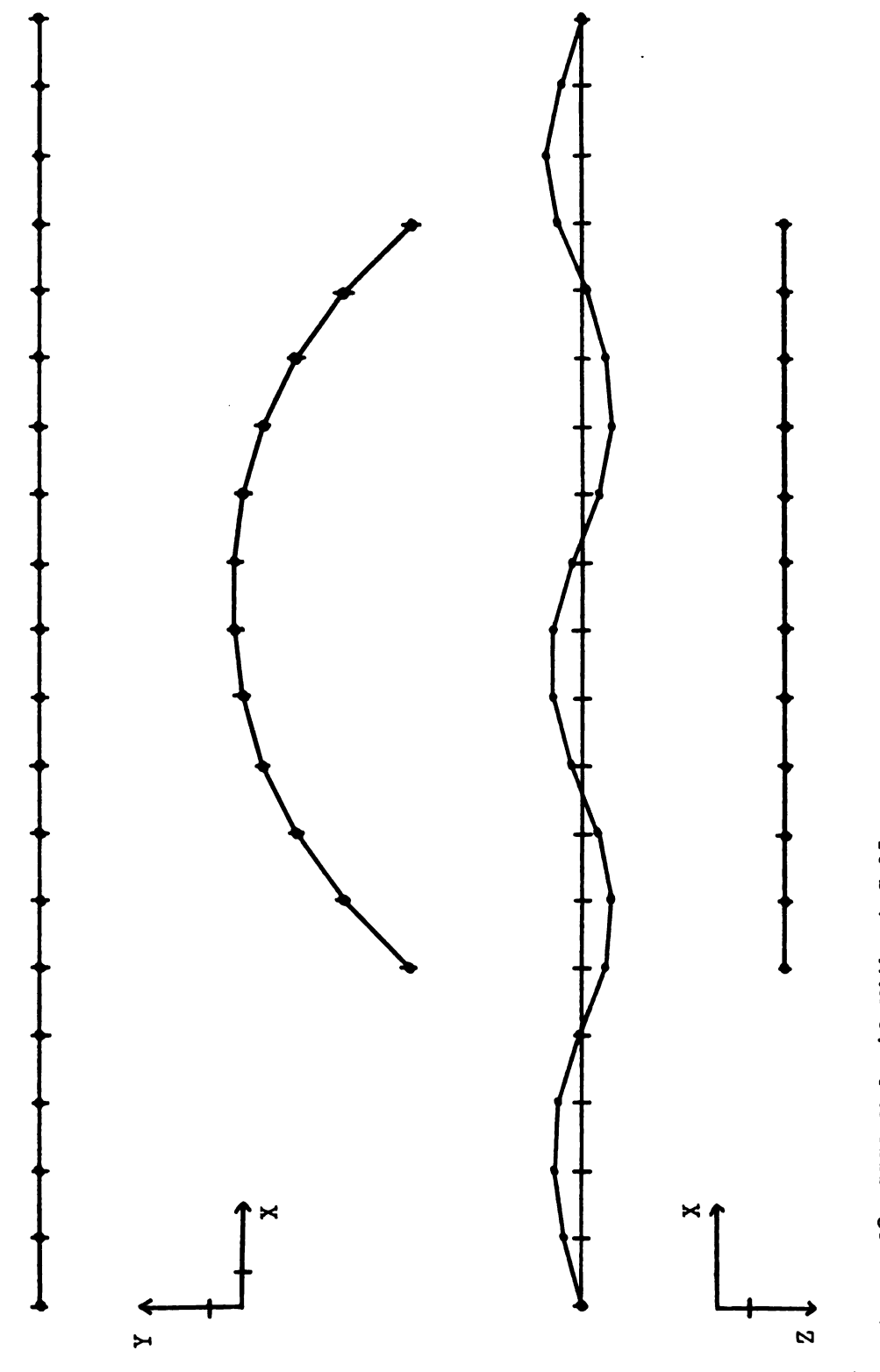


Figure 98 CSCB Mode 12 Without Cables

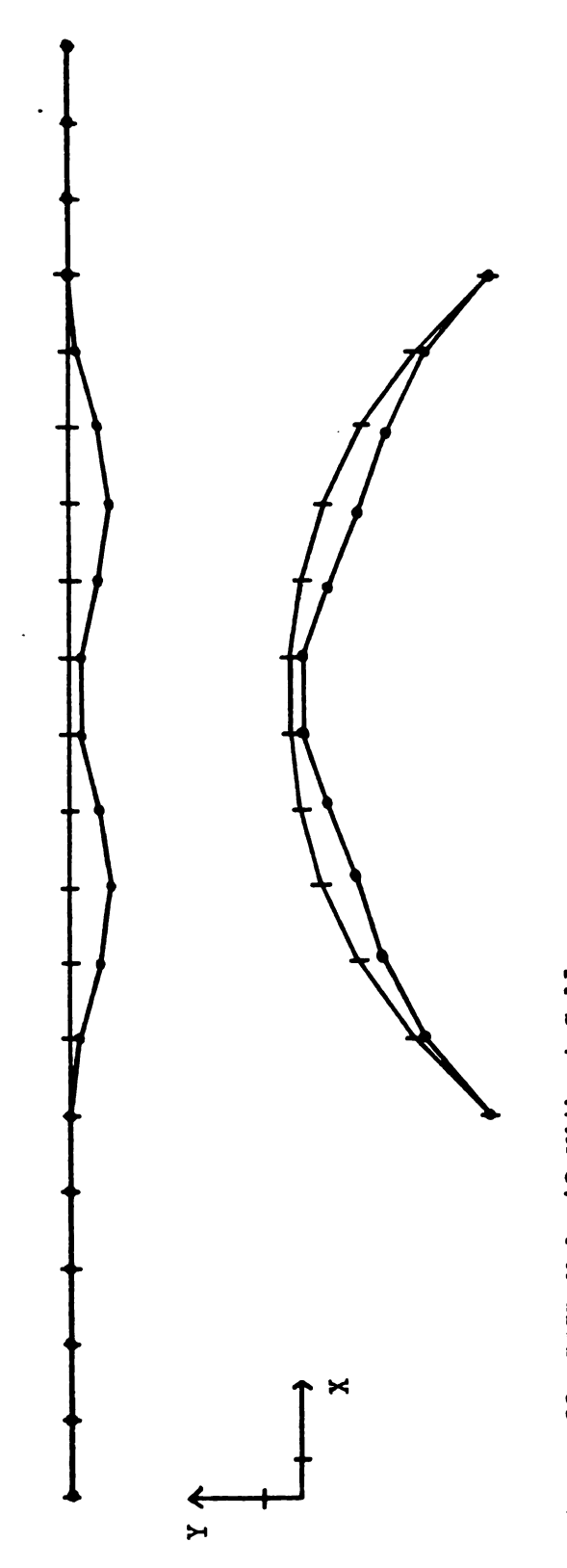


Figure 99 GSGB Mode 13 Without Gables

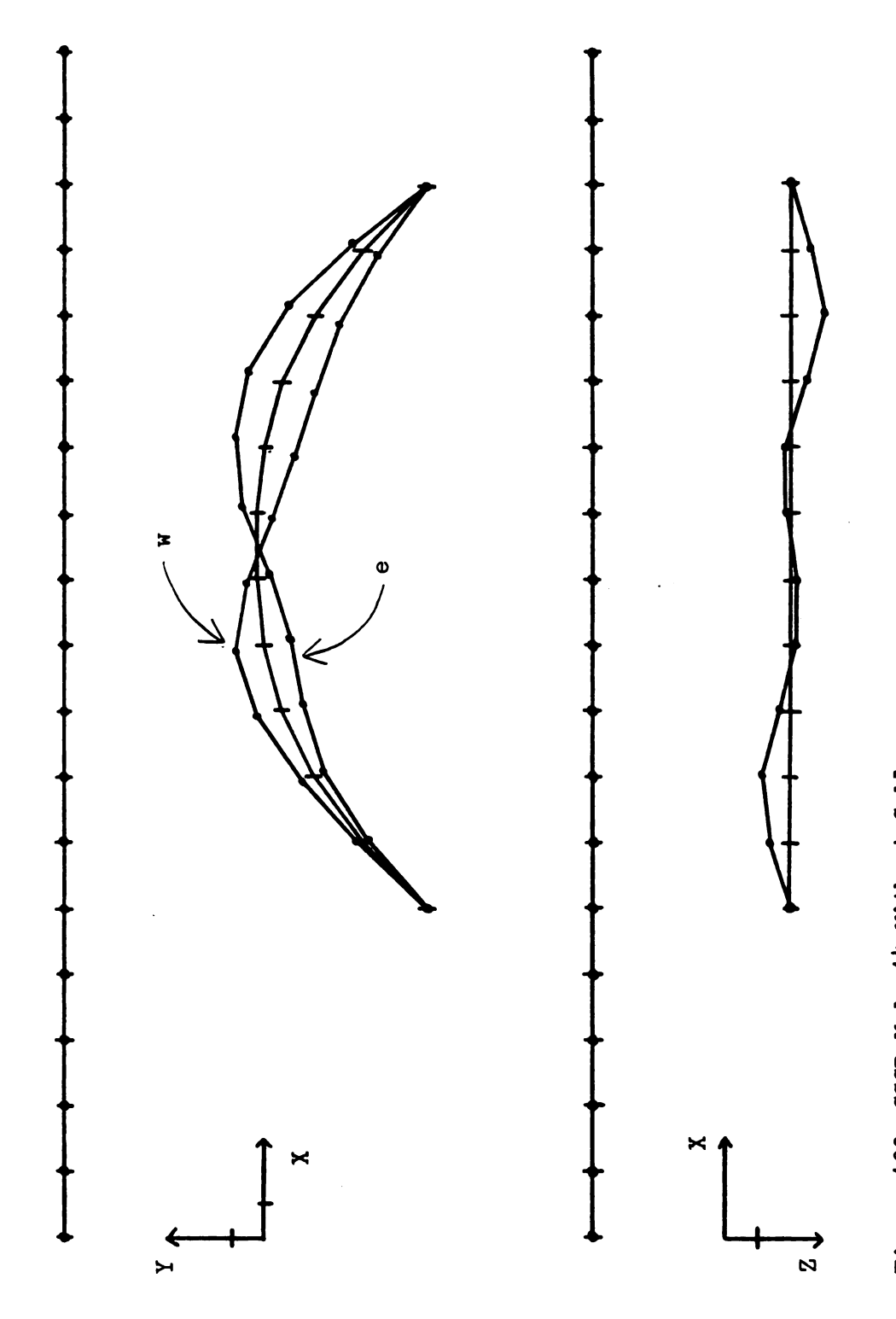


Figure 100 GSGB Mode 14 Without Cables

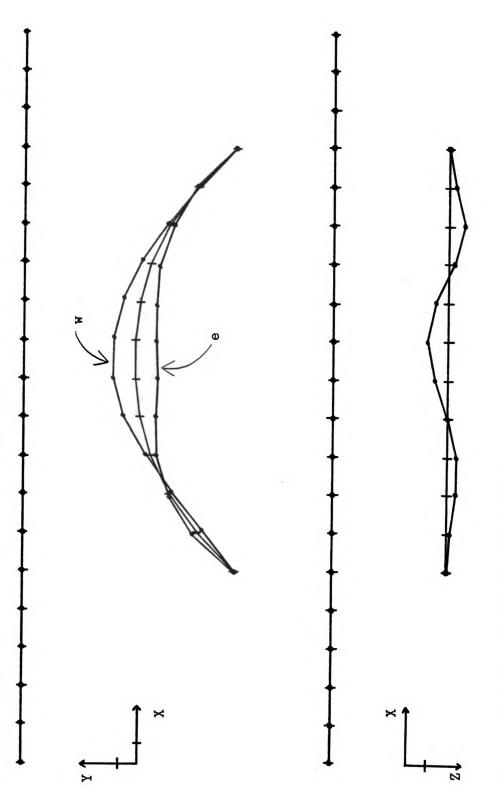
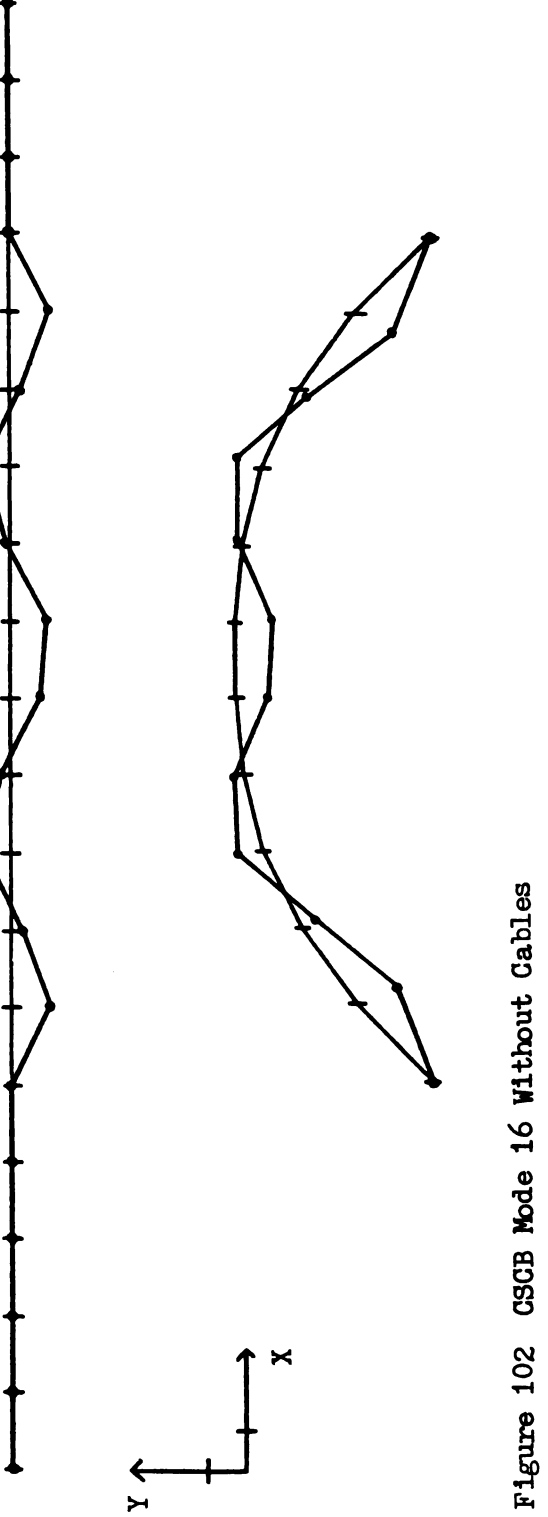


Figure 101 CSCB Mode 15 Without Cables



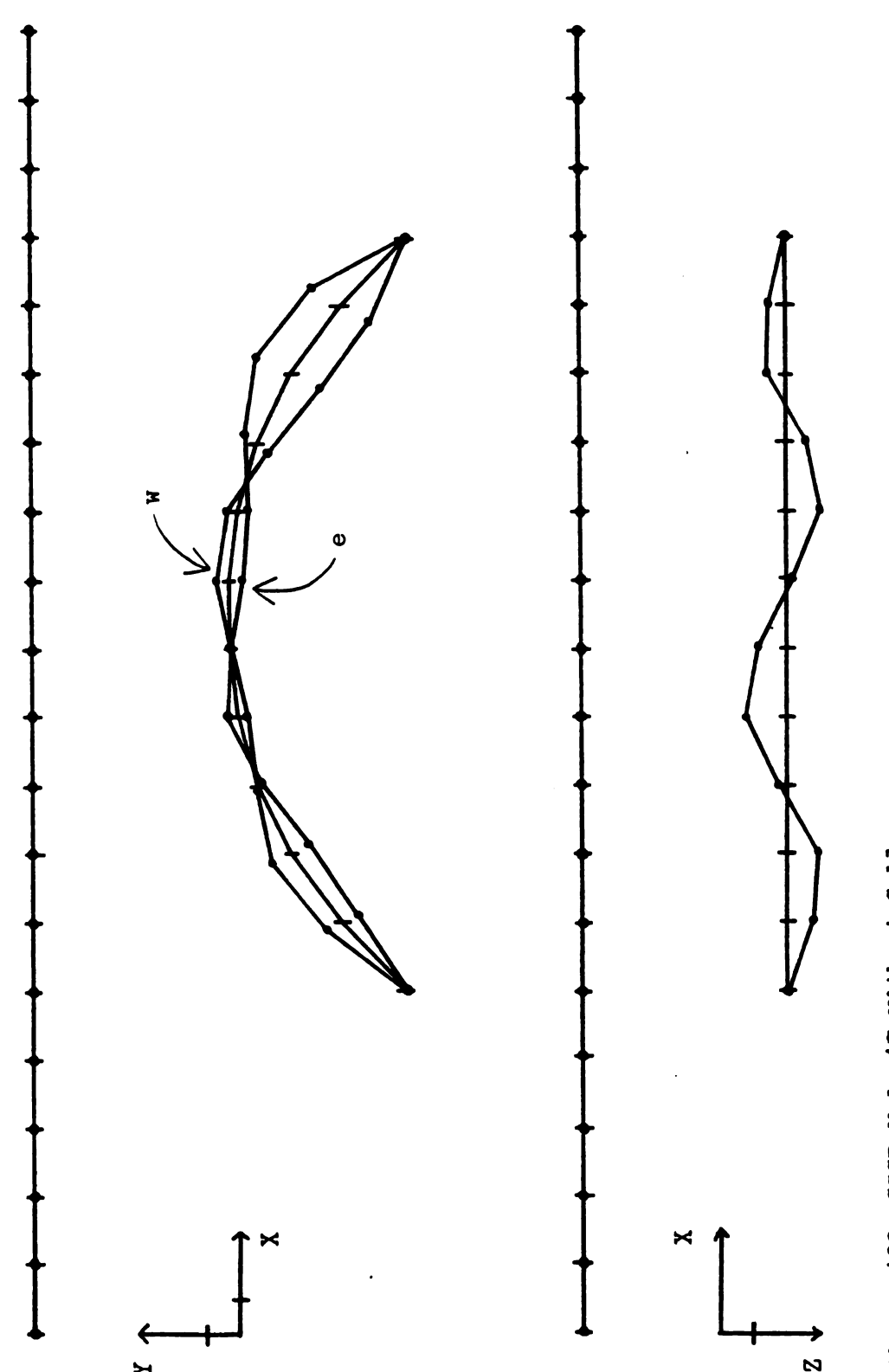


Figure 103 CSCB Mode 17 Without Cables

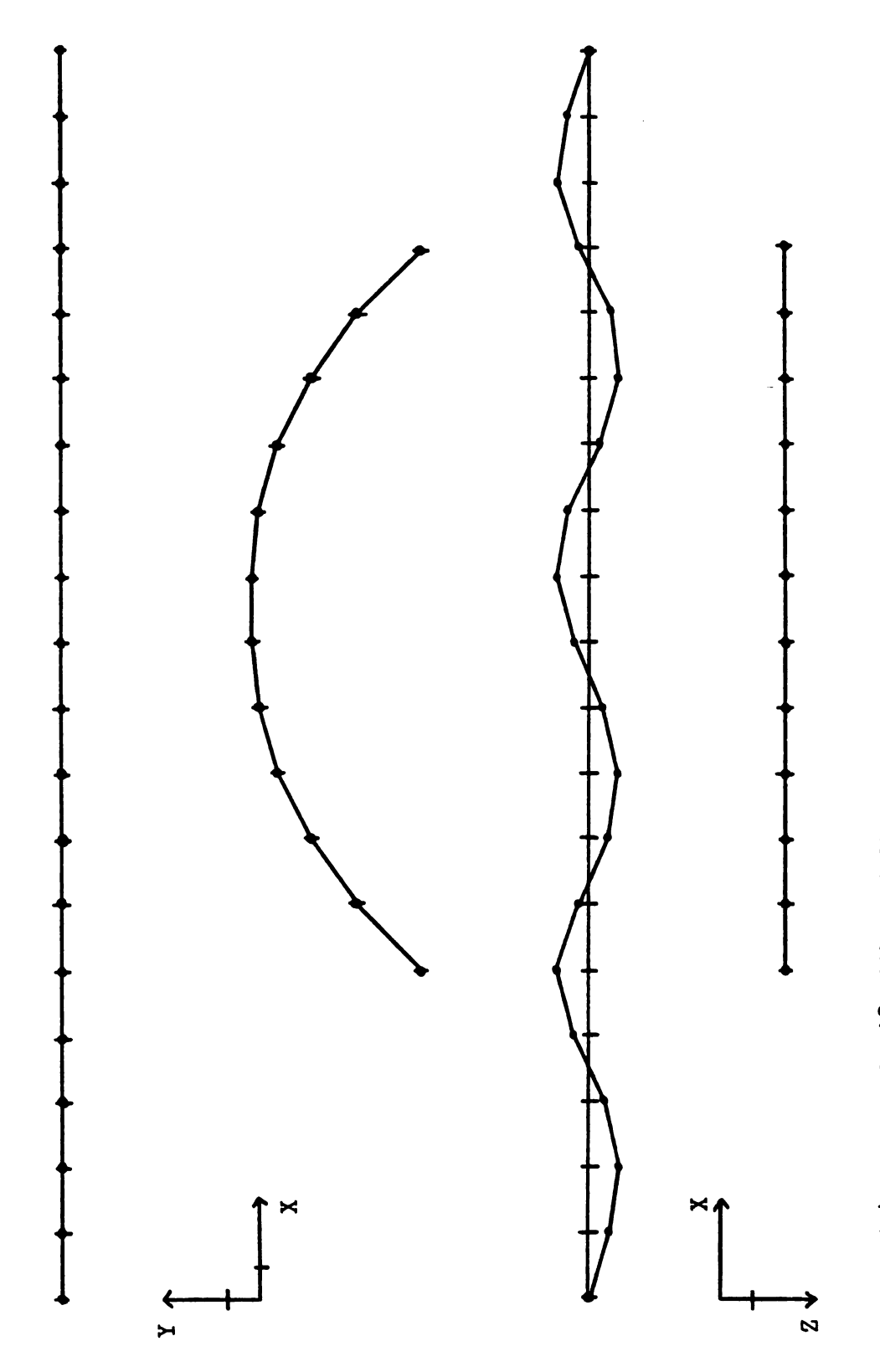


Figure 104 CSCB Mode 18 Without Cables

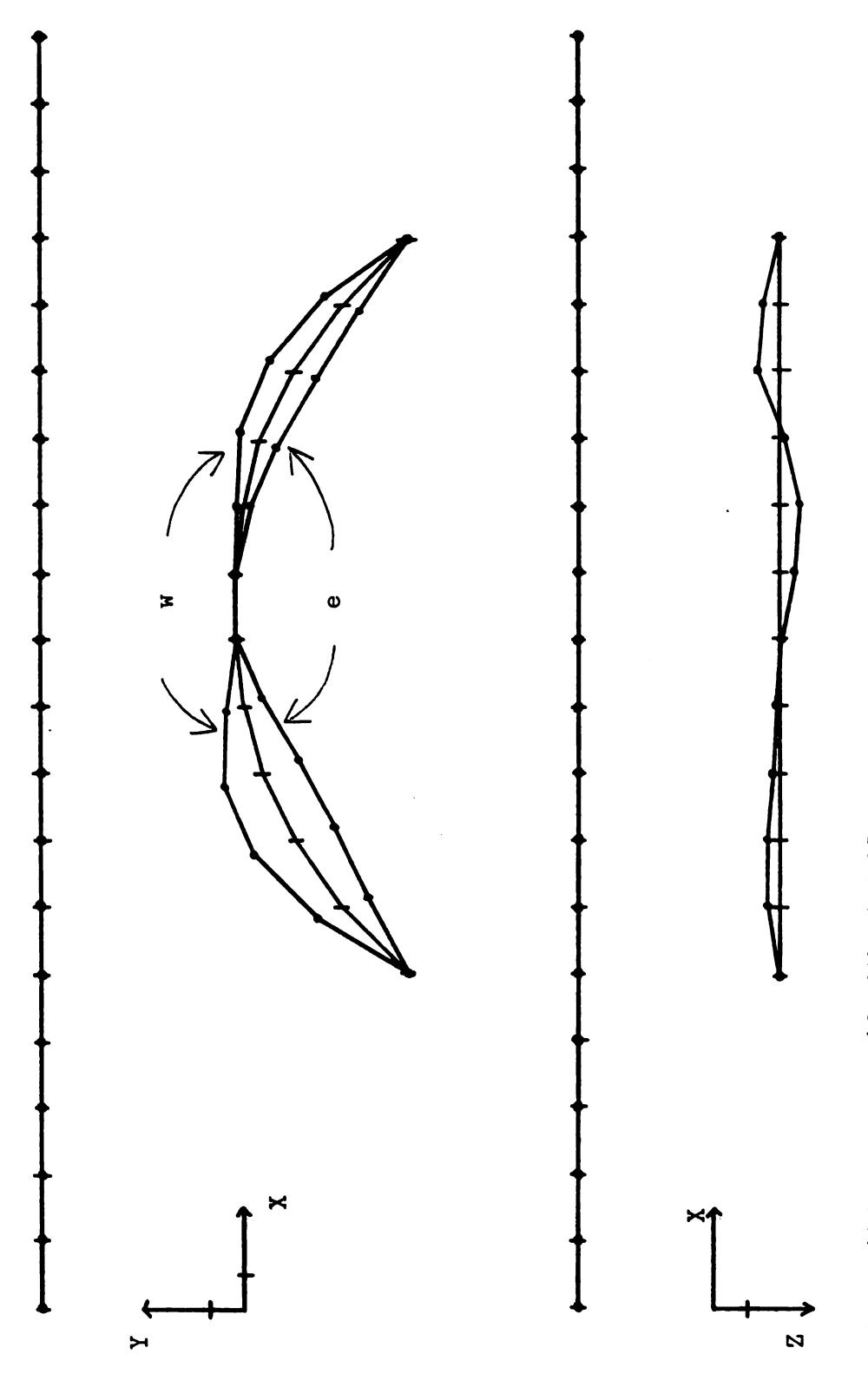


Figure 105 CSCB Mode 19 Without Cables

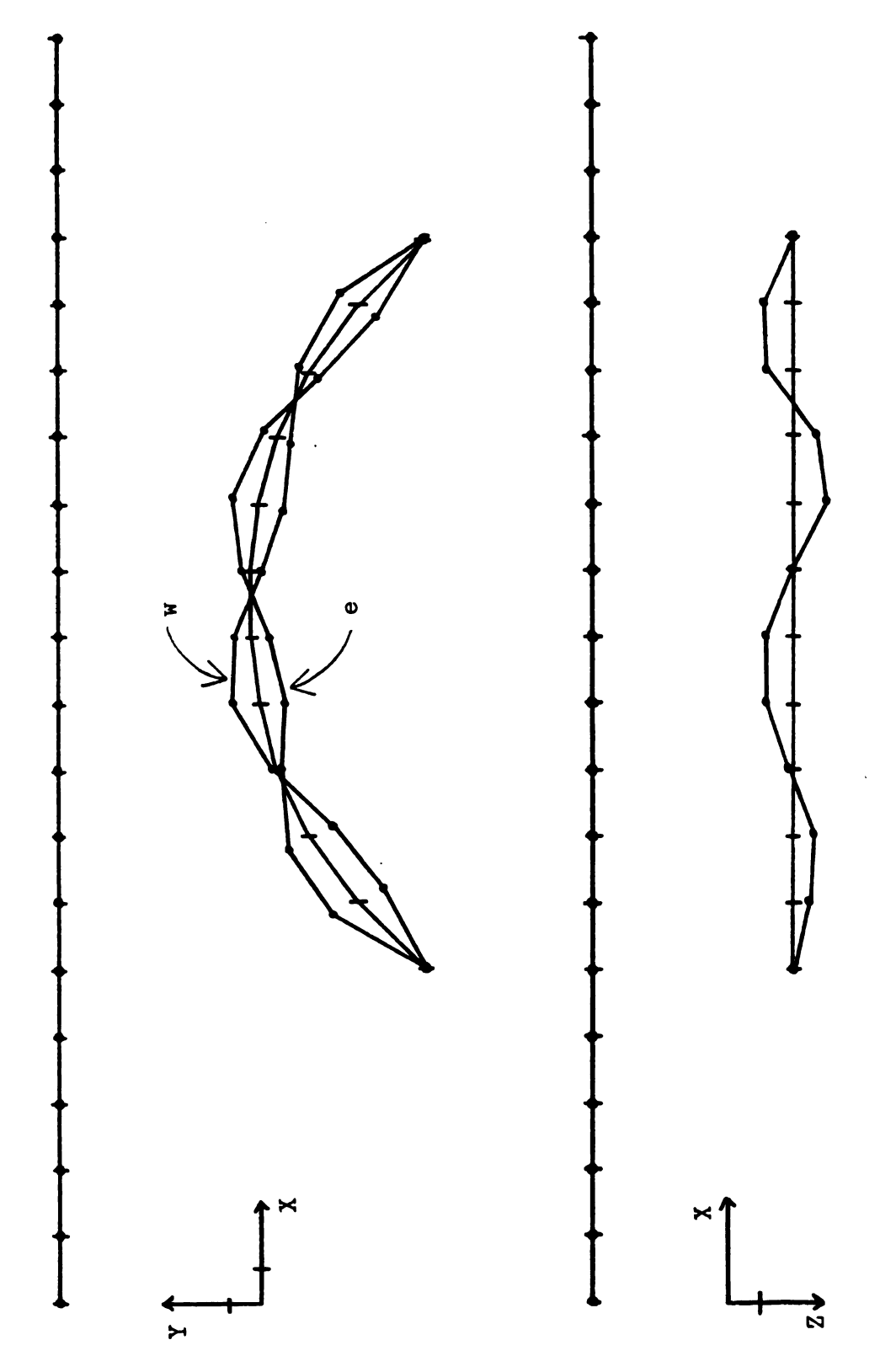


Figure 106 GSGB Mode 20 Without Gables

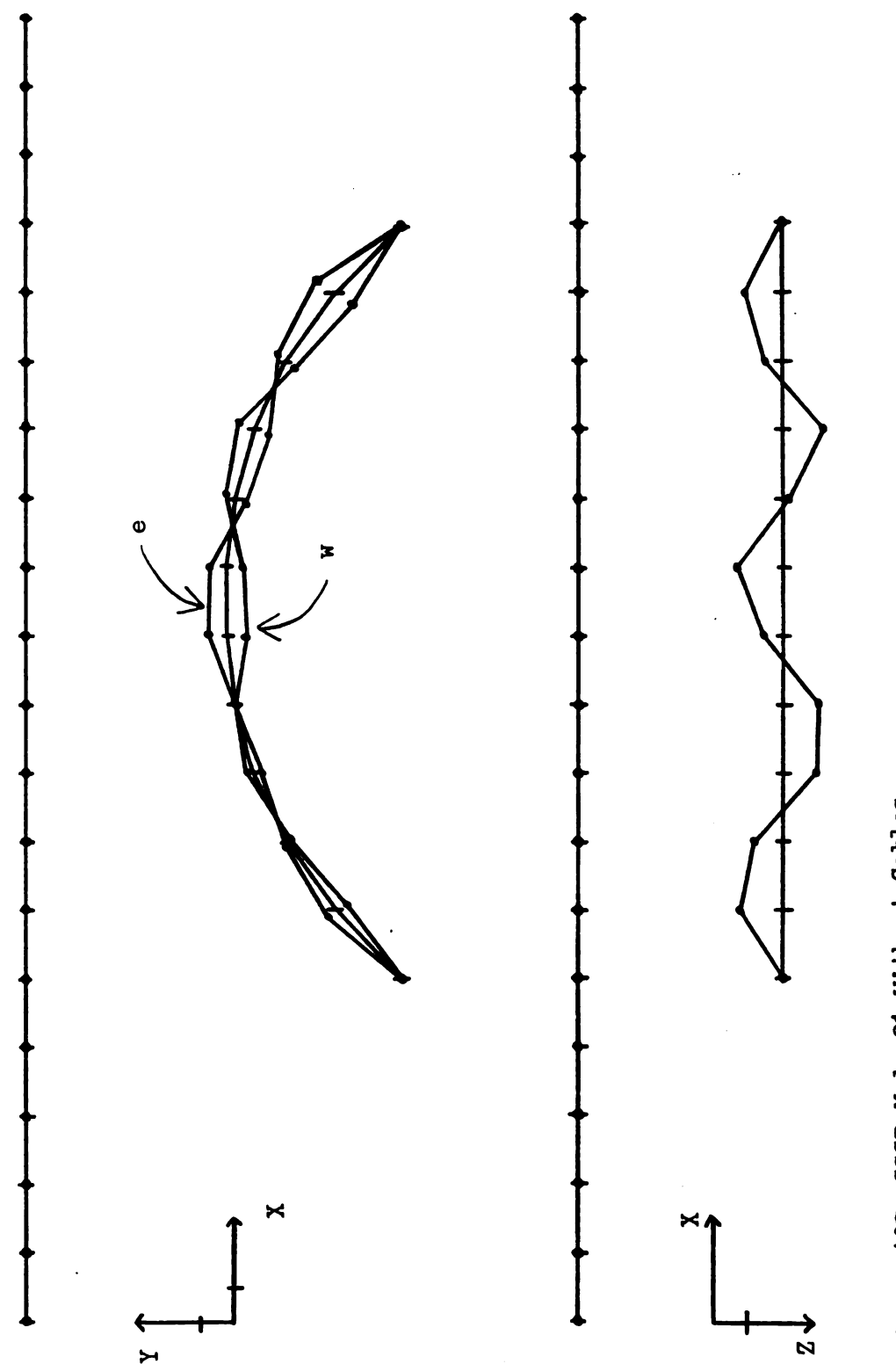


Figure 107 GSCB Mode 21 Without Cables

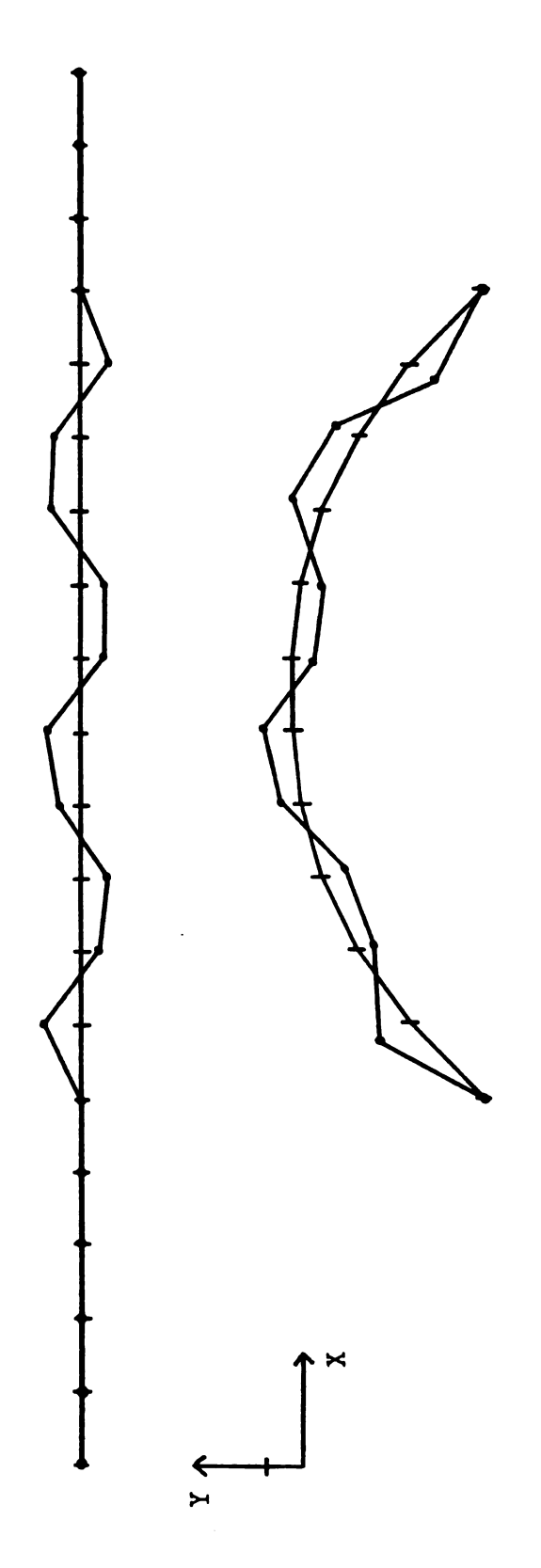


Figure 108 CSCB Mode 22 Without Cables

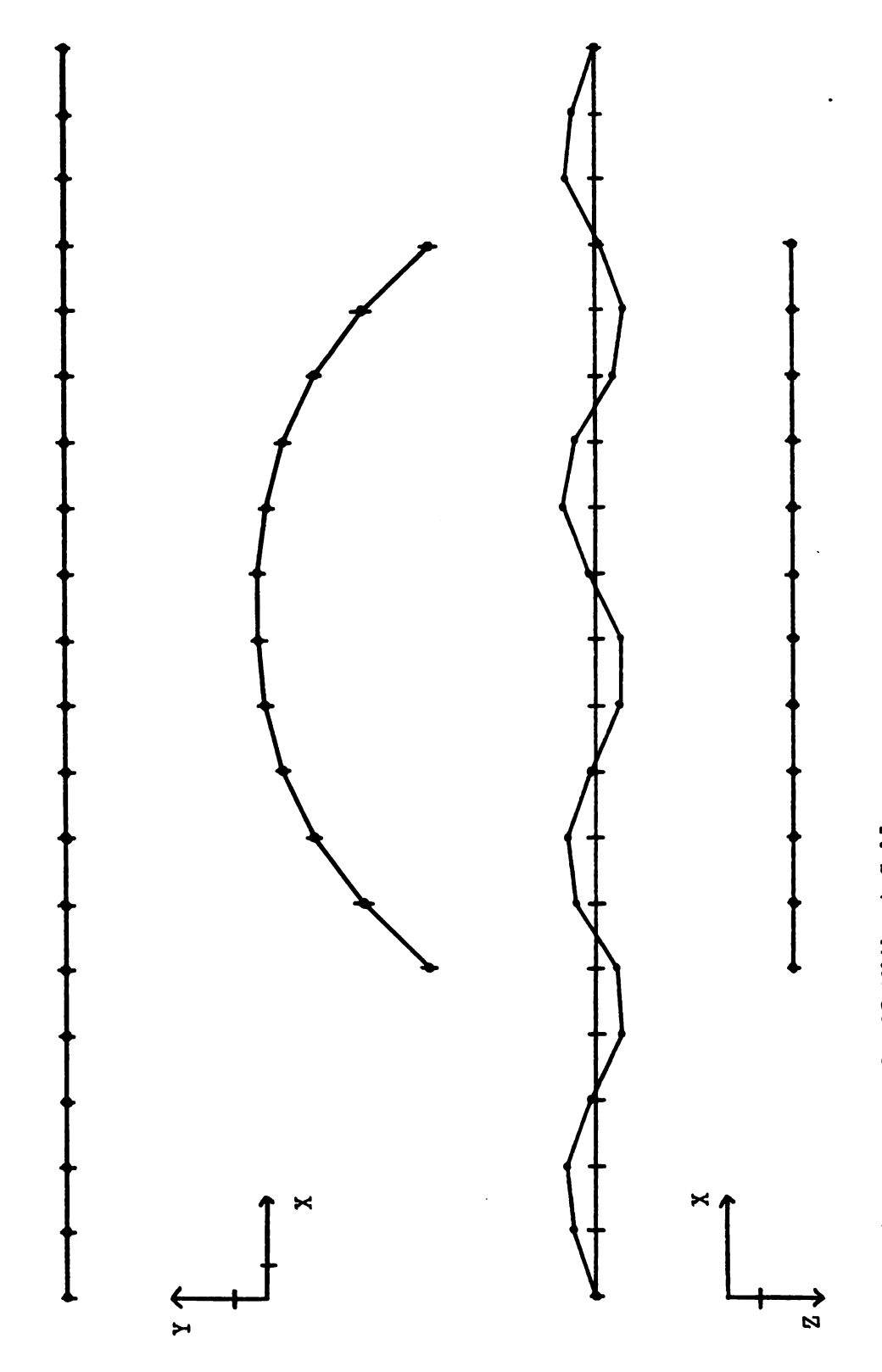


Figure 109 GSCB Mode 23 Without Cables

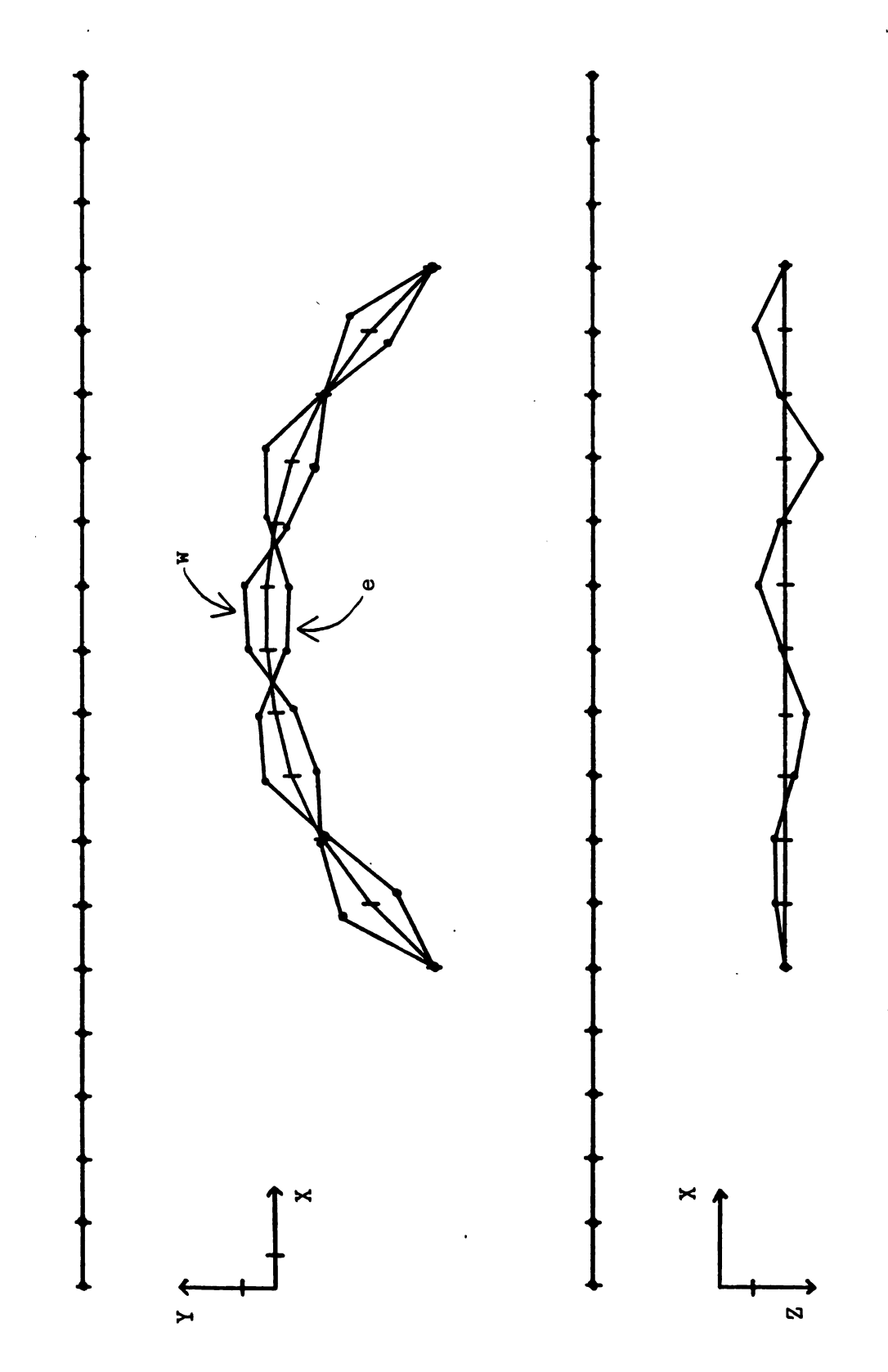


Figure 110 CSCB Mode 24 Without Cables

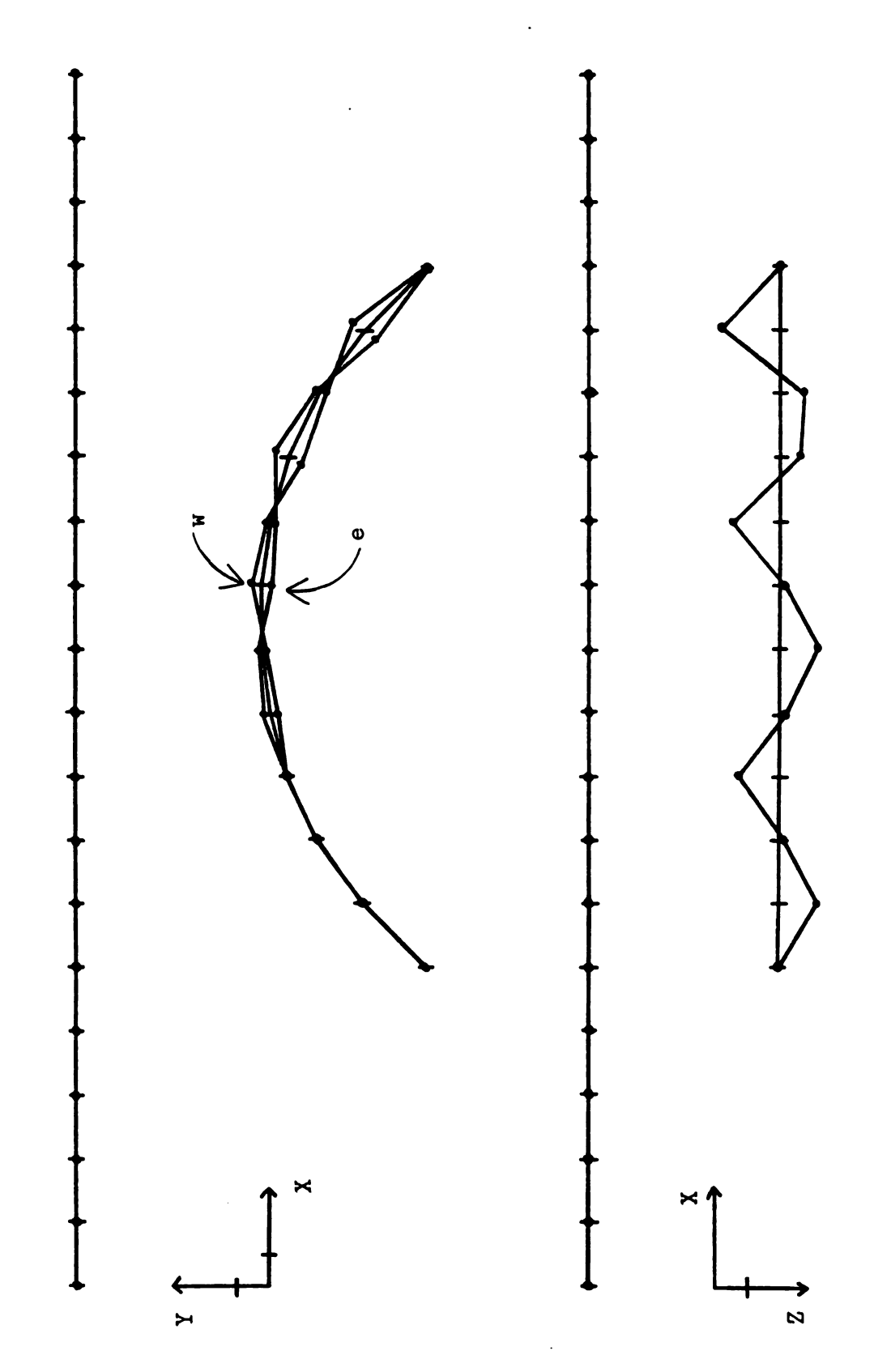
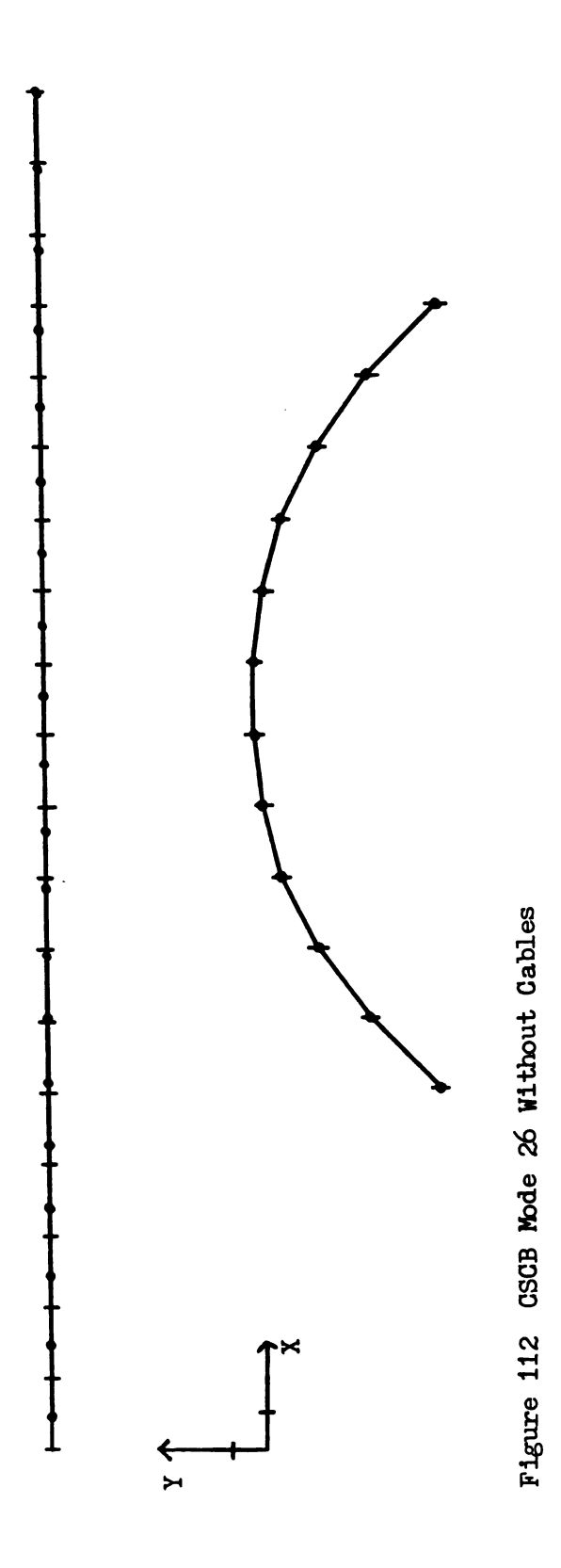


Figure 111 GSGB Mode 25 Without Cables



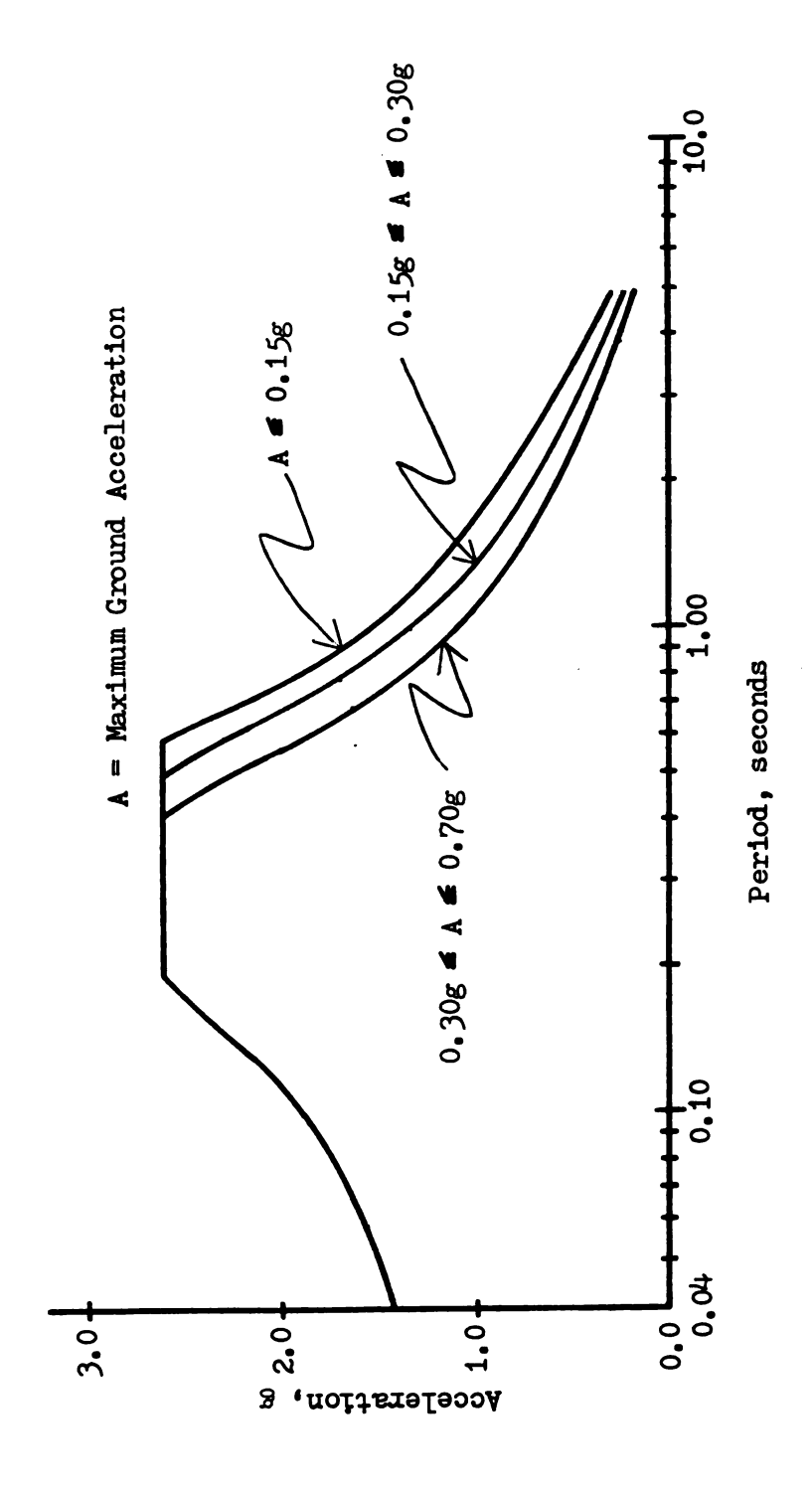


Figure 113 Normalized Rock Spectra

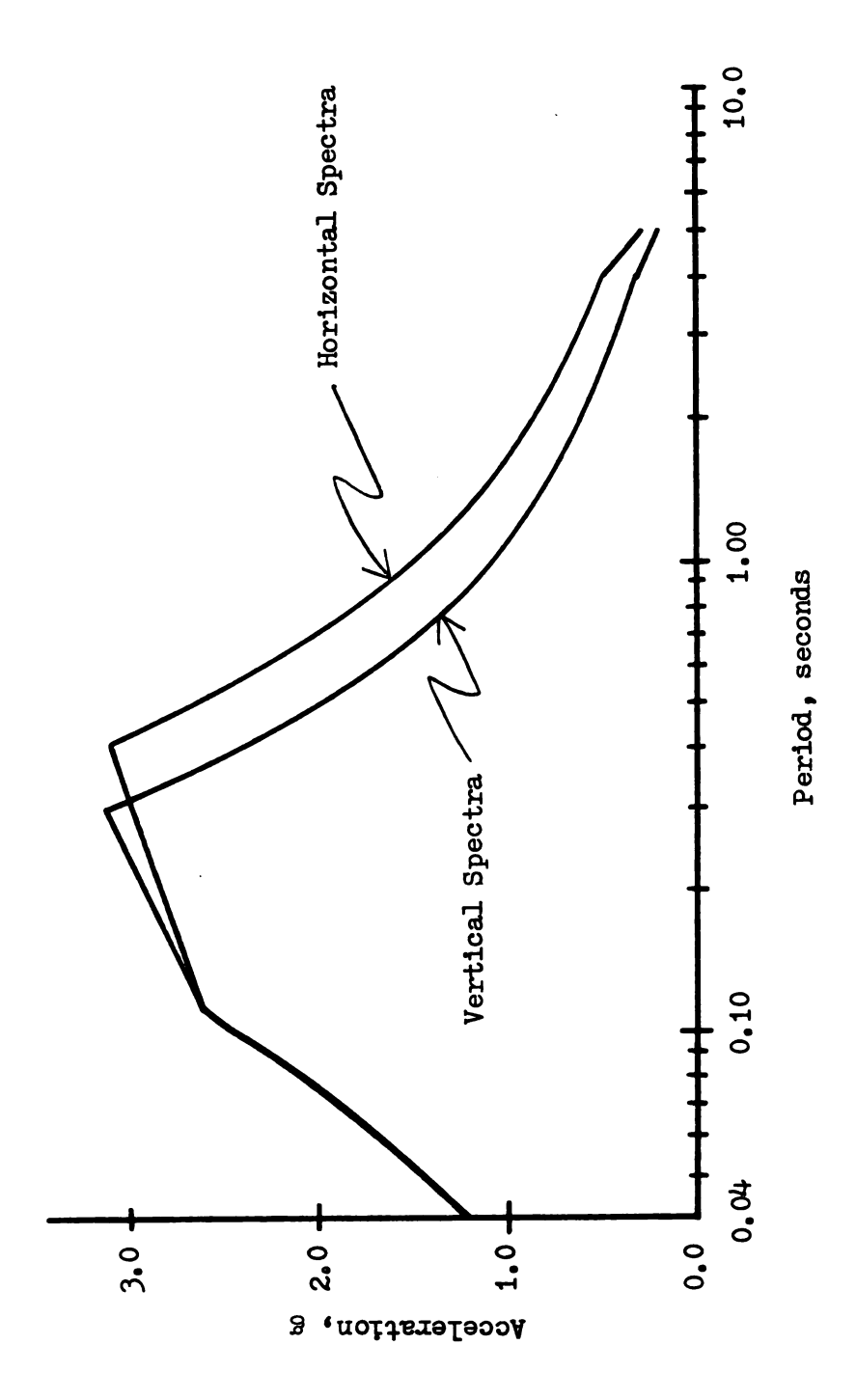


Figure 114 NRC Spectra

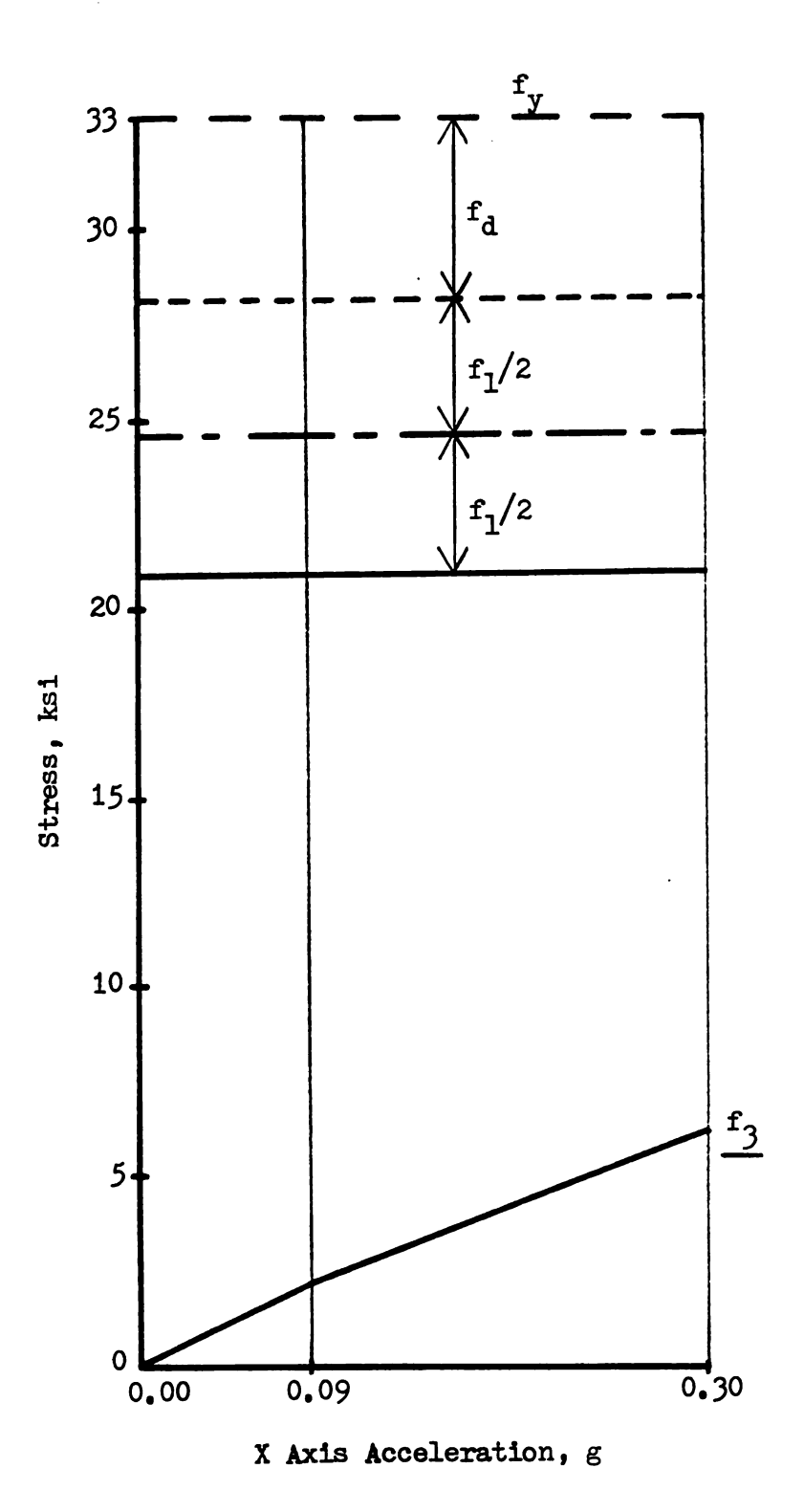


Figure 115 SSB Arch Rib Stresses in Elements DE Versus X Axis Acceleration

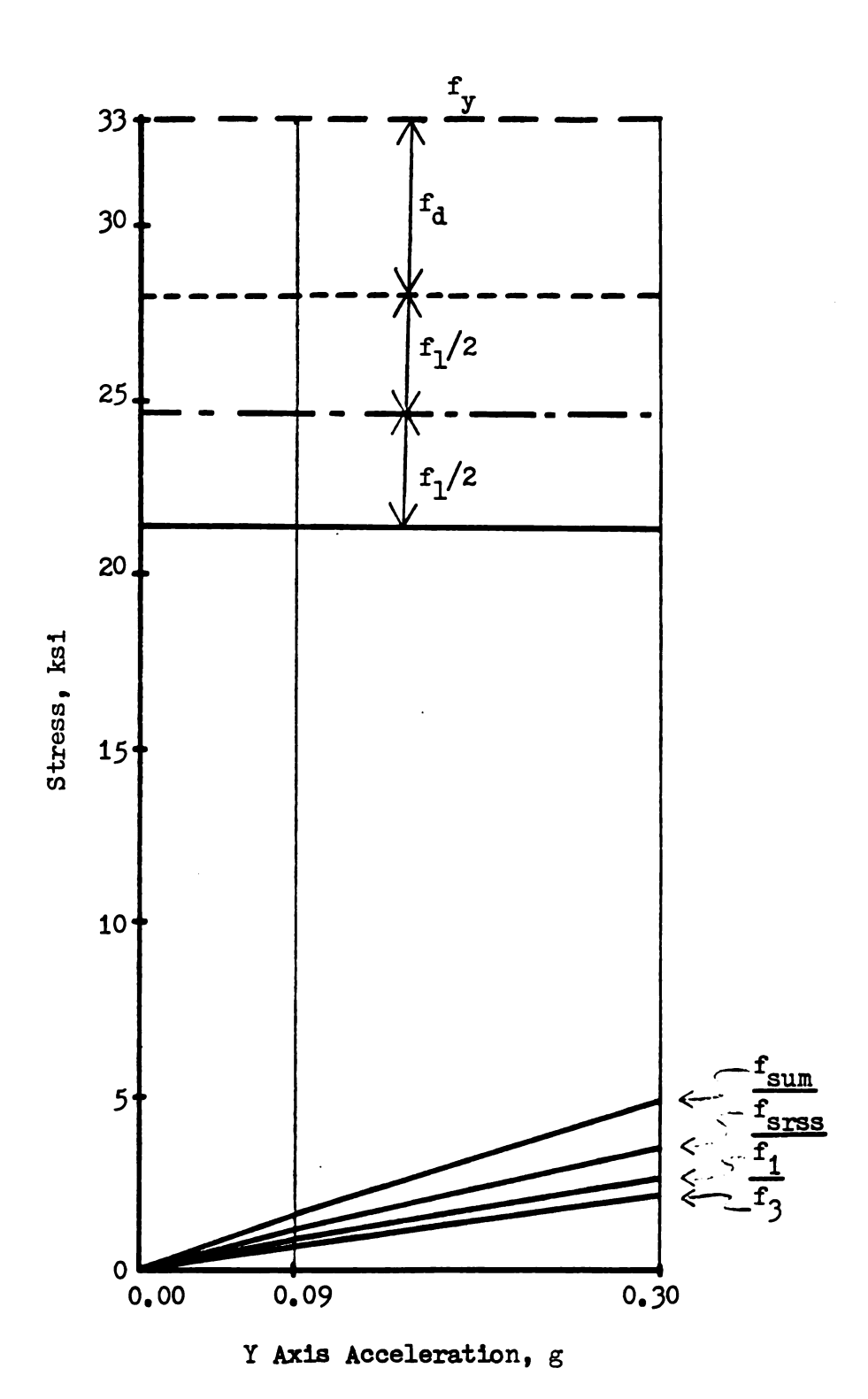


Figure 116 SSB Arch Rib Stresses in Elements D°C° Versus Y Axis Acceleration

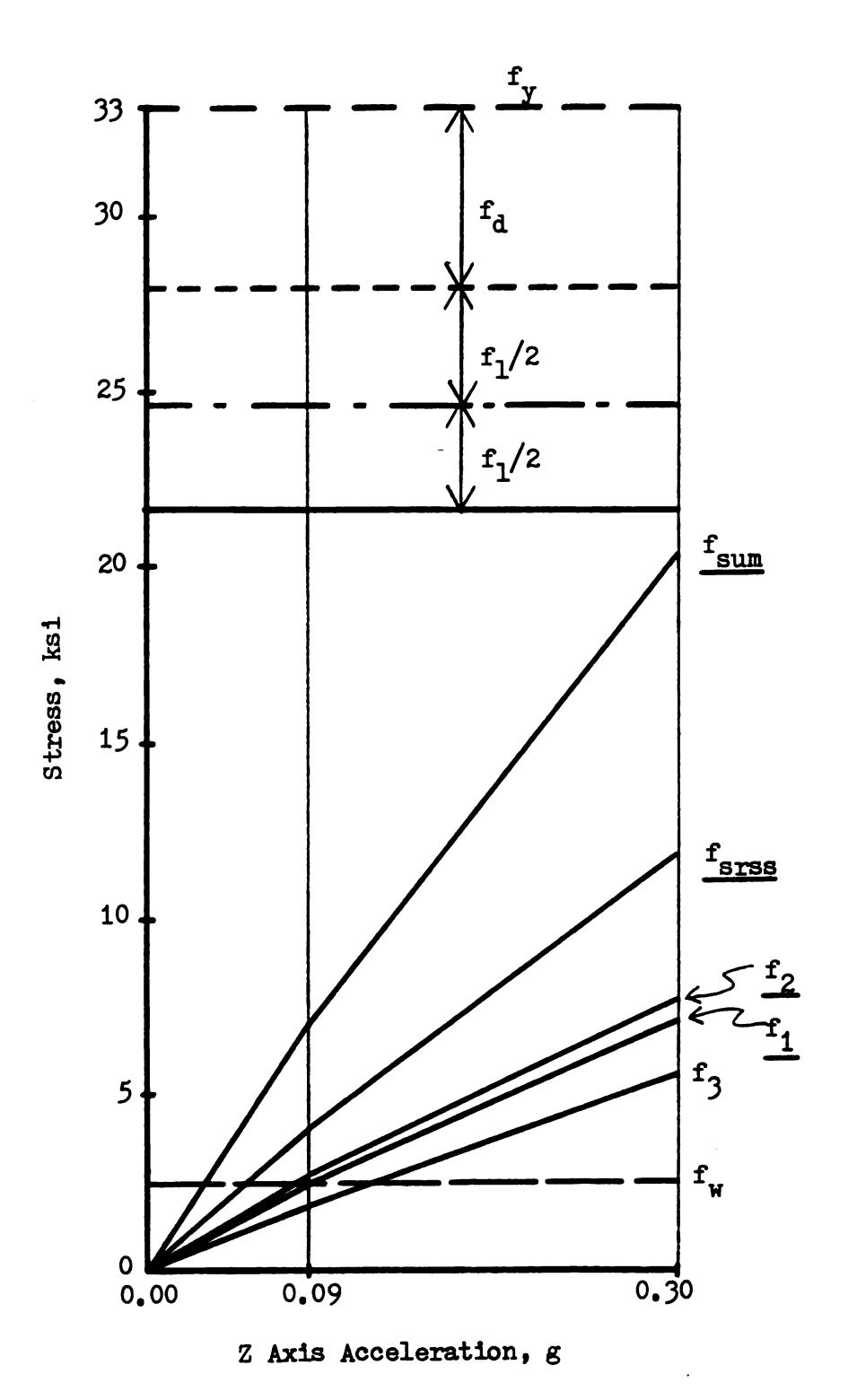


Figure 117 SSB Arch Rib Stresses in Elements CD Versus Z Axis Acceleration

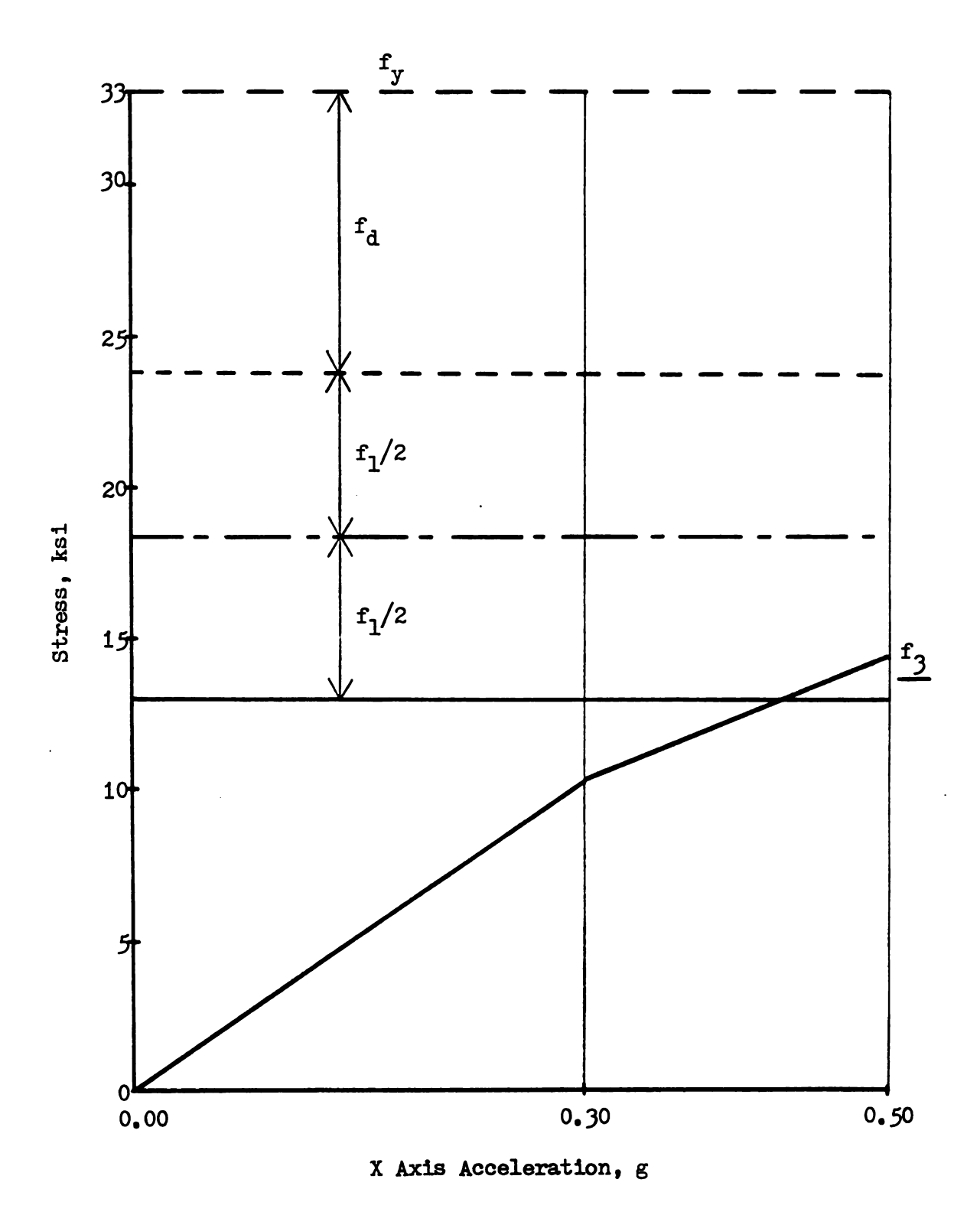


Figure 118 CSCB Arch Rib Stresses in Elements 15c-16 Versus X Axis Acceleration

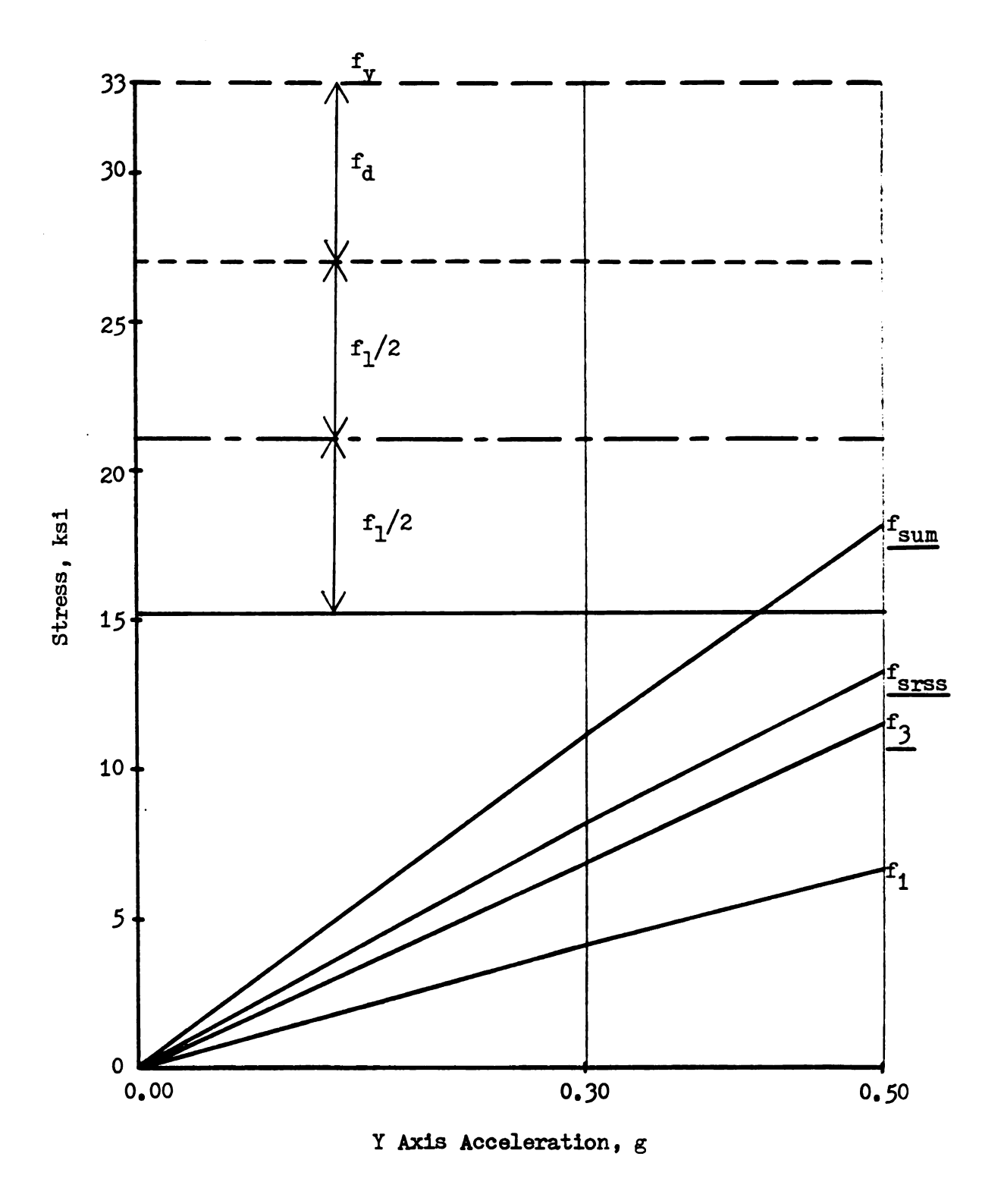


Figure 119 CSCB Arch Rib Stresses in Elements 13c-14 Versus Y Axis Acceleration

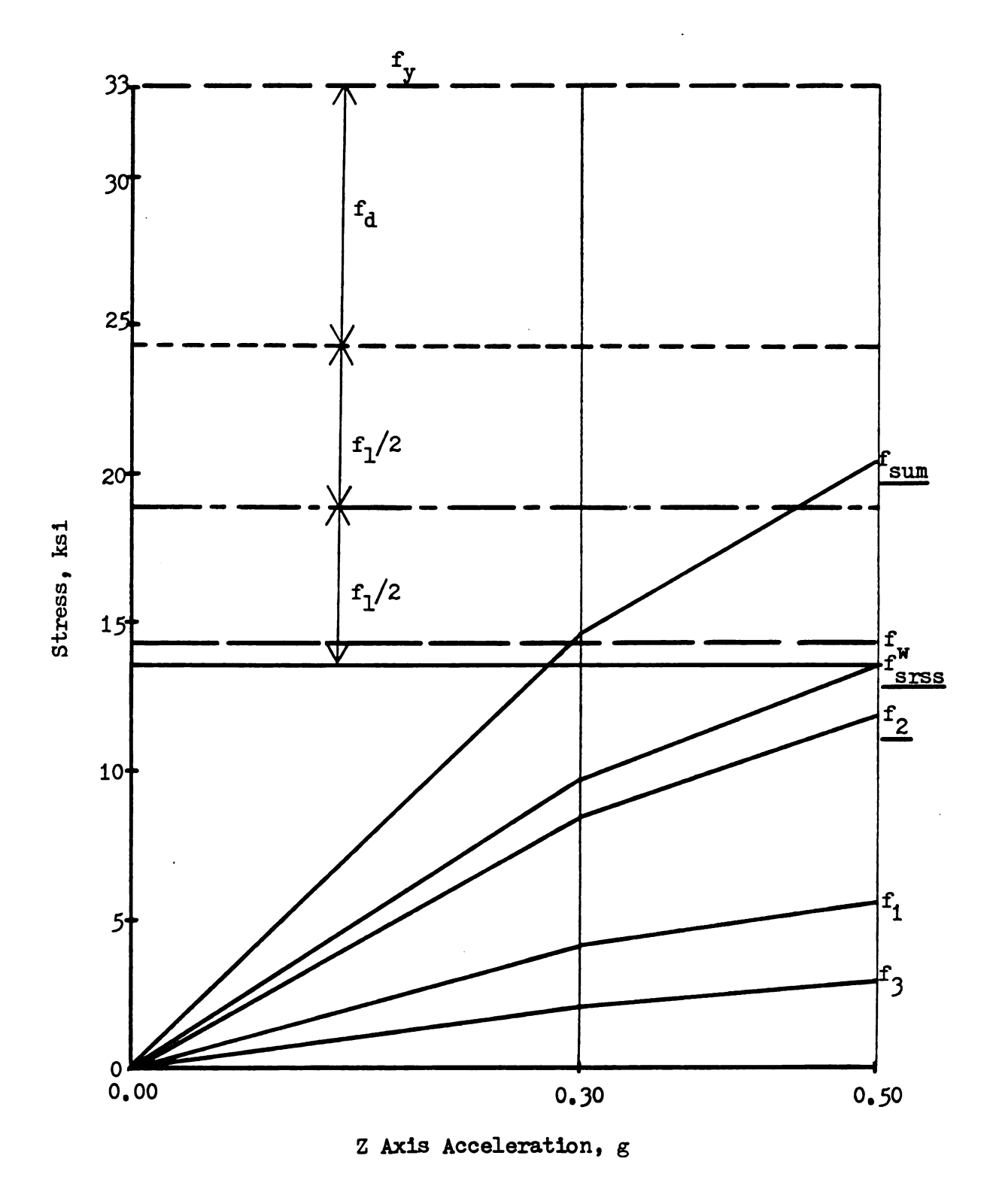
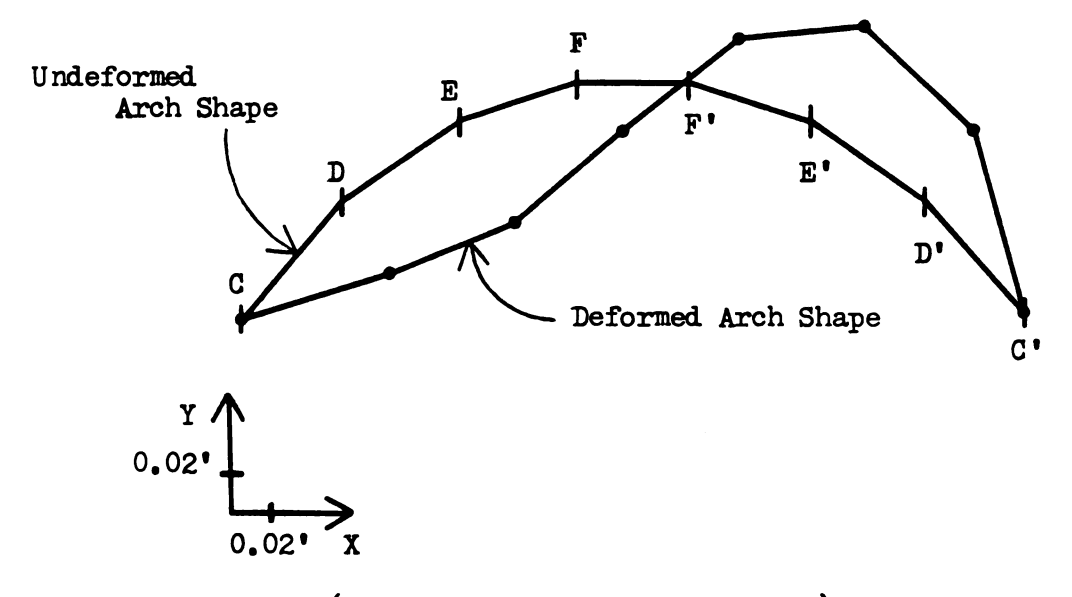


Figure 120 CSCB Arch Rib Stresses in Elements 6c-7 Versus Z Axis Acceleration



Scale (applies to displacements only)

Displacements

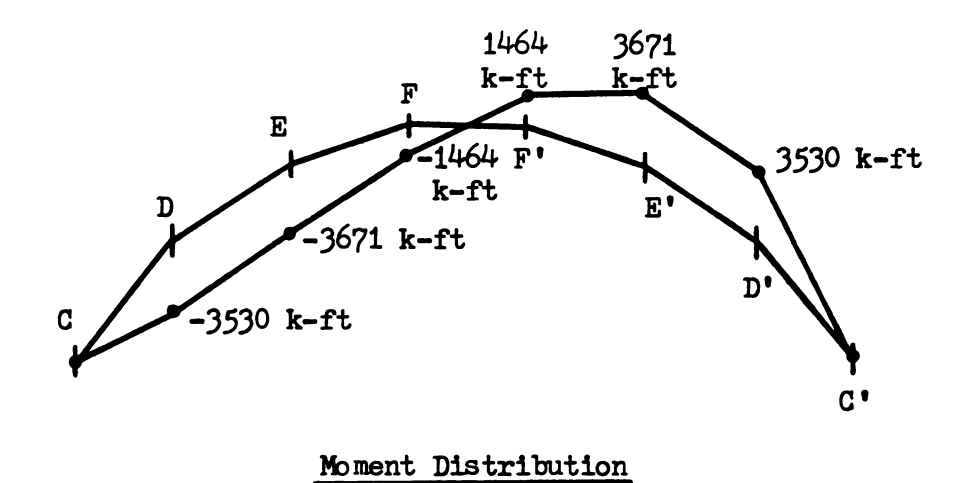


Figure 121 SSB Arch Rib Responses to X Axis Application of Self Weight

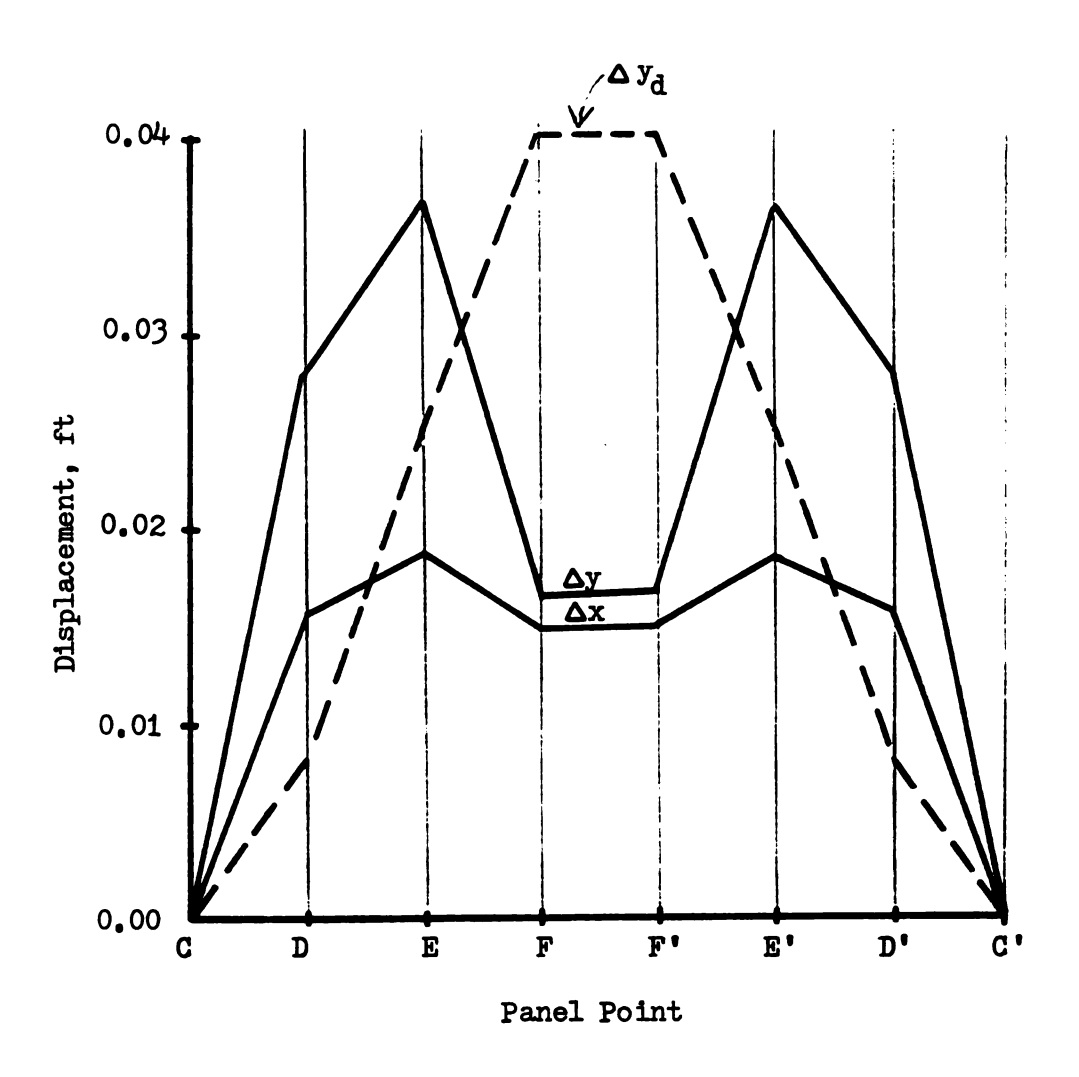


Figure 122 SSB Arch Rib Displacements at X Axis Accelerations of 0.09g

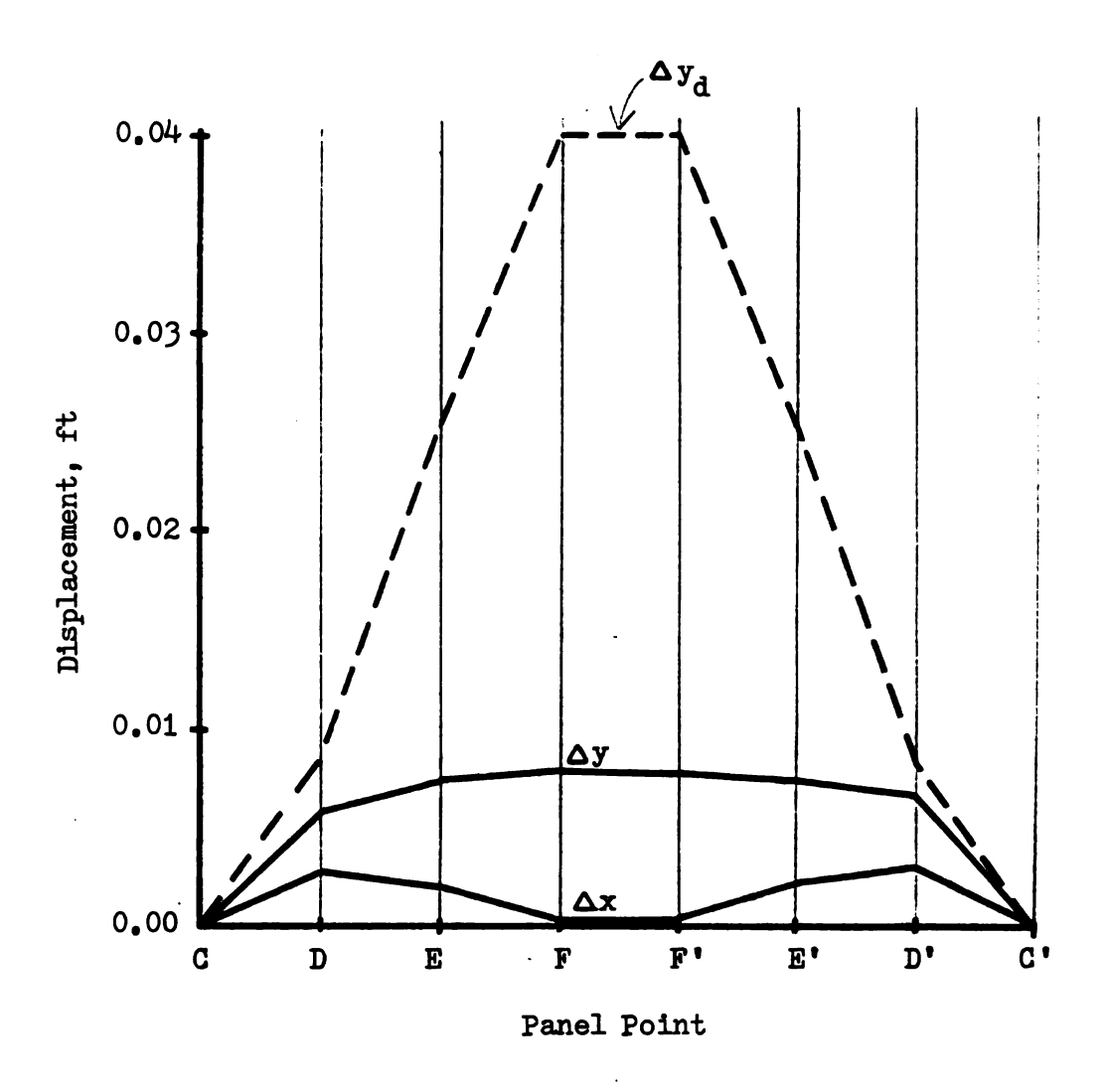
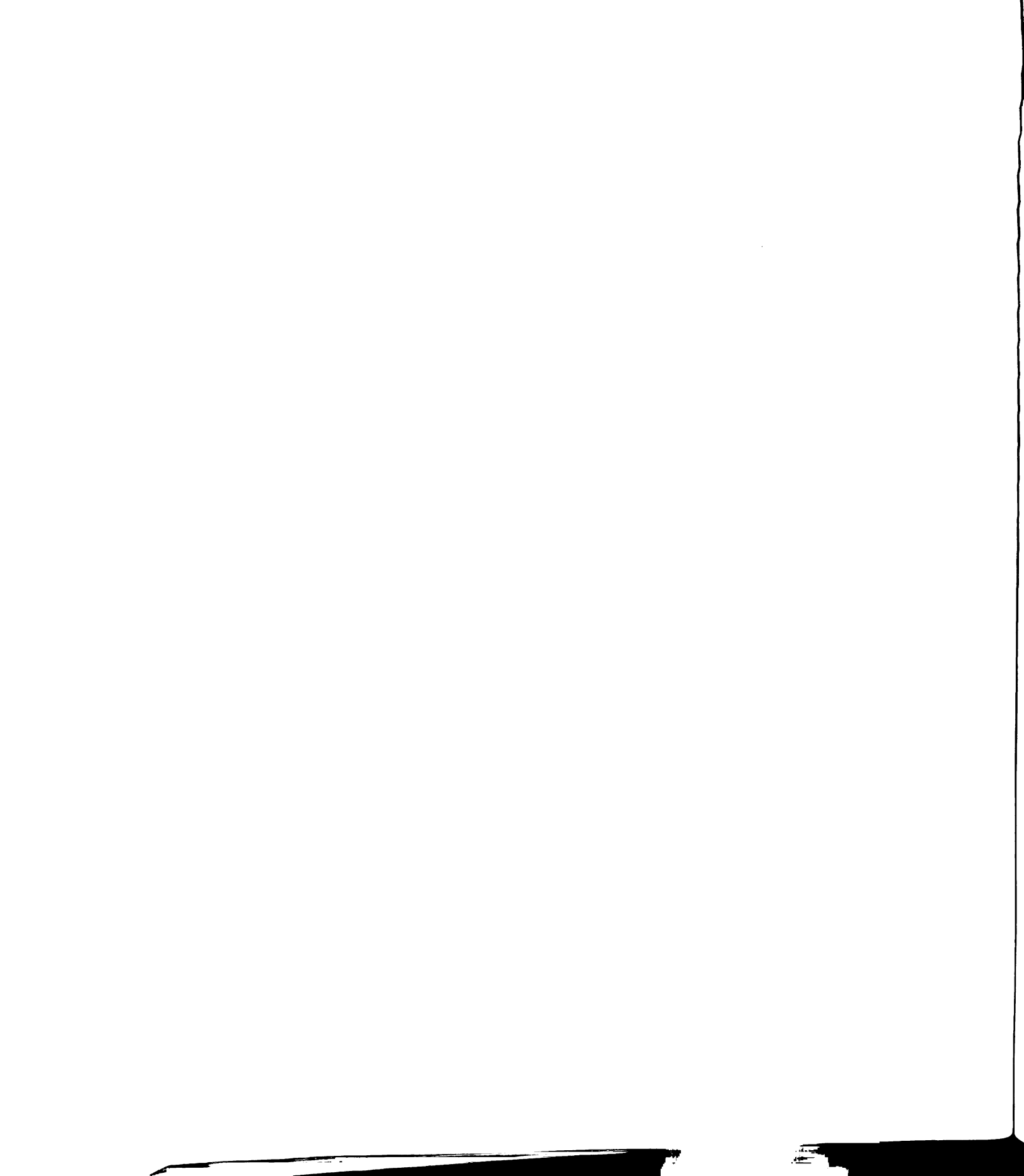


Figure 123 SSB Arch Rib Displacements at Y Axis Accelerations of $0.09 \mathrm{g}$



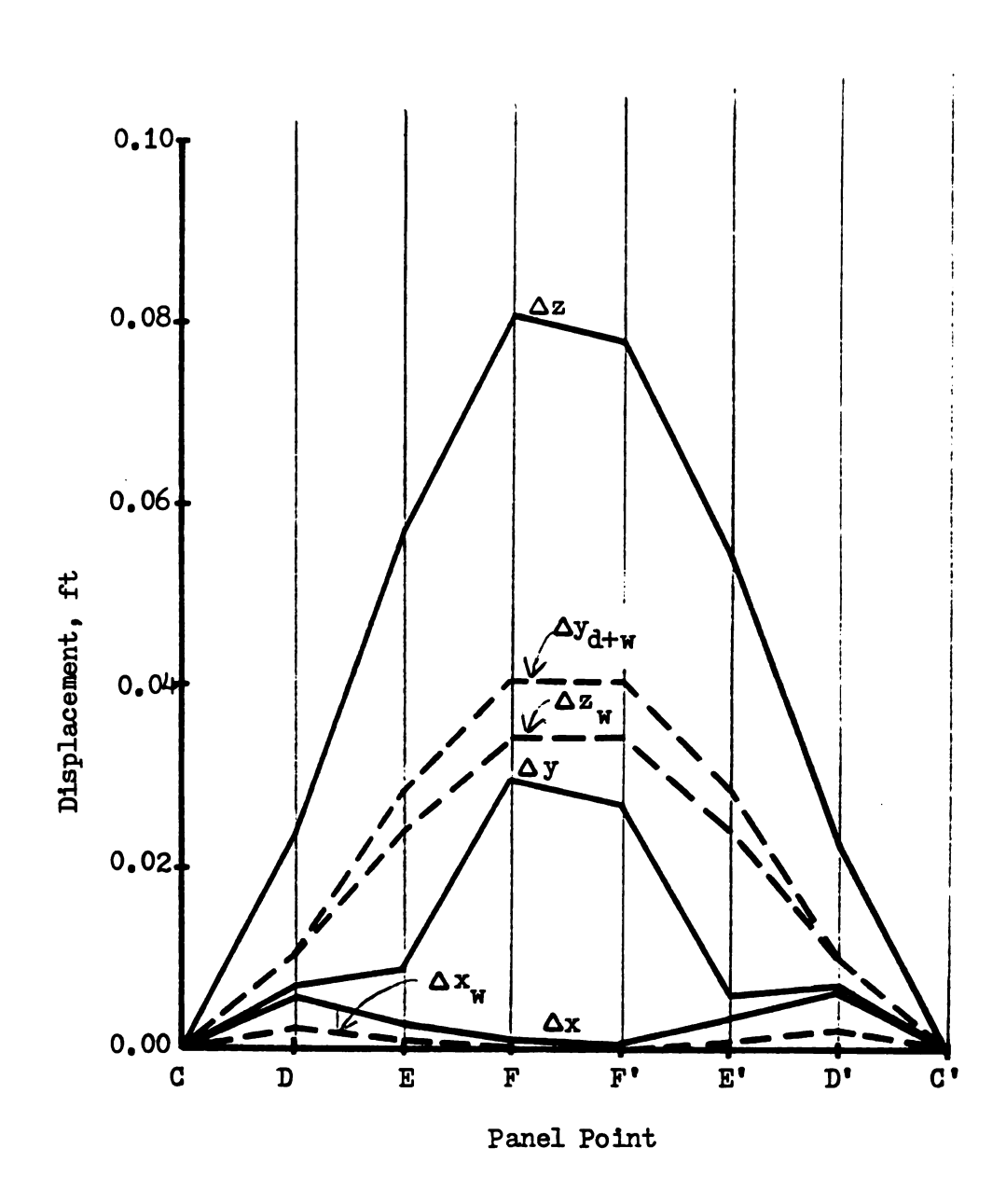


Figure 124 SSB Arch Rib Displacements at Z Axis Accelerations of 0.09g

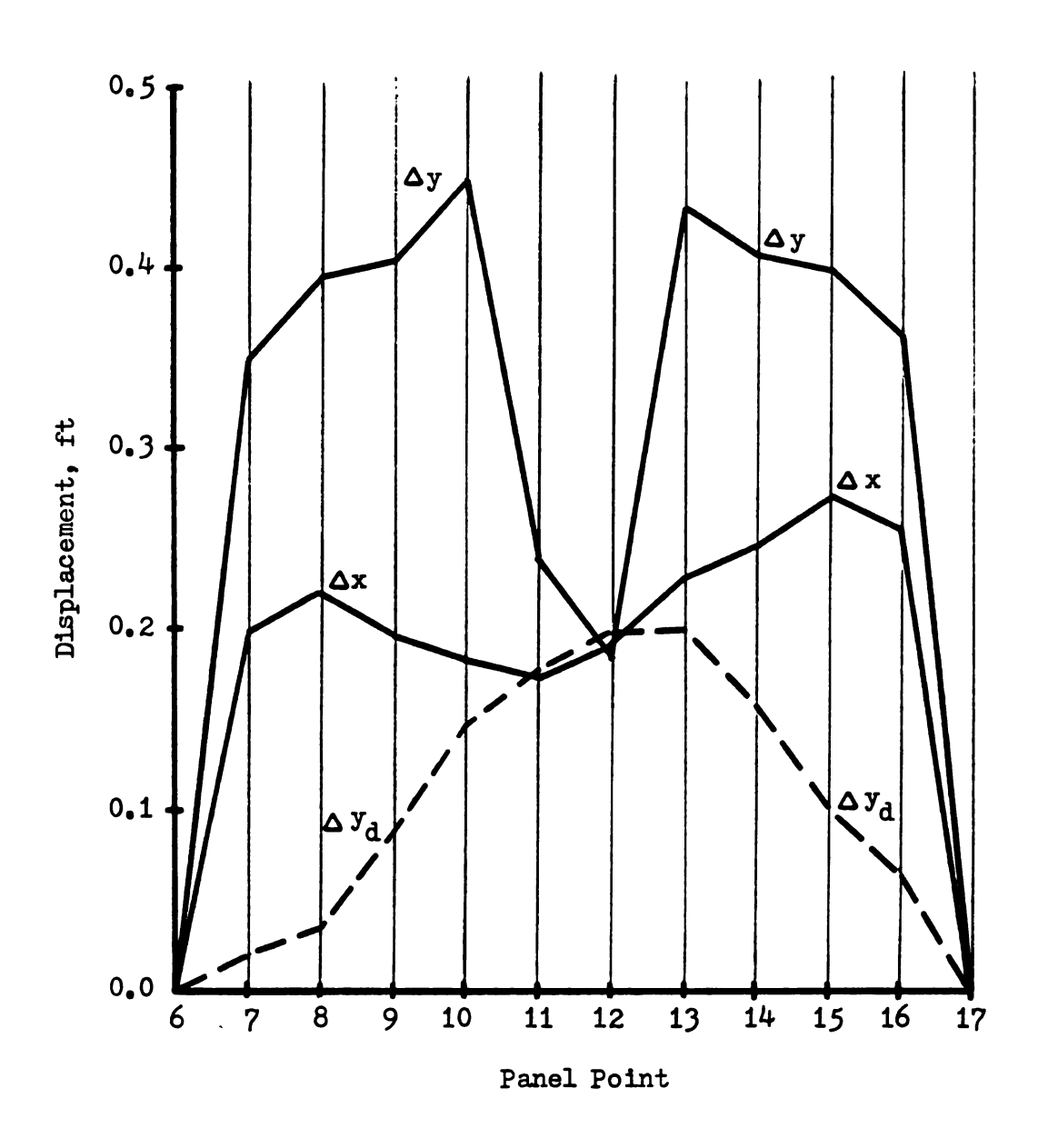


Figure 125 CSCB Arch Rib Displacements at X Axis Accelerations of 0.50g

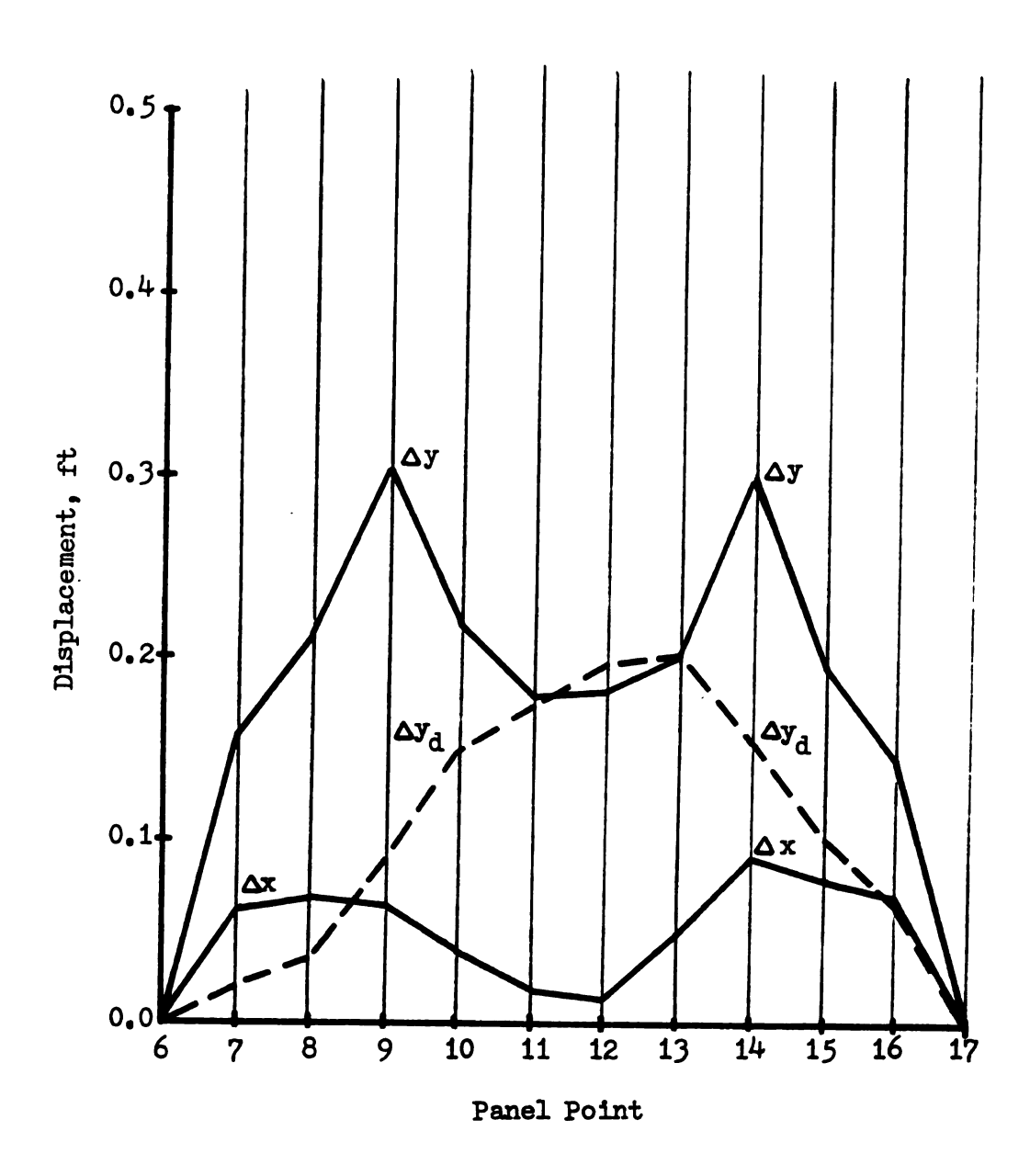


Figure 126 CSCB Arch Rib Displacements at Y Axis Accelerations of 0.50g

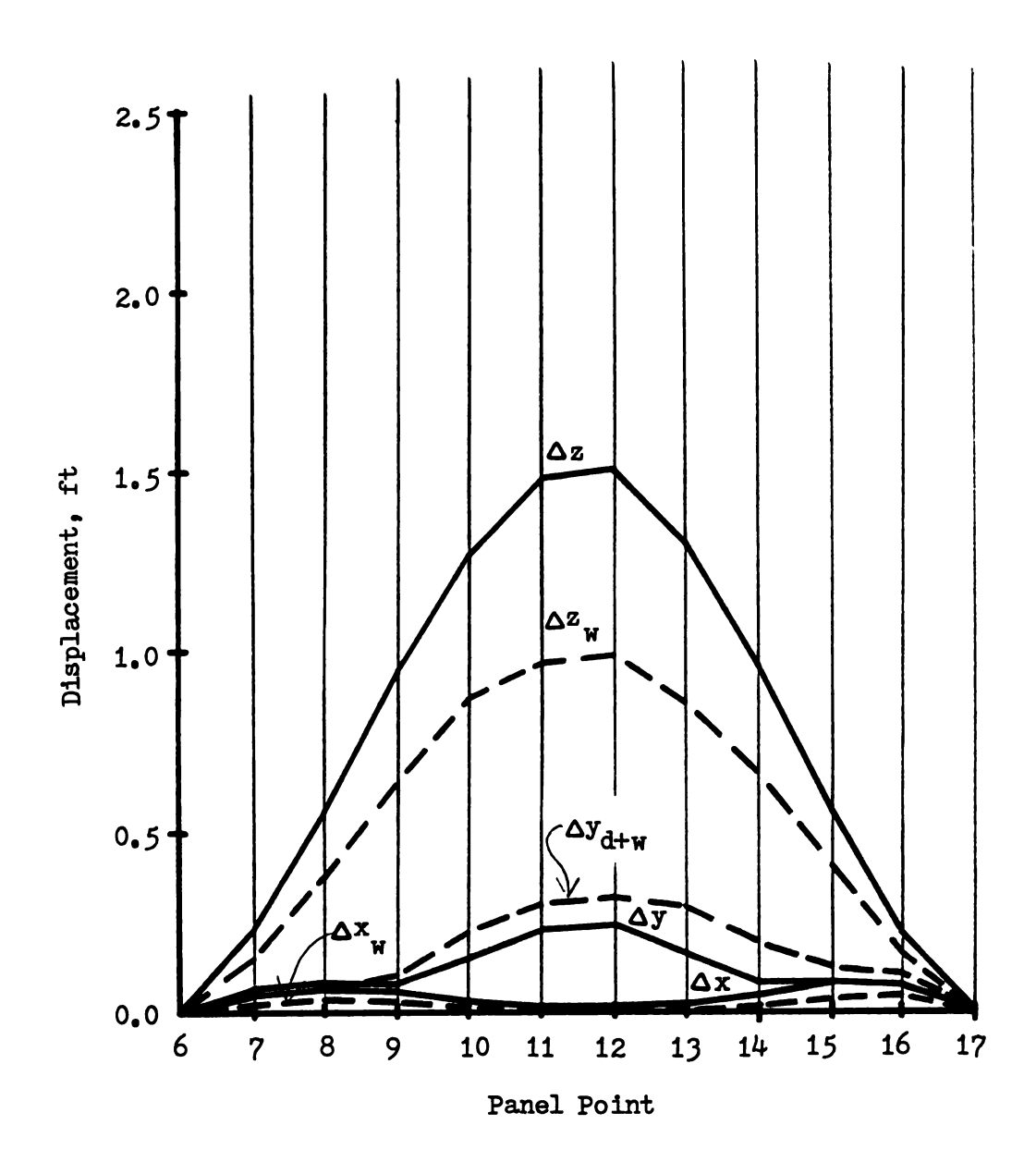
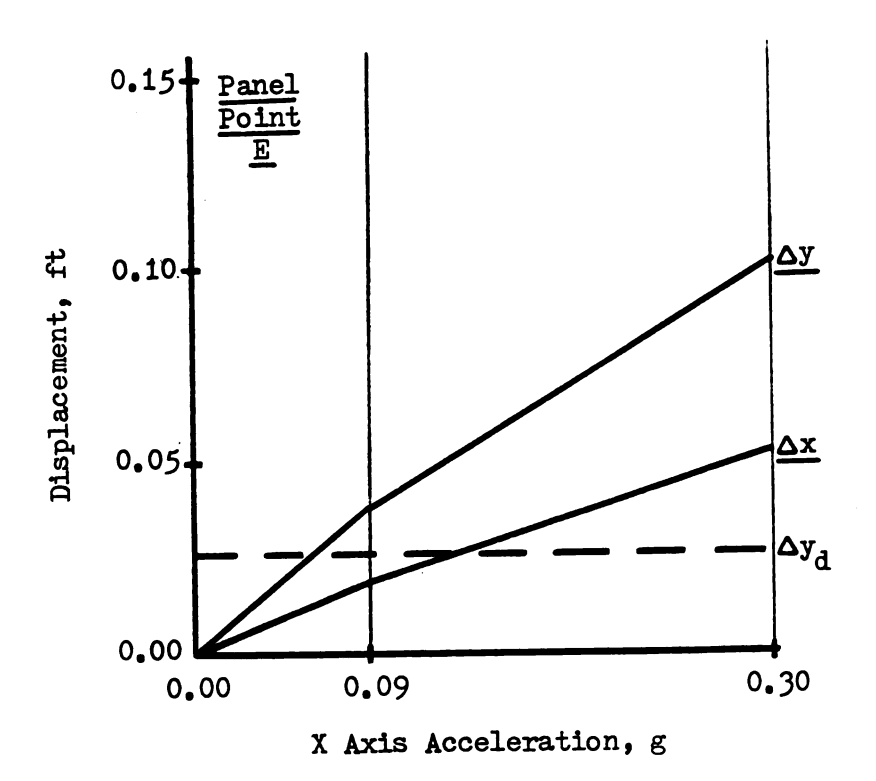


Figure 127 CSCB Arch Rib Displacements at Z Axis Accelerations of 0.50g



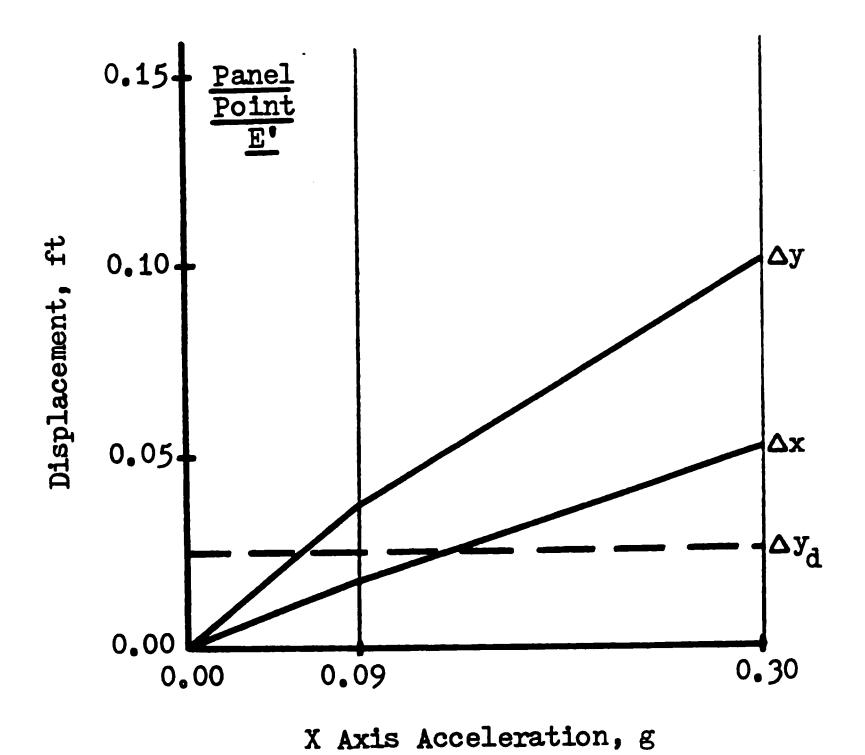
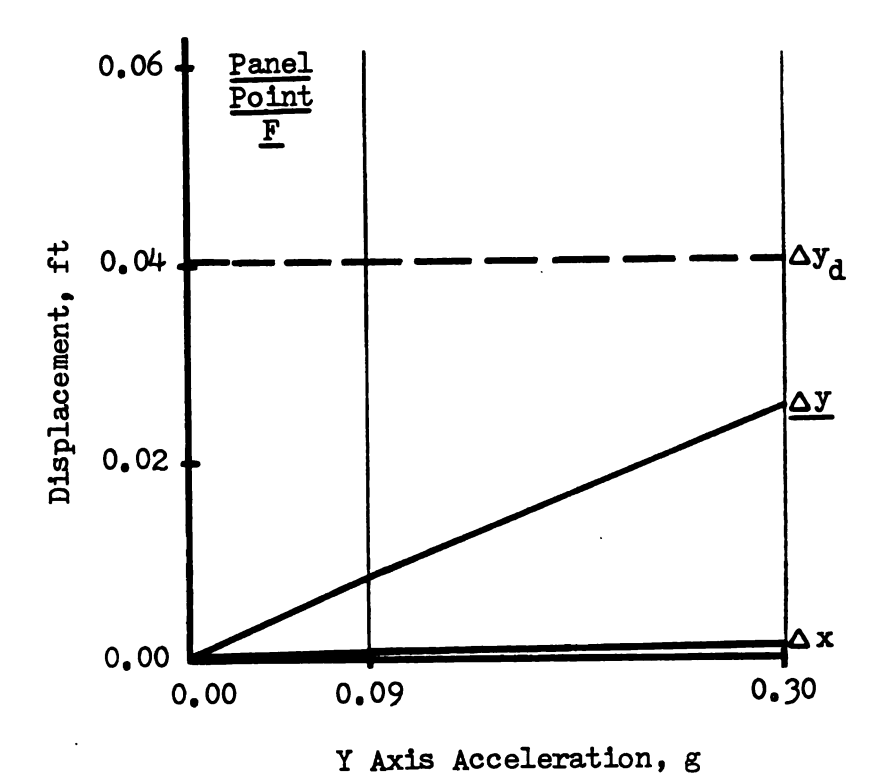


Figure 128 SSB Arch Rib Displacements Versus X Axis Acceleration



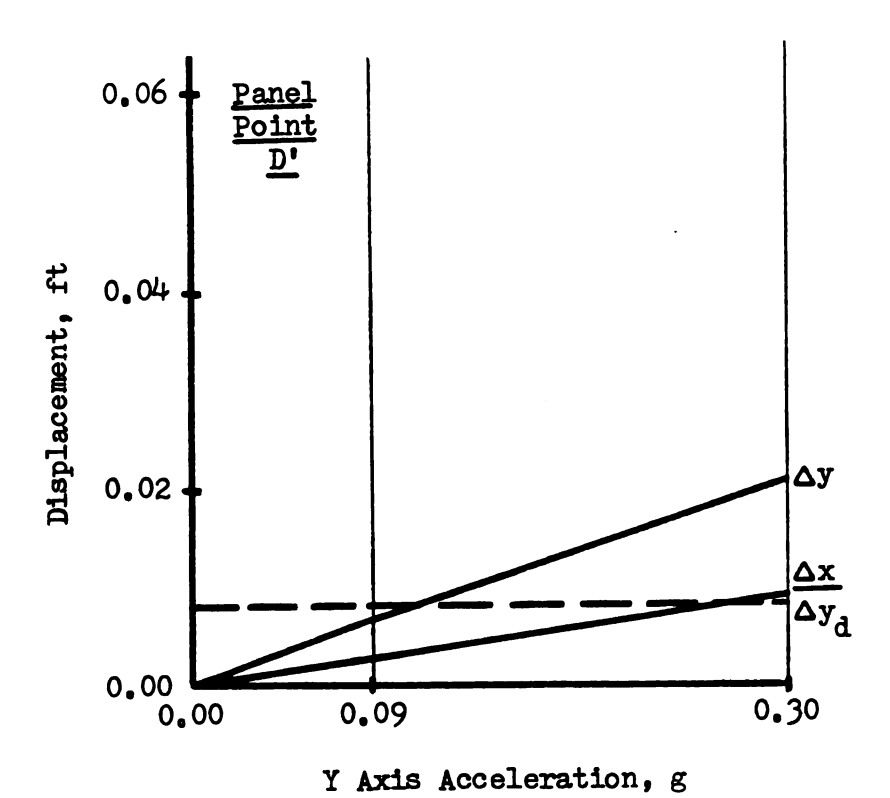
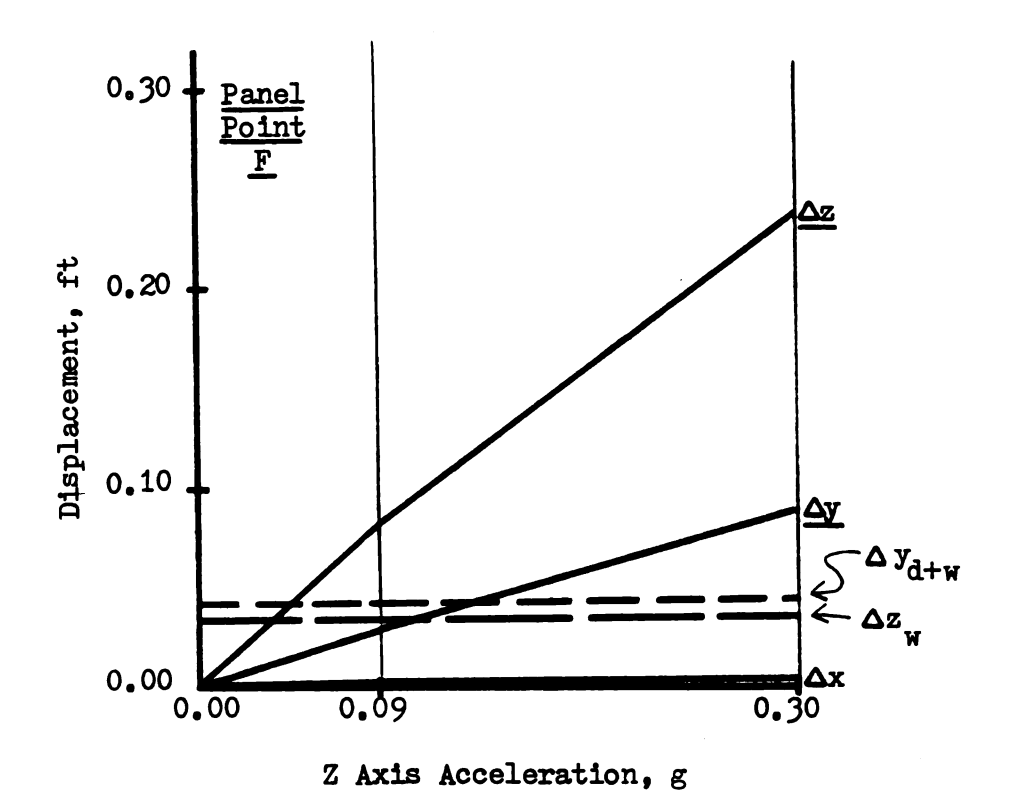


Figure 129 SSB Arch Rib Displacements Versus Y Axis Acceleration



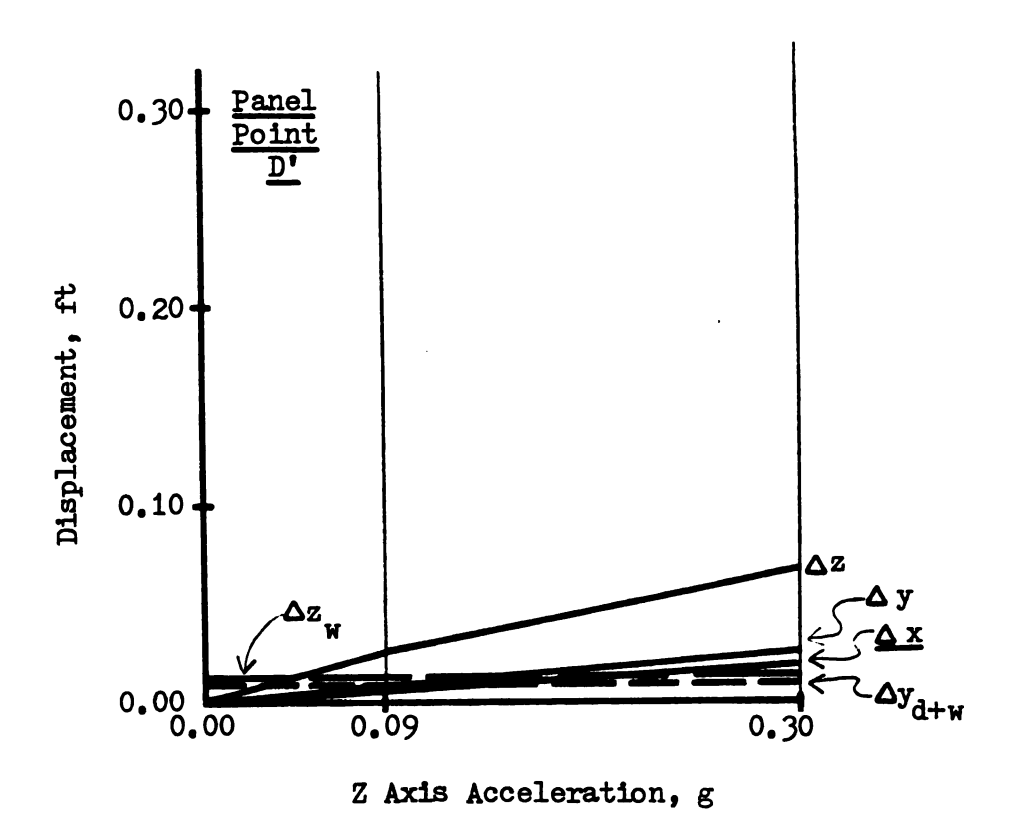


Figure 130 SSB Arch Rib Displacements Versus Z Axis Acceleration

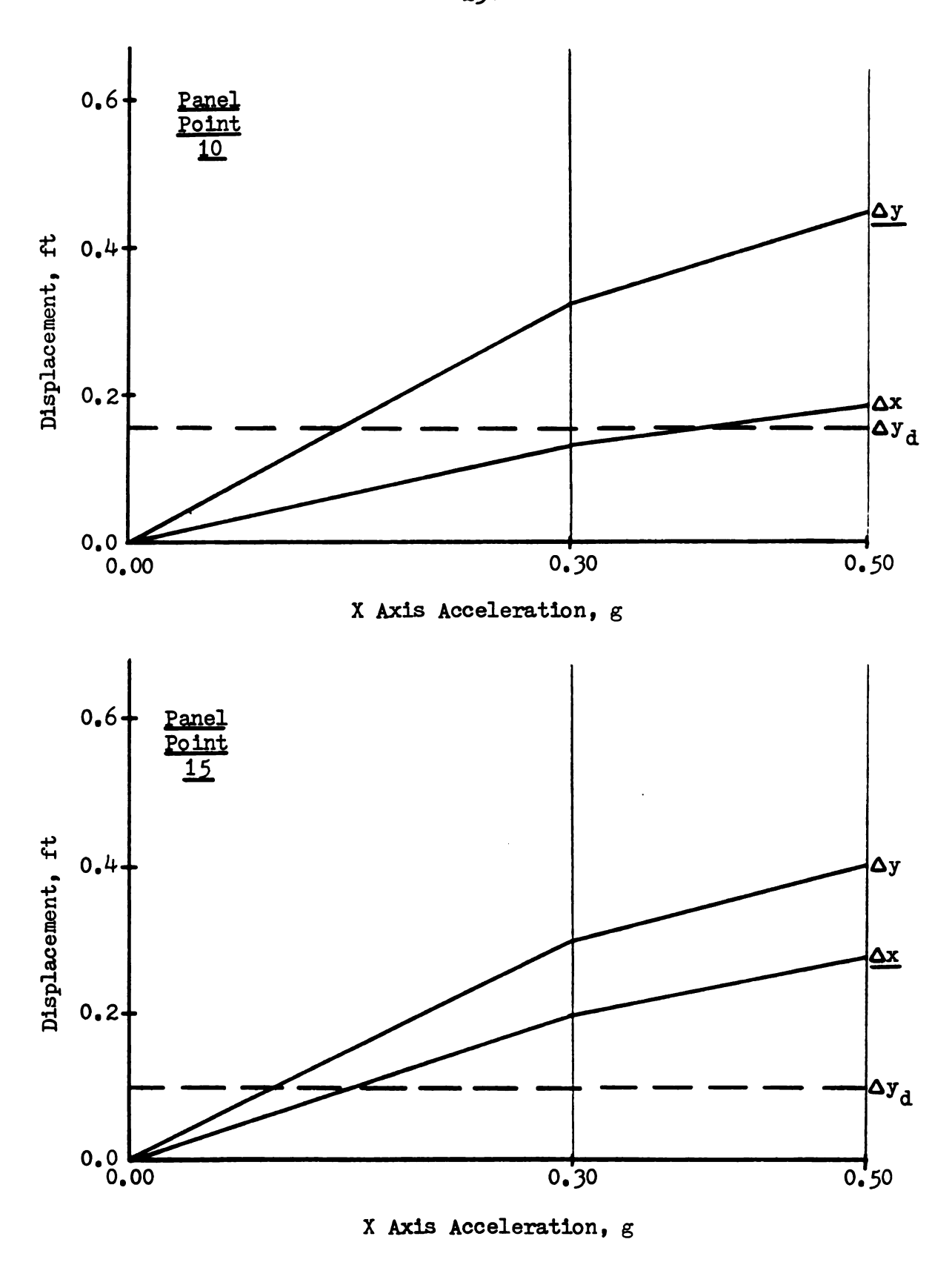


Figure 131 CSCB Arch Rib Displacements Versus X Axis Acceleration



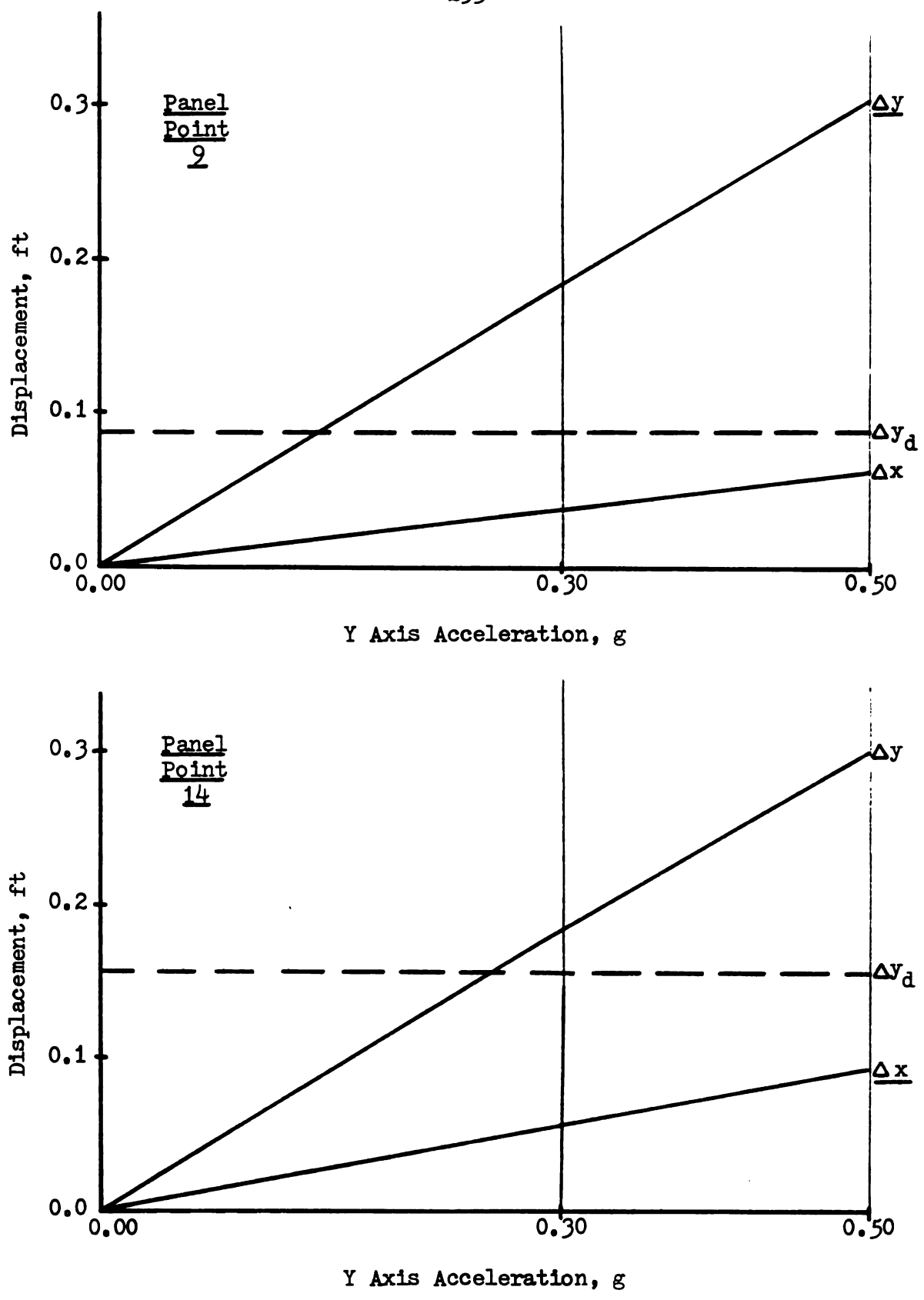


Figure 132 CSCB Arch Rib Displacements Versus Y Axis Acceleration

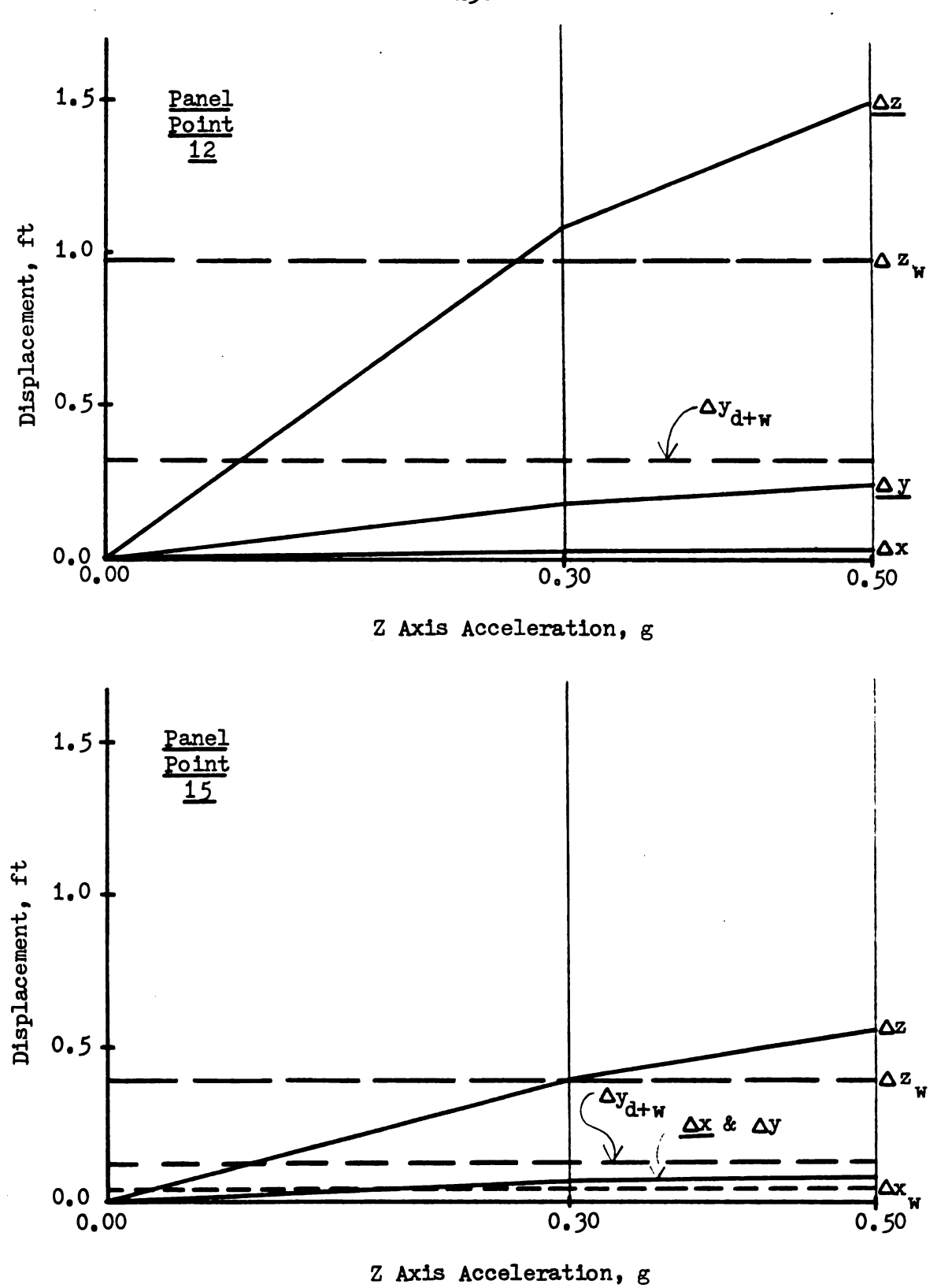


Figure 133 CSCB Arch Rib Displacements Versus Z Axis Acceleration

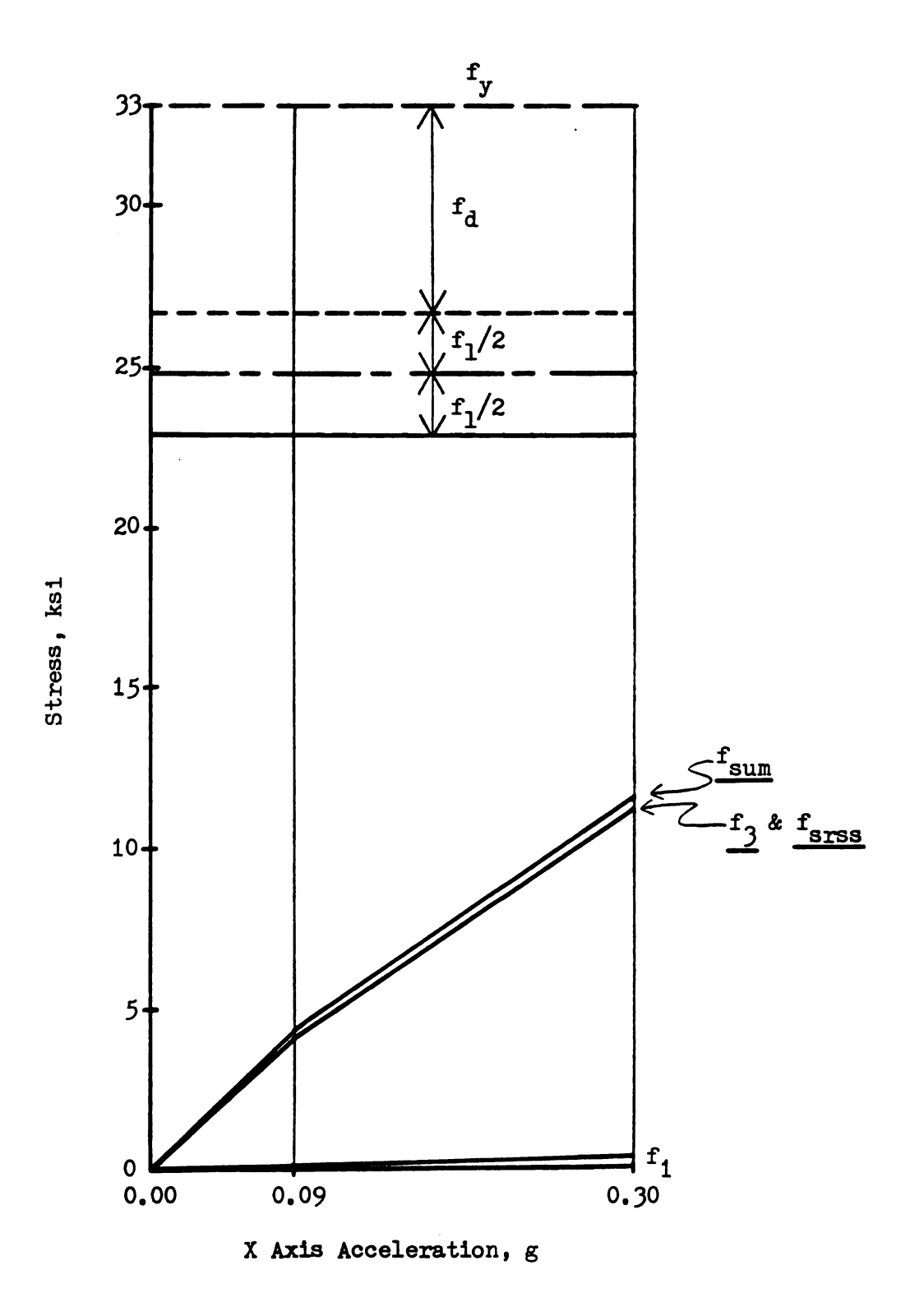


Figure 134 SSB Deck Stresses in Element DE Versus X Axis Acceleration

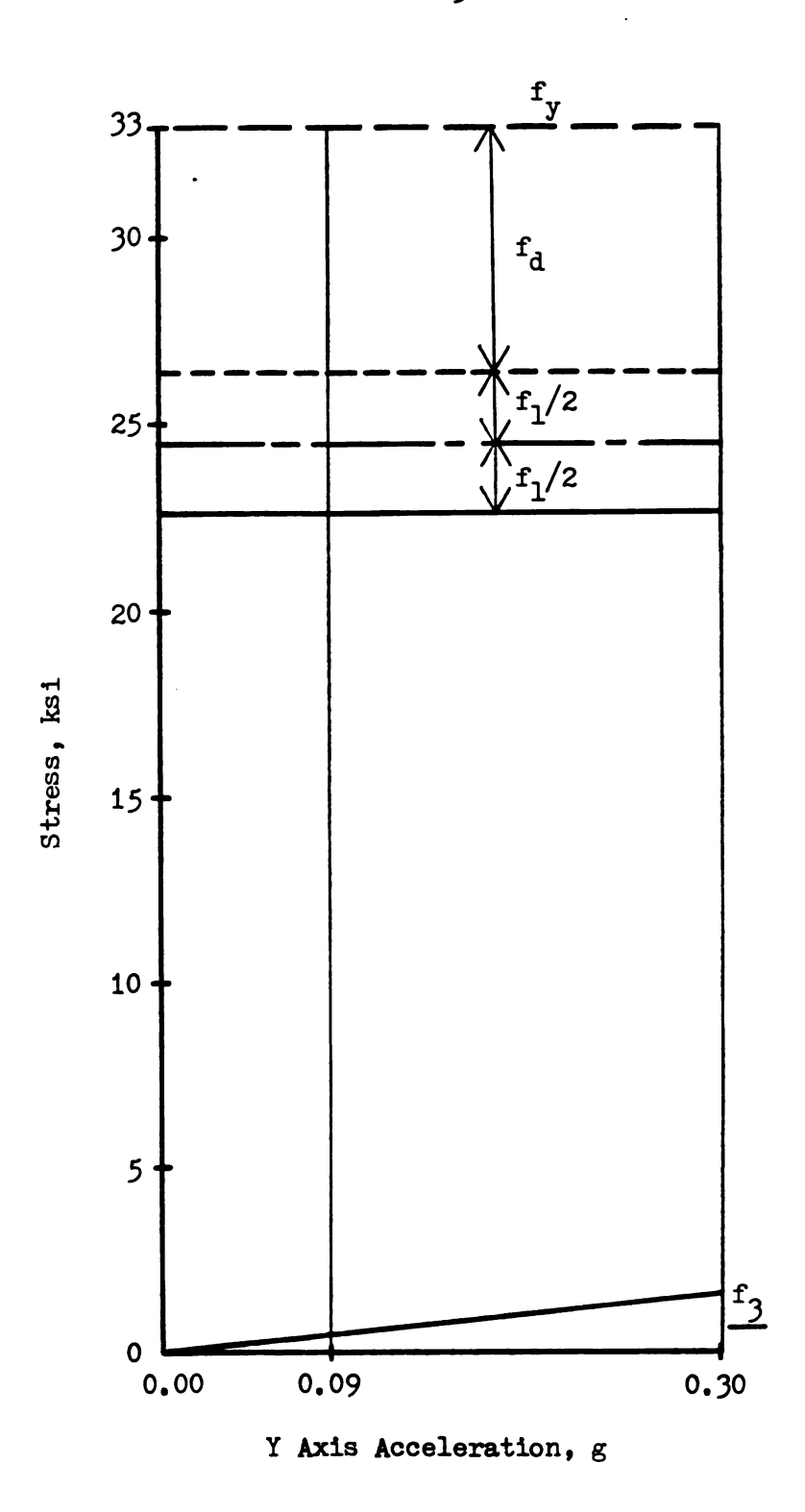


Figure 135 SSB Deck Stresses in Element D°C' Versus Y Axis Acceleration

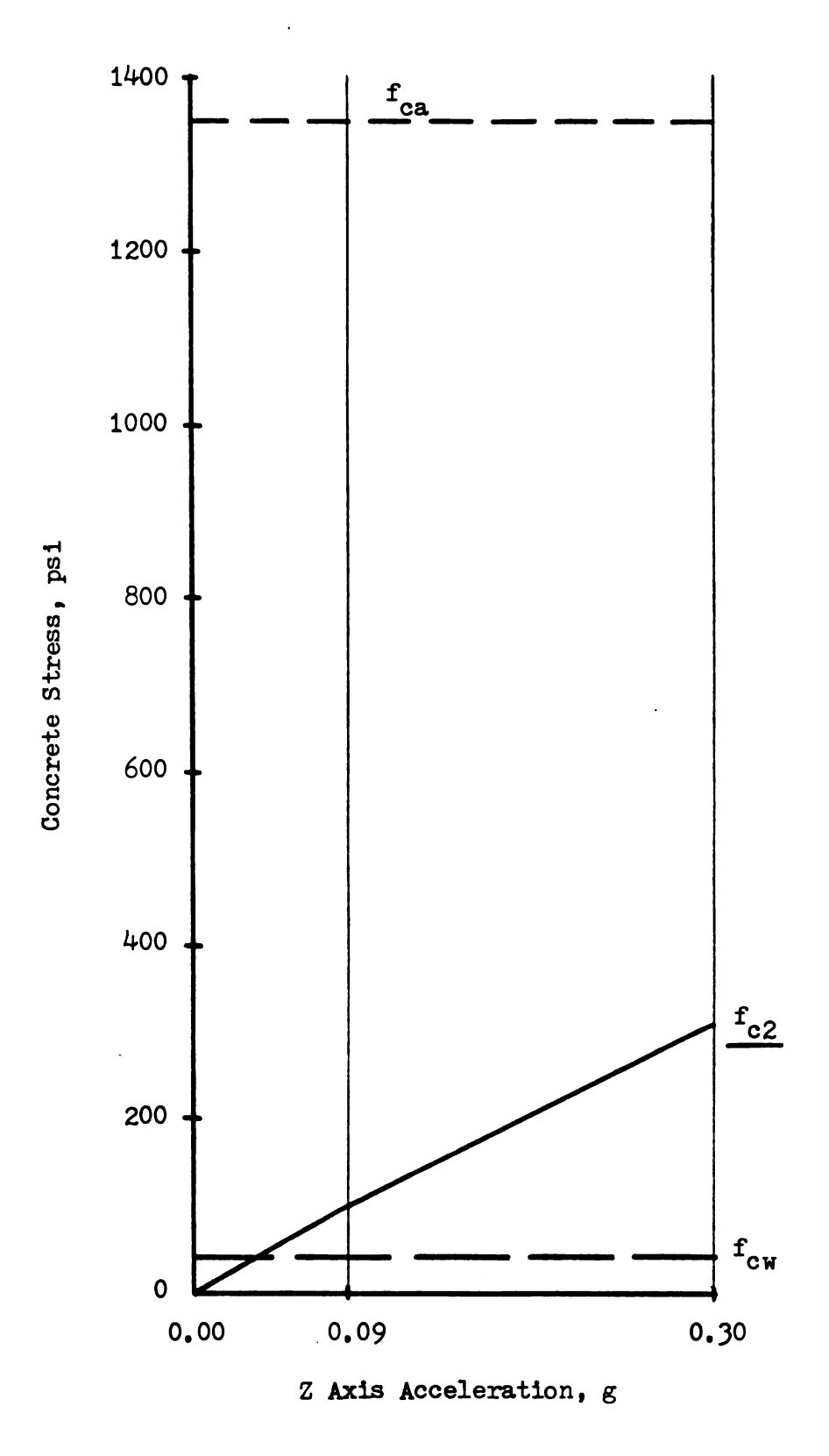


Figure 136 SSB Deck Concrete Stress in Element CD Versus Z Axis Acceleration

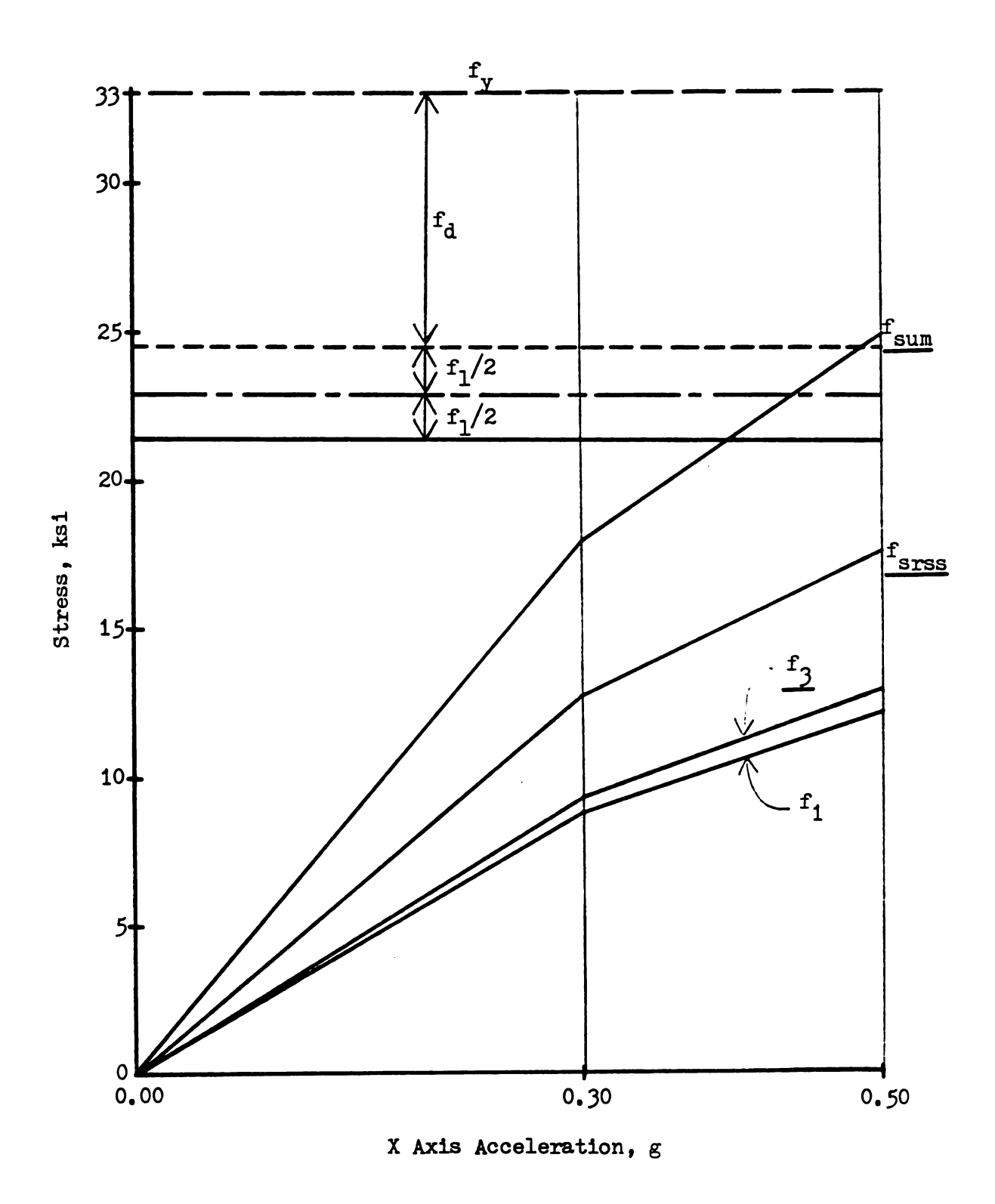


Figure 137 CSCB Deck Stresses in Element 15-16 Versus X Axis Acceleration

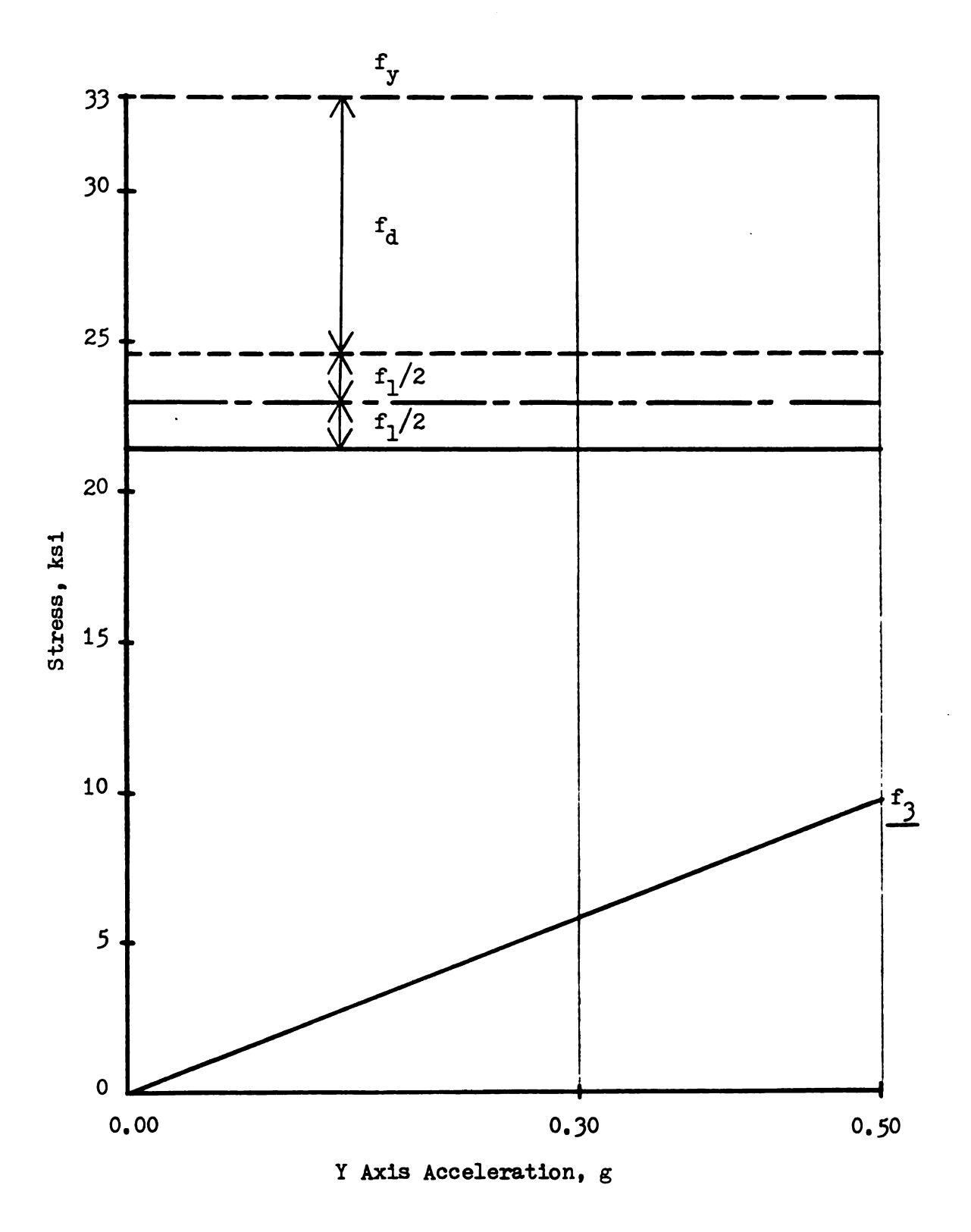


Figure 138 CSCB Deck Stresses in Element 15-16 Versus Y Axis Acceleration

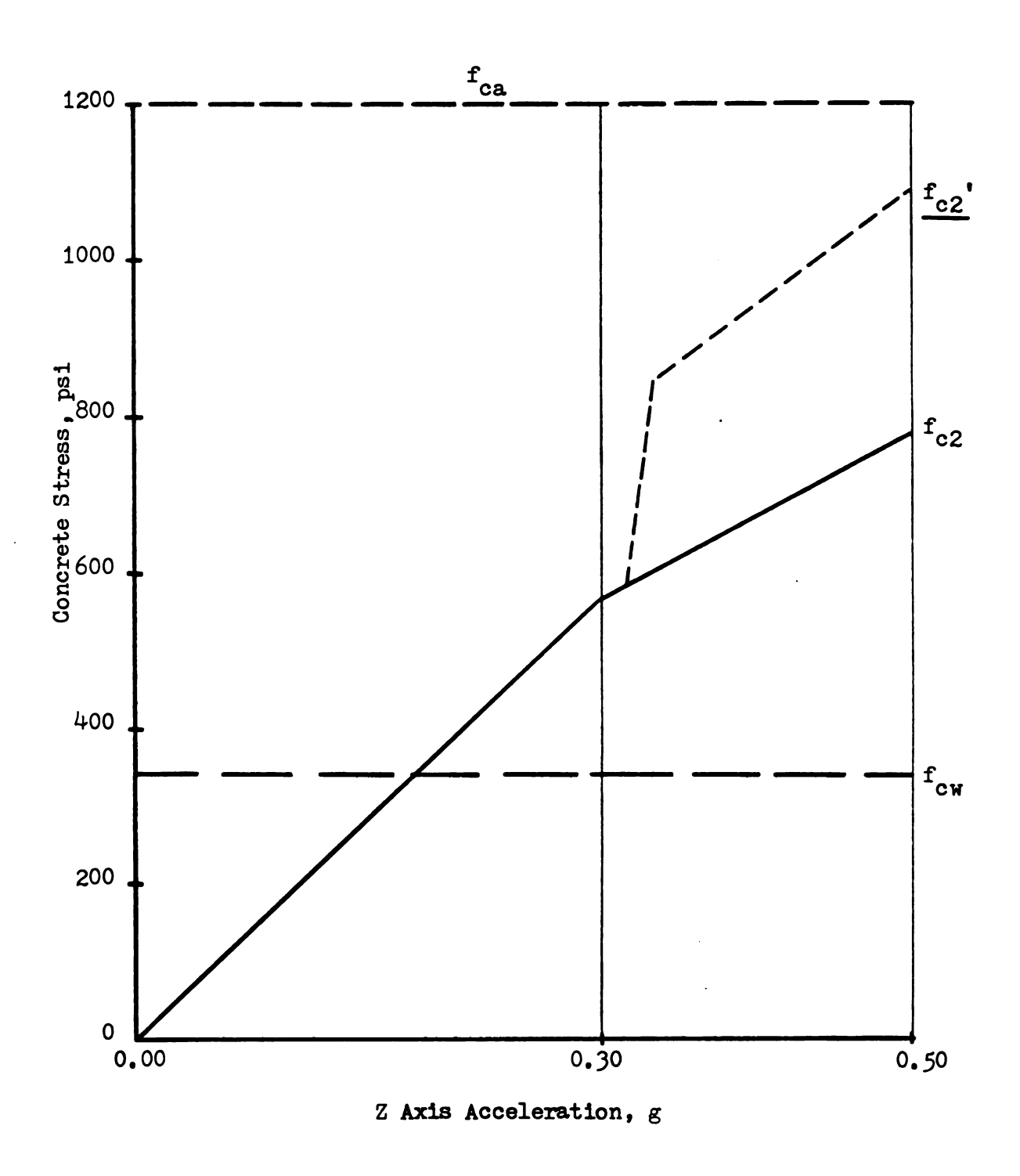


Figure 139 GSCB Deck Concrete Stresses in Element 10-11 Versus Z Axis Acceleration

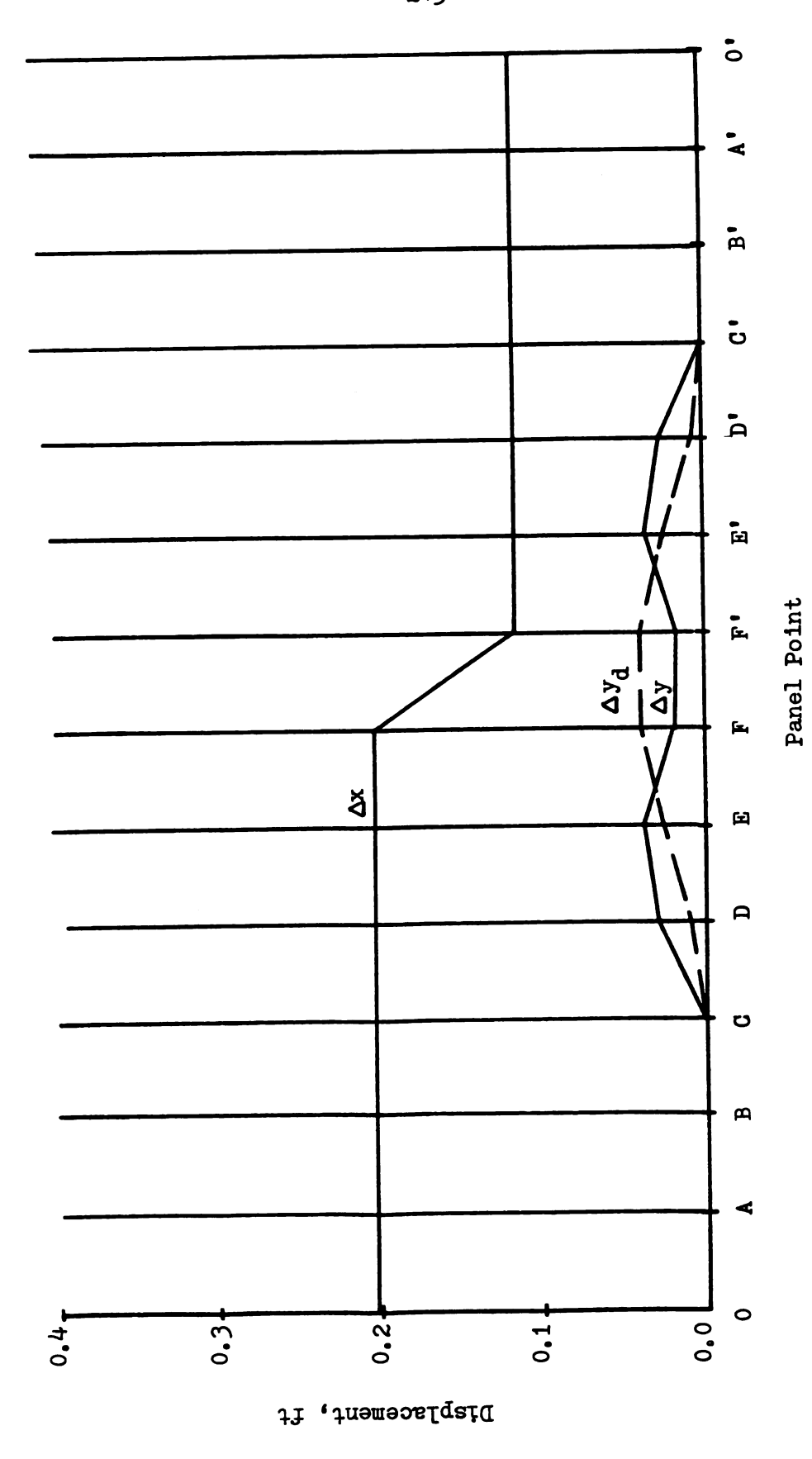


Figure 140 SSB Deck Displacements at X Axis Accelerations of 0.09g

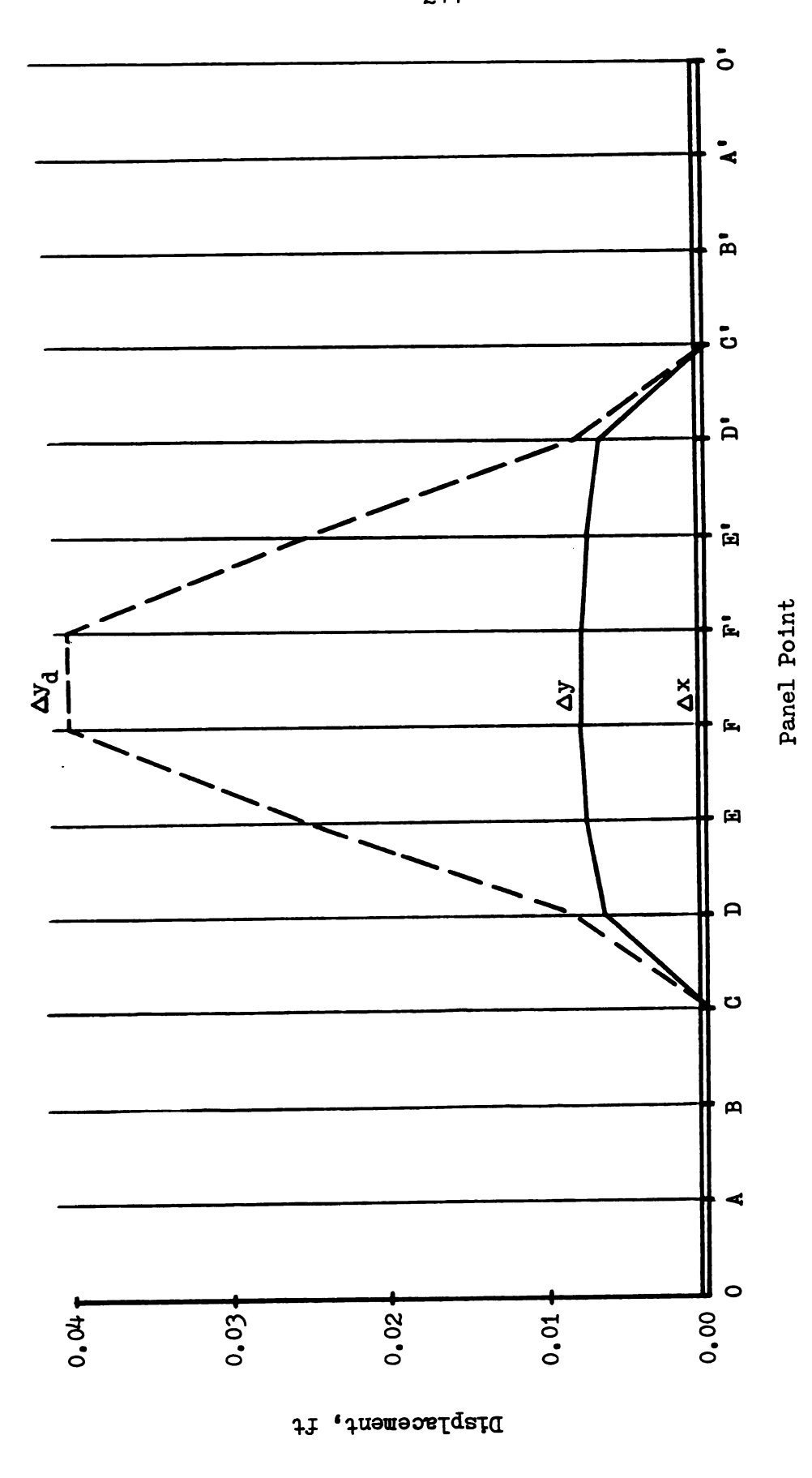


Figure 141 SSB Deck Displacements at Y Axis Accelerations of 0.09g

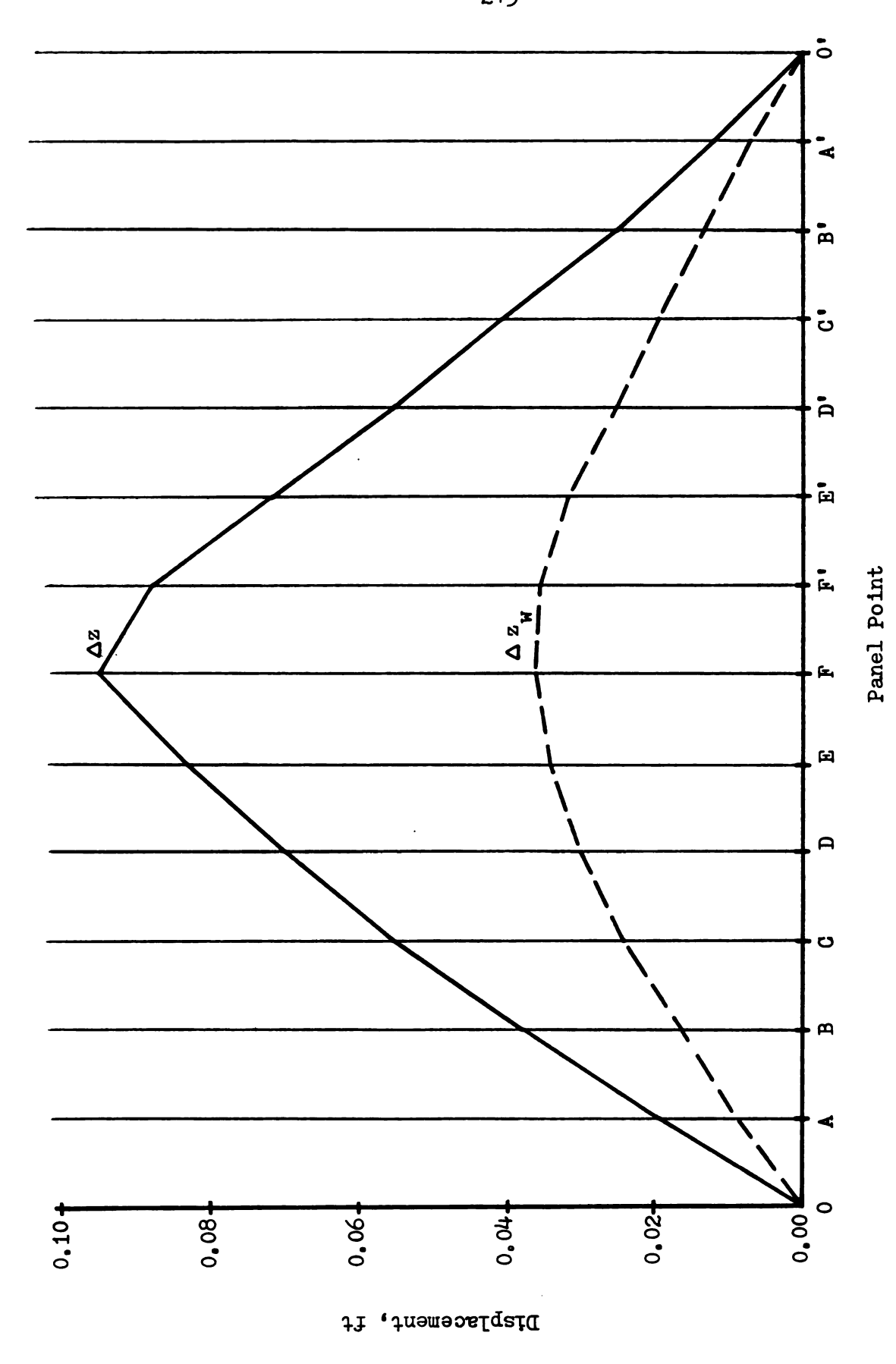


Figure 142 SSB Deck Displacements at Z Axis Accelerations of 0.09g

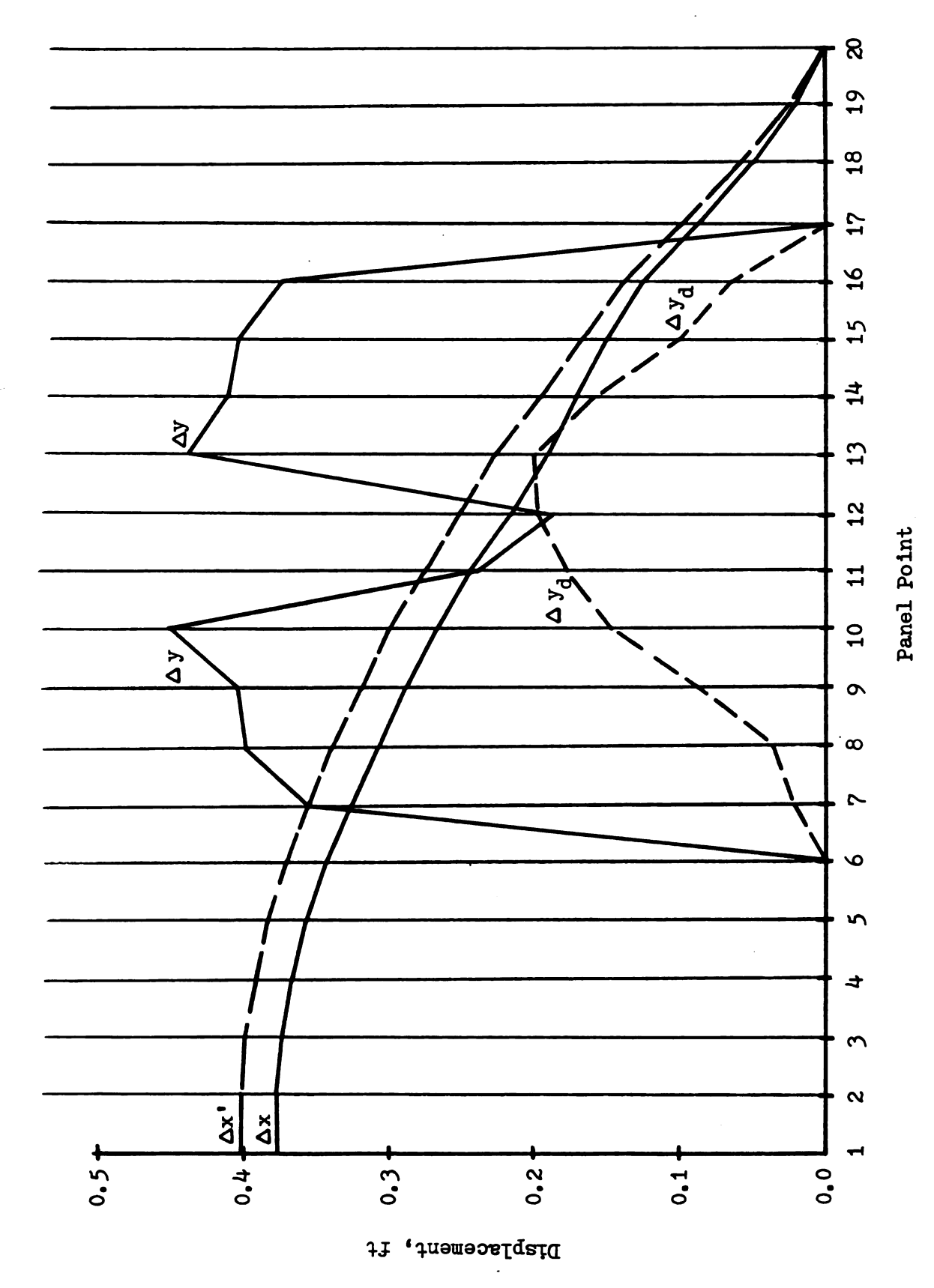


Figure 143 GSCB Deck Displacements at X Axis Accelerations of 0.50g

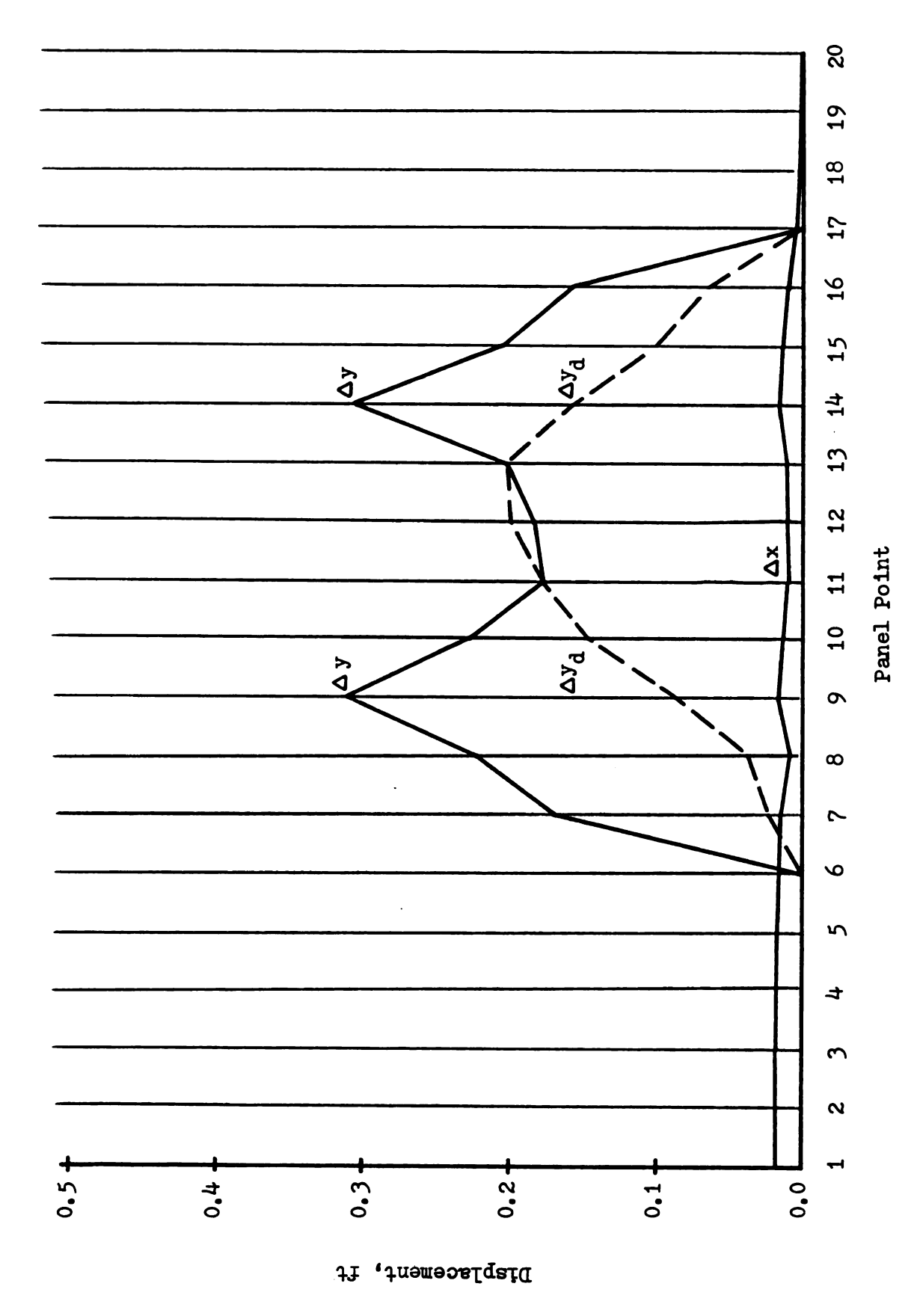


Figure 144 CSCB Deck Displacements at Y Axis Accelerations of 0.50g

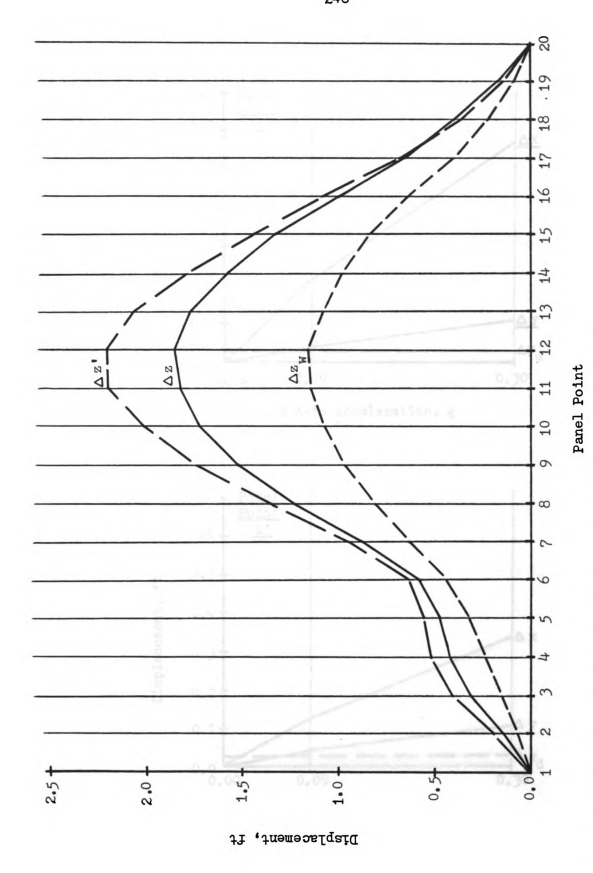
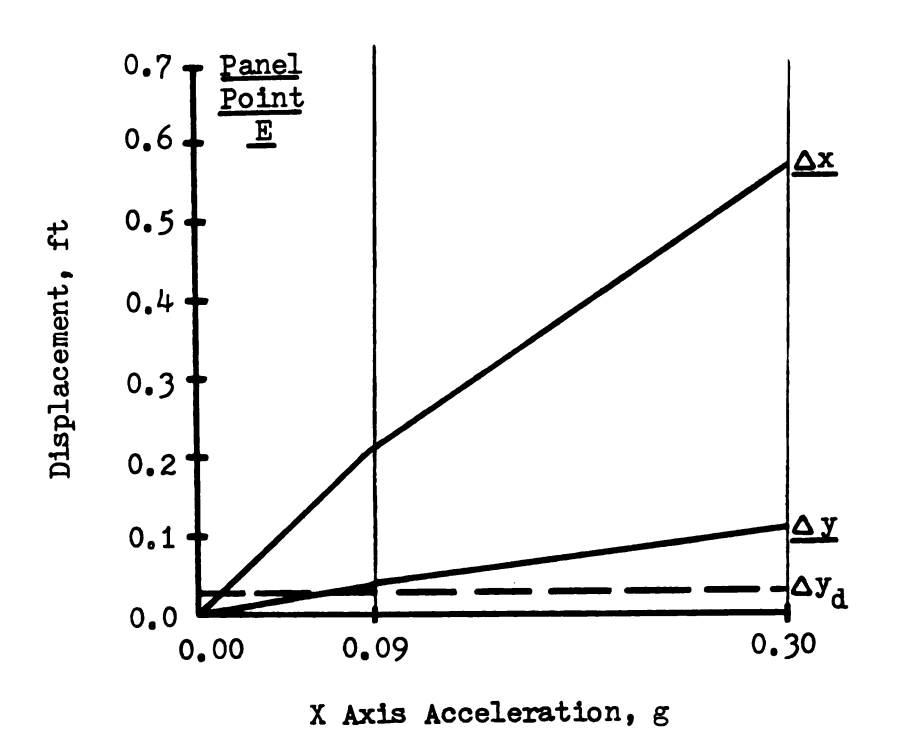


Figure 145 GSCB Deck Displacements at Z Axis Accelerations of 0,50g



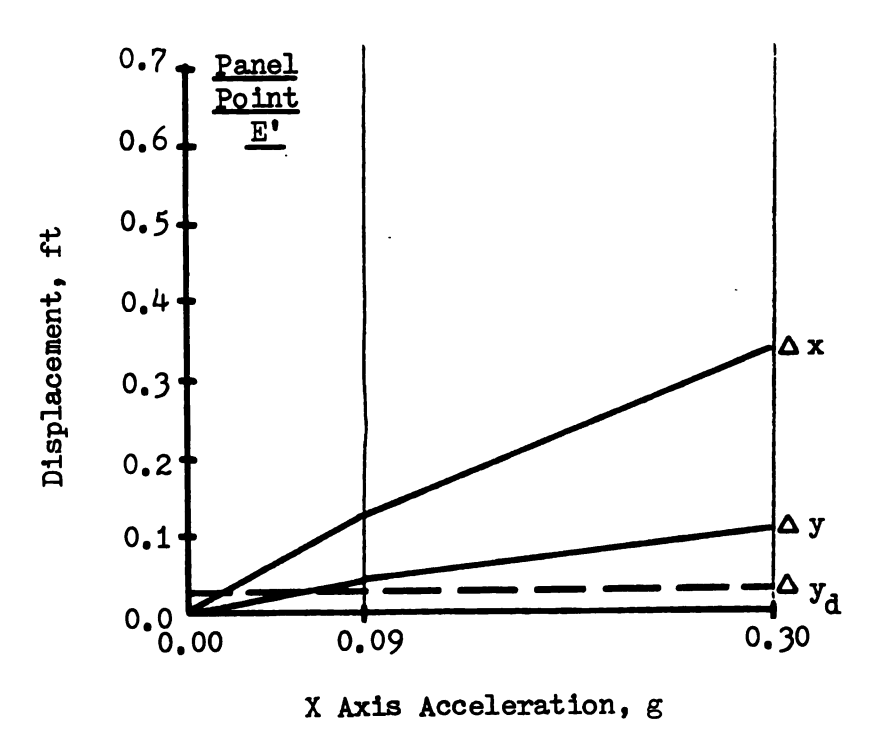
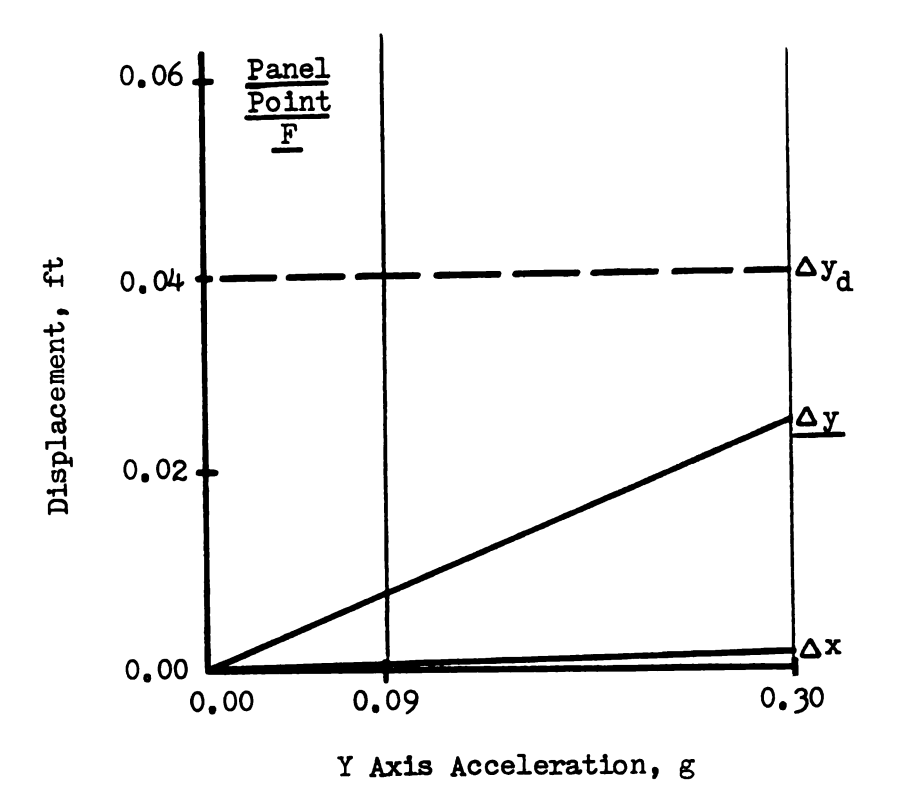


Figure 146 SSB Deck Displacements Versus X Axis Acceleration



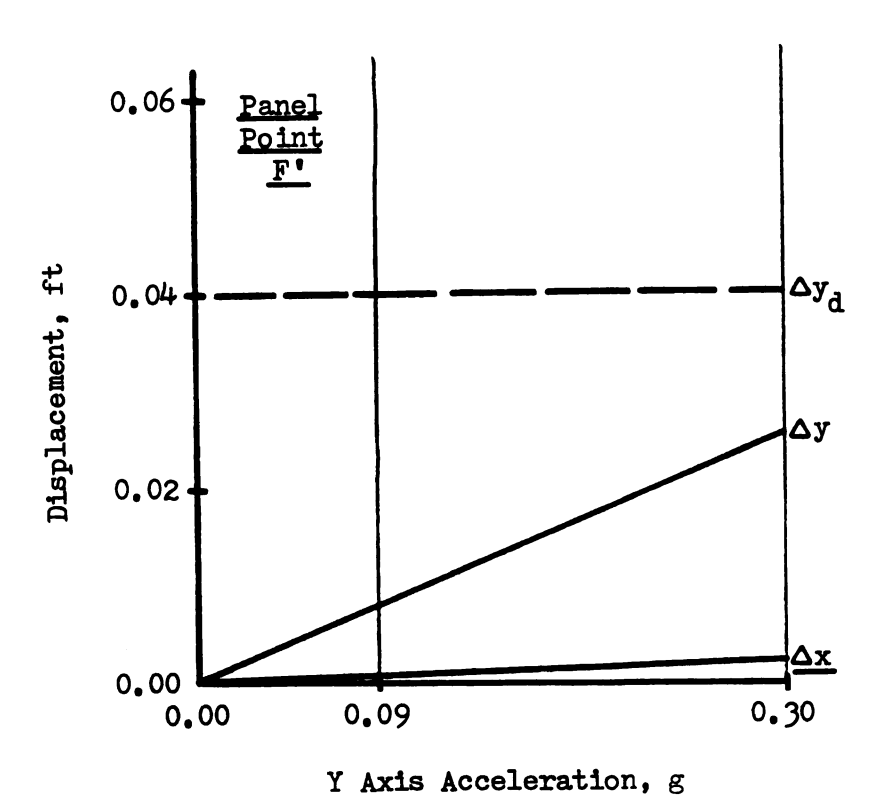


Figure 147 SSB Deck Displacements Versus Y Axis Acceleration

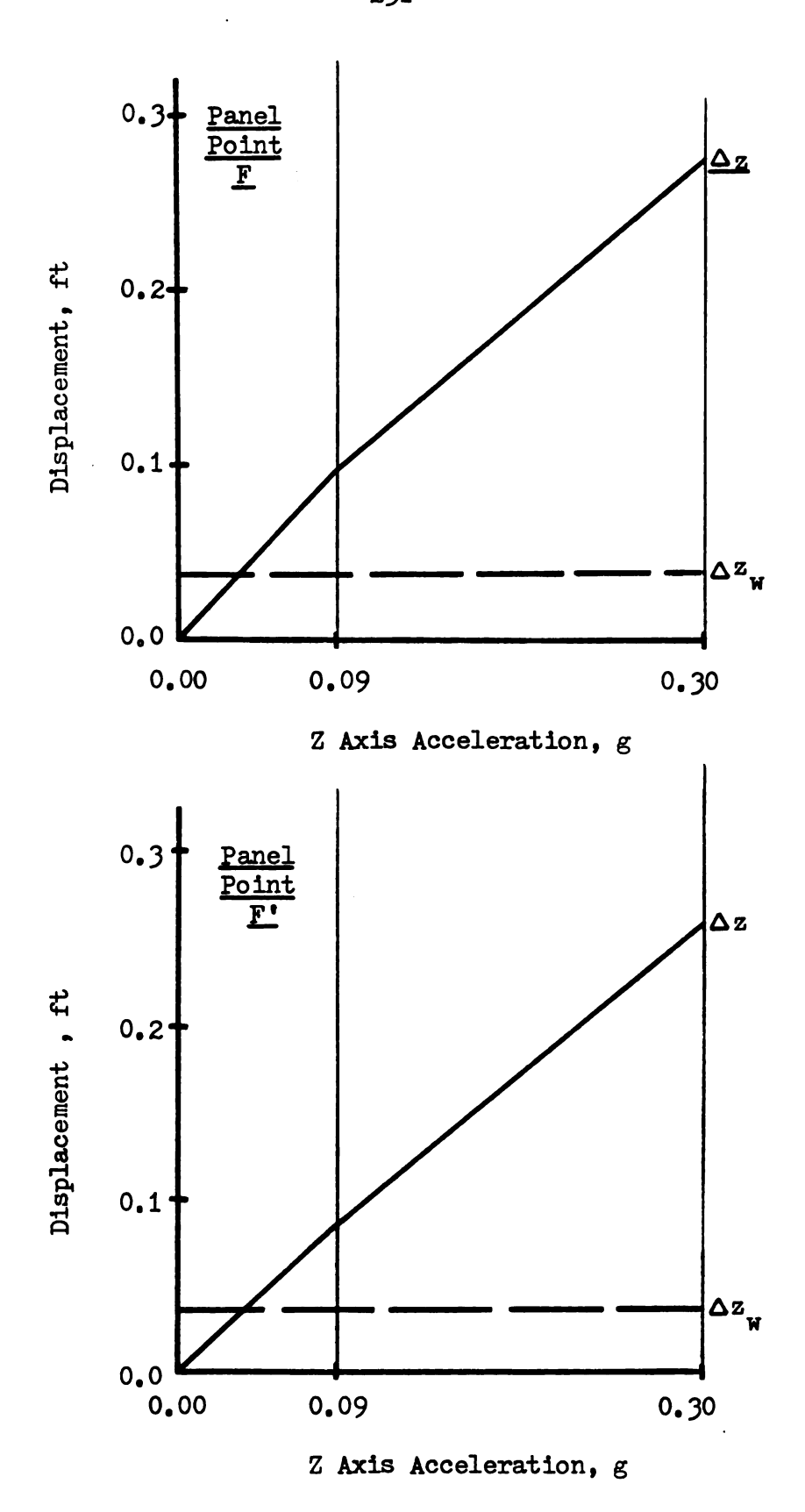


Figure 148 SSB Deck Displacements Versus Z Axis Acceleration



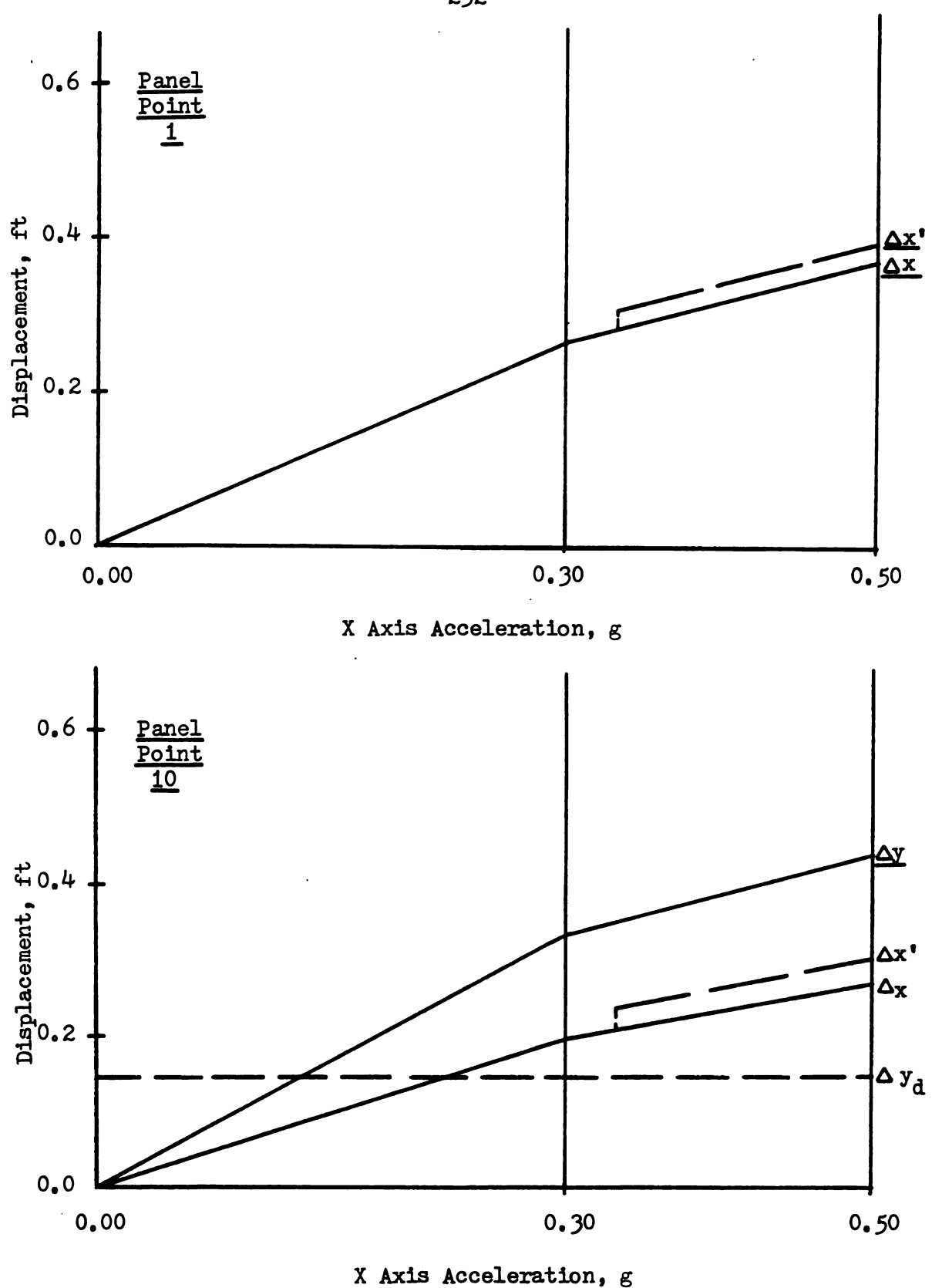


Figure 149 CSCB Deck Displacements Versus X Axis Acceleration

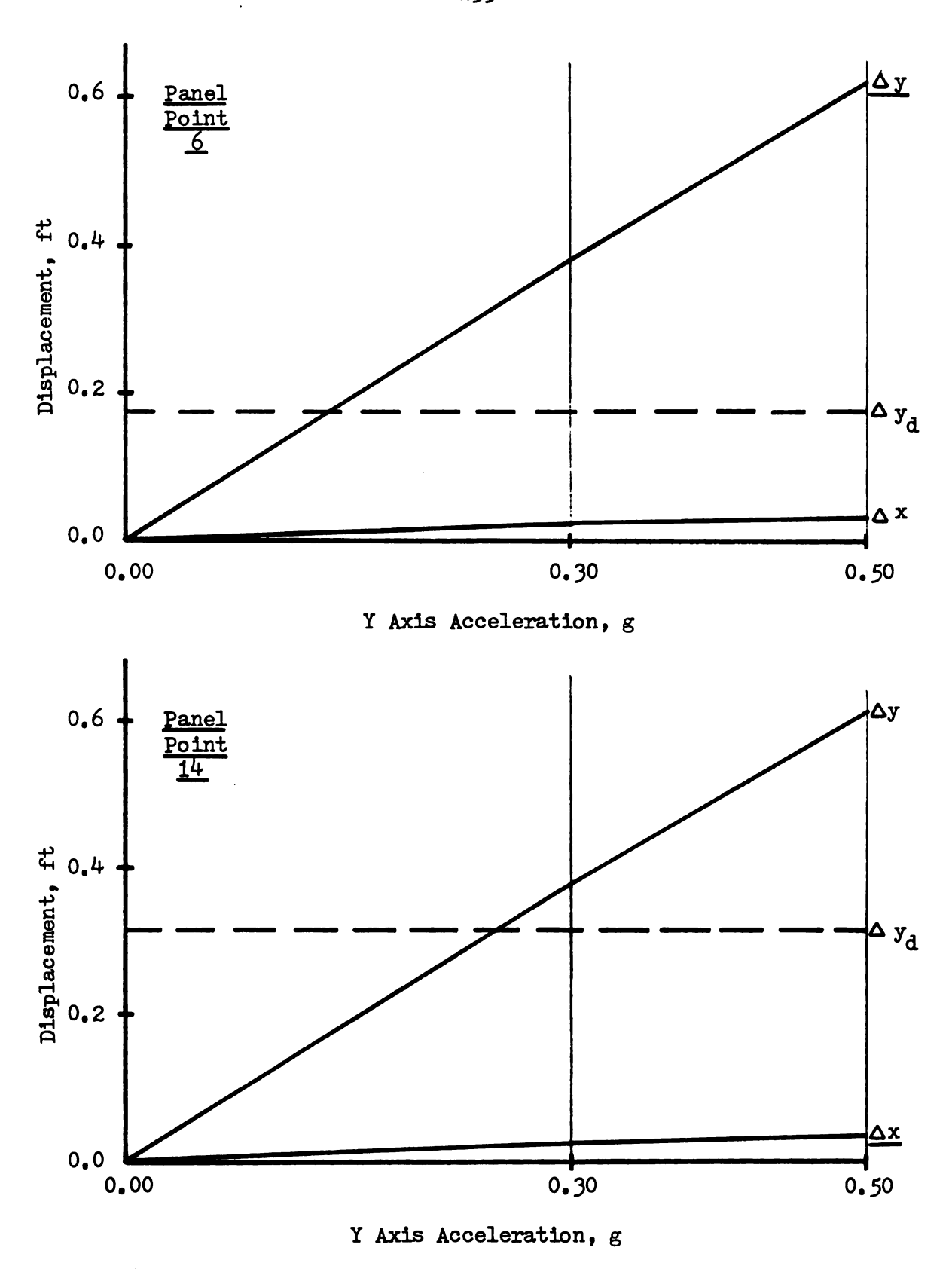


Figure 150 CSCB Deck Displacements Versus Y Axis Acceleration

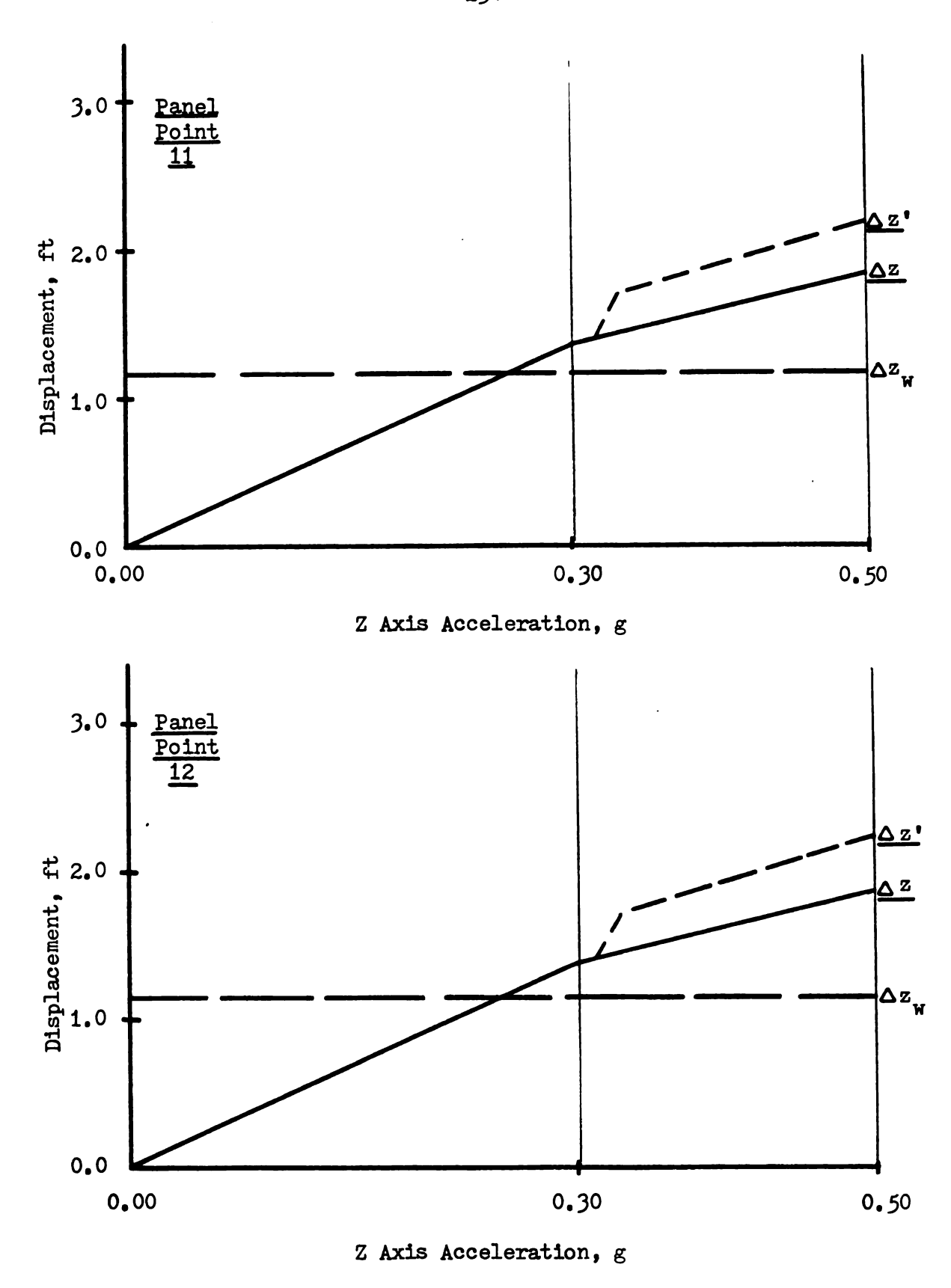
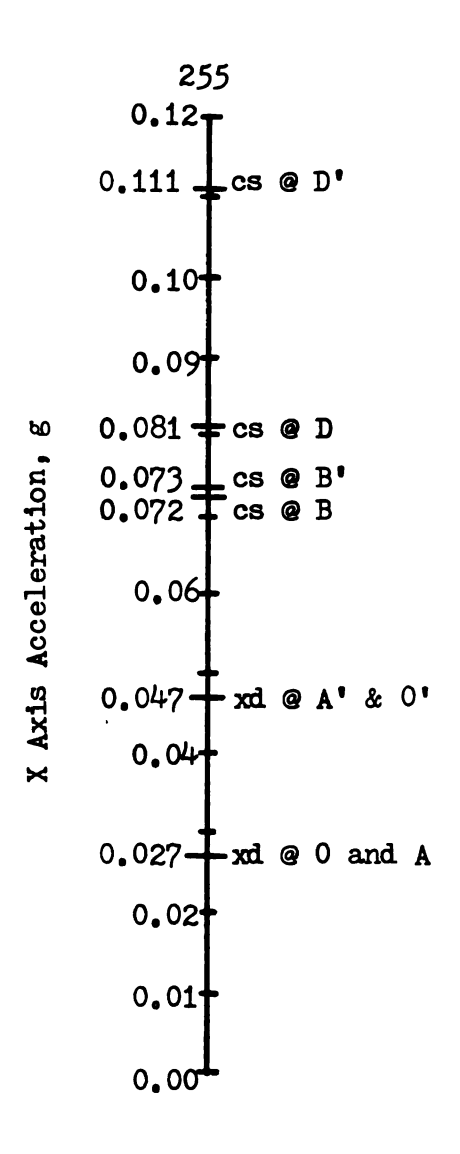
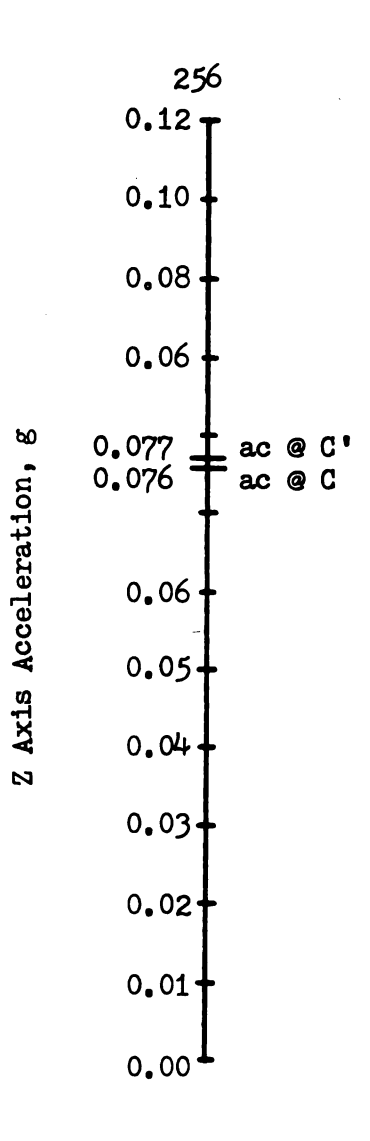


Figure 151 CSCB Deck Displacements Versus Z Axis Acceleration



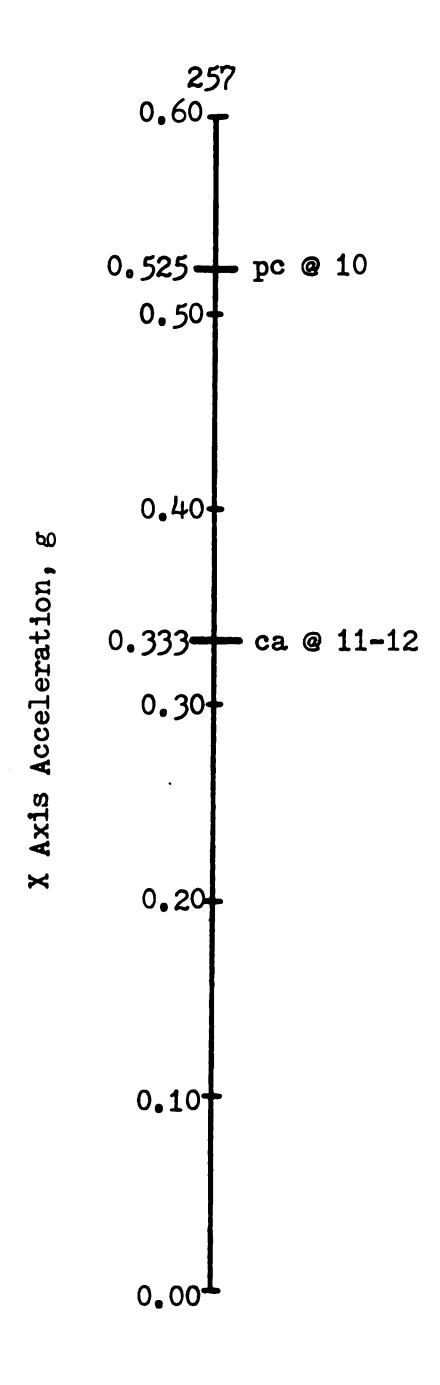
- xd = x axis deck displacement exceeds $\pm 3/4$ inch at this panel point
- cs = column combined stress by SRSS exceeds reserve strength after dead
 load at this panel point

Figure 152 Limits of Assumption Validity for SSB Under X Axis Acceleration



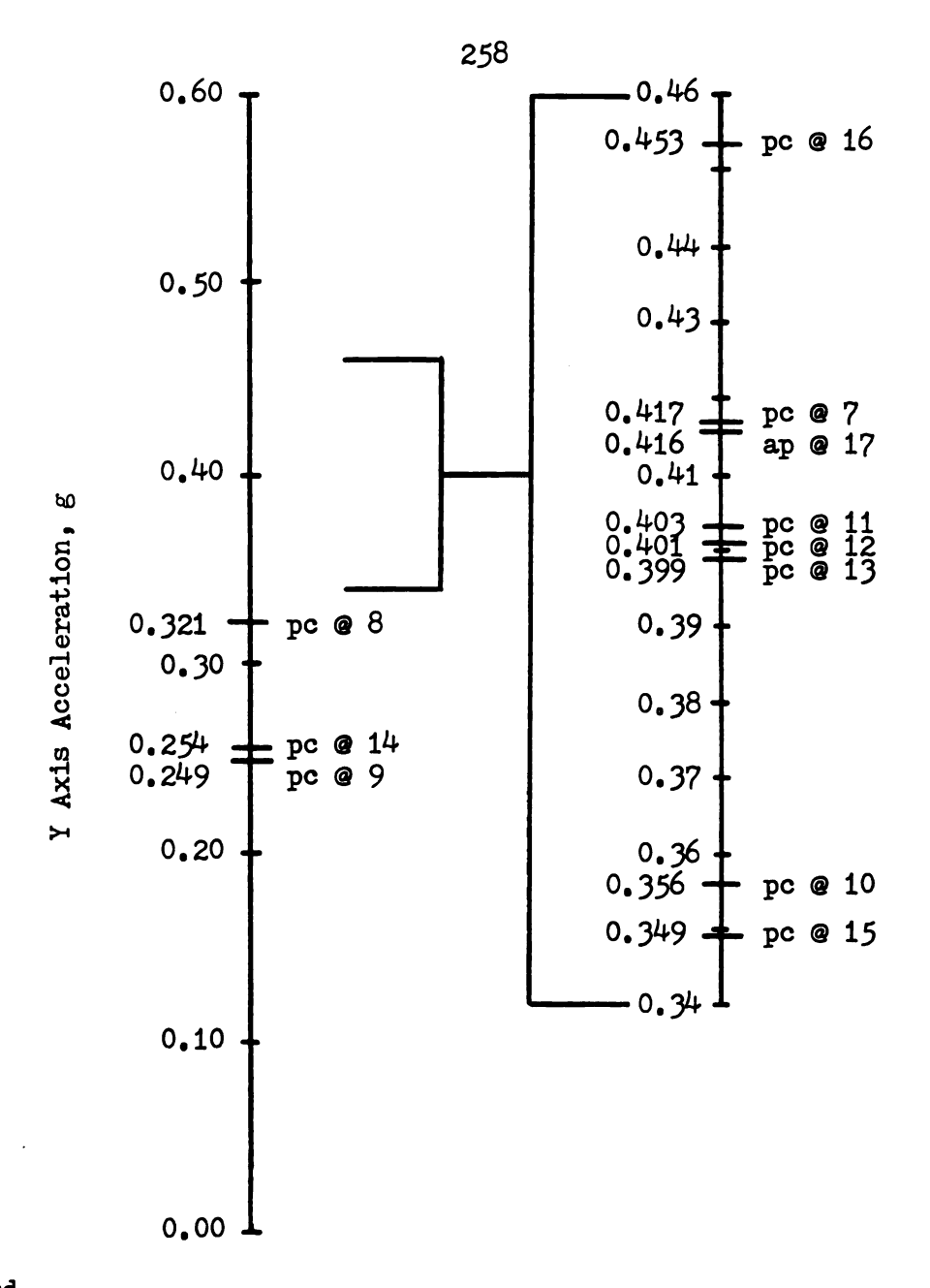
ac = arch rib combined stress by SRSS exceeds dead load prestress at
 this abutment

Figure 153 Limits of Assumption Validity for SSB Under Z Axis Acceleration



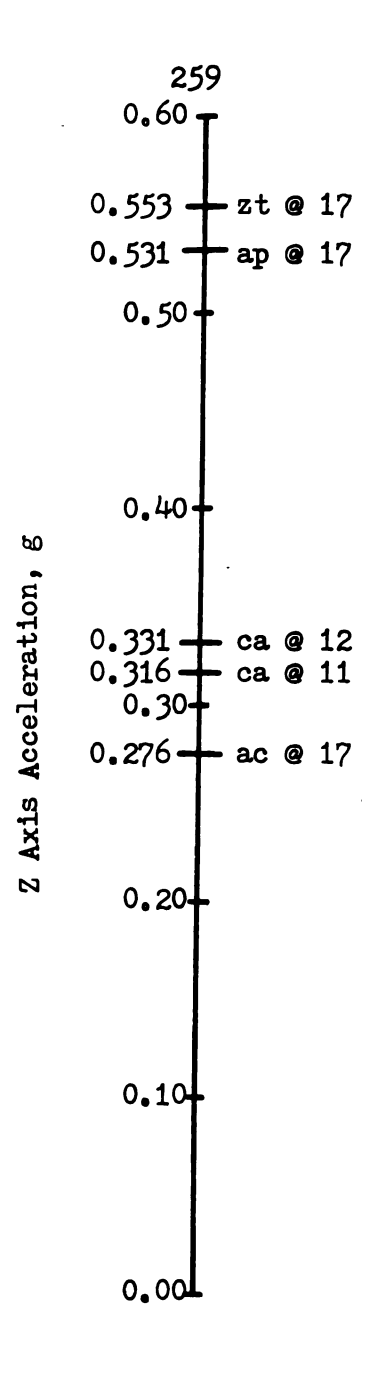
- pc = column axial stress exceeds dead load compressive stress at this
 panel point
- ca = sum of absolute value of axial stresses in pair of longitudinal cables exceeds minimum breaking strength of one cable at this panel

Figure 154 Limits of Assumption Validity for CSCB With Cables Under X Axis Acceleration



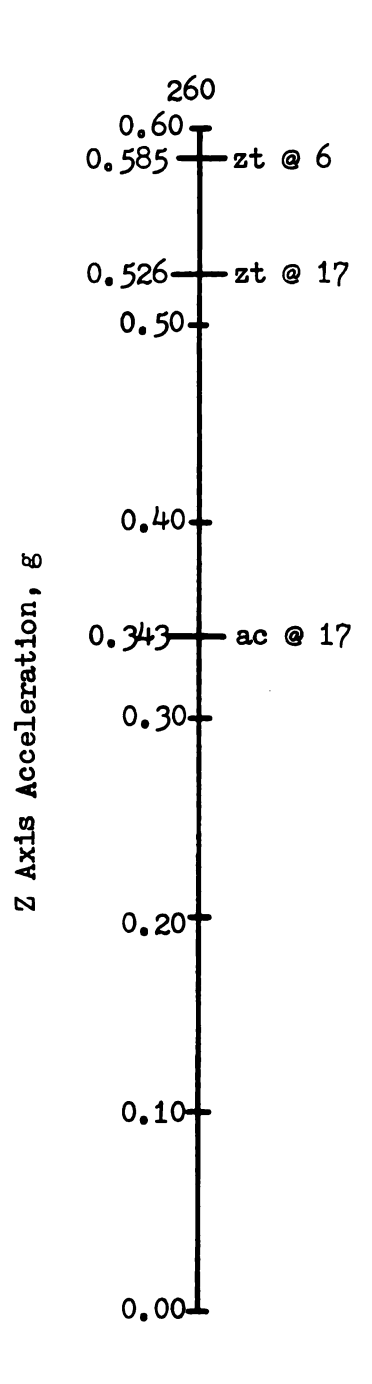
ap = arch rib axial stress exceeds dead load prestress at this abutment
pc = column axial stress exceeds dead load compressive stress at this
panel point

Figure 155 Limits of Assumption Validity for CSCB With Cables Under Y Axis Acceleration



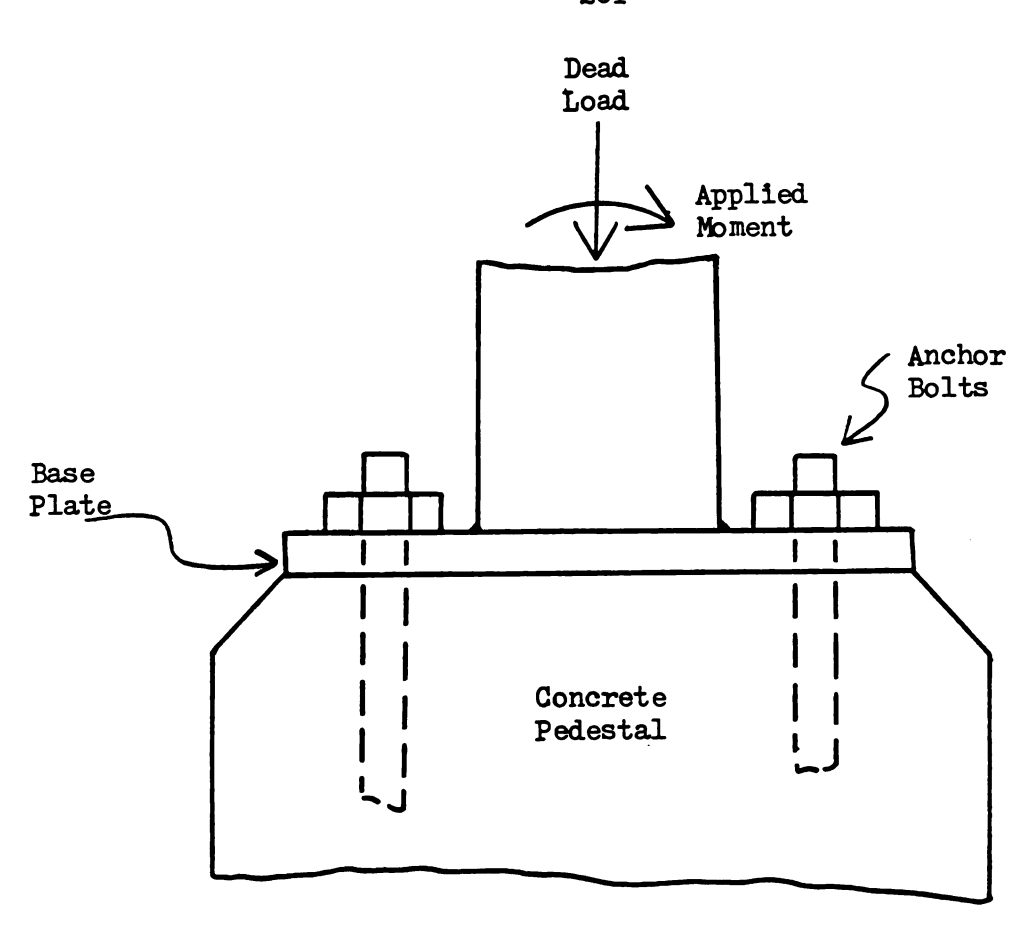
- ap = arch rib axial stress exceeds dead load prestress at this abutment
- ac = arch rib combined stress by SRSS exceeds dead load prestress at
 this abutment
- ca = sum of absolute value of axial stresses in pair of lateral cables exceeds minimum breaking strength of one cable at this panel point
- zt = z axis tower displacement exceeds value required for tower column stress to surpass the yield stress of 33 ksi at this panel point

Figure 156 Limits of Assumption Validity for CSCB With Cables Under Z Axis Acceleration

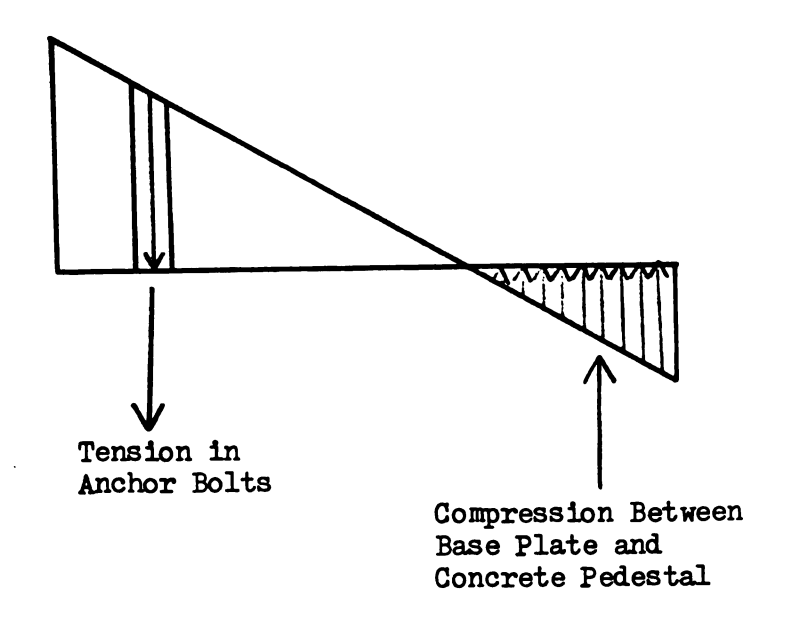


- ac = arch rib combined stress by SRSS exceeds dead load prestress at
 this abutment
- zt = z axis tower displacement exceeds value required for tower column stress to surpass the yield stress of 33 ksi at this panel point

Figure 157 Limits of Assumption Validity for CSCB Without Cables Under Z Axis Acceleration



Joint Diagram



Stress Distribution

Figure 158 Typical SSB Column to Pedestal Joint and Linear Joint Stress Distribution



LIST OF REFERENCES

- 1) Tseng, W. S. and Penzien, J., "Seismic Response of Long Multi-span Highway Bridges", Earthquake Engineering and Structural Dynamics, Volume 4, pages 25-48, 1975.
- 2) Abdel-Ghaffer, A. M., "Dynamic Analyses of Suspension Bridge Structures", California Institute of Technology, Earthquake Engineering Research Laboratory, Pasadena, California, May 1976.
- 3) Thakkar, S. K. and Arya, A. S., "Earthquake Response of Circular Arches", 4th Symposium of Earthquake Engineering, University of Roorkee, Roorkee, November 1970.
- 4) Thakkar, S. K. and Arya, A. S., "Dynamic Response of Arches Under Seismic Forces", Proceedings of the 5th World Conference on Earthquake Engineering, Rome, 1973.
- 5) Okamoto, S., "Introduction to Earthquake Engineering", University of Tokyo Press, 1973.
- 6) Merritt, C. S., "Structural Steel Designer's Handbook", McGraw-Hill Book Company, New York, 1972.
- 7) AASHTO, "Standard Specifications for Highway Bridges", American Association of State Highway Officials, 12th edition, Washington, D. C., 1977.
- 8) Clough, R. W. and Penzien, J., "Dynamics of Structures", chapters 26 and 27, McGraw-Hill Book Company, New York, 1975.
- 9) NRC, "Regulatory Buide 1.92: Combining Modal Responses and Spatial Components in Seismic Response Analysis", Nuclear Regulatory Commission, February 1976.
- 10) Gates, J. M., "Factors Considered in the Development of the California Seismic Design Criteria", Proceedings of a Workshop on Earthquake Resistance of Highway Bridges, pages 142-162, January 1979.
- 11) Imbsen, R. A., Nutt, R. V., and Penzien, J., "Evaluation of Analytical Procedures Used in Bridge Seismic Design Practice", Proceedings of a Workshop on Earthquake Resistance of Highway Bridges, pages 468-497, January 1979.

LIST OF REFERENCES (Continued)

12) AEC, "Regulatory Guide 1.60: Design Response Spectra for Seismic Design of Nuclear Power Plants", Atomic Energy Commission, October 1975.

APPENDIX GLOSSARY OF SYMBOLS

APPENDIX

GLOSSARY OF SYMBOLS

A = maximum ground acceleration

 $\Delta x = x$ axis displacement

 $\Delta x^{\bullet} = x$ axis deck displacement of CSCB without cables

 $\Delta x_{x} = x$ axis wind load displacement

 $\Delta y = y$ axis displacement

 $\Delta y_d = y$ axis dead load displacement

 $\Delta y_{d+w} = y$ axis dead load plus wind load displacement

 $\Delta z = z$ axis displacement

 $\Delta z' = z$ axis deck displacement of CSCB without cables

 $\Delta z_{u} = z$ axis wind load displacement

e = east arch rib

F = modal frequency of vibration

 f_1 = axial stress

 f_2 = arch rib minor axis bending stress or deck lateral bending stress

 f_3 = arch rib major axis bending stress or deck vertical bending stress

 f_{c2} = deck concrete slab lateral bending stress

 f_{c2}^{\bullet} = deck concrete slab lateral bending stress in CSCB without cables

f = allowable stress in deck concrete slab

 f_{cw} = wind load stress in deck concrete slab

 f_d = dead load stress

 f_1 = live load stress

GLOSSARY OF SYMBOLS (Continued)

- f = combined stress by SRSS
- $f_{sum} = combined stress by summation$
- f = wind load stress
- f_y = yield stress of steel (33 ksi)
- N = total number of modes
- n = modular ratio of elasticity
- R = representative maximum value of a particular response
- $R_{k}^{}$ = peak value of a particular response due to the kth mode only
- w = west arch rib
- x = global and local joint coordinate axes which are horizontal and are
 parallel with the bridge centerlines
- y = global and local joint coordinate axes which are vertical
- z = global and local joint coordinate axes which are horizontal and are perpendicular to the bridge centerlines